UNIVERSITEIT VAN PRETORIA
UNIVERSITY OF PRETORIA
YUNIBESITHI YA PRETORIA

Computational Fluid Dynamics Analysis of Flow Patterns in a Thermal Tray Dryer

Reginald Badenhorst

Department of Mechanical and Aeronautical Engineering

University of Pretoria

Supervised by Prof. L. Liebenberg

A dissertation submitted in partial fulfilment for the degree of

Masters in Engineering

November 2009

Summary

Industrial tray air-dryers are increasingly used for the drying of agricultural products. The main drawback of these dryers is the non-uniform velocity distribution in the drying zone resulting in a non-uniform drying of the product. Computational Fluid Dynamics (CFD) software was implemented to predict and decrease the non-uniform velocity distribution of various dryer configurations. Tunnel dryers in commercial use were used to obtain experimental data. The CFD results were correlated with the test data.

Trolley and tray tunnel dryers provide a relatively simple, low capital intensive and versatile method for drying a wide range of products. Artificial drying has the advantage of controlled drying conditions compared to traditional sun drying. The main focus of every tunnel design should be the improvement of the quality of the product in terms of colour, texture and aroma. Increasing the evaporation rate without increasing the energy required to do so, should always be done in-line with this main objective. Many studies focus on the mango structure and food dehydration principles that influence the uniform drying product with the assumption that the airflow over the produce is uniform. Few have been conducted on the air movement inside industrial dryers. CFD analysis predicts the airflow without influencing the airflow pattern compared to the measuring equipment inside test dryers.

The experimental data were obtained from an empty dryer without a flow diverter. This was compared to dryer with the flow diverter included and compared to a dryer with the trolleys, trays and mango slices included. The test results showed that turbulence created by this configuration, still played a major role in the non-uniform velocity distribution along the drying zone of the tunnel. The inclusion of a flow diverter did however dampen the swirl effect of the main fan. Measuring the velocity distribution was practically difficult with the handheld devices used, which influenced the accuracy of the measurements taken. This justified the CFD analysis in order to better visualise and predict the airflow pattern inside the dryer.

The total average speed CFD results of the sections in the drying zone (without mangoes and trolleys) of the dryer without a flow diverter was 11.2% higher compared to the test results. It was 14% higher for the dryer with the flow diverter included. The dryer with the mangoes, trays, trolleys and flow diverter showed a large difference where the total average speed of the CFD analysis was 49% higher compared to the test results. The main reason for the difference of the CFD analysis compared to the measured results are the factors that influenced the uncertainty of the experimental set up. The CFD analysis showed that the coefficient of variance (*CV*) of the dryer with the flow diverter (mangoes and trolleys included) was 3% lower compared to the dryer without one.

Various dryer configurations were analysed using the CFD software to investigate what the best combination of flow diverter, vanes and blanking-off plates would be. A dryer configuration where flow diverters (Up-and-downstream of the main fan) above the false ceiling and inside the drying zone was analysed. A 16% decrease in terms of the *CV* value was obtained compared to the dryer with just the flow diverter downstream of main fan above the false ceiling. There was however a large region of swirl upstream of the main above the false ceiling resulting in a larger loss of heated air through the outlet fan before it reached the drying zone.

The cost of manufacturing a simple vane and flow diverter for an existing dryer is 4% of the initial building costs (excluding the initial cost of the trolleys). The overall drying uniformity of this dryer is improved according to the CFD analysis by 7%. A cost analysis (taking into account the 15 year life cycle of a dryer) in terms of the energy requirement to evaporate water from the drying zone, showed that the dryer with the flow diverter was 6% less expensive to run on a yearly basis. Labour costs will be lower due to man-hours saved in terms of sorting out the wet slices from the dried product. Resources (dryers and trolleys) that would have been used for re-drying the wet produce, could now be implemented to increase the production rate of the plant.

Acknowledgements

I wish to thank the following people that contributed their time and knowledge:

- C. A. Badenhorst
- R. de Beer
- Dr. D.J. de Kock
- C. Gans from Swisscool
- Prof. L. Liebenberg
- Management and production staff at M-Pak Musina
- Construction staff of Precool
- S. Schmitt

Contents

List of Symbols

English Symbols

$\pm a$	end points of the distribution		Equation 10-3
a_i	sensitivity coefficient		Equation 10-4
a_w	water activity	%	Equation 2-4
A	area available for heat transfer	m^2	Equation 2-7
b	breadth of the drying zone in the dehydrator	m	Equation 2-18
C_a	constant pressure specific heat for dry air	kJ/kg·°C	Equation 2-10
C_f	skin-friction coefficient		Equation 4-13
C_{pe}	product specific heat at product exit	kJ/kg·℃	Equation 2-10
d	reference direction for the angular deviation		
D	diameter of circular pipe.	m	Equation 4-1
D	ratio of mass diffusion	m^2/s	Equation 3-2
D_H	hydraulic diameter of a duct	m	Equation 4-1
E_c	cycle efficiency	%	Equation 2-16
FP	measured fan input power	W	Equation 4-17
h	convective heat transfer coefficient	$kW/m^{2\circ}C$	Equation 2-7
h	height of the drying zone in the dehydrator	m	Equation 2-18
h_{fg}	latent heat of evaporation evaluated at T_s	kJ/kg	Equation 2-7
h_{fg_vapour}	latent heat of vaporisation	J/kg	Equation 2-11
h_{li}	enthalpy of liquid H_2O	kJ/kg	Equation 2-10
h_{ve}	enthalpy of the water vapour at the air exit	kJ/kg	Equation 2-10
h_{vi}	enthalpy of water vapour at the air entrance	kJ/kg	Equation 2-10
H_d	rate at which sensible heat is lost by in the dehydration section	J/s	Equation 2-13
H_h	rate at which heat has to be supplied to heat the air during the heating stage	J/s	Equation 2-15
H_i	rate at which latent heat is absorbed to evaporate the water in the product in the dehydrator	J/s	Equation 2-17
I	Turbulent intensity	%	Equation 4-3
k	critical value from the t-table		Equation 10-1
k	surface roughness height	m	Equation 4-10
k	thermal conductivity	W/m K	Equation 3-2
k	turbulent kinetic energy (TKE)		Equation 4-9
k^+	law- of-the-wall variable		Equation 4-10
k_m	mass transfer coefficient	$kg/s.m^2.kPa$	Equation 2-8

ℓ	turbulent length scale	m	Equation 4-6
l_{c1}	loss coefficient of the filter	m/s	Equation 4-14
L	distance from the nearest wall	m	Equation 4-22
L	length of the drying zone in the dehydrator	m	Equation 2-18
L	length of a flat plate	m	Equation 4-1
m	mass of the gas	kg	Equation 4-15
m	loading of the material on the trays	kg/m^2	Equation 2-18
M	drying rate	kg/s	Equation 2-7
M_a	dry mass flow rate entering the dryer	kg/h	Equation 2-10
Ma	free stream Mach number		Equation 4-13
M_{evap}	evaporation rate within the dryer	kg/h	Equation 2-10
M_{evap}	evaporation rate	kg/s	Equation 2-11
M_g	mass of the dry air in the mixture	kg	Equation 2-2
M_i	$B.D.B$ of the material being dried on the product inlet side		Equation 2-18
M_o	$B.D.B$ of the material being dried on the product outlet side		Equation 2-18
M_{pe}	product mass flow rate leaving the system	kg/h	Equation 2-10
M_v	mass of the vapour in the mixture	kg	Equation 2-2
n	number of trays per unit height	n/m	Equation 2-18
p	pressure of the gas	Pa	Equation 4-15
p	total fan pressure	Pa	Equation 4-16
Δp	The pressure drop over the filter	Pa	Equation 4-14
P	total air power of the fan	W	Equation 4-16
P	total pressure	kPa	Equation 2-5
P_a	partial pressure of the dry air in the mixture	kPa	Equation 2-3
P_g	saturation pressure at temperature of mixture	kPa	Equation 2-1
P_v	pressure of the vapour	kPa	Equation 2-1
Q	heat transfer required	kW	Equation 2-10
Q	volume flow rate of air	m^3/s	Equation 2-13
Q	volume flow	m^3/s	Equation 4-16
Q_{actual}	measured dryer energy consumption rate	J/s	Equation 2-11
Q_{loss}	heat loss through the walls and by air leaks	kW	Equation 2-10
r	radial coordinate		Equation 4-18
R	gas constant (8.3145 kJ/kmolK for a particular gas having a molecular mass M)	kJ/kmolK	Equation 4-15
R	percentage of re-circulated air	%	Equation 2-14
s_i	standard deviation		Equation 10-4
$t_{\alpha/2}(v)$	Values on t-table to determine high level confidence coverage		Equation 10-1

T	absolute temperature of the gas	K	Equation 4-15
T_a	fresh outside air at dry bulb temperature	℃	Equation 2-14
T_{ae}	temperature of the air at the exit	℃	Equation 2-10
T_{ai}	temperature of the air at the entrance	℃	Equation 2-10
T_i	circulating air at dry bulb temperature	℃	Equation 2-14
T_i	dry bulb temperature of the air on the side where the fruit enters	℃	Equation 2-13
T_m	dry bulb temperature of the mixture	℃	Equation 2-14
T_o	dry bulb temperature of the air on the side where the fruit leaves the	℃	Equation 2-13
T_{pe}	product temperature at the exit	℃	Equation 2-10
T_{pi}	product temperature at the entrance	℃	Equation 2-10
T_s	surface temperature	°C	Equation 2-7
T_{source}	surface temperature of the heat source	°C	Equation 2-9
T_∞	air stream temperature	°C	Equation 2-7
$\bar{u}$	mean flow velocity	m/s	Equation 4-3
u	standard uncertainty		Equation 10-1
u'	Turbulent velocity fluctuations	m/s	Equation 4-2
u'_{rms}	root mean square of the velocity fluctuations	m/s	Equation 4-2
u_w	finite slip velocity	m/s	Equation 4-13
u_θ	velocity in the direction of revolution	m/s	Equation 4-18
u_τ	friction velocity	m/s	Equation 4-10
u_τ	friction velocity		Equation 4-20
U	expanded uncertainty		Equation 10-1
U	free-stream velocity	m/s	Equation 4-1
U	overall heat transfer coefficient between the heat source and the surface	W/m^2.°C	Equation 2-9
v	The local velocity magnitude	m/s	Equation 4-22
ν	kinematic viscosity	m^2/s	Equation 4-8
v_{app}	velocity of the fluid as it approaches the filter	m/s	Equation 4-14
V	air speed in a dehydrator	m/s	Equation 2-20
V	volume occupied by the gas	m^3	Equation 4-15
W	the rate at which water is evaporated in the dehydrator	kg/s	Equation 2-18
x	length of pipe connected to the fan	m	Equation 4-5
X_w	mole fraction of H_2O in the liquid phase		Equation 2-5
y_1	wall function	m	Equation 4-21
Y	measurement result		Equation 10-5
Y_w	mole fraction of H_2O in the gas phase		Equation 2-5

Greek Symbols

α	thermal diffusion	m^2/s	Equation 3-2
$\delta_{99\%}$	boundary layer thickness	m	Equation 4-5
ε	turbulent dissipation rate	m^2/s^3	
Λ	pipe-friction factor		Equation 4-12
η	fan efficiency	%	Equation 4-17
η_t	thermal efficiency	%	Equation 2-11
μ	dynamic viscosity	kg/m·s	Equation 4-1
μ_t	turbulent viscosity	kg/m·s	Equation 4-22
ν	degrees of freedom listed on t-table		Equation 10-1
Φ	relative humidity	%	Equation 2-1
θ	angular deviation	°	Equation 4-24
θ	time that it takes for the product to dry	s	Equation 2-18
ρ	density of air	kg/m^3	Equation 2-13
ω	absolute humidity	%	Equation 2-2
ω	vorticity	s^{-1}	Equation 4-23
ω_{ai}	absolute humidity of air entering the dryer	%	Equation 2-10

Dimensionless Groups

Le	Lewis number	Equation 3-2
Pe	Peclet number	Equation 4-7
Pr	Prandtl number	Equation 4-8
Re	Reynolds number	Equation 4-1

Abbreviations

$B.D.B$	dry base moisture content	%	Equation 2-19
RPM	revolutions per minute	r/min	Equation 4-18
$W.W.B$	Wet Weight Basis moisture content	%	Equation 3-1

1 Introduction

1.1 Background

An increasing number of industrial tray-air dryers are used in the drying of agricultural products. The advantages in using these types of dryers are well documented. Tests that were conducted in previous studies showed that the drying rate is a strong function of air flow or air velocity over the product (Mathioulakis, Karathanos and Belesssiotis, 1998). The main drawback in using tunnel dryers is the variation of air velocities across the trays thus resulting in a non-uniform drying of the product (Mathioulakis et al., 1998). A drying chamber is required to improve the uniform air-velocity flowing over the food produce.

Few studies have been conducted on the air movement in these dryers. Computational Fluid Dynamics (CFD) software is increasingly being implemented in the design of drying chambers or to predict the airflow. It is shown to be a useful tool in predicting non-uniform air velocities in the drying chamber (Mathioulakis et al., 1998).

1.2 Justification of the study

'The drying of agricultural products such as fruits and vegetables is usually performed using the sun. Traditional sun drying takes place under direct sunlight or under transparent plastic films for the protection against rain or other environmental factors. Sun drying has the advantage of low installation costs and low drying temperatures. The disadvantages are the long process times, labour cost and the deterioration of the food quality due to several factors, such as dust, moisture and insects. A method of increasing importance is by drying of fresh products in large, forced-air circulation dryers at relatively high temperatures within a few hours. Such artificial drying has the advantage of controlled drying conditions. It also minimizes the necessity for handling during drying and thus the operating costs are significantly reduced. The risks of several environmental factors, applied to sun drying, such as rain, dust, insects, problems from stones and other foreign matter, are absent in artificial drying and the dehydrated products are of good quality' (Mathioulakis et al., 1998, pp. 183-184).

1.3 Goal of study

Airpak 2.1, a CFD software program, will be implemented to improve the uniform velocity distribution in present-day tunnel dryers. The simulation model of the tunnel dryer will be validated against test data.

The different factors that have an influence on the airflow in the tunnel dryers will be discussed including methods that can be implemented to optimise the drying

tunnel. Information obtained will be implemented in creating a dryer that is more efficient in drying the food product. This will lead to lower energy consumption and thus reducing the running cost of the dryer.

1.4 Structure of this dissertation

The literature study focuses on the mango structure and food dehydration principles that influence the uniform drying of the food product in the dryers. Tunnel dryers in commercial use at M-Pak in Musina, South Africa, were used to obtained experimental data. The average air-speed over the food product was measured. Various factors to obtain a CFD analysis that accurately models the tunnel dryer in terms of air-flow are discussed. In order to reduce the computational effort and time required, the simulation of the heat and water transfer from the mangoes and distribution inside the dryer were omitted. The results are correlated with the test data. Conclusions and recommendations are given to improve the drying uniformity of the dryer.

2 Literature study

2.1 Mango structure

To understand why it is important to have the correct air velocity and uniformity when drying, one has to look at the structure and composition of fruits and vegetables. According to Wills et al. (1981) the cells of fruit and vegetables are typical plant cells, and the principal components of these are shown in Figure 2-1. Pant cells are bound together by a rigid cell wall. The cell wall is permeable to water and solutes.
Other functions of the cell wall that will have an influence on the heat and mass transfer of the fruit are:

- to contain the cell contents by supporting the outer cell membrane, the plasma lemma, against the hydrostatic pressures of the cell contents which would otherwise burst the membrane.
- it gives structural support to the fluid reservoirs called the vacuoles, which are surrounded by semi-permeable membranes, the tonoplast. Together with the semi-permeable plasma lemma, the tonoplast is responsible for maintaining the hydrostatic pressure of the cell, allowing the passage of water.

Most produce contains more than 80% water. Quite large variations in water content can occur within the species, since the water content of individual cells varies considerably (Wills et al., 1981).

A basic fact important in the post harvest handling of produce is that harvested fruit and vegetables are 'living' structures. After harvest the produce is still living as it continues to perform the metabolic reactions and maintain the physiological systems, which were present when it was attached to the plant. Fruits and vegetables respire by taking up oxygen (O_2) and giving off carbon dioxide (CO_2) and heat. They also transpire, that is, lose water. Respiration and transpiration continue after harvest, and since the produce is now removed from its normal source of water, the produce is dependent entirely on its own moisture content (Wills et al., 1981).

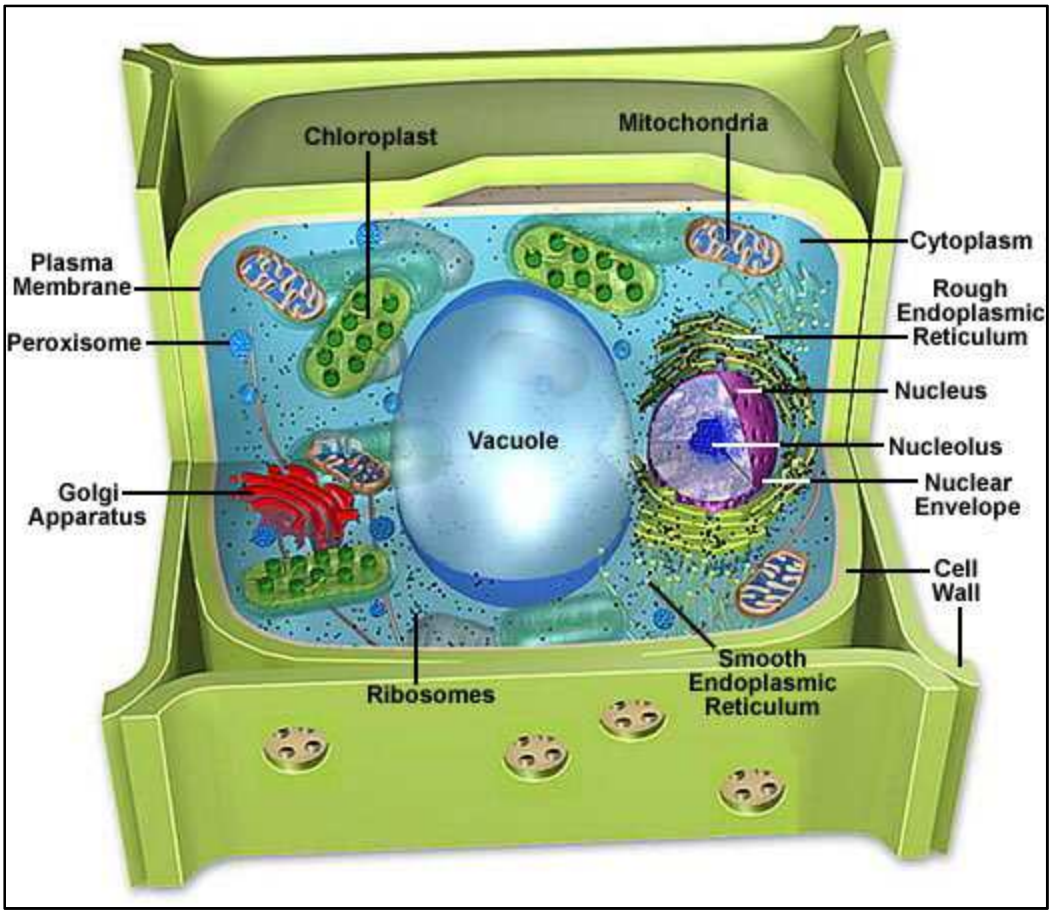

Figure 2-1 Anatomy of a plant cell

Source: http://micro.magnet.fsu.edu/cells/plantcell.html

'Relative humidity (RH), expressed as a percentage, is probably the best-known term for expressing the humidity of moist air and it is defined as the ratio of the water vapour pressure in the air to the saturation vapour pressure possible at the same temperature. When fruit is placed in an enclosure filled with air, the water content of the air increases or decreases until equilibrium is reached. Equilibrium occurs when the number of water molecules entering and leaving the vapour phase is equal. The relative humidity at equilibrium is called the equilibrium

relative humidity (ERH), which is a property of the material and its moisture content' (Wills et al., 1981, pp. 53-54).

'The humidity ratio (ω) of an air-water vapour mixture is the mass of the vapour in the mixture (M_v) divided by the mass of the dry air in the mixture(M_g). The term *dry air* is used to emphasize that this refers only to air and not the water vapour' (Sonntag, Borgnakke and van Wylen, 1998, p 446). An important process for an air-water vapour mixture is the adiabatic saturation process. This is a process where the air-vapour mixture comes in contact with a body of water (fruit) in a well insulated duct. If the relative humidity is less than 100%, some of the water will evaporate and the temperature of the air-vapour mixture will decrease. If the mixture leaving the duct is saturated and if the process is adiabatic, the temperature of the mixture on leaving is known as the adiabatic saturation temperature. Also known or termed as thermodynamic wet-bulb temperature. If it is assumed that the pressure is constant a steady state process will occur if water at the adiabatic saturation temperature is added at the same rate at which water is evaporated. The saturation temperature is a function of the pressure, temperature, and relative humidity of the entering air-water vapour mixture and of the exit pressure (Sonntag et al., 1998). The evaporation of water is a physical process that requires energy (Wills et al., 1981).

'Fresh fruit and vegetables can be regarded as essentially water in fancy and expansive packages. The high water content of fruit and vegetables is held within the produce by osmotic forces within the cells, mostly as free water, although a small proportion is chemically bound and, therefore, is more tightly held and stable. Water in plant tissues contains varying amounts of solutes, which slightly depress the vapour pressure of the water. When fresh plant tissue is placed in an enclosure, the air will not become completely saturated due to the presence of these solutes and chemically bounded water. For most fresh produce an equilibrium relative humidity of at least 97% is established. The small reduction in ERH due to the presence of solutes can also be related to the terms water activity and water potential. Water activity and water potential are expressions of the energy status of water within living tissues and this determines the availability of water for life processes' (Wills et al., 1981, p. 54).

'A major factor in the rate of water loss from the produce is the surface to volume ratio of the material. On purely physical grounds, there is a greater loss by evaporation from produce with a high surface area to unit volume ratio' (Wills et al., 1981, p. 55).

'The types of surfaces and the underlying tissues of fruit and vegetables have a marked effect on the rate of water loss. Many types of produce have a waxy coating on the surface (cuticle) that is resistant to the passage of water or water vapour. Before harvest, the cuticle plays an essential part in maintaining within the tissues of the produce the high water content that is necessary for normal

metabolism and growth by restricting water loss by evaporation' (Wills et al., 1981, p. 56).

'The structure of the wax coating is more important than its thickness. Waxy coatings that consist of a complex, well ordered structure of overlapping platelets provide more resistance to the permeation of water than coatings that are thicker but are flat and with less structure. In the former, the water vapour must follow a more diverse path as it escapes into the atmosphere' (Wills et al., 1981, p. 56).

Underneath the waxy layer and the cuticle, many fruits comprise of cork cells tightly packed together. These are toughened hypodermal cells. Lenticels are narrow openings formed between the cork cells. There is no mechanism provided for the closing of lenticels. The rate of transpiration thus depends on the number and the size of the pore openings and the nature of the waxy coating. In mature fruit the lenticels are often blocked with wax and debris and are therefore non-functional. Thus loss of water as vapour, and respiratory gas exchange take place only by diffusion through the cuticle. Therefore by removing these protective surface layers and directly exposing the underlying tissues to the atmosphere can greatly accelerate the rate of water loss from the produce (Wills et al., 1981).

'Air movement over the produce is a significant factor influencing the rate of moisture loss. There is always a microscopically thin layer of air (the boundary layer) adjacent to the surface of the produce in which the water vapour pressure is approximately in equilibrium with that of the produce itself. Air movement tends to sweep away this moist air from around the produce. Increasing the rate of air movement reduces the thickness of the boundary layer, increases the vapour pressure difference near the surface, and so increases the rate of moisture loss' (Wills et al., 1981, p. 58).

2.2 The simulation of airflow in a dryer using CFD

Previous studies of the simulation of airflow in a tunnel dryer using Computational Fluid Dynamics (CFD) is now evaluated. It is important to know how accurate the model created with CFD recreates the real inner workings of a tunnel dryer. Factors that influence the model of the tunnel dryer are evaluated.

Mathioulakis et al., (1998) conducted several drying tests on an industrial batch-type, tray air fruit dryer and expressed the result as a weight loss fraction. They determined that there was a variation in the degree of the dryness in several trays and the non-uniformity was traced to certain areas of the drying chamber. Modelling the pressure profile and air velocities of the drying chamber with CFD, they found a lack of spatial homogeneity of the air velocities above the product.

According to Mathioulakis et al.,(1998) there is still a lack of knowledge of the drying behaviour inside a fruit dryer and may be in part responsible for the relatively high cost of such a drying installation. It is of primary importance to know the air flow in the drying chamber, because one may know the areas of adequate or inadequate air velocities, which respectively leads to proper or improper (or slow) drying. Adams and Thompson (cited in Mathioulakis et al., 1998) found that the variation in air velocities reduced with the addition of baffles.

'In processes which may use air as a reaction or as a heat transfer medium, a simulation of the air movement in the system may be applied, in order to predict the air flow and therefore several transport processes which are connected with the air flow or air velocity. CFD software may be used to predict air velocities in the drying chamber. Measurement of the air velocities during the operation is difficult, since several sensors need to be placed at various directions of airflow and location which may disturb the flow pattern. The simulation results by CFD may be tested with the actual drying experiments and if there is an agreement between predicted and experimental results then the CFD code may be reapplied for other drying conditions to optimise the drying performance of the unit. CFD may thus be used as a drying optimisation tool' (Mathioulakis et al., 1998, p. 184).

Most algebraic, plug flows, or balance type models are based on the assumption of spatial homogeneity of the flow. Experimentally this assumption could not be fully verified. Lack of homogeneity seems to be the main factor for the malfunction of dryers. There are very few literature references concerning numerical simulation of airflows in the interior of industrial dryers (Mathioulakis et al., 1998).

'Numerical simulation, in contrast to the algebraic models, is based on the resolution of the Navier-Stokes equations at each point in the flow field. This kind of model, taking into consideration the exact topography of the plant, is able to describe the spatial and time distributions of velocities, temperatures, pressures and other physically meaningful quantities' (Gouvalias, Markatos, Panagopoulos, Tierny, Huberson and Zhong cited in Mathioulakis et al.,1998, p. 184).

'Turbulence is an intrinsic attribute of this type of flow, which is characterised by the relative high velocities, and the presence of many obstacles. The main objective of the numerical simulation of turbulent flows is to propose a representation of the mean motion. The Navier-Stokes equations of instantaneous motion are averaged to produce the equations of mean motion. The statistical averaging process introduces an unknown turbulent correlation, the so-called Reynolds stresses and fluxes, in the mean flow equations, which represent the transport of momentum, heat and mass due to turbulence. A turbulence model is a set of equations, additional to the averaged Navier-Stokes equations, which may express approximate relationships between otherwise unknown terms and the dependent variables' (Mathioulakis et al., 1998, p. 189).

The use of different turbulence models might lead to completely different results, especially in a complex geometry configuration. The choice of the appropriate turbulence model must be done after taking into consideration both the physical and numerical aspects of the problem. Consequently, the use of models that are based on the assumption of isotropic spatial distribution of the turbulence production, as the constant effective turbulence and standard $k-\varepsilon$ turbulence models are not recommended (Mathioulakis et al., 1998).

Most designs of drying chambers assume that the airflow will be uniform over the produce, allowing the air to pass only one tray per pass. Non-uniform drying is the limitation of many drying units because of differences in air humidity or temperature as the same air passes from tray to tray (e.g. vertical motion of air moving through the trays) (Mathioulakis et al.,1998).

The tests of Mathioulakis et al., (1998) showed that artificial drying resulted in a relatively uniform dried product in each tray and was of an excellent quality, regarding the cleanliness, flavour, colour, texture and foreign matter and other infestation. The only problem with the application of artificial drying in fruits was the non-uniformity of drying in some areas of the drying chamber. In industrial terms this means that the produce has to be sorted and the wet produce has to re-dried, increasing the cost of the drying process.

Mathioulakis et al., (1998) then measured the velocities above the produce with an anemometer and found that the results agreed remarkably well with the results obtained with the simulation using CFD.

2.2.1 The influence of grid density on CFD simulation

‘Due to the fact that the main flow evolves in all three directions, the use of a three-dimensional grid is necessary. As a consequence, the dependent variables of the problem are the three velocity components in the x, y and z directions. Because the flow is forced, the air density and viscosity can be assumed to be constant’ (Mathioulakis et al., 1998, p. 187).

‘A crucial factor for the numerical simulation to be realistic is the appropriate definition of the computational grid, which comes as a result of a compromise between the necessity to use the geometry very close to the real-world model and the necessity to decrease the computational time and achieve a rapid convergence of the numerical process’ (Mathioulakis et al., 1998, p. 188). A finer grid would be a great strain on the computational time without significant improvement of the quality of results, while a coarser grid would not allow the realistic representation of the flow, especially in the vicinity of the solids. Mathioulakis et al., (1998) represented the fruit on the tray as ‘blockages’, which means solid bodies with zero porosity and friction on their surfaces.

2.3 Ideal gas mixtures and psychrometrics

'An understanding of the behaviour of the air-water vapour mixture is essential in designing and operating food drying systems. While the ideal gas equation of state is only an approximate model of the real gas behaviour, it is accurate enough to be used in the modelling equations of food drying systems' (Batty & Folkman, 1983, p. 111). Jones (1977) produced compressibility tables for air free of CO_2. Air at 301 K, 95 kPa and 50% RH, which is similar to the ambient values of experiment one (see chapter 3.2), the compressibility factor (Z) according to Jones (1977) is 0.99967. A second, less accurate option is to use the compressibility chart of nitrogen for the ranges of temperature and pressure in the dryer. At low density all gas and vapour approach ideal gas behaviour. At higher densities the compressibility chart should be used to check whether the gas deviates from the ideal gas law of state (Sonntag et al., 1998). It was found that for the temperature ranges and pressure field in the flow domain of the dryer that the ideal gas law can be applied.

'Consider a mixture of a gas and a vapour such as the air and water vapour. The difference between the gas and a vapour is not always clear, but in general a substance is called a gas if it is very highly superheated and a vapour if its temperature is not very much greater than the saturation temperature corresponding to its partial pressure. If the temperature is reduced sufficiently, part of the vapour will condense to liquid if the partial pressure of the vapour is greater than the triple point pressure or it will solidify if the partial pressure is below the triple point pressure. The dew point of a gas-vapour mixture is the saturation temperature corresponding to the partial pressure of the vapour in the mixture. If the partial pressure of the vapour equals the saturation pressure corresponding to the temperature of the mixture, the mixture is to be saturated' (Batty & Folkman, 1983, p. 114).

'The relative humidity of a gas vapour mixture is defined as the mole fraction of the vapour divided by the mole fraction of the vapour in a saturated mixture at the same temperature and total pressure. Usually, for the mixtures of interests, the partial pressure of vapour is sufficiently low that the vapour may be treated as an ideal gas with good accuracy. In such a case the, the relative humidity (Φ) of the mixtures may be taken as the ratio of the partial pressure of the vapour (P_v) to the saturation pressure (P_g) corresponding to the temperature of the mixture' (Batty & Folkman, 1983, pp. 114-115).

$$\Phi = \frac{P_v}{P_g}$$

Equation 2-1

The absolute humidity (ω) of an air-water vapour mixture is the mass of the vapour in the mixture (M_v) divided by the mass of the dry air in the mixture (M_g) (Batty & Folkman, 1983).

$$\omega = \frac{M_v}{M_g}$$

Equation 2-2

A useful relationship between relative humidity (Φ) and absolute humidity (ω) is:

$$\omega = 0.622\Phi \frac{P_g}{P_a}$$

Equation 2-3

where:

- P_a – partial pressure of the dry air in the mixture

'The evaporation process lowers the temperature of the wet surface. The faster the evaporation rate, the cooler the surface becomes. The rate at which evaporation takes place depends on a number of factors including the humidity of the surrounding air. If the air is saturated with water vapour (100% relative humidity), there will be essentially no net evaporation, and the wet surface temperature will be the same as the ambient air temperature. If the air were dry then the evaporation would proceed at a maximum rate' (Batty & Folkman, 1983, pp. 118-119).

2.4 Water activity

'The relative humidity obtained when a substance is sealed in a container and allowed to come to equilibrium is called the equilibrium relative humidity or water activity (a_w) of the substance' (Batty & Folkman, 1983, p. 119).

$$a_w = \Phi = \frac{P_v}{P_g}$$

Equation 2-4

'Lowering the water activity value will generally reduce the susceptibility of a food to microbial spoilage. Also, water activity indicates the relative ease at which water could be removed from a product during hydration. Thus a basic

understanding of the variables affecting water activity is important' (Batty & Folkman, 1983, p. 119).

The presence of more than one component in the liquid phase reduces the relative humidity at equilibrium. Raoult's law describes the behaviour of an ideal solution with a non-volatile solute as (Batty & Folkman, 1983, p. 119):

$$Y_w = X_w \frac{P_g}{P}$$

Equation 2-5

where:

- X_w – mole fraction of H_2O in the liquid phase
- Y_w – mole fraction of H_2O in the gas phase
- P_g – saturation pressure of H_2O at the temperature of the solution
- P – total pressure

The basic reasoning behind Raoult's law is that as the concentration of water goes down, there will be fewer water molecules on the surface of the liquid-vapour interface; consequently the rate at which water molecules will evaporate and enter the gas phase will be reduced. Since $Y_w = P_v/P$, Equation 2-5 can be rearranged to give:

$$X_w = \frac{P_v}{P_g} = a_w$$

Equation 2-6

Thus, for an ideal solution at equilibrium the water activity is equal to the water concentration in the liquid phase. Most foods do not behave as ideal solutions due to the many factors such as capillary effects, incomplete disassociation of ions, and chemically bounded water. Thus, Raoults's law gives an approximate, but still very useful, estimate of water activity (Batty & Folkman, 1983).

2.5 Basic principles on the dehydration of food

'Drying is a process wherein moisture is removed from the food product to enhance its storability, transportability, flavour, or texture. Consider the typical wet food product having its surface exposed to an air stream with a specified velocity, temperature, pressure, and relative humidity. If the weight of material is measured and plotted as a function of time, a curve of the measured moisture content similar to that shown in Figure 2-2 would be obtained. Between points 1 and 2, a nearly linear relationship between moisture content and time would exist. Between points 2 and 3 the curve will asymptotically approach an

equilibrium moisture content dependant on the temperature and the relative humidity of the air stream. The rate of moisture removal or drying rate can be found by determining the slope of the curve in Figure 2-2 at any point' (Batty & Folkman, 1983, p. 234).

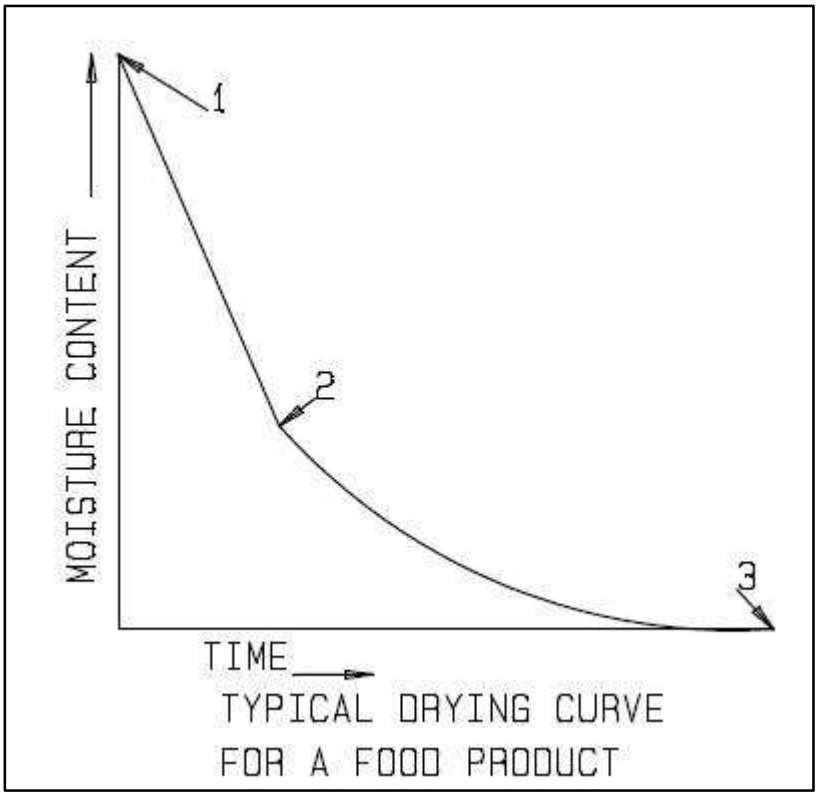

Figure 2-2 Drying curve of fruit

Source: Batty & Folkman, 1983

Figure 2-3 illustrates a typical drying rate curve. The portion of this curve from point 1 to point 2 is called the constant rate period. The curve from point 2 to point 3 is called the falling rate period. The moisture content at point 2 is called the critical moisture content (Batty & Folkman, 1983).

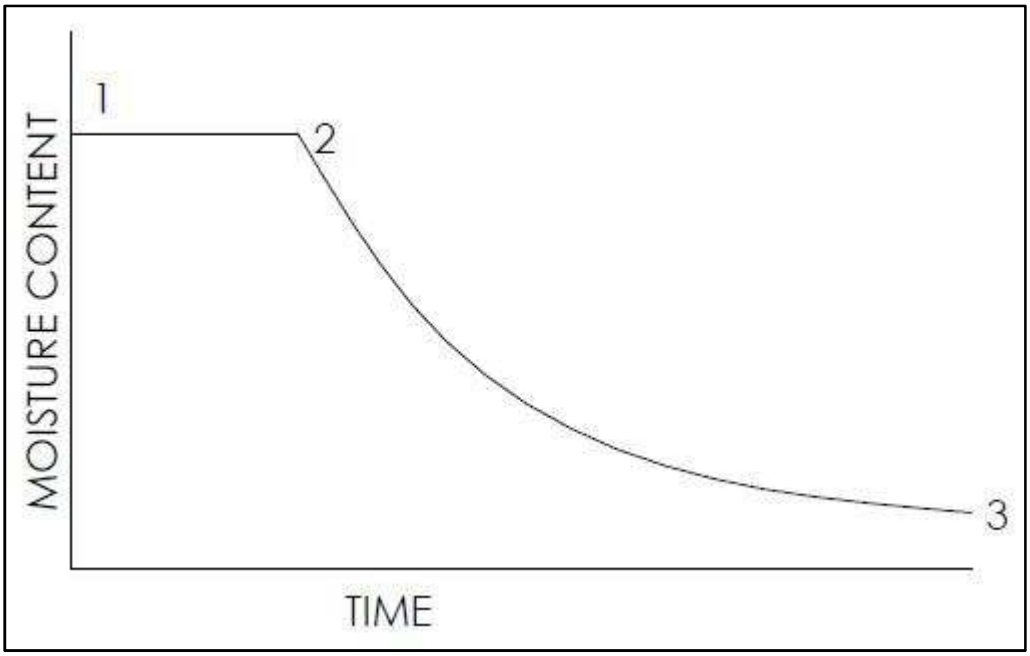

Figure 2-3 Illustration of drying rates for a typical food product

Source: Batty & Folkman, 1983

2.5.1 Constant-rate drying period

'During the constant-rate drying period, moisture is always present on the surface of the material being dried. The water within this material is able to diffuse to the surface at a rate faster than the rate at which it leaves the surface. The heat transfer to the material usually determines the drying rate in the constant-rate period' (Batty & Folkman, 1983, p. 234). For heat addition by forced convection from the air stream, the drying rate is given by:

$$M = \frac{hAT_{\infty} - T_s}{h_{fg}}$$

Equation 2-7

where:

- M – drying rate (kg/s)
- h – convective heat transfer coefficient (kW/m^2°C)
- A – area available for heat transfer (m^2)
- T_{∞} – air stream temperature (°C)
- T_s – surface temperature (°C)
- h_{fg} – latent heat of evaporation evaluated at T_s (kJ/kg)

'The surface temperature (T_s) can usually be approximated as the wet bulb temperature of the air stream. The air stream flowing over a wet bulb thermometer lowers the temperature of the thermometer. In a similar manner, the surface temperature of a wet material subjected to forced convection heat transfer will reach the wet bulb temperature given sufficient time' (Batty & Folkman, 1983, p. 235).

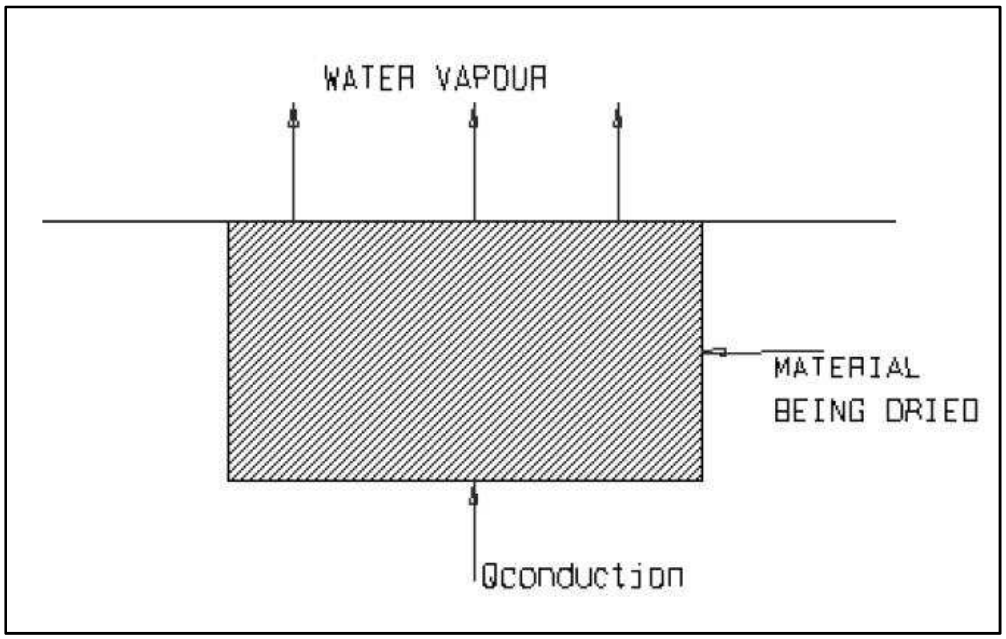

Figure 2-4 Illustration of the slab material being dried via conduction heat transfer

Source: Batty & Folkman, 1983

'Conduction is another mechanism for transferring heat to the material being dried. Figure 2-4 illustrates how this is accomplished. Heat transfer occurs on one side of the wet product while water vapour leaves on the other. If all the heat transfer occurs by conduction, the surface temperature of the material being dried will approximately equal the boiling point temperature. If both the conduction and convection heat transfer modes are present, the surface temperature will be somewhere between the wet bulb and boiling point temperature. Calculation of the drying rates during the constant-rate time period is often made with the following equation' (Batty & Folkman, 1983, p. 236).

$$M = k_m A(P_g - P_v)$$

Equation 2-8

where:

- k_m – mass transfer coefficient (kg/s.m^2.kPa)

- P_g – saturation pressure of water corresponding to the surface temperature (kPa)
- P_v – partial pressure of the water vapour in the air, kPa

The value of the mass transfer coefficient (k_m) is dependent on the dryer design. Equation 2-8 indicates that for a given dryer design, the drying rate is proportional to the surface area and the water vapour partial pressure difference. Another equation for estimating evaporation rates due to the conduction heat transfer is:

$$M = UA(T_{source} - T_s)/h_{fg}$$

Equation 2-9

where:

- U – overall heat transfer coefficient between the heat source and the surface (W/m^2.°C)
- T_{source} – surface temperature of the heat source (°C)

'It is important to note that the material properties do not affect the drying rate during the constant-rate time period' (Batty & Folkman, 1983, p. 237).

It should be noted that the constant rate period is formulated around the assumption that the free stream air temperature is constant. In a dryer due to air re-circulation and fresh air inserted at various rates and ambient temperature over the drying cycle, the drying does not occur at a constant rate. It is however a zone in which the surface temperature of the material remains constant at the adiabatic saturation temperature of the air. Since the air temperature varies and the surface temperature is constant, the rate of heat transfer and the rate of drying must vary in this zone (Charm, 1971).

2.5.2 Falling-rate time period

'The falling-rate time period begins when the water within the material being dried can go longer to diffuse to the surface at a rate fast enough to keep the entire surface saturated with moisture. It is at this point that the properties of the material being dried begin to influence the drying rate. As the moisture content decreases below the critical moisture content, the influence of the water mobility on the drying rate increases. Water mobility is determined primarily by diffusion and capillary flow. Relationships have been developed for predicting drying rates in the falling-rate time period' (Batty & Folkman, 1983, p. 237).

2.5.3 Tunnel dryers

Tunnel dryers use a hot circulating air stream to provide the energy required for drying and the product being dried does not move or moves at a low velocity compared to the circulating air velocity. In a tunnel dryer, trays are loaded onto carts and the carts can be loaded into the dryer tunnel on a quasi-continuous basis. The air stream in a tunnel dryer could be arranged to flow in the same direction (parallel flow), opposite direction (counter flow) or at right angles (cross flow) with respect to the direction in which the carts move through the tunnel. Parallel flow results in less severe drying conditions in that the material being dried does not attain the high temperatures in the falling rate section realised in counter-current flow. However, a longer tunnel would be required to obtain the same drying capacity (Charm, 1971).

One also gets counter-current and co-current centre flow. The dry heated air enters the tunnel at the finishing end. It passes in a counter-current direction over the driest part of the charge. About half way along the tunnel it is led off and reintroduced at the wet end to flow concurrently with the wet material. This procedure gives the greatest driving force for heat transfer where the material has the lowest moisture content (Charm, 1971).

The energy required for the operation of tray dryers can be estimated if the properties of all the mass flows leaving the dryer are known. Consider the dryer system illustrated in Figure 2-5 (Batty & Folkman, 1983).

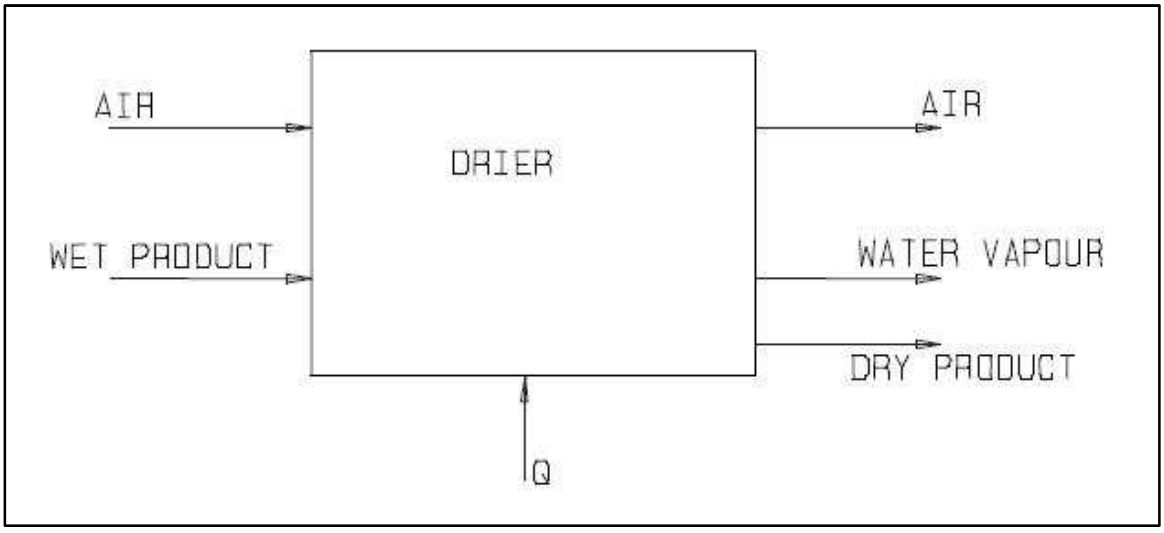

Figure 2-5 A control volume for a tunnel dryer

Source: Batty & Folkman, 1983

An energy balance for this system gives:

$$Q = M_{pe}C_{pe}(T_{pe} - T_{pi}) + M_a[C_a(T_{ae} - T_{ai}) + \omega_{ai}(h_{ve} - h_{vi})] + M_{evap}(h_{ve} - h_{li}) + Q_{loss}$$

Equation 2-10

where:

- Q – heat transfer needed (kW)
- M_{pe} – product mass flow rate leaving the system (kg/h)
- C_{pe} – product specific heat at product exit (kJ/kg·℃)
- T_{pe} – product temperature at the exit (℃)
- T_{pi} – product temperature at the entrance (℃)
- M_a – dry air mass flow rate entering the dryer (kg/h)
- C_a – constant pressure specific heat for the dry air (kJ/kg·℃)
- T_{ae} – temperature of the air at the exit (℃)
- T_{ai} – temperature of the air at the entrance (℃)
- ω_{ai} – absolute humidity of air entering the dryer
- h_{ve} – enthalpy of the water vapour at the air exit (kJ/kg)
- h_{vi} – enthalpy of the water vapour at the air entrance (kJ/kg)
- M_{evap} – evaporation rate within the dryer (kg/h)
- h_{li} – enthalpy of liquid H_2O (kJ/kg)
- Q_{loss} – heat loss through the walls and by air leaks (kW)

'For a given dryer production rate, the mass flow rates (M_{pe}) and (M_{evap}) in Equation 2-10 are fixed. However, the air mass flow rate (M_a) can vary, depending on the temperature and relative humidity within the dryer. The heat loss (Q_{loss}) accounts for the conduction through the walls and air leaks. These losses can be significant and should be included for an accurate analysis. Typically these heat losses amount to 20% of the total heat input but can vary significantly depending on such factors as how well the dryers are insulated and air leakage. An important consideration in the operation of tunnel dryer systems that re-circulate air is to determine the fraction of the air stream to be exhausted. Reducing the amount of air exhausted will generally reduce the energy costs, but it will also increase the humidity within the dryer. Increasing the humidity within the dryer will generously reduce the evaporation rate. Thus, there is a trade-off between production rate and energy costs. Predicting the influence of humidity on production rates is difficult and accurate data can often only be obtained by measurement' (Batty & Folkman, 1983, p. 241).

If the rate at which air is exhausted from the tunnel were reduced, the relative humidity of the air leaving the drying zone will increase. In most cases, this will result in a decrease in the drying rate and the energy cost per kilogram of product. But if the production rate is reduced, the dryer must operate more hours per day and/or additional dryers must be installed to obtain a set production rate.

It is easy to see that in selecting the optimum air exhaust rate one must consider not only energy cost, but also labour and equipment costs (Batty & Folkman, 1983).

2.5.4 Dryer thermal efficiency

'One measure of the dryer performance often used to compare energy consumption is the dryer's thermal efficiency computed by the following formula' (Batty & Folkman, 1983, p. 247):

$$\eta_t = \frac{M_{evap} h_{fg\_vapour}}{Q_{actual}}$$

Equation 2-11

Where:

- η_t – thermal efficiency
- Q_{actual} – measured dryer energy consumption rate (J/s)
- M_{evap} – evaporation rate (kg/s)
- h_{fg_vapour} – latent heat of vaporisation (J/kg)

A dryer with a thermal efficiency of 100% ($\eta_t = 1$) would be impossible to obtain with conventional designs. Implementing Equation 2-10 a thermal efficiency of 100% would only occur if the product and air exit temperatures are equal to the product and air entrance temperatures (Batty & Folkman, 1983). If $\eta_t = 1$, then:

$$Q_{actual} = M_{evap} h_{fg\_vapour}$$

Equation 2-12

From Equation 2-10 we see that this could occur only if the product and the air exit temperatures are equal to the product and air temperatures. This would be very difficult to achieve in actual practice. Thus the thermal efficiency of a dryer gives a good measure of the relative dryer performance compared with an ideal process. Tunnel dryers have typical thermal efficiencies of 0.7 or less (Batty & Folkman, 1983).

2.6 Diffusion of moisture content in food

'When the moisture content of substrate is reduced below 10%, the microorganisms are not active. This forms the basis for the preservation of food through dehydration. It is necessary however to reduce the moisture content below 5% in order to preserve nutrition and flavour. In addition to preserving the food from a microbiological standpoint, it is also necessary to preserve its flavour and nutritional characteristics. The delicate characteristics of food require the skilful operation and design of the dehydration system' (Charm, 1971, p. 294).

2.6.1 Evaporation of water below its boiling point

'Heat is transferred from the air to the water and water is evaporated from the surface. At equilibrium, the rate of heat transfer is equal to the rate of mass transfer times the latent heat of the vaporization of the water. The driving force for the vaporising water from the surface is the difference between the vapour pressure of water at the temperature of the surface (T_s) and the partial pressure of the water in the air (P_v). When all the heat is transferred to the surface from the air, the surface temperature (T_s) is equal to the wet bulb temperature of the air. The wet bulb temperature is the temperature assumed by a thermometer whose bulb is surrounded by a wick moistened with water' (Charm, 1971, p. 295).

'If drying occurs at too high a temperature, the surface forms a layer of closely packed shrunken cells, which are sealed together. This presents a barrier to moisture migration and tends to keep the moisture sealed within. This condition is known as "case hardening" (Charm, 1971, p. 302).

2.6.2 The removal of moisture in the falling rate period

If the rate of the heat transfer to the object is sufficiently high, vaporization takes place within the material. The rate of drying is determined by the rate of heat transfer into the object. There are several mechanisms by which water migrates from the interior. Charm (1971) summarizes these as follows:

- Liquid movement caused by capillary forces. The liquid conductivity is dependent on the capillary distribution and its value varies greatly with the moisture content.
- Diffusion of liquids caused by the differences in concentration.
- Surface diffusion in liquid layers absorbed at the boundary of solid substances.

- Water vapour diffusion in air-filled pores caused by differential partial pressures. Vapour flow causes differences in the pressure in dehydration processes where the heat transfer occurs in a special way or when dehydration is effected in a vacuum at the boiling point of the moisture present. When pore diameters exceed the mean free path of the vapour molecules, the vapour flow is thought to obey Poiseuille's equation.

It should be realised that it is possible for several of these mechanisms to be occurring at the same time. In many food materials the migration of moisture in the falling rate period occurs through the mechanism of diffusion. In practise the diffusion constant is dependent on some extent on moisture content (Charm, 1971).

'Water activity rather than moisture content influences biological reactions. The interrelationship between water activity and moisture content is expressed by the sorption isotherm. In the region of water absorption on polar sites or when a monomolecular layer exits, there is little enzyme activity. Enzyme activity begins only above the region of monomolecular adsorption. In this region, some of the water exists in the liquid state. Under these conditions, dissolution and diffusion of glucose is possible, water does not function so much as a reactant, but rather serves as a medium for the enzymatic process' (Acker cited in Charm, 1971).

2.7 Results of non-uniform velocity distribution

'One of the major problems in tunnel dryer design and operation is obtaining a uniform velocity distribution throughout the drying sections. When the velocity distribution varies, the heat transfer coefficient and drying rate will also vary. This results in a non-uniform product. Very often the material at the edges of a tray dries out at different rates than other parts of the tray. This is due to the variation in airflow pattern at the edges of the tray (edge effect). Guide ducts in the path of the air are often employed for producing uniform velocity distributions' (Charm, 1971, p. 322).

2.8 Improving drying uniformity in concurrent flow tunnel dehydrators

Experiments conducted by Adams and Thompson, (1985), confirmed that the moisture content variation in fruit dried in concurrent flow tunnel dehydrators is dependent on the uniformity of the airflow entering the wet end of the tunnel. Improvements in dehydrator performance was obtained by using a flow diverter and turning vanes to produce a more uniform flow distribution, thereby reducing the moisture content variation. The experiment that Adams and Thompson, (1985) conducted in prune tunnel dehydrators indicated that the modification could reduce the range in final fruit moisture content by approximately 40%.

According to Adams and Thompson (1985), Christie and Nichols (1929) were one of the first to recognise that drying time was controlled by factors such as air temperature, air humidity, fruit variety, pre-treatment of the fruit and the air speed over the fruit. Adams and Thompson (1985) stated that many dryer operators regularly observed wide variations in fruit moisture content within individual cars. In order to ensure that the wettest fruit has reached low enough moisture content, much of the fruit is over dried. In some operations, wet fruit in the load is recollected and re-dried using a tunnel dedicated for this task. Both of these practices may result in longer drying time and increased energy use compared to the operation of a tunnel, which produces uniform moisture content.

Adams and Thompson (1985) used in their experiments the tunnel dryer design of Rodda and Gentry (1969), which was used in drying prunes. The modifications they used to improve the uniform velocity distribution over the product were turning vanes, a flow diverter and screens in front of the first trolley and a suction slot located just above the front cars (see Figure 2-6). Adams and Thompson (1985) found that the turning vanes helped to eliminate part of the flow asymmetry, which is produced by fan swirl. This effect is best removed using a flow-straightening device attached to the fan. The best results were obtained with the turning vane configuration and the worst with the suction slot. The suction pressure was obtained using a duct connected to the upstream side of the fan and was insufficient to control the flow. Though the screen performance was comparable to that of the vanes, the additional pressure loss and need to move the screens during the tunnel filling made it a less desirable modification. There was less moisture variation in the prunes after the drying process, using the turning vanes.

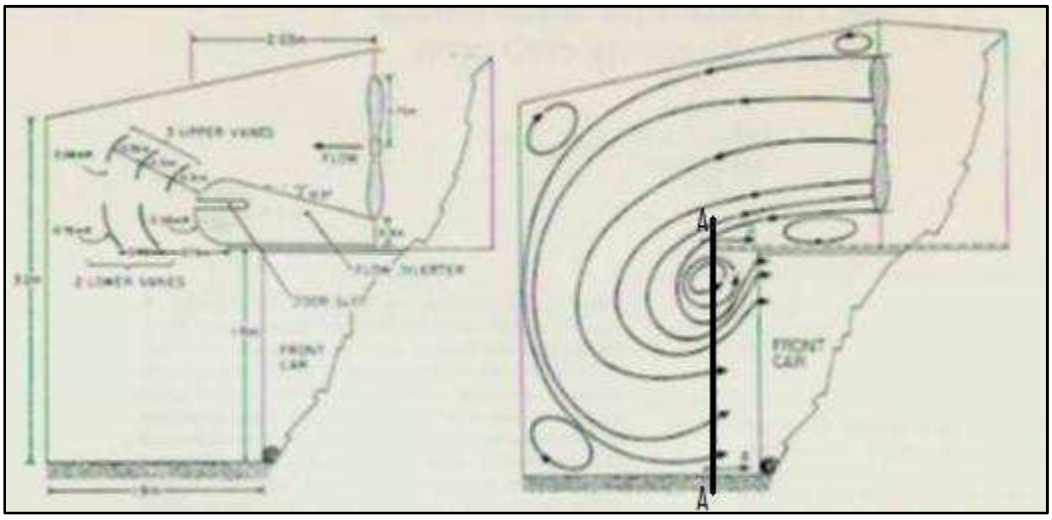

Figure 2-6 Turning vane and flow diverter on the left. Estimated flow field at centre line AA in front of first car on the right

Source: Adams and Thompson (1985)

Adams and Thompson (1985) showed in Figure 2-6 and Figure 2-7 that the position of the low air speed coincided with the location of the centres of the vortices and where the operators observed the wettest food product. The turning vanes of the fan inside the tunnel dryer cause the swirl action in Figure 2-7.

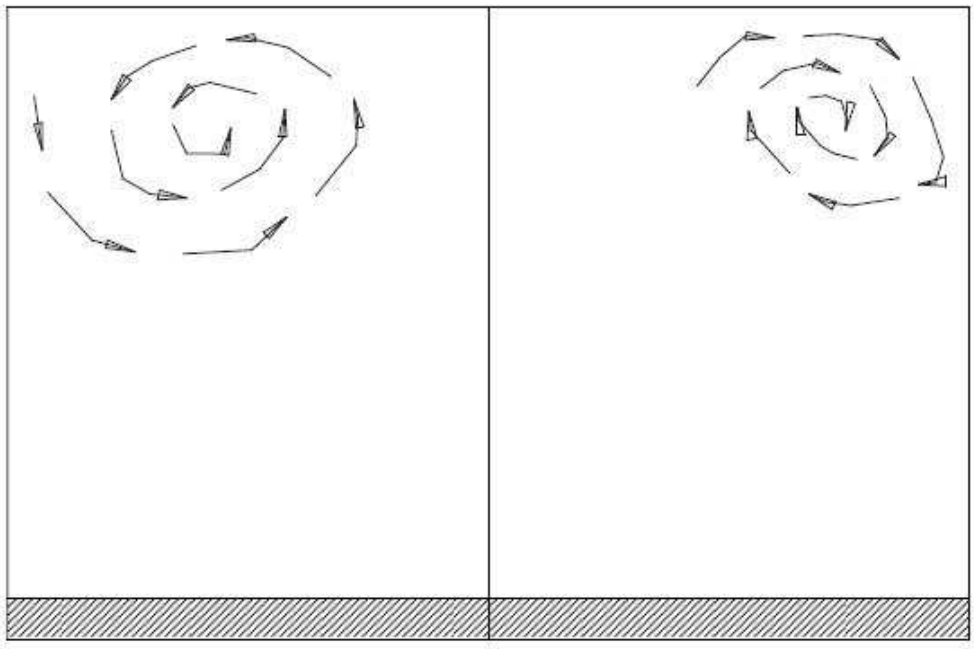

Figure 2-7 Plane view of the cross flow at centre line AA

Source: Adams and Thompson, 1985

Adams and Thompson (1985) also noted that the airflow distribution at the dry end of the dehydrator was more uniform as a result of adjustments taking place within the tunnel. The flow field has its strongest influence during the convective phase of drying at the wet end. The air speed ranges of the modified tunnels were much smaller than that of the conventional tunnels. The effect of the counter-rotating vortices was also weakened by the modification. The results of the dried fruit moisture testing conducted by Adams and Thompson (1985) showed that with the modifications in place the range of the moisture content of the prunes was reduced. The data also implicated that there were no significant difference in the average fruit moisture content for the different configurations. The differences in average speed were within the range of the variations among the tunnels without the modifications. The dryer operator found that the tunnels with the airflow modifications eliminated the need to re-dry the fruit, resulting in increased drying capacity and possibly a small reduction in energy use (Adams and Thompson, 1985).

2.9 Shrinkage of food produce caused by dehydration

The drying calculations thus far represented have assumed the material being dried maintains a constant shape and no shrinkage occurs. In practise this is often not the case. Charm (1971) has suggested that the drying rate may not be constant in certain materials, because the surface area is changing as moisture is removed.

2.10 Laboratory simulation of a commercial dehydration tunnel

The paper of Reddek (1973) deals with the relationship between the many parameters, which effect the drying of a material in a dehydrator. The dehydration of a material can be studied on macroscopic and on a microscopic scale. On the microscopic scale the dehydration of an organic material is extremely complicated and is effected by so many parameters that it is nearly impossible to predict, from calculation, the behaviour of dehydrators with any degree of accuracy.

The psychrometric cycle of air in a counter-flow dehydration tunnel can be divided in three stages, namely the dehydration stage, the mixing stage, and the heating stage. Figure 2-8 shows schematically the airflow in a commercial counter flow tunnel. The psychrometric cycle is shown schematically in Figure 2-9. The dry bulb temperature of the air on the side where the fruit enters (fruit inlet side) is referred to as T_i. The dry bulb temperature of the air on the side where the fruit leaves the tunnel (fruit outlet side) is referred to as T_o. T_a and T_m refer to the dry bulb temperature of the outside air and the mixture of outside and re-circulated air respectively (Reddek, 1973).

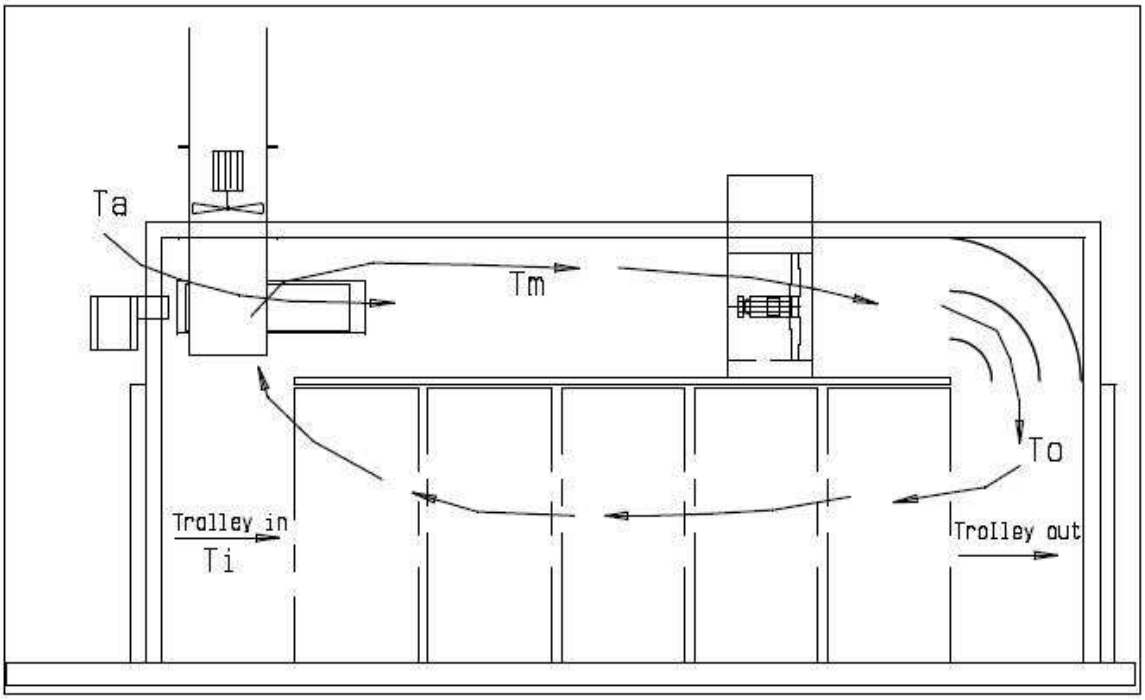

Figure 2-8 Schematic representation of a counter flow dehydration tunnel showing the nomenclature used for the dry bulb air temperature at the various points in the tunnel

Source: Reddek, 1973

'During the dehydration stage, when the air flows over the fruit the wet bulb air temperature remains constant. During this stage the air loses sensible heat energy to the product and gains latent heat energy, in the form of moisture, in return. The rate at which sensible heat is lost by the air in the dehydration section of the tunnel is calculated as follows' (Reddek, 1973, p. 23):

$$H_d = \rho Q C_a (T_o - T_i)$$

Equation 2-13

where:

- H_d – Rate at which sensible heat is lost by in the dehydration section (J/s)
- ρ – Density of air (kg/m^3)
- Q – the volume flow rate of air (m^3/s)
- C_a – Specific heat of air (J/kg-K)

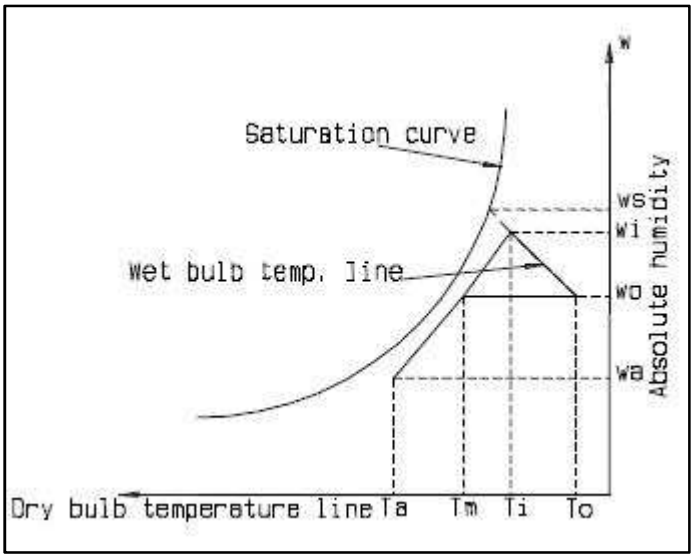

Figure 2-9 Psychometric cycle of air in a counter-flow dehydration tunnel. The symbols used correspond with those in Figure 2-8

Source: Reddek, 1973

During the mixing stage a large percentage of the circulating air at dry bulb temperature (T_i), is re-circulated and mixed with a small percentage of fresh outside air at dry bulb temperature (T_a). The resultant dry bulb temperature of the mixture (T_m) can be calculated as follows:

$$T_m = T_a + R(T_i - T_a)$$

Equation 2-14

where:

- R – percentage of re-circulated air

During the heating stage, when the air passes through the heat exchanger, the dry bulb temperature of the circulating air is increased from (T_m) to(T_o). On the psychometric chart (See Figure 2-9) this process is shown as the horizontal line because the moisture content of the air does not change during this stage. The rate at which heat energy has to be supplied to heat the air during this stage is calculated as follows (Reddek, 1973):

$$H_h = QC_p(T_o - T_m)$$

Equation 2-15

where:

- H_h – Rate at which heat has to be supplied to heat the air during the heating stage (J/s)

Figure 2-9 clearly shows that the amount of heat used to dehydrate the material in the tunnel (Equation 2-13) is less than that delivered by the heaters (Equation 2-15). The balance is lost to the atmosphere in the air that is exhausted by the outlet fan. The loss is reduced by increasing the length of the drying section of the dehydrator (L) and by re-circulating more air. The ratio of H_d to H_h is known as the cycle efficiency (E_c) (Reddek, 1973).

$$E_c = H_h / H_d$$

Equation 2-16

The most useful mathematical relationship between most of the parameters that affect the rate at which material dries in dehydrators is obtained by using the conservation of the energy law. The rate at which sensible heat is lost from the air (H_d) as it flows over the material in a dehydrator must equal the rate at which latent heat is absorbed to evaporate the water in the product in the dehydrator (H_i). Equation 2-13 expresses the sensible heat (H_d) in terms of the dry bulb temperature on the two ends of the drying section of the dehydrator. H_i can be expressed in terms of the rate at which water is evaporated in the dehydrator (W) as follows (Reddek, 1973):

$$H_i = h_{fg} W$$

Equation 2-17

$$W = \frac{mbLnh(M_i - M_o)}{\theta(M_i + 1)}$$

Equation 2-18

where:

- W – the rate at which water is evaporated in the dehydrator (kg/s)
- m – loading of the material on the trays (kg/m^2)
- L – the length of the drying zone in the dehydrator (m)
- h – the height of the drying zone in the dehydrator (m)
- b – breadth of the drying zone in the dehydrator (m)
- n – the number of the trays per unit height in the dehydrator (n/m)

- θ – the time that it takes for the product to dry (s)
- M_i – the dry base moisture content $(B.D.B)$ of the material being dehydrated on the product inlet side
- M_o – the dry base moisture content $(B.D.B)$ of the material being dehydrated on the product outlet side (See Equation 2-19)

$$B.D.B = \frac{Wet\ weight - Bone\ dry\ weight}{Bone\ dry\ weight}$$

Equation 2-19

The air speed in a dehydrator (V) is defined as follows:

$$V = \frac{Q}{hb}$$

Equation 2-20

Combining Equation 2-13, Equation 2-17 , Equation 2-18 and Equation 2-20 the following is obtained:

$$T_o - T_i = \pm \frac{h_{fg} m Ln(M_i - M_o)}{C_p \theta \rho V (M_i + 1)}$$

Equation 2-21

This equation, together with the Equation 2-14 gives the relationship between all the dry bulb temperatures shown on Figure 2-9. Equation 2-21 holds true only for tunnel dehydrators and when parallel flow tunnels are being considered the negative sign is applicable (Reddek, 1973).

To determine the capacity and efficiency of the dehydrator with any degree of accuracy it is necessary to know how long the product will take to dry (θ). The drying time will depend on many factors including V, n, m, T_o and T_i and a host of other factors, e.g. the way the product is cut for dehydration, the type of pre-treatment it is given and the type of tray it is loaded to. This information is usually determined by dehydrating a large number of samples of the material in question under various drying conditions in laboratory dehydrators (Reddek, 1973).

3 Tunnel dryer design on which experiments were conducted

The design is based on the California tunnel principle, utilising trays on trolleys, and has been adapted for Southern African fruit and climatic conditions. The California type trolley-and-tray drying tunnel is ideal for South African conditions and provides a relative simple, low capital intensive and versatile dryer suitable for a wide range of products. Figure 3-1 shows a schematic representation of the tunnel dryer adapted for South African conditions (de Beer and Muller, 2003).

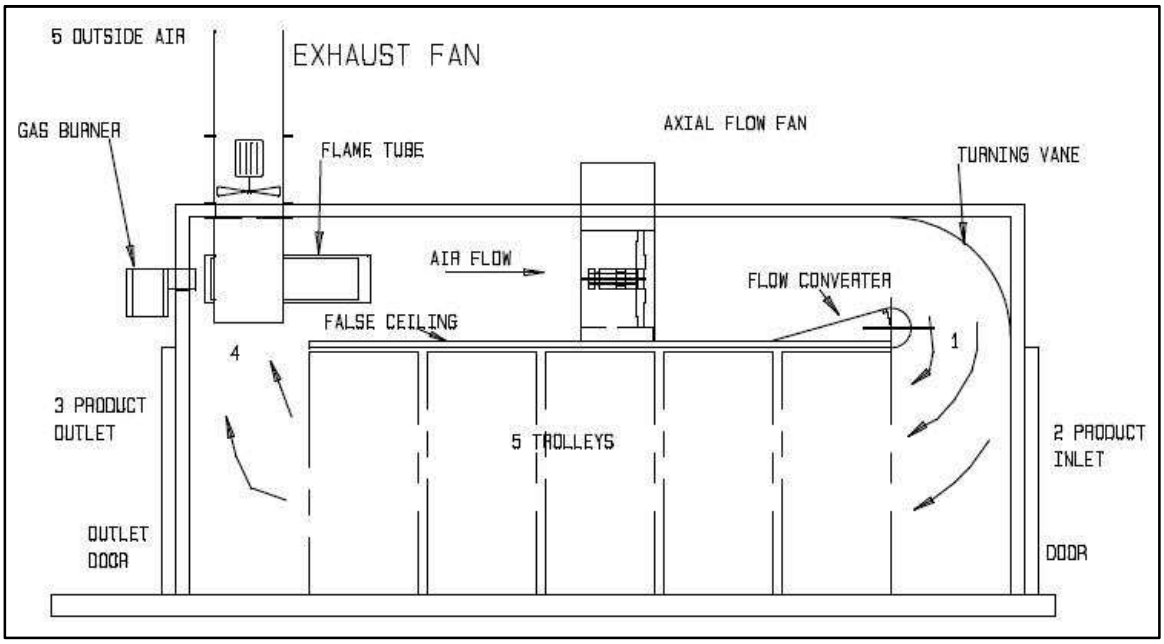

Figure 3-1 Schematic representation of tunnel dryer (parallel flow)

Source: de Beer and Muller, 2003

No other type of dryer for piece-form materials so successfully exposes a very large area of product to controlled drying conditions within a single moderately sized piece of equipment. Dehydration provides a means of adding value to fruit with skin blemishes and to obtain a product**,** which is far less perishable. In dehydrated products tastes and flavours are concentrated. Typically 15 kg of mango fruit is needed to produce 1 kg of end product (De Beer and Muller, 2003).

According to De Beer and Muller (2003) a drying curve can be determined for Mango slices by Hansman (1995) from the variables presented in Figure 3-2. The curve was determined for different inlet conditions at the drying zone (54℃/20% RH and 67℃/30% RH). This was done on a c ounter-flow drying tunnel (de Beer and Muller, 2003).

'An important consideration in the operation of tunnel dryer systems is to determine the fraction of the air stream to be exhausted. Reducing this amount will generally reduce energy costs, but it will also increase the humidity within the dryer. Increasing the humidity within the dryer will generally reduce the evaporation rate plus it will prevent the formation of "case hardening" or sealing at the surface of the product, which retards further moisture diffusion' (De Beer and Muller, 2003, p. 1). The equations mentioned in Chapter 2 were implemented in Appendix 10.3. to obtain the fraction of air exhausted and energy required for the dryer configurations mentioned below in paragraph 3.2. It was calculated that 35.7% of the air circulated through the dryer must exit the dryer at the outflow fan to maintain a relative humidity of 0.2 of air entering the drying zone. In order to evaporate 43.7 kg/s of water, 69 kW (with 20% heat losses included) of heating energy was required.

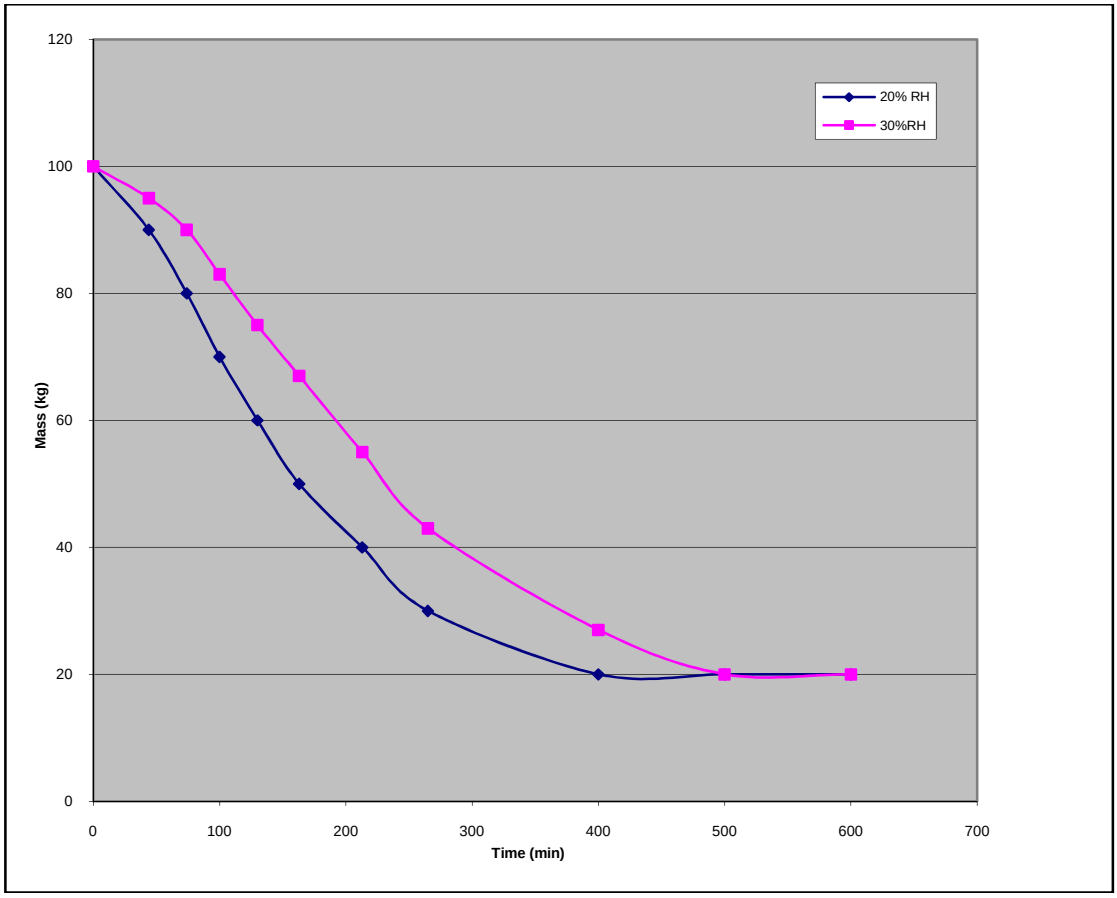

Figure 3-2 Drying rate of mango slices in simulated counter flow dehydration

Source: De Beer and Muller, 2003

Thus there is a trade-off between production rate, energy costs and drying defects. Energy to evaporate the water is obtained in South Africa from gas, electricity or coal.

'Both internal and external air properties need to be monitored and taken into account in selecting the process control set points. If this is not done, un-attainable balance points may be asked of the control instrumentation' (de Beer and Muller, 2003, p. 3).

Analysing the drying curve of Figure 3-2 it can be seen that constant rate drying occurs down to about 66% Wet Weight Basis ($W.W.B$) moisture content. The drying rate during the constant rate period is in the order of five times the average drying rate over the falling rate period (de Beer and Muller, 2003).

$$W.W.B = \frac{Wet\ weight - Bone\ dry\ weight}{Wet\ weight} \times 100$$

Equation 3-1

The work by Hansman (1995) indicates that before the constant period sets in, an increase in the drying rate actually occurs. This is explained as follows:

- Immediately upon loading a wet trolley, the hot air stream will at first condense water vapour onto the product (negative drying). As the product and the surface moisture increases in temperature, the drying becomes positive and proceeds at an increasing rate until a balance point is established.

- The wetted surface temperature will be driven towards the dry bulb temperature of the drying air. The air properties change according to the straight-line law.

- The rates of heat and mass transfer are uniquely related, so that the path for the drying air is a straight line, driving towards the temperature of the wetted surface (Lewis number of unity). The driving forces for water removal are thus established at a tremendous rate. The Lewis number (Le) is the ratio of mass diffusion, D, compared to thermal diffusion , α (White, 1991):

$$Le = \frac{\rho C_p D}{\alpha} = \frac{D}{\alpha}$$

$$\alpha = k/\rho C_p$$

Equation 3-2

where:

- D – has the same dimensions as kinematic viscosity or the thermal diffusivity , α (m^2/s)

- C_p – Specific heat at constant pressure (kJ/kg K)
- k – thermal conductivity (W/m K)
- ρ – density (kg/m^3)

'To provide for such wide variations in drying rate in a single tunnel is problematic. Equipping for an average drying rate for the process will result in too small heating and too large fan capacity during the first three to five hours in a 24-hour cycle. During the remaining 10 to 15 hours of the cycle, the heating capacity will be too high for good temperature control' (de Beer and Muller, 2003, p. 3).

'The optimum solution would be to complete the drying in two phases in two different sets of dryers namely one high-capacity constant-rate tunnel in combination with two low-capacity falling-rate tunnels' (de Beer and Muller, 2003, p. 3):

- Constant rate parallel flow at 65℃, 30% RH
- Falling rate counter flow at 45℃, 20% RH

The same conditions are recommended for cross flow tunnel configuration.

3.1 Prediction of airflow using different vane and flow configurations

A CFD program, Fluent 6.1, was used to construct a simple two-dimensional model of the airflow over different turning vanes and flow diverters. This was done in order to predict the best combination of a flow diverter and a turning vane. The design principles were based on the findings of Adams and Thompson (1985).

The two-dimensional (2D) model does not take in account the swirl action of the air leaving the fan. All the factors that were mentioned in paragraph 2.2 were taken in account when the model was constructed to give the most realistic representation of the real dryer. One has to remember that these 2D models are a fast and easy way to predict the airflow distribution, before doing a complete and detailed three-dimensional (3D) CFD simulation on the dryer.

Three designs were considered:

- The drying tunnel with only a false ceiling dividing the drying zone from the downstream area of the fan.
- A three turning vane construction.
- A flow diverter and one turning vane.

The inlet value of 8 m/s and the outlet pressure boundary value of 0 Pa relative to atmospheric pressure was only an estimate due to the fact that the design of the dryers was not yet finalised at the time of this simulation. These values were based on the previous designs of Roelf de Beer (de Beer and Muller, 2003).

Figure 3-3 shows the downstream zone of the fan with only a false ceiling. The range of the velocity-contours along the X-axis changes rapidly in the middle of the drying section from –3.6 m/s to –6.87 m/s.

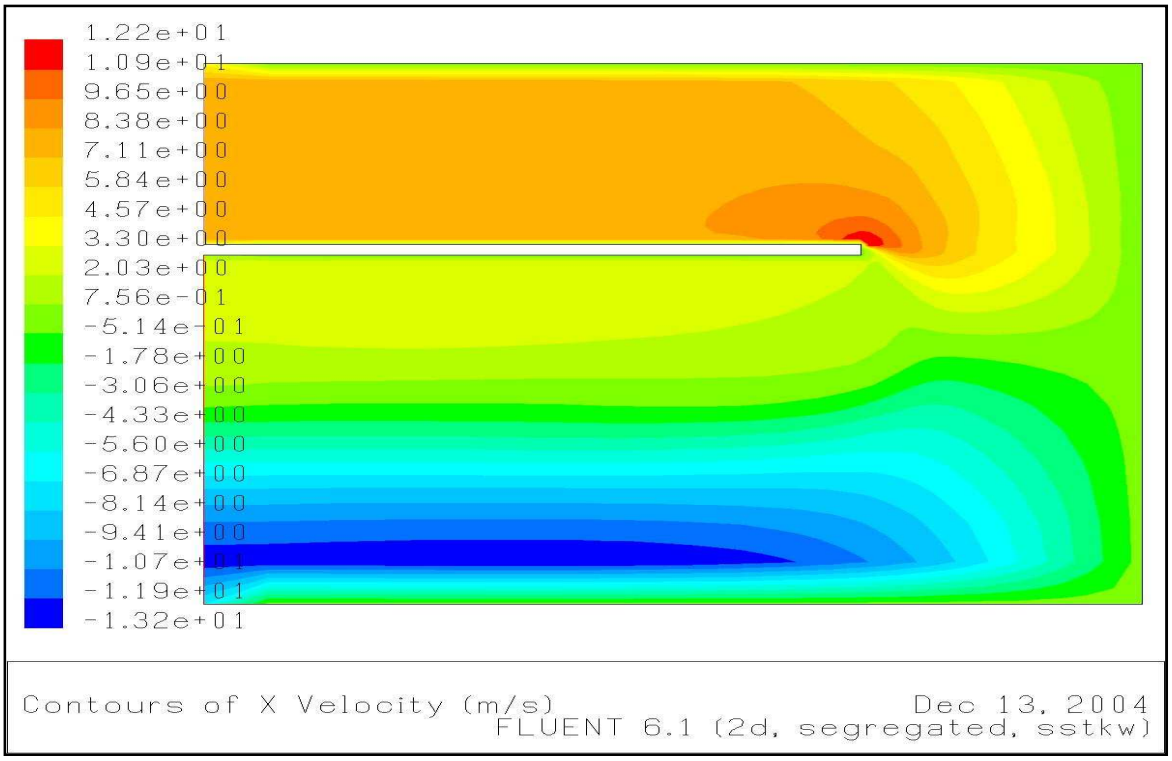

Figure 3-3 2D Fluent model of dryer without flow diverter and turning vane

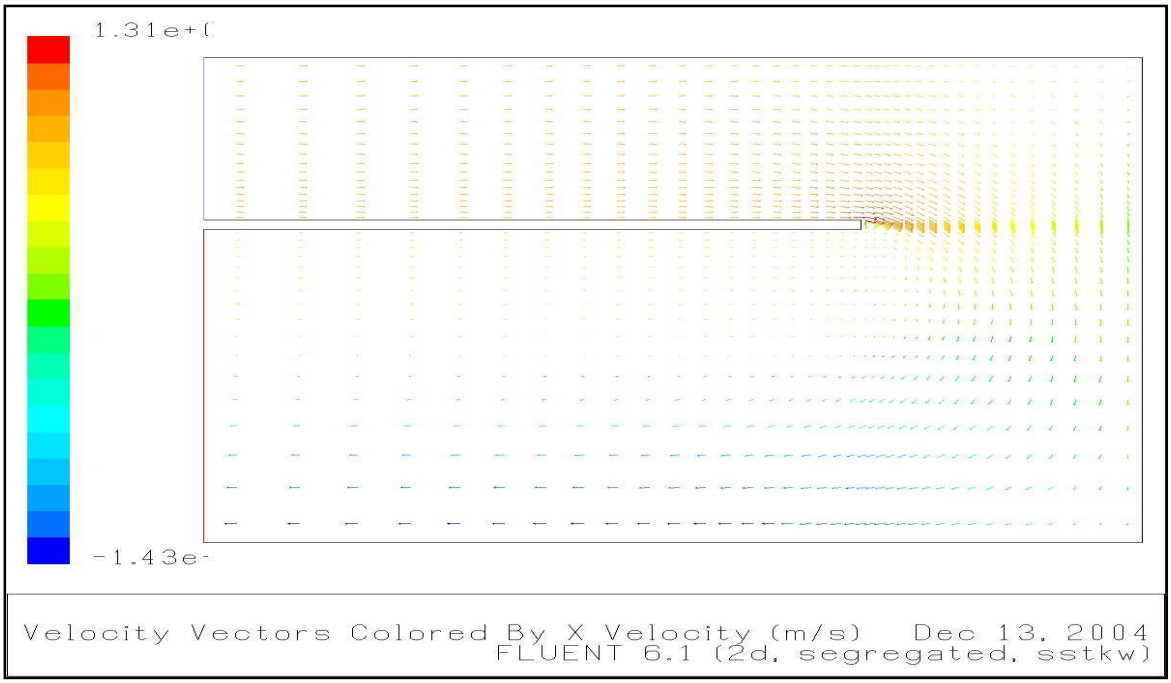

Figure 3-4 2D Fluent model of dryer without flow diverter and turning vane

One can clearly see that a vortex is formed at the tip of the false ceiling where the first trolley would be situated. In the middle of a vortex the direction of the velocity changes and goes to zero. This is normally where one would find the wettest food product. It is clear from these figures that a flow and turning vane design should be considered.

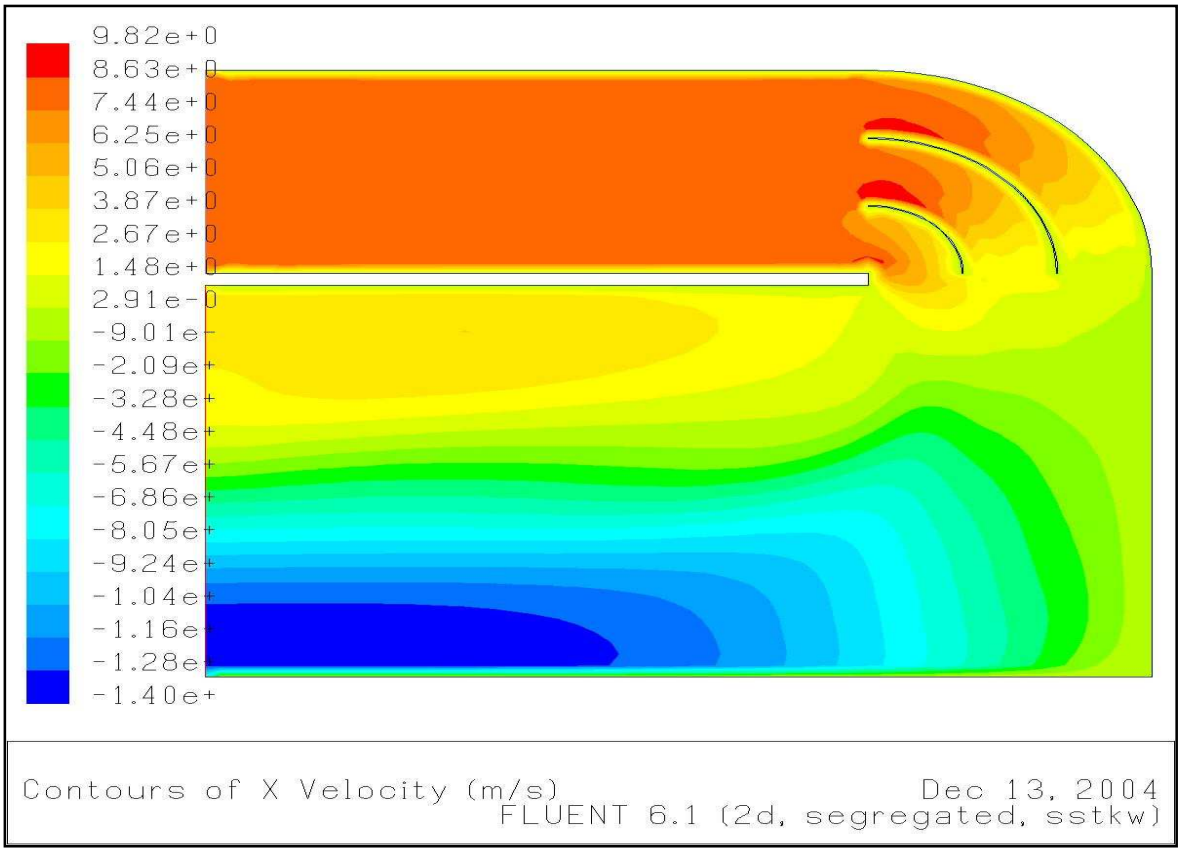

Figure 3-5 2D Fluent model of dryer with turning vane

Figure 3-5 is a representation of the three-vane turning construction. The X-velocity range still changes abruptly in the middle of the drying zone where the first trolley will be situated. These trends continue forwards in the positive X-direction. This non-uniform velocity distribution will affect all the trays on the trolleys and still further design changes are required. The construction of three vanes will not increase the uniform velocity distribution dramatically. It is also difficult to construct this set-up in commercial or industrial settings.

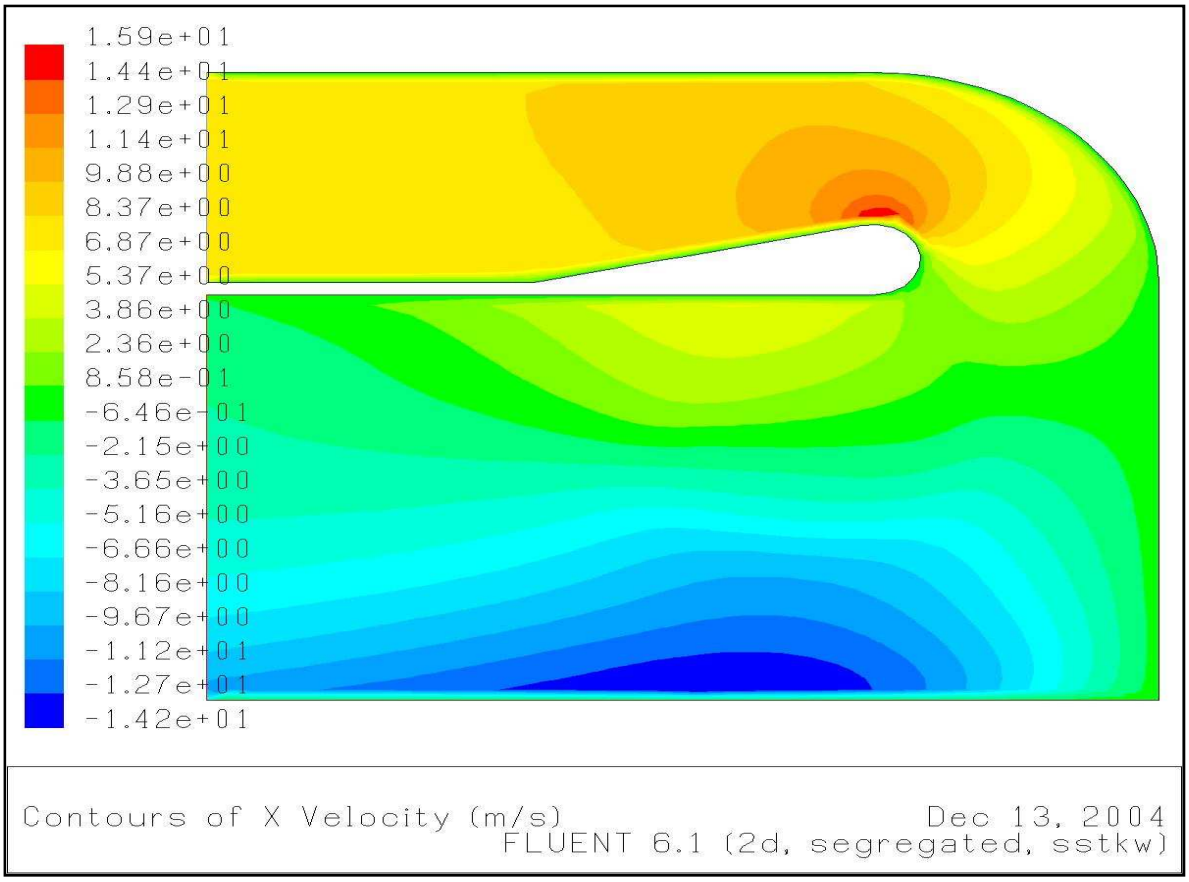

Figure 3-6 2D Fluent model of dryer with turning vane and flow diverter

In Figure 3-6 the velocity distribution in the X-direction is more uniformly distributed across the Z-Y section in front of the first trolley in the drying zone. The range of the velocity distribution is not that great as the previous design considerations.

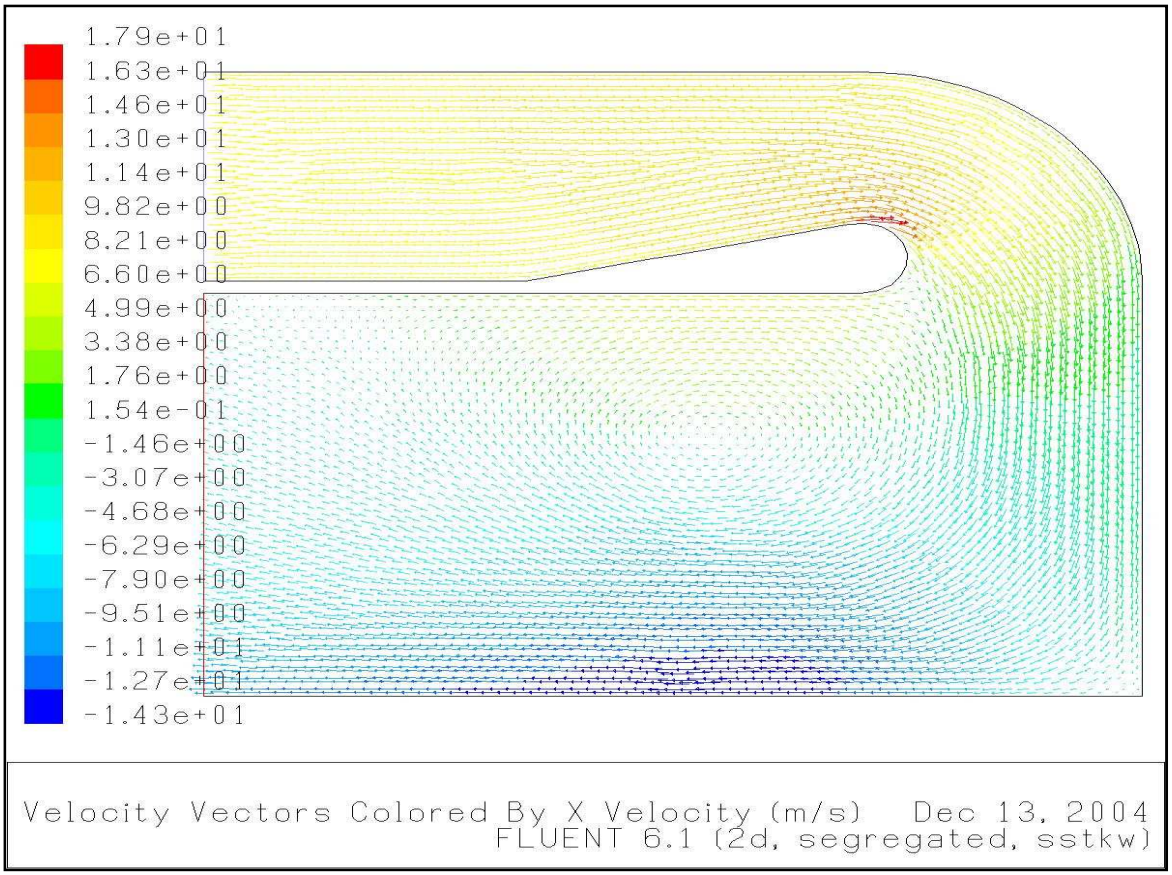

Figure 3-7 Turning vane and flow diverter of 2D Fluent model showing velocity vectors

The vortex system is reduced by a small margin and moved more towards the right with this set-up, as shown in Figure 3-7. The flow diverter also helps to move the air volume better around the false ceiling into the drying zone. The less the change in the vector direction of the velocity in the X-direction, the less the range of the velocity distribution will be across the drying zone.

3.2 Methodology

The experiments were conducted on tunnel dryers in the Musina industrial area. These tunnels are used for drying mangoes for the company M-Pak Musina. The tunnels can be used in a counter current or parallel airflow set-up. The walls of the dryer are insulated to minimize the heat loss to the environment. The tunnels are divided into high and low capacity dryers depending on which dryers contain two or one axial fans and the sizes of the electric motors driving the fans. A single dryer unit inside dimensions are 5.990 m in length, 1.565 m in width and 2.6 m in height. The actual drying zone (The volume inside the dryer which is occupied by the trolleys) is 4.250 m in length, 1.565 m in width and 1.680 m in

height. The openings at the doors have the same dimensions in height and width as the drying zone. The distance between the roof and the false ceiling is 870 mm.

The design of the tunnels was done in such a way that all the dryers could be upgraded to high or low capacity dryers. Roelf de Beer designed the dryers so that 5 trolleys, each containing 50 trays (250 kg-wet products per trolley could be dried in a 24 hour drying cycle (De Beer and Muller, 2003).

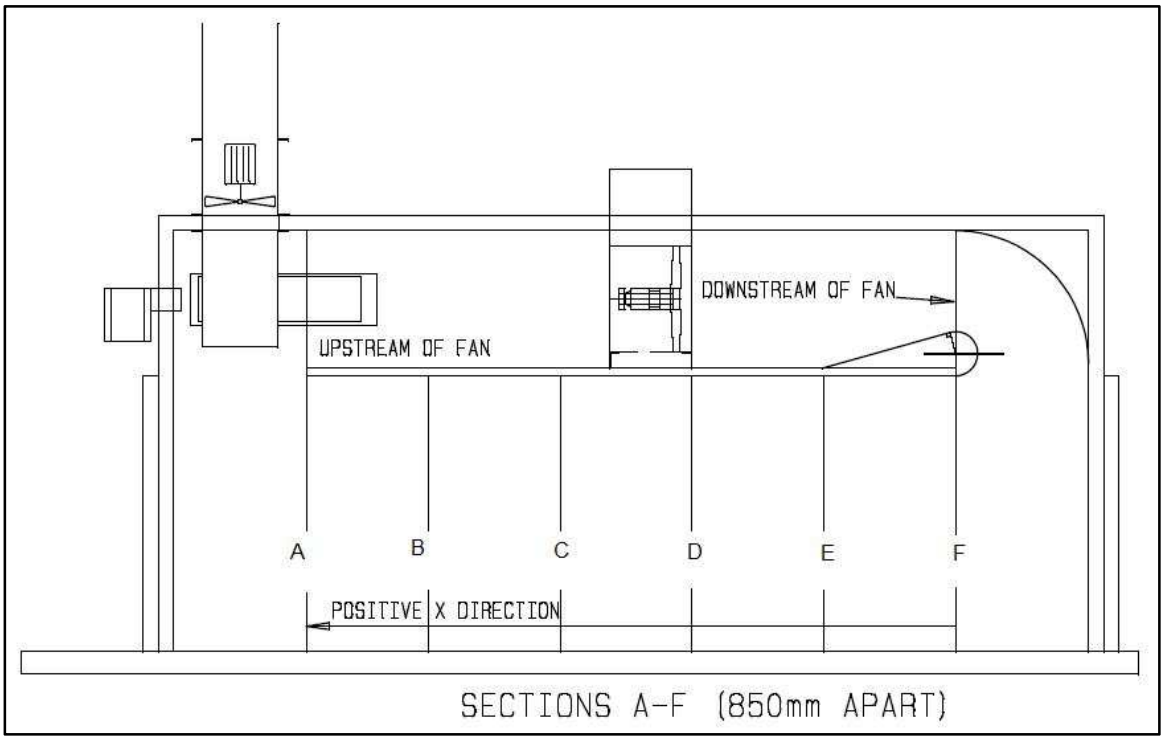

Figure 3-8 Schematic presentation of dryer showing the sections across the X-axis

There were six cross sections in the drying zone where the mean velocity magnitude (speed) was measured. Figure 3-8 shows the placing of the sections. The position of the section was done in such a way that it coincides with the front of each trolley. Two measuring sections up-and-downstream of the main fan were situated above the false ceiling. Figure 3-9 shows the cross section of the measuring points along the tunnel dryer.

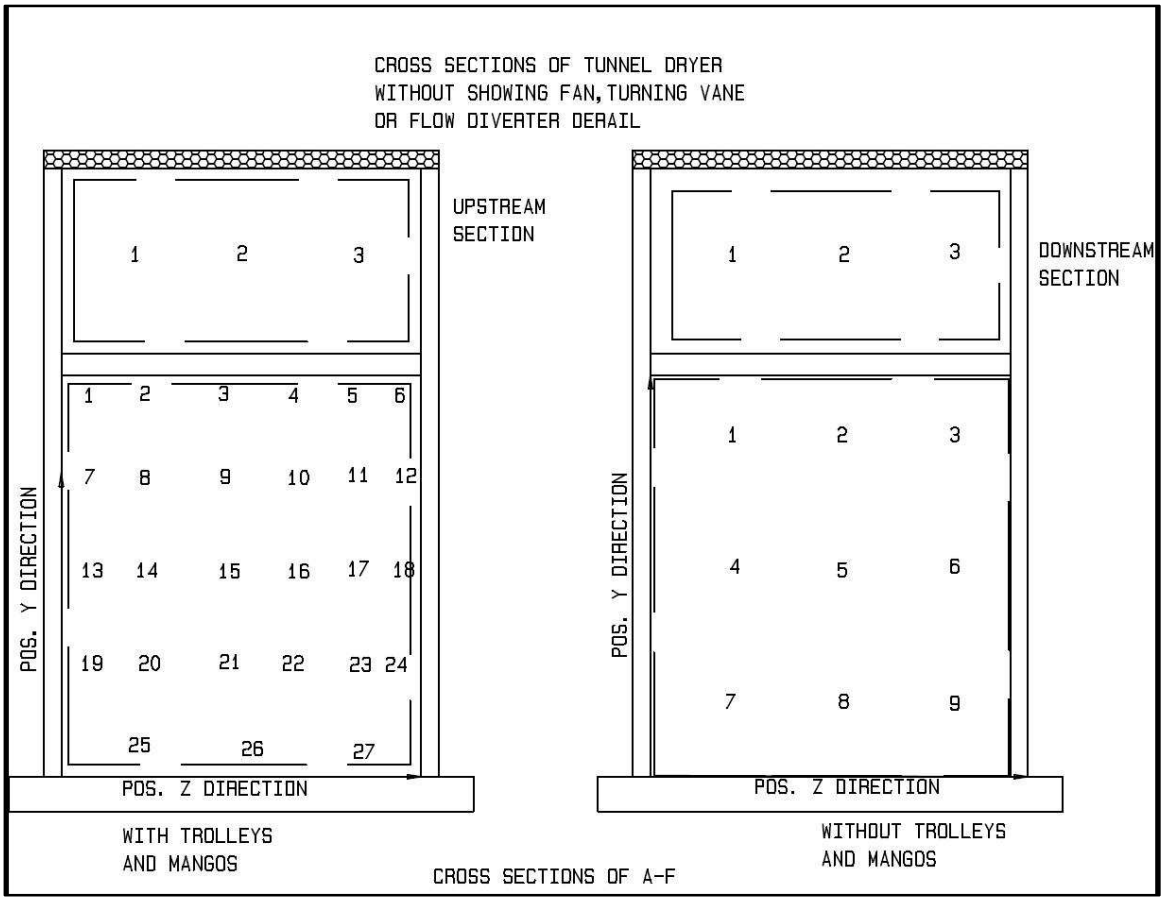

Figure 3-9 Measuring points

Three experimental set-ups were done:

- Measuring speed over sections with no trolleys or mangoes with the flow diverter removed. The mean velocity magnitude was taken with a handheld anemometer (Testo 451), which takes speed-readings over 10 seconds and then calculates the average speed at each measuring point. Nine readings were taken in each area of the sections in the drying zone and three in the up-and-downstream sections. The readings were taken on the 4th of January 2006 between 11 and 12 am; the RH of the outside air was 45.6% and the outside temperature 32.6 °C.
- The second set-up is the same as the first set-up, except only the flow diverter was installed.
- The third set-up was done with the flow diverter installed, 1 March 2005 14:30. The outside temperature was 34 °C and the RH was 40%. The first section A was measured at the back of the last trolley (with trays and mangoes on it). The trolley was then removed and the next section was then measured. A second anemometer (AV6) was used

for this set-up. The speed over 27 points in each section were taken. This anemometer was better suited for this experimental set-up, due to the fact that it's fan area which measures the speed is larger, and therefore giving a better overall reading between the trays with turbulence (at local area) not playing such a big role then. The first anemometer was more sensitive. There was up to a 30% difference in the readings using the two anemometers to measure the speed at the same point and time. Keeping in mind that the average speed over the sections was 1.3 m/s for the dryers without mangoes the choice of the anemometer used to obtain the various results used in the analysis played a major role. Uncertainty analyses were done on all the measurements taken in the drying zone of each experimental set-up (Please see Appendix 10.2).

For the first two experimental set-ups the dryer was configured in the following way:

- The dryer had an air-filter installed at the louvers
- The louvers were closed
- Door on gas burner side was open
- The gas burner was off
- Outlet fan was running at 1440 revolutions per minute
- Door on the downstream side was closed
- Main axial fan was running at 1440 revolutions per minute
- Cooled off system
- The settings of the controllers that control the inlet vent, gas burner and outlet fan was constant for the entire 24 hour drying cycle

For the third set-up the dryer was configured in the same way except the air-filters were not yet installed at the inlet louvers.

3.3 Test results

The contour of the average speed was created in each section of the drying zone. The results will be discussed in terms of the velocity magnitude distribution across the various sections in the drying tunnel. The speed contour is only constructed between the points and wall effects were excluded, as speed measurements were not taken near the wall. As in the study of thermo-dynamic and fluid flow it can be assumed that at the wall the velocity will be zero.

The drying zone was divided into six sections. The sections F and E of each set-up will be discussed in detail. These sections are the nearest to the flow diverter and turning vane and will give a good indication if the configuration works better than a normal tunnel configuration with no flow or turning vanes. The figures of

the other sections will be put next to each other, so that one can visualise of how the speed contour changes along the drying zone.

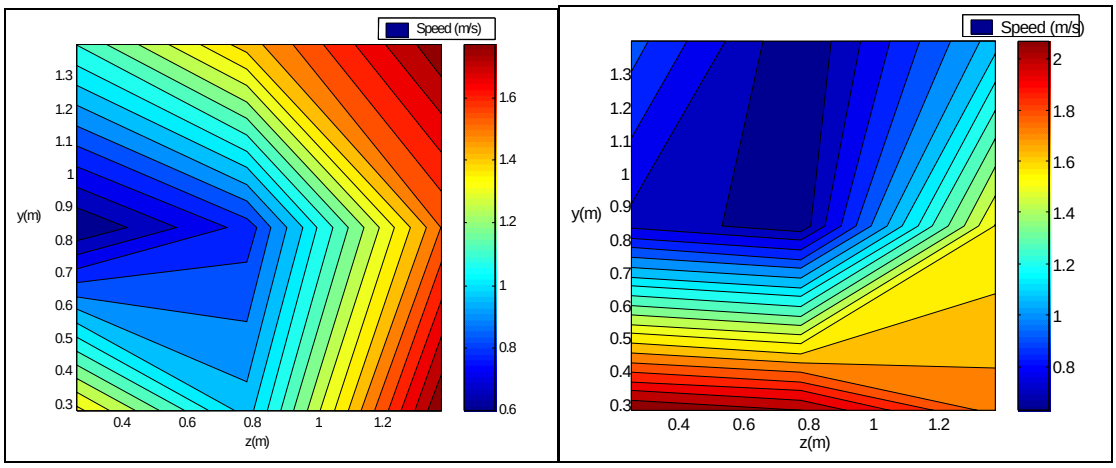

Figure 3-10 (Left) Section E: No flow diverter (No Trolleys) (Right) Section E: With flow diverter and turning vane (No trolleys)

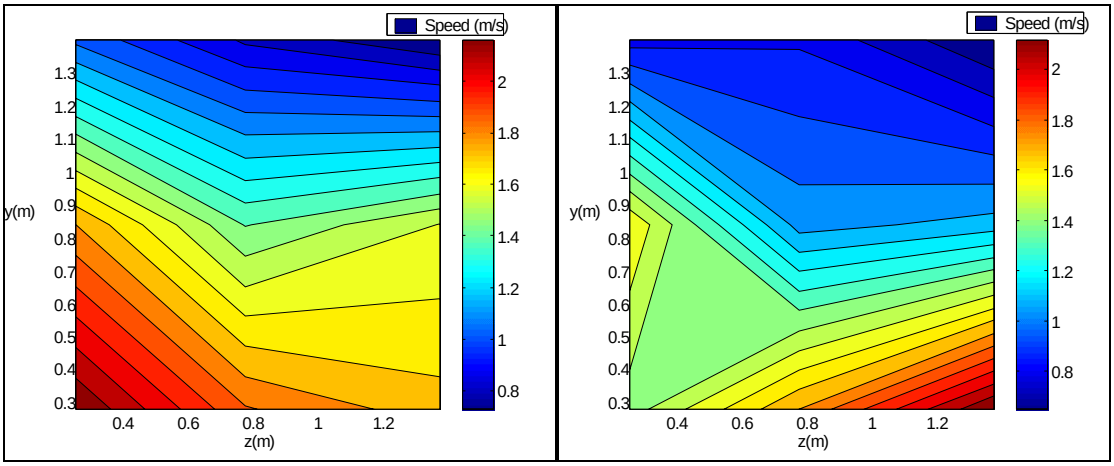

Figure 3-11 (Left) Section F: No flow diverter (No Trolleys) (Right) Section F: With flow diverter and turning vane (No trolleys)

In Figure 3-10 one clearly sees the swirl effect of the fan as the speed contour rotates in a clockwise direction. In this case the overall uniformity of the velocity distribution was better for the configuration without any flow diverter.

Section F of Figure 3-11 with the flow diverter and turning vanes shows that the range of the speed distribution varies less than the figure showing section F of the dryer with no flow converter. A larger area of the cross section is covered with the speed range area between 0 m/s and 1.4 m/s with the flow and vane configuration. There is still a non-uniform velocity distribution along the Y-axis but less then without the flow and vane configuration. The velocity distribution along

the Z-axis is more constant than that of the dryer without any flow and vane configuration.

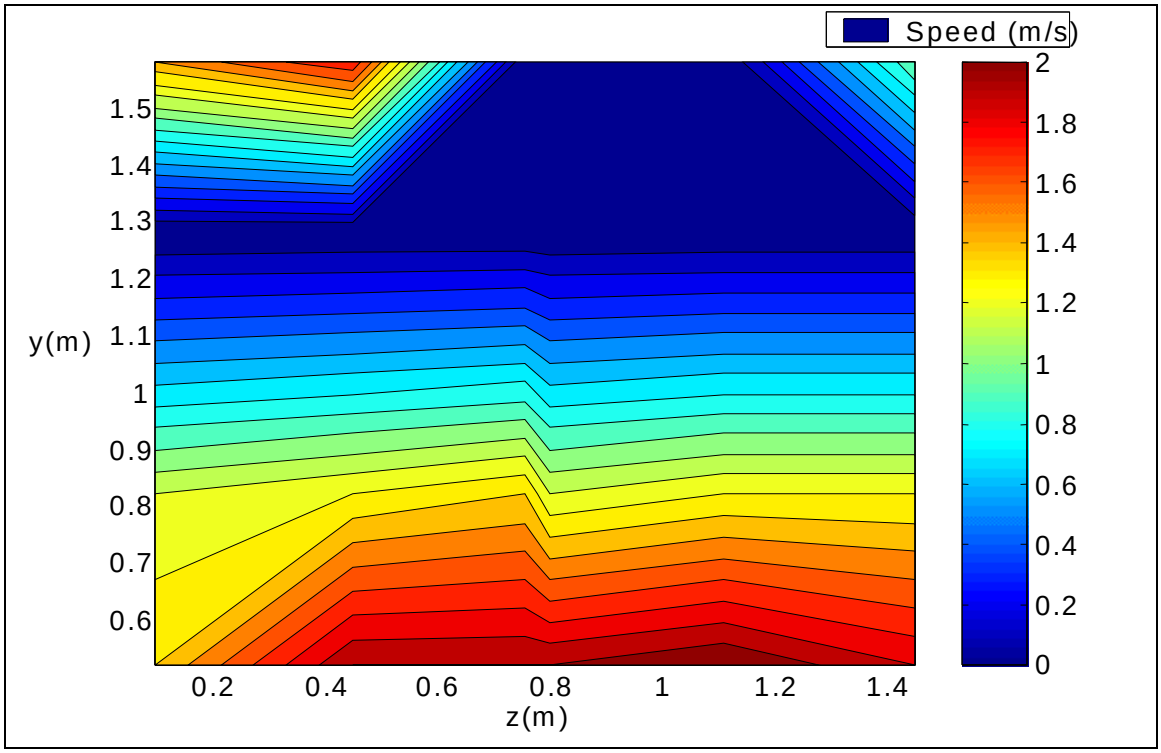

Figure 3-12 Section F: With flow diverter and turning vane (with trolleys & mangoes)

The velocity distribution along the Z-axis for the section F of the configuration with trolleys and mangoes are constant (See Figure 3-12). The velocity distribution along the Y-axis still varies, but Jinnie Nel (2006), part of the production staff of M-Pak Musina, confirmed that the produce dried more evenly along this axis than with the configuration with no vane or flow diverter.

In Figure 3-13 and Figure 3-14 section B and C of the dryer with the flow diverter and mango trolleys included the speed increases in the middle of the trays between the mango slices. In section F of all the trails the speed contour in the Z-axis does not vary as much compared to the variation in the Y-axis. The speed contour in all three trails increases towards the lower part of the Y-axis, showing that the velocity magnitude increases near the floor of the dryer. This is due to the relatively large gap between the floor and the first tray compared to the gap between the rests of the trays on the trolley. The speed contour increases toward the edges of the trolleys. There is little to no resistance to the airflow in the gap between the sides of the trolleys and the walls.

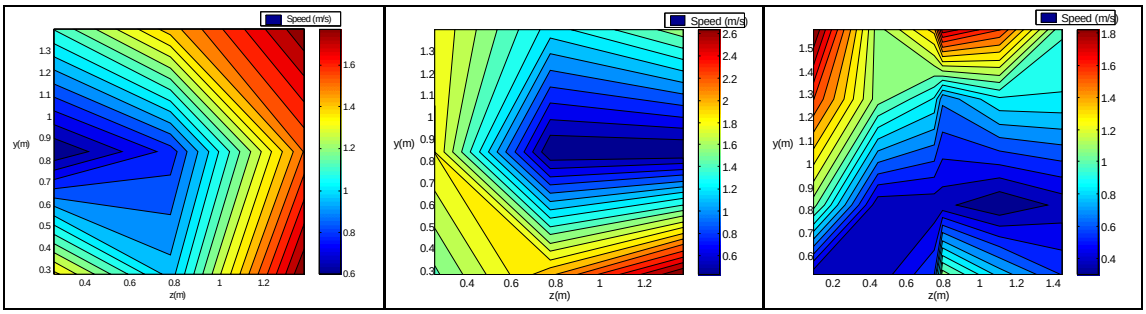

Section A

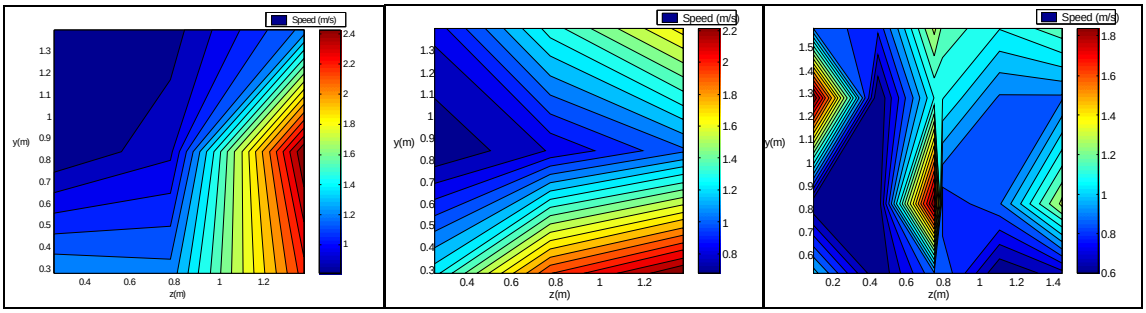

Section B

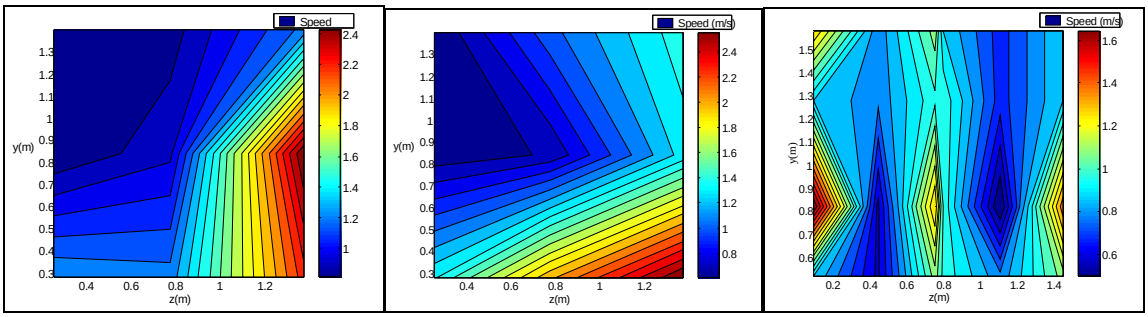

Section C

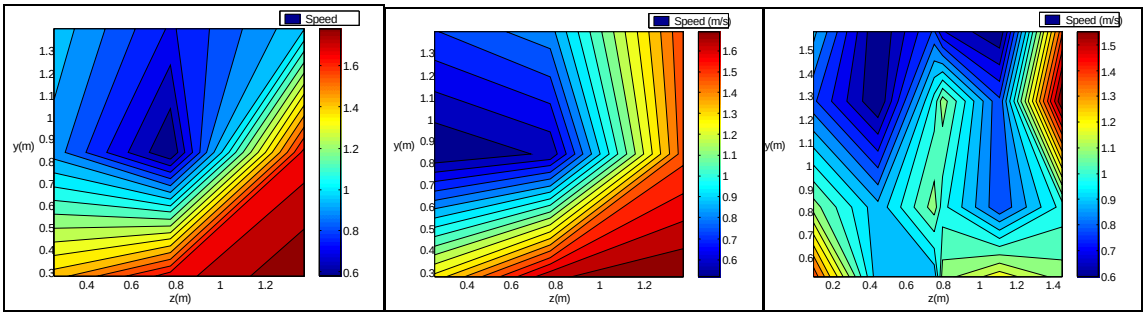

Section D

Figure 3-13 Speed contours - Left: No flow diverter, Middle: With flow diverter, Right: With flow diverter and mango trolleys

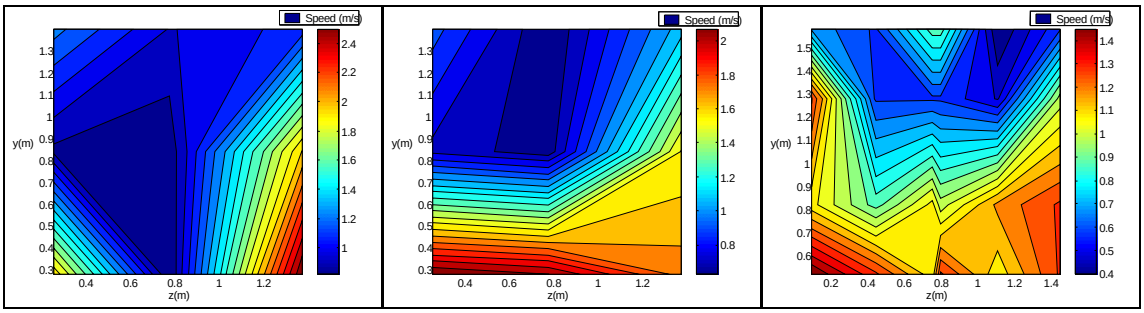

Section E

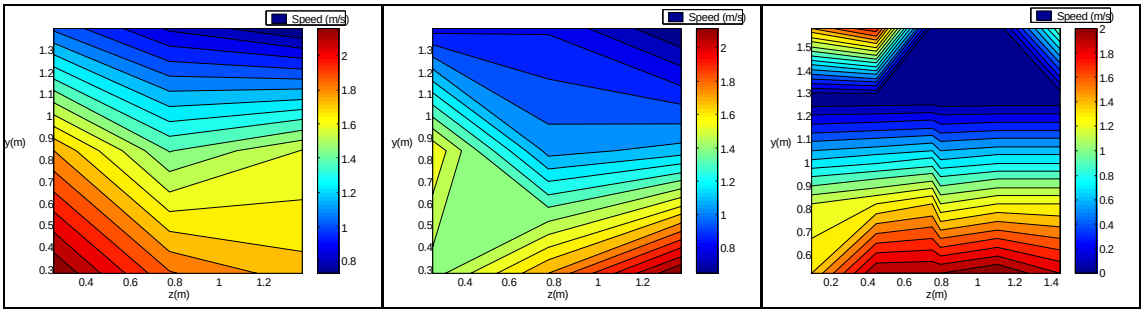

Section F

Figure 3-14 (Contd.) Speed contours - Left: No flow diverter, Middle: With flow diverter, Right: With flow diverter and mango trolleys

3.4 Conclusion based on test results

The effect of turbulence created by the trolleys and mangoes still played a major role in the non-uniform velocity distribution along the cross-sections of the drying zone. The trolley and mangoes in the drying zone dampened the swirl affect of the fan. It must be noted that measuring the velocity distribution is practically difficult. The operator measuring the velocity magnitude, calibration (accuracy) of the equipment and the misalignment of the handheld devices are all factors that influence the accuracy of the measurements. Uncertainty analyses in Appendix 10.2 calculate the random and bias errors as a result of these factors mentioned above. This is why it is important to construct a CFD model of the tunnel, to get a better picture and understanding of what is happening inside the dryer and between the trolleys and mangoes.

It must be taken into account that the pre-treatment of the mango and the quality of the produce plays an important role in the uniform drying of the food product. The production staff of M-Pak Musina confirmed this (Nel, 2006).

To add a flow and vane configuration is relatively cheap compared to installation costs to construct a dryer. It is also easy to add to an already constructed dryer.

4 Airpak project

The program used to solve the velocity and pressure distribution is called Airpak 2.1. It is commonly use in the ventilation industry. The main advantage of the program is the quick and easy-to-use interface that is integrated with the computational fluid dynamics solver of Fluent. For the design of mango dryers it had all the necessary features to capture the results required to optimise the whole system. The user of this program must take in account that the product is limited to creating complex geometries and the refinement options in terms of meshing the fluid volume. This program is more focussed on the practical side of designing an airflow system, compared to the other products used for analytical purposes.

4.1 Specifying the steady-state solution

The tunnel dryer at M-Pak Musina is equipped with a controller (VT30 Series from Vertex Technology Corporation) that can divide the temperature and humidity settings into sections so that it can follow the drying rate curve of the mangoes. The mango dryers would run on a 24-hour cycle where the temperature and humidity requirements would be controlled via the inlet vent, gas heater and outlet suction fan. The controller attached to the equipment mentioned above could be programmed into eight stages to control the temperature and relative humidity settings over time (Vertex Technology Corp. 2009). Humidity and temperature sensors are placed on the downstream side of the fan (See Figure 4-1). The sensors measure the actual relative humidity and temperature in the room and the data is relayed back to the controller.

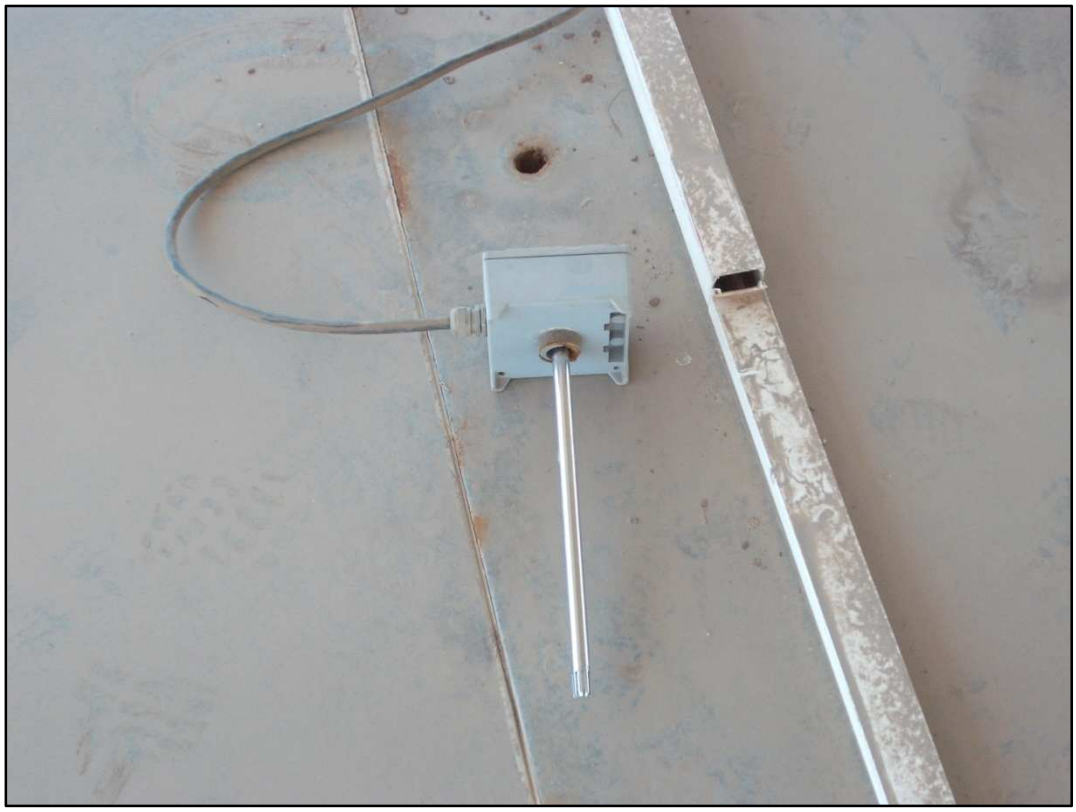

Figure 4-1 Humidity and temperature sensor

Source: M-Pak Musina

The controller compares this data to what the temperature and relative humidity should be at that time stage and setting. The controller then sends a signal to the actuators that controls the equipment. The whole system is built according to a real-time continuous loop. The relative humidity is mainly controlled by the inlet vent and outlet fan and varies one percent from the setting at the specific time stage. The outlet fan is either on or off, but the vanes on the inlet vane open or close continuously over time. Temperature is controlled via the gas heater, which heats up the air upstream from the fan. The gas heater has got a high and low flame. Most of the time, the low flame is burning to control the temperature to within one degree Celsius of the required setting. If the temperature falls below five degrees Celsius of the required setting, the high flame is activated to heat up the air. When the temperature rises above five degrees Celsius of the required setting the gas burner shuts off the low flame with only the pilot flame burning until the air has cooled down.

The controller can be programmed with either a step or linear ramped function to control the output signal. Although the output signal controlling the equipment can be a ramp function, the actuators (except the one on the inlet vent) can only respond in a step function (See Figure 4-2). Thus for a very short period (a couple of minutes) the temperature and relative humidity can change quite abruptly over a large spectrum of the set ranges. This situation usually occurs

when the controller changes over from one stage to another with large step up or down setting.

Figure 4-2 Actuator controlling inlet vent

Source: M-Pak Musina

A typical relative humidity and temperature setting is shown in Figure 4-3 and Figure 4-4 respectively. A company called Bavaria Fruit Estates uses these settings on their batch-type mango dryers. Roelf de Beer also designed these dryers. The relative humidity varies over a large spectrum in the first and last couple of stages. For most of the time especially in the midsection it varies linearly over a small spectrum. The same goes for the temperature setting, which is constant for most of the time. One has to take in account that the equipment is of such a manner that it can quickly stabilise the temperature and relative humidity values to coincide with the respective settings.

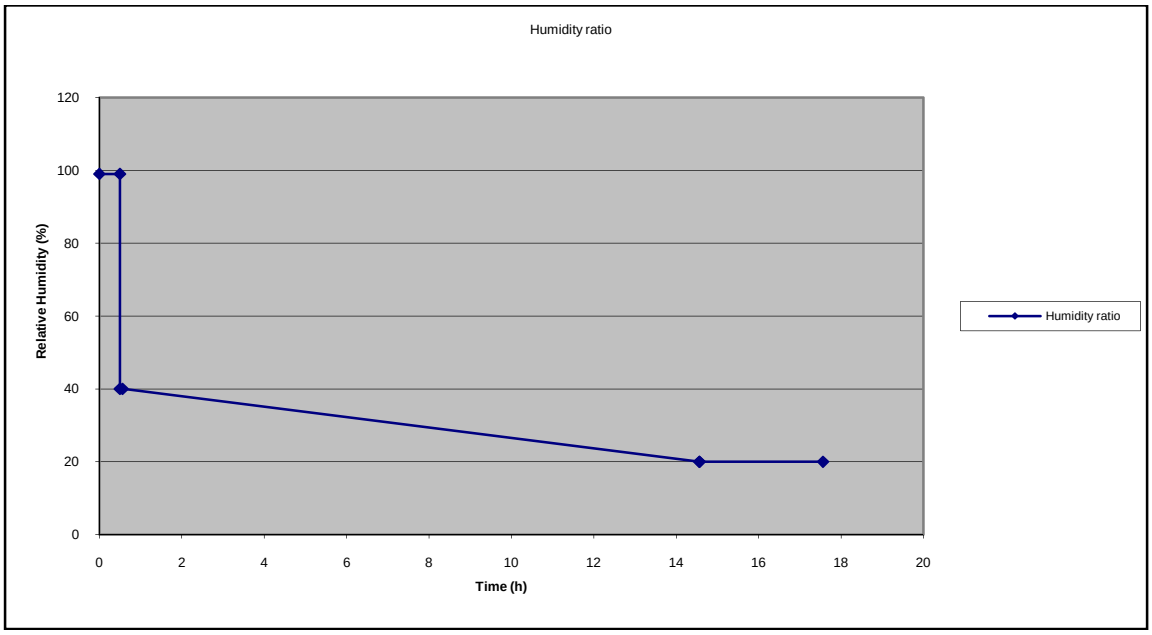

Figure 4-3 Relative humidity settings

Source : Bavaria Fruit Estates

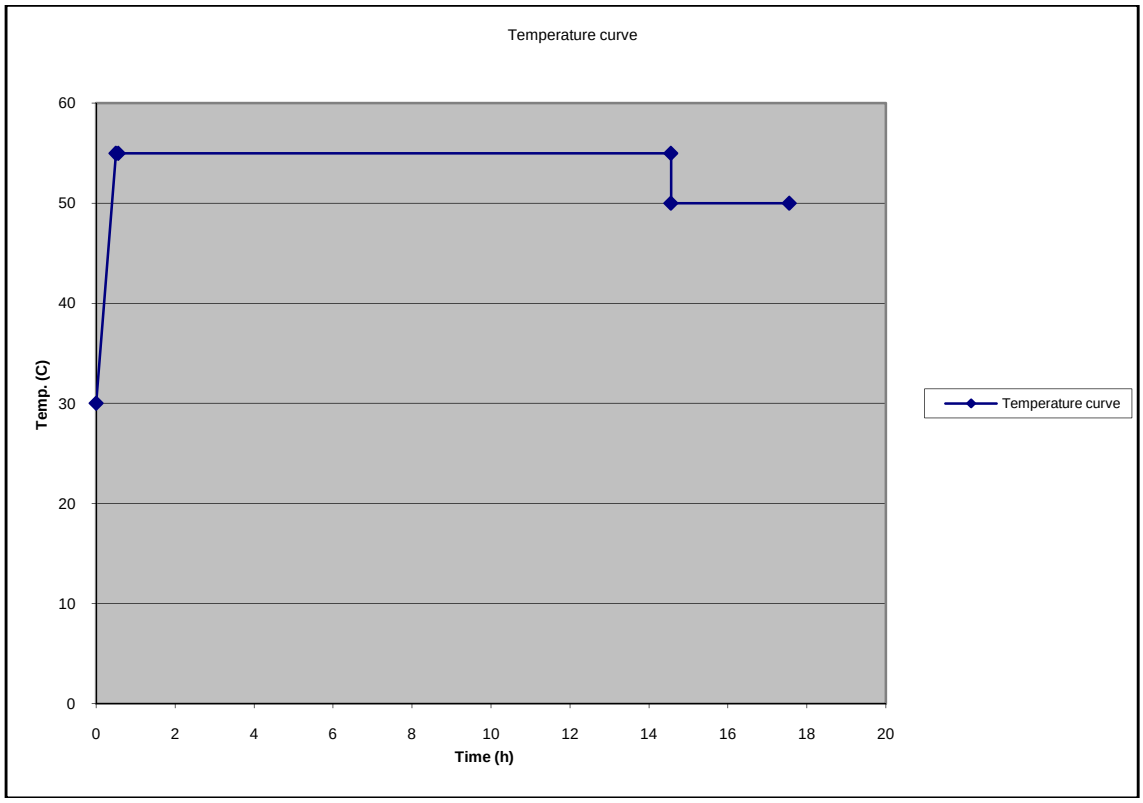

Figure 4-4 Temperature settings

Source: Bavaria Fruit Estates

The main reason for specifying the problem in CFD as a steady-state solution is the fact that the main fan runs constantly through the 24 hour cycle. This is the largest factor controlling the airflow pattern inside the room. Although the airflow patterns would change in the areas near the inlet vent and suction fans as the air passes through the openings, it would only vary across a short time-span. For the rest of the time the setting in each stage is constant over time. Airpak models of the dryer will be run where the inlet vent and outlet fan will be fully opened or closed.

Shrinkage of the mango slices over the 24-hour cycle has not been taken into account, thus the air-volume inside the room stays constant. The results of the CFD model will be compared to the experimental data. The data was gathered during one stage and in each stage the volume of the mango slices do not decrease that significantly.

For the purpose of using the Airpak program as a design tool, savings are made in terms of computational time and effort in modelling the problem as a steady-state solution for each of the control stages or settings.

4.2 Flow regime

Turbulent flows are characterised by fluctuating velocity fields. The Reynolds number (Re_D) is used as measurement in forced convection flow to determine whether the flow is turbulent or laminar. Thus the relative importance of the inertial forces and viscous forces are measured (Airpak 2.1 Documentation, 2002). If the dimensionless Reynolds number of internal flow is above 2300 the flow should be treated as turbulent. Earlier transitions to turbulent flow can be caused by free-stream turbulence, surface conditions and disturbances (De Kock, 2004). It is recommended that a turbulence model should be used when the Reynolds number is greater than 2000 (Airpak 2.1 Documentation, 2002).

$$Re_D = \frac{\rho U D}{\mu}$$

Equation 4-1

where:

- U – The free-stream velocity (m/s)
- D – The diameter (m) of a circular pipe. Note that (D) can be any characteristic geometric size for example, (L) for flow over the length of a flat plate or (D_H) the hydraulic diameter of a duct (White, 1991).

In turbulent flow the degree of mixing and in heat transfer is much greater than in laminar flow. An effective viscosity measures the amount of fluid mixing, which is the sum of the dynamic viscosity (μ) and turbulent eddy viscosity. Eddy viscosity

is part of the turbulence model and not a measurable quantity (Airpak 2.1 Documentation, 2002).

The RNG $k-\varepsilon$ turbulent model was used in Airpak 2.1 to determine the flow field. Turbulent intensity (I) and turbulent length scale (ℓ) are the two parameters used to determine the transported scalar quantities of the fans, vents and free openings in the model. Turbulent intensity is defined as the ratio of the root mean square of the velocity fluctuations (u'_{rms}), to the mean flow velocity $(\bar{u})$.

$$u'_{rms} = (\overline{u'^2})^{1/2}$$

Equation 4-2

where:

- u' – Turbulent velocity fluctuations

$$I = \frac{u'_{rms}}{\bar{u}}$$

Equation 4-3

For internal flows, the turbulent intensity at the fan is dependent on the upstream history of the flow. An empirical correlation is used by Airpak 2.1 to determine the turbulent intensity (See Equation 4-4) of a fully developed flow. For wall-bounded flow at a fan where a turbulent boundary layer exits, the boundary layer thickness $(\delta_{99\%})$ should be used to determine the turbulent length scale. Equation 4-5 is used to estimate boundary layer thickness over a flat plate when a large Reynolds number is present (White, 1991). Although this equation was determined for flow over a flat plate, assuming that the inlet profile of the velocity would be uniform, it was used as a first estimate for the turbulent scale in a large fan tube.

$$I = 0.16(Re_{D_H})^{-1/8}$$

Equation 4-4

$$\delta_{99\%} \approx \frac{5.5x}{\sqrt{Re_{D_x}}}$$

Equation 4-5

$$\ell \approx 0.4\delta_{99\%}$$

Equation 4-6

For the first initial run a free stream velocity (U) of 16 m/s was used to determine the two parameters. This was according to the fan manufacturers the mean free-steam velocity at the downstream side at the outlet of the internal fan (0.630 m in diameter), working under ideal conditions and optimum set-up. A Reynolds

number (Re_{D_H}) of 5.22×10^5 gave a turbulent intensity (I) of 3.08%. The circular tube or pipe that surrounded the fan was 0.5 m in length(x), and was used to estimate the turbulent length scale of 2.4×10^{-3} m. See Table 10-1 for calculation detail of the equations.

Prior to solving the model Airpak 2.1 computes the Reynolds number and the Peclet number for forced flow with the given initial conditions. The Peclet number (Pe) measures the rate of advection to the rate of thermal diffusion (Airpak 2.1 Documentation, 2002). The Reynolds number ranged between 450,000 up to 500,000 for all the runs made with the model in Airpak 2.1. The Peclet number ranged between 340,000-380,000.

$$Pe_L = Re_L Pr = \frac{LU}{\alpha}$$

Equation 4-7

The Prandtl number (Pr) is the ratio of momentum diffusivity (kinematic viscosity) and thermal diffusivity (White, 1991).

$$Pr = \frac{\nu}{\alpha} = \frac{viscous\ diffusion\ rate}{thermal\ diffusion\ rate} = \frac{C_p \mu}{k}$$

Equation 4-8

where:

- ν – kinematic viscosity, $\nu = \mu/\rho$ (m^2/s)
- α – thermal diffusivity, $\alpha = k/(\rho Cp)$ (m^2/s)
- k – thermal conductivity (W/(m K))

In the runs that followed the initial run using the RNG $k-\varepsilon$ turbulent model, the turbulent intensity (I) was increased to 8% and the turbulent length scale (ℓ) reduced to 0.0015. The turbulent length scale is the physical quantity related to the size of the large eddies containing the energy in turbulent flow. Thus by reducing the turbulent length scale the turbulent dissipation rate (ε) is increased. The turbulent kinetic energy (k) is increased, by increasing the turbulent intensity(I). This produced a better convergence rate of the (k) and (ε) residuals, showing that the turbulence created or values chosen were in good agreement with the turbulence created within the shear layers of the domain. Calculation of the turbulence can become sensitive in terms of convergence if the effective viscosity of the free-stream entering at the boundary condition is too high (Airpak 2.1 Documentation, 2002).

$$k \equiv \frac{\overline{u'^2}}{2}$$

Equation 4-9

In Equation 4-9 it is assumed that the turbulence is isotropic whereby the normal stresses are equal. Epsilon is the dissipation rate of the turbulent kinetic energy (k) to thermal energy (de Kock, 2004).

4.3 Ambient values

The project mainly focuses on achieving a uniform velocity flow field in the drying chamber, so the runs performed with the Airpak program will be of a steady state isothermal set-up. The main fan influences the airflow pattern inside the drying chamber. Due to the fact that this is a forced flow problem the temperature of the air does not play that big a role on the airflow pattern as during natural convection. The main two variables, the pressure field and velocity flow will be investigated in order to evaluate the uniform velocity flow-distribution inside the dryer. Ambient values surrounding the room can be set in terms of the temperature and gauge pressure. The average temperature was 35°C in the Musina district when the experimental data was captured. The gauge pressure was taken as zero. The ambient value was set to 35°C together with the velocity field set to zero in each coordinate axis as the initial conditions for each run.

The Southern African Weather Service (2009) reported that the average daily maximum temperature for a drying season (November-March) in Musina was 32℃. The height above sea level for that district is 522 m. The Engineering Toolbox (2009) gives the absolute atmospheric pressure for this height above sea level as 95.2 kPa. This is 6% lower than absolute atmospheric pressure at sea level (101.3 kPa) at a standard temperature of 298 K (25℃). The value of the air properties listed in Table 4-1 was at 300 K and 100 KPa. The decrease in density due to the temperature increase (from 300 K up to 306 K (32℃) was 0.5%. These values were chosen to compare to the data obtain through measurements taken when the air that circulated in the dryer was at ambient values. The gas burner was off during the experiments compared to when the dryer is in full production mode and the average temperature inside the dryer is 55℃.

4.4 Material and surface properties

The properties listed for the various fluid and materials are required to obtain the velocity, pressure and temperature variables calculated by the Airpak program.

Table 4-1 Properties of air at 300 K used in Airpak program

Properties	Value	Unit
Density	1.1614	kg/m^3
Specific heat	1005.0	J/kg-K
Conductivity	0.0261	W/m-K
Volume Expansion	0.003333	1/K
Viscosity	1.853×10^{-5}	kg/m-s
Diffusivity	2.92×10^{-5}	m^2/s
Molecular weight	28.966	kg/kmol

Source: Airpak 2.1 Documentation, 2002

The walls, false ceiling and doors were constructed by laminating polyurethane foam between 0.6 mm Chromadek sheets. The properties of the foam are given below in Table 4-2.

Table 4-2 Material properties of polyurethane foam

Properties	Value	Unit
Density	70.0	kg/m^3
Specific heat	1400	J/kg-K
Conductivity	0.026	W/m-K

Source: Mills, 1991 and http://www.bath.ac.uk/~absmaw/Benv1/properties.pdf

The flow diverters and vane were constructed of 0.6 mm Chromadek sheets. Chromadek is hot-dip galvanised steel. Galvanised steel is obtained by dipping carbon steel in a bath of molten zinc. The properties are given in Table 4-3. (http://www.colmaccoil.com/pdf/AluminumAdTP.pdf)

Table 4-3 Material properties of Chromadek sheets

Properties	Value	Unit
Density	7800	kg/m^3
Specific heat	486	J/kg-K
Conductivity	36	W/m-K

Source: Airpak material library of carbon steel (Airpak 2.1 Documentation, 2002)

All the trolleys and burner tube were constructed of 3Cr12 steel, with the following properties:

Table 4-4 Material properties of 3Cr12 steel

Properties	Value	Unit
Density	7740	kg/m^3
Specific heat	478	J/kg-K
Conductivity @ 100°C	30.5	W/m-K

Source: http://www.fanagalo.co.za/tech/tech_grade_3cr12.htm

The floor was constructed of concrete, with the following properties:

Table 4-5 Material properties of concrete

Properties	Value	Unit
Density	2100	kg/m^3
Specific heat	880	J/kg-K
Conductivity	1.4	W/m-K

Source: Mills, 1999

All the surfaces from the equipment mentioned above were modelled with non-metallic paint finishing. The default value of non-metallic paint finishing in Airpak 2.1 is zero; this represents a perfectly smooth surface (Airpak 2.1 Documentation, 2002).

In turbulent flow even a small roughness will break up the thin viscous sub-layer and greatly increase the wall friction. It is common engineering practice to compute noncircular duct friction by using the hydraulic diameter, D_h, and pipe-friction relation. Adding the surface roughness height, k, as parameter to the law-of-the-wall variable, k^+, the following is obtained (White, 1991):

$$k^+ = \frac{k u_\tau}{\nu}$$

Equation 4-10

where:

- u_τ – friction velocity (m/s)
- ν – kinematic viscosity (m^2/s)

Surfaces are defined as a hydraulically smooth (no roughness effect) if $k^+ < 4$. A transitional-roughness regime is considered when $4 < k^+ < 60$. When applying the pipe-friction equation a second denominator that can be used to determine if surface roughness is an unimportant factor when determining the law-of-the-wall variables, is (White, 1991):

$$\left(\frac{k}{D_h}\right) Re_{D_h} < 10\text{: roughness unimportant}$$

$$\left(\frac{k}{D_h}\right) Re_{D_h} > 1000\text{: fully rough (Independent of } Re_{D_h})$$

Equation 4-11

White (1991) used the explicit equation of Haaland (1983) to determine the pipe-friction factor, Λ:

$$\frac{1}{\Lambda^{1/2}} \approx -1.8 log_{10}\left[\frac{6.9}{Re_{D_h}} + \left(\frac{k/D_h}{3.7}\right)^{1.11}\right]$$

Equation 4-12

The surface roughness, k, of the chromadek sheets (hot dip galvanised steel) was 0.15×10^{-3} m (The Engineering Toolbox, 2009). The hydraulic diameter was calculated for the cross section (a = the width and b = the height) above the false ceiling and the roof on the downstream side of the fan. The highest average velocity distribution (except in the fan tube) was found in this region of the dryer domain (See Table 10-8).

Table 4-6 Surface roughness factors for dryer without trolleys and flow-diverter

Friction factors	Value	Unit
a	1.565	m
b	0.87	m
D_h	1.118	m
Density, ρ	1.1614	kg/m^3
Avg. velocity, U	3.56	m/s
Dynamic viscosity, μ	1.853×10^{-5}	kg/m-s
Re_{D_h}	$2.50\times10^{+5}$	
k	0.00015	m
$(k/D_h)Re_{D_h}$	33.5	
Friction velocity, u_τ	2.03×10^{-1}	m/s
Kinematic viscosity, ν	1.60×10^{-5}	m^2/s
k^+	1.91	
Λ	0.015	

The table above shows that the surfaces of the dryer are hydraulically smooth. If the cross section of the drying zone is considered (b =1.68 m, and U = 1.33 m/s (See Table 5-4)) the factor, $(k/D_h)Re_{D_h}$, reduces to 12.5. Surface roughness for this project is considered unimportant. A Moody chart (shown below) can be used as a second option to determine the friction factor.

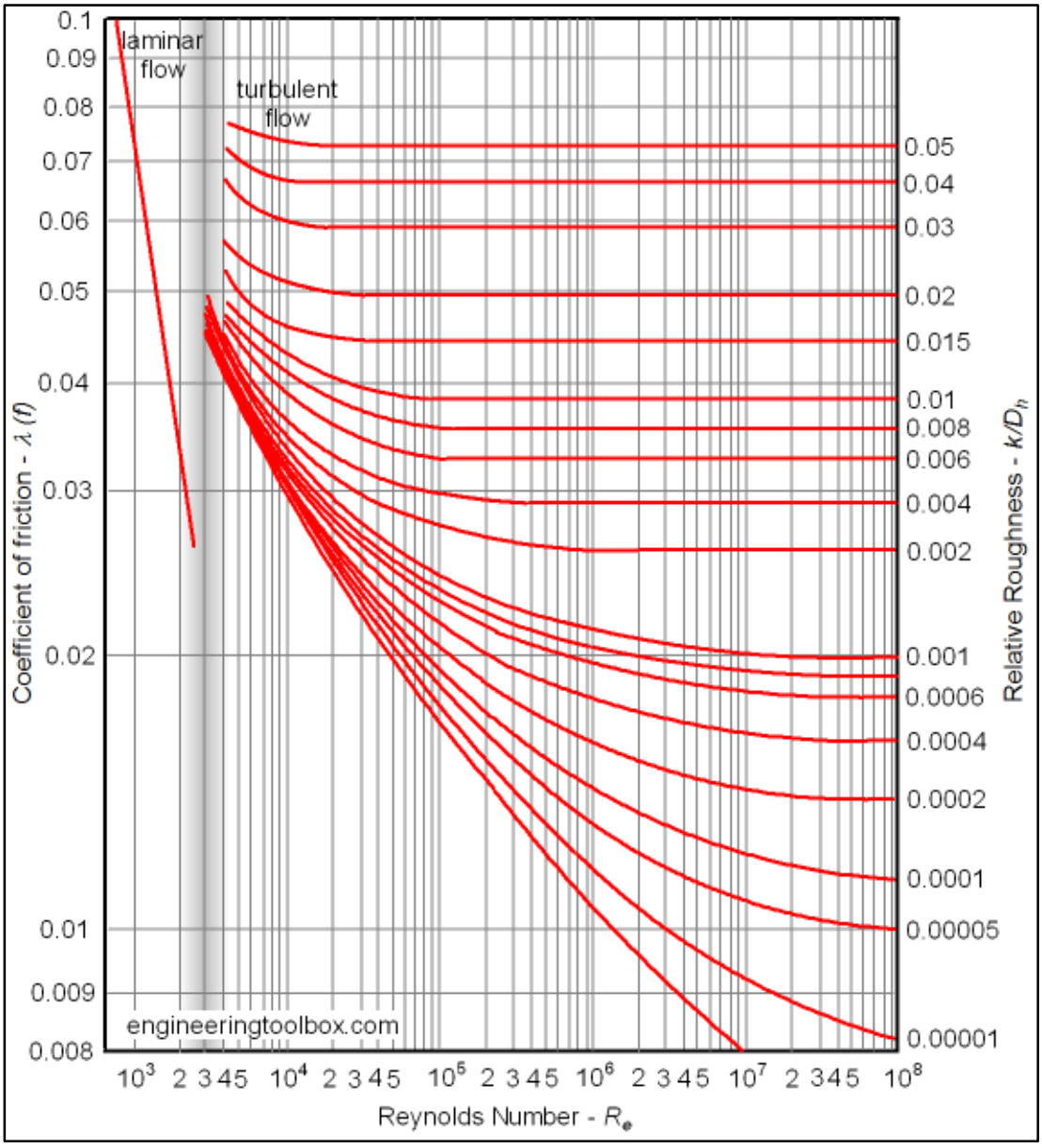

Figure 4-5 Moody Diagram

Source: The Engineering Toolbox, 2009

4.5 Building the model in the Airpak 2.1 program

It is a simple process creating the simulation model in Airpak 2.1. The main advantage of Airpak 2.1 is how it logically sets out the way of building the model and setting the conditions, recreating the physical world or boundaries. The main parts of the dryer will be discussed in this section.

4.5.1 Room

The room represents the physical boundary or the entire computational domain of the model. All objects should be created within the walls of the room. As previously stated only a single stand-alone unit would be modelled. The size of the room is 6 × 2.6 × 1.565. Figure 4-6 shows the global coordinate axes of the room from which all other objects were placed.

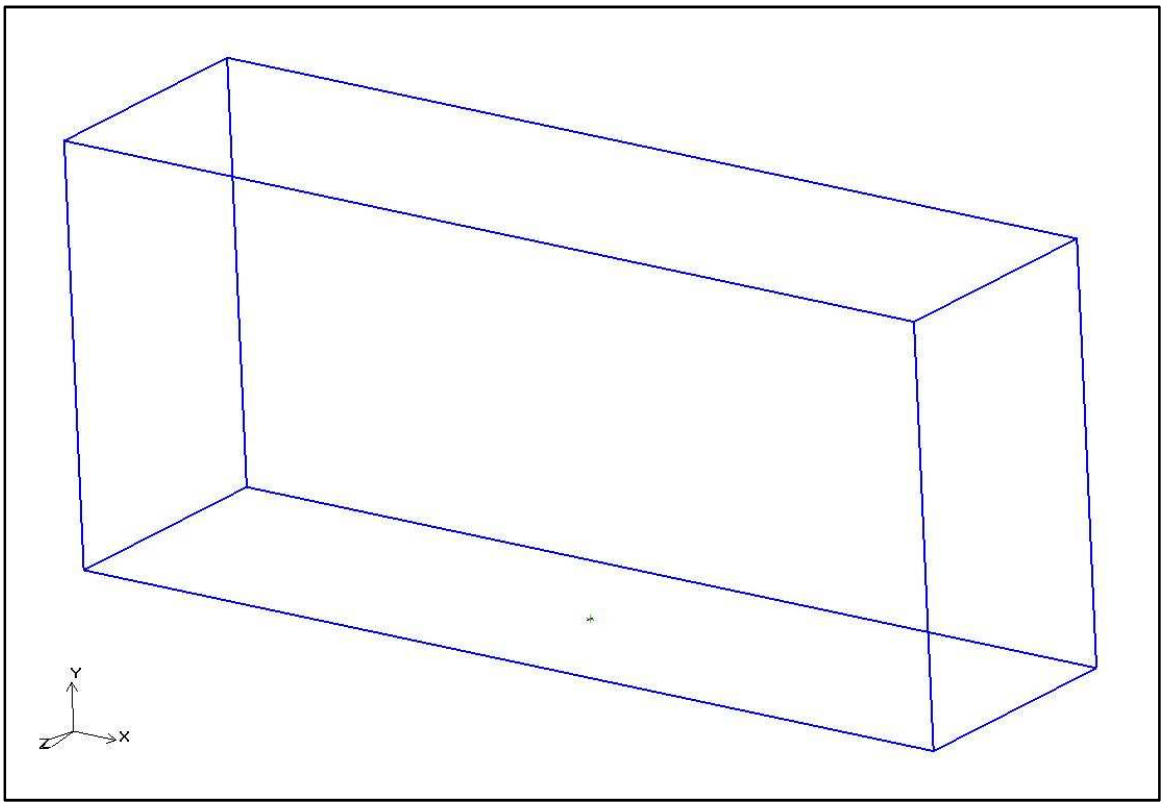

Figure 4-6 Room shown with coordinate axes

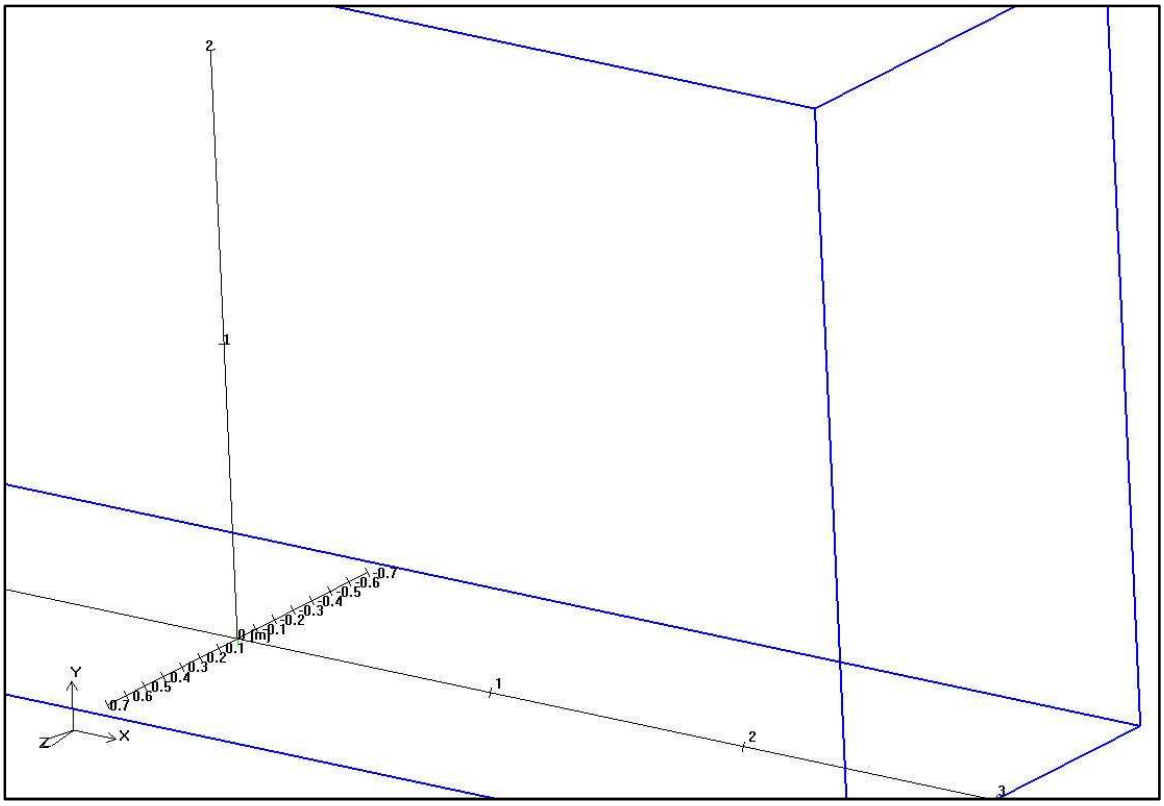

4-7 Global coordinate axis situated at the centre of the floor

4.5.2 Walls

Walls are objects that constitute all or part of the room boundary. The inner surface of an external wall is in direct contact with the fluid in the room, and its outer surface is exposed to the external environment. A no-slip velocity boundary condition is applied in the inner surface of the wall. For turbulent flows, you can also specify the surface roughness of the wall, the effect of which is to increase resistance to the flow. For a wall with zero thickness, the inner and outer sides of the wall will coincide. To configure a wall in the model, you must specify its geometry (including location and dimensions), velocity, thickness, thermal characteristics, and the material the wall is made of (Airpak 2.1 Documentation, 2002).

The walls created in this model are external and rectangular, located on the boundaries of the room. In practice most dryers are built alongside each other, thus side panels are shared between rooms. This means the outer surface of one room is not exposed to the external environment, but to the internal fluid of the room built alongside it. This procedure saves costs in using less building material in the construction of the rooms. Heat loss through the walls is lower thus saving in energy or running costs. For the purpose of this project the side panels of the room will be exposed to the external environment, thus modelling the room as

single unit, standing alone. The end panel contains the air inlet and gas burner. The front and end panel contains large sliding doors made from the same material as the wall of the dryer. Butyl rubber lining (gasket), ensuring minimal heat loss, seals of the gap created between the door and wall (Precool, 2009). The roof contains the outlet fan. A small cut-out of 140mm × 75mm is made on the roof; this contains the fan belt that drives the internal fan. The cut-out is covered by a housing made of structural-steel. The heat and airflow loss through this hole are negligible and will not be included in the Airpak 2.1 model of the room.

Effective-thickness walls will be used in this model; the interior of the walls will not be meshed. These walls have the same properties as non-zero-thickness walls, except that they have no physical thickness: they can possess only effective thickness. The interior heat flow inside the walls will not be examined for this project (Airpak 2.1 Documentation, 2002).

For turbulent flow it is sometimes necessary to account for surface roughness. The length scales of typical rough surfaces can be larger than the length scale of flow eddies in turbulent flow. Surface roughness acts to increase resistance to flow, leading to higher rates of heat transfer. For turbulent-flow simulations in which roughness is significant, however, one can specify a roughness factor for the entire wall (Airpak 2.1 Documentation, 2002).

No thermal boundaries were specified for the model due to the fact that the emphasis was on the airflow, rather than the heat distribution inside the room. When no thermal boundaries are specified Airpak 2.1 assumes that the walls are adiabatic and thus the heat fluxes across the walls is zero (Airpak 2.1 Documentation, 2002).

When a gas is used as a fluid one has to be careful in assuming that the velocity of the fluid equals the velocity of the solid it is in contact with, as established by Maxwell (1860) from the kinetic theory (White, 1991).

In Equation 4-13 the finite slip velocity (u_w) is expressed in terms of the free stream Mach number (Ma), the skin-friction coefficient (C_f), and the free stream velocity (U).

As the Reynolds numbers increases the flow near the wall becomes more turbulent and the skin coefficient decreases. The Mach number is very low considering that the maximum velocity calculated for this model does not exceed 16 m/s.

$$\frac{u_w}{U} = 0.75 Ma C_f$$

Equation 4-13

For a turbulent boundary layer the finite slip velocity:$u_w \approx 0$, resulting in a no-slip condition at the walls.

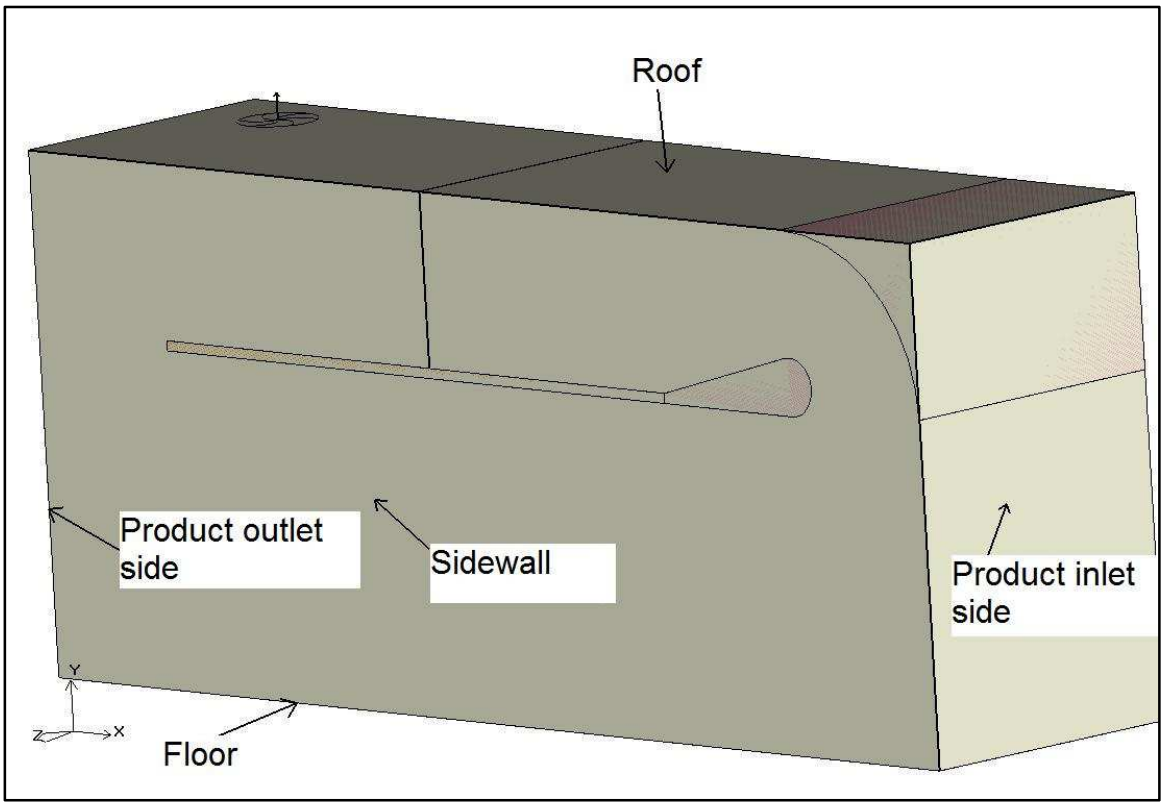

Figure 4-8 Solid view of the walls at the boundary of the room (parallel set-up)

4.5.3 Doors

The sliding doors are modelled as openings. This was one of the new design features at M-Pak Musina compared to previous dryers designed by Roelf de Beer for Bavaria Fruit Estates in Hoedspruit (South Africa). The previous door design had a pulley and weight system that lifted the door vertically upwards. This created problems in sealing of the doors and the placement of the gas burner and inlet vent (See Figure 3-1). A 20 mm thick butyl rubber lining at the floor and sidewalls seals off the doors, thus very little air and heat escapes between the gaps created (Precool, 2009). If a vertical door is used, a large frame is constructed to support the structure. This could create a large gap (up to a 100 mm) between the trolleys and the sidewalls of the dryer. With the sliding door system the gap is decreased to only 20 mm. When the velocity measurements were taken the outlet door was open. A model was created with this situation taken into account.

In Airpak 2.1 Documentation (2002) a free opening represents an area on the surface of the exterior wall, through which fluid is free to flow in any direction.

Thus the fluid inside the room is exposed to the external environment. Ambient pressure and temperature are used for the boundary conditions and flow rate at the door opening.

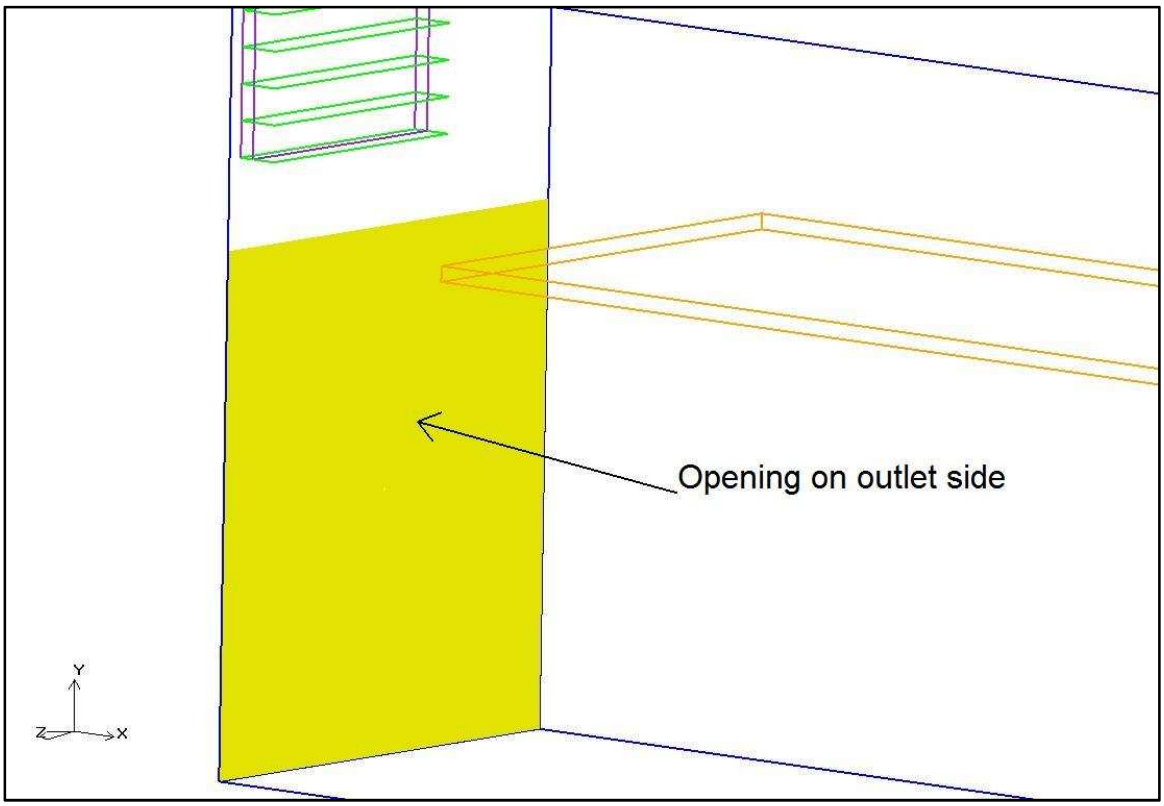

Figure 4-9 Door modelled as opening on outlet side of dryer

4.5.4 False ceiling

The false ceiling is made from the same material as the walls of the dryer. It is there to separate the trolleys from the fan, thus creating a circular flow inside the room. It protects the trolleys and mangoes from the direct heat of the gas-burner flame at the back of the dryer. During construction the false ceiling must be securely fastened to the sidewalls. The pressure difference between the topside volume between the false ceiling at the upstream side of the fan and the drying zone below can cause the panels to lift up. The gap between the false ceiling and the top of the trolleys must be as small as possible, to ensure minimum airflow at that cross section. The construction tolerances for these types of dryers are usually within 5 mm compared to the distances or measurements given in the manufacture-drawings. Taking in account dryers are built on floors that are sometimes uneven or slopes at a slight angle the gap is between 10-20 mm.

The false ceiling is defined as a hollow, 50 mm thick partition in the Airpak 2.1 program. A partition is impervious to flow. The partition can be seen as an interior

wall with all the same settings or boundary conditions as mentioned in section 4.5.2 for the exterior walls.

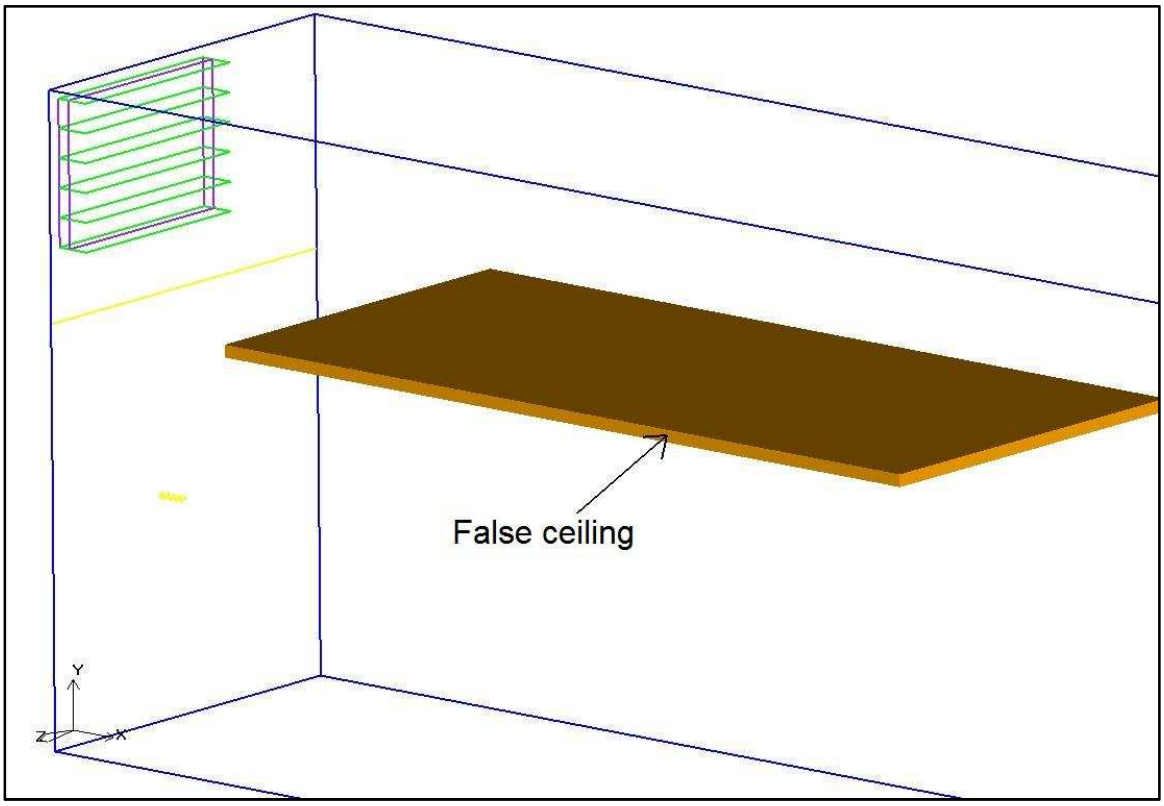

Figure 4-10 False ceiling

4.5.5 Inlet vent

Vents represent holes through which fluid can enter or leave the room (Airpak 2.1 Documentation, 2002). Airpak 2.1 assumes the ambient pressure is static to calculate the pressure drop and flow at the cross section of the vent. It contains angled slats, which create a secondary pressure drop across the plane of the vent-surface. The user specifies the direction of flow through the vent. The free area ratio (can be obtained from any adjustable louver manufacturer) is required by Airpak 2.1 to calculate the pressure drop over the angled slats. The slats for all the models used to simulate the dryer will be fully opened (See Figure 4-11). The airflow is thus normal across the plane surface of the vent. The vent is modelled as a perforated thin vent. This is one of the advantages in using Airpak 2.1, which has already got built-in models of various vents used in the ventilation industry. The free area ratio for the vent (Model: VRLA-6) used in this dryer was 0.58 m^2/s (Ventrite, 2009).

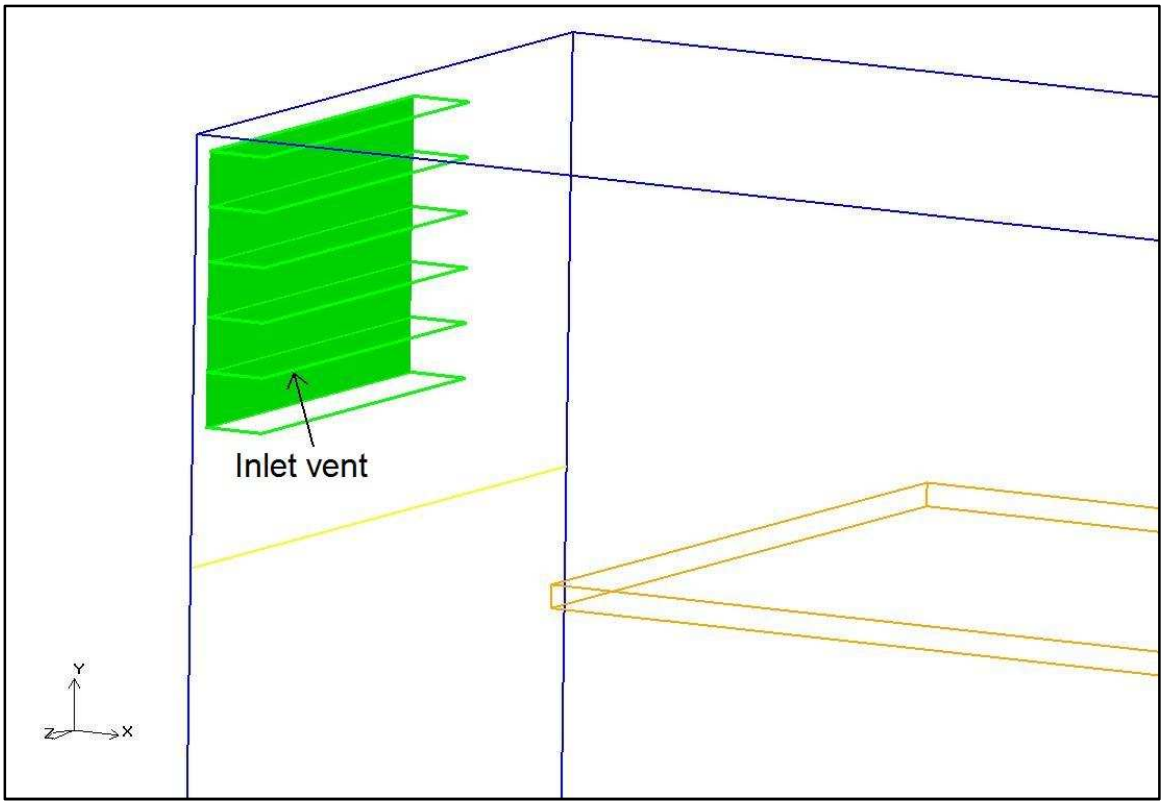

Figure 4-11 Inlet vent placed above the outlet door

4.5.6 Filter

A filter is placed at the cross section of the inlet vent to prevent dust particles and insects to contaminate the mangoes (See Figure 4-12). This filter is made from washable non-woven needle-punched synthetic media and is fixed within a galvanized channel frame with urethane, ensuring no air bypass (Trox Technik, 2004). This creates another pressure drop over the vent. The filter is modelled in Airpak 2.1 by inserting a 50 mm thick resistance in terms of the fluid flow in the X-axis. A resistance is a partial obstruction to the flow within the room. The manufacturer usually supplies pressure drops on the three stages of the filter. When the filter is new or fairly unused the pressure drop over the filter is very low. The filter used in this dryer had an initial pressure drop range of between 45-60 Pa. The second stage is the normal working stage, and then the pressure drop ranges from 50-70 Pa. The last stage is when the filter is not continuously cleaned or replaced and the pressure drop can jump as high as 250 Pa. These values are usually given in combination with the face velocity or rated airflow (m^3/h at specified velocity, filter area and thickness).

Airpak 2.1 provides two methods for calculating the pressure drop over the filter:

- The approach-velocity method which relates the pressure drop to the fluid velocity
- The device-velocity method, which relates the pressure drop induced by the resistance to the fluid velocity.

Due to the uncertainty of the specific pressure drop that the filter will induce over time to the fluid velocity, the approach-velocity method will be used. Airpak 2.1 suggests using the quadratic relationship between the pressure drop and velocity for turbulent flow.

$$\Delta p = \frac{\rho}{2} l_{c1} v_{app}^2$$

Equation 4-14

where:

- Δp – The pressure drop over the filter (Pa)
- ρ – The density of the fluid flowing through the filter (kg/m^3)
- l_{c1} – The loss coefficient of the filter (m/s)
- v_{app} – The velocity of the fluid as it approaches the filter (m/s)

The main factor that is unknown before the first run of the model is the loss coefficient (l_{c1}). The loss coefficient (l_{c1}) was chosen to be 1 m/s. The pressure drop is directly linked to the quadratic velocity approach, with the loss coefficient not being a factor for the first couple of runs.

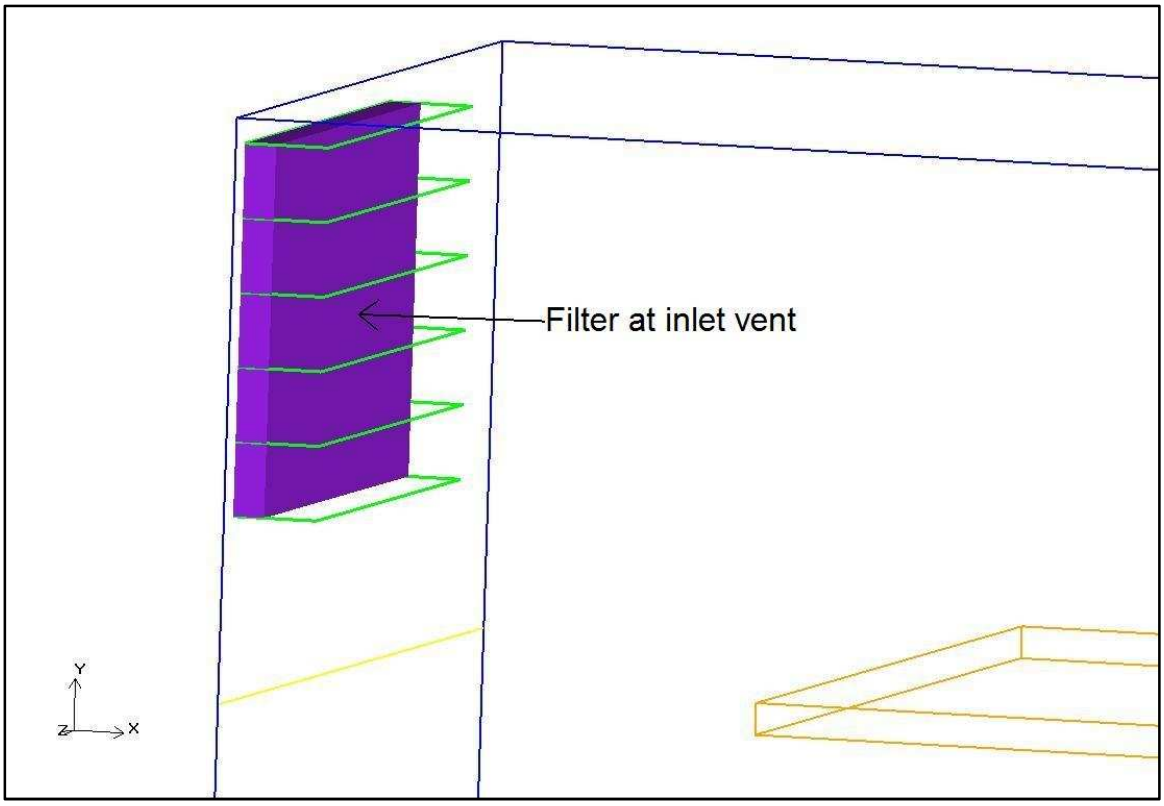

Figure 4-12 A 50 mm thick primary washable unsupported filter at the inlet vent

4.5.7 Heat source

In the food drying industry gas burners, electrical elements or steam are used to heat up the circulating air in a dryer. The production staff at Musina chose Liquefied petroleum gas (LPG) burners. It is up to the specific client to choose a heat source that satisfies their needs. In some cases it would be more cost effective to heat up the air by using electrical elements. Availability and maintenance played a major role in choosing gas burners at the Musina plant. Gas burners have the added advantage in heating up the air faster compared to electrical heating elements. Thus the temperature inside the room can be adjusted faster over a shorter period and thus the control over the temperature is better.

Figure 4-13 Gas burner, inlet vent and outlet fan

Source: M-Pak Musina

The gas burner is surrounded or enclosed by a circular metal tube (See Figure 4-13 and Figure 4-14). The air does not come into direct contact with the flame produced by the burning gas. The main focus will be placed on the airflow pattern around the volume of the circular tube. The nearby wall and false ceiling are also protected from the direct gas flame by the metal tube.

Airpak 2.1 has the feature of inserting a separate heat source with capability of changing the factors like thermal specification, radiation and species entering the room through the heat source. For the purpose of this simulation a hollow block type was used to model the gas burner, where only the surface and heat specification were given.

The gas burner produced an average thermal power of 50 kW when the low flame is burning as mentioned in paragraph 4.1. The power output of the high flame ranges between the values of 60-150 kW, depending on the gas-to-air mixture ratio and the nominal pressure settings (F.B.R Gas Burners Series X, 2009). The total power output of the tube in the dryer model was set to 50 kW to simulate the low flame burning. The burner tube is made of 3Cr12 steel with a

smooth finish. The gas burner is placed near the inlet vent to heat up the fresh inflowing air and the air that just past through the trolleys. For safety reasons the gas burner will automatically shut off if the main fan is not running due to mechanical failure.

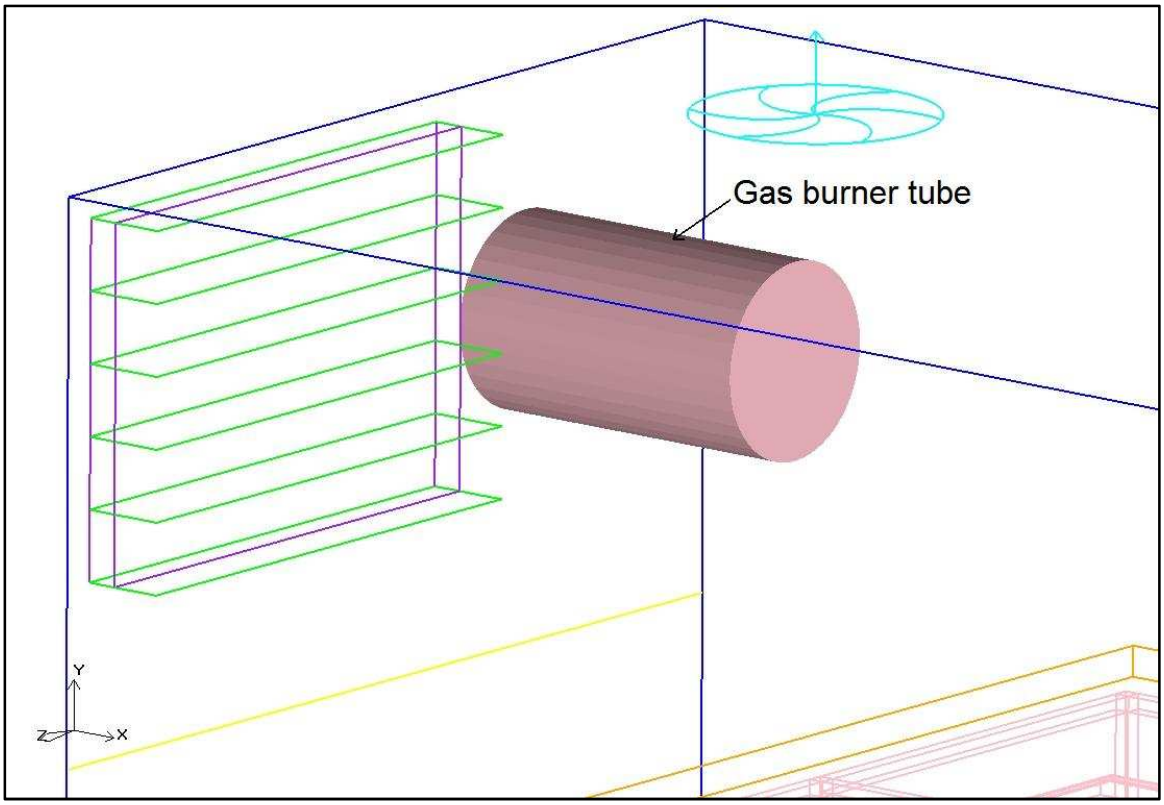

Figure 4-14 Tube enclosing the gas burner

4.5.8 Fans

According to Osborne (1977) air is considered as incompressible in fan engineering. From the gas laws:

$$\rho = \frac{m}{V} = \frac{p}{RT}$$

Equation 4-15

where:

- ρ – The density of the gas (kg/m^3)
- m – The mass of the gas (kg)
- V – The volume occupied by the gas (m^3)
- p – The pressure of the gas (Pa)
- T – The absolute temperature of the gas (K)
- R – The gas constant (8.3145 kJ/kmolK for a particular gas having a molecular mass M

Density is seen to be a variable quantity according to the conditions. In recording the performance of fans it is convenient to work in terms of some standard air density value and to make a correction for practical working pressure. The Musina district is 522 m above sea level (Southern African Weather Service, 2009). It is therefore necessary to compute the partial pressure of water vapour pressure (Osborne, 1977).

The purpose of a fan is to move air continuously against moderate pressures. Although under some circumstances a little compression occurs, it is customary to consider air fan flow as being incompressible. Often fan manufacturers will provide the fan characteristic curve of the specific fan. The graph will plot the total, static and velocity pressure against the volume flow. Static pressure is often regarded as the useful pressure and is defined as the total pressure minus the velocity pressure. Fan total pressure is the difference between the total pressures at the fan outlet and inlet. Fan velocity pressure is the velocity pressure corresponding to the average velocity at the fan outlet (found by dividing the volume flow of air by the area of the fan discharge orifice) (Osborne, 1977).

The total power output is found by using the total fan pressure multiplied by the volume flow.

$$P = pQ$$

Equation 4-16

where:

- P – The total air power of the fan (W, J/s)
- p – The total fan pressure (Pa, N/m^2)
- Q – The volume flow (m^3/s)

Fan efficiency (η) is the ratio of output power to the mechanical input power and is usually expressed as a percentage:

$$\eta = \frac{P}{FP} \times 100\%$$

Equation 4-17

where:

- FP – The measured fan input power

The power and fan efficiency of the main and outlet fan were calculated for the various dryer configurations mentioned in 3.2 in Appendix 10.3.

According to Osborne (1977) the performance of a fan in terms of pressure, volume flow and power absorbed depends mostly on the following factors:

- The design and the type of fan
- The point of operation on the volume flow/pressure characteristic fan curve
- The size of the fan
- The speed of rotation of the impeller
- The condition of the air passing through the fan

It is important to notice that the Reynolds number of the fan is based on the impeller diameter and peripheral velocity. It is found that an increase in the Reynolds number tends to result in an increase in fan performance and efficiency. Relative roughness of the fan surface is generally less as the fan size increases leading to an increase in fan performance (Osborne, 1977).

An axial flow fan may be described as a fan in which the flow of air is substantially parallel to the axis of the impeller. In the simplest form of the unit, air approaches the impeller in an axial direction and leaves with the rotational component due to the work done by the impeller torque. Thus the absolute velocity of the air leaving is higher than the axial velocity with the result that some of the total pressure developed by the impeller does not appear as useful total pressure (Osborne, 1977).

More advanced designs have guide-vanes downstream of the impeller which remove the rotational component, thus slowing down the air and converting some of the excess velocity pressure to more useful static pressure. One has to keep in mind that the major pressure losses in axial flow fans occur through the blades and guide vanes. Therefore many commercial designs are produced without guide-vanes to reduce costs, and if the fan operates at low power, the gain in efficiency is negligible (Osborne, 1977).

Another way to achieve the maximum amount of useful pressure is to have pre-rotational vanes upstream of the impeller. These rotate the air in a direction opposite to that of the impeller rotation and with careful design the air will leave the fan in an axial direction. A third way to achieve maximum amount of useful pressure is to have a second impeller downstream of the first, but rotating in the opposite direction. True axial discharge from any of these units will be possible only for a single operating condition (Osborne, 1977).

The pressure/volume flow characteristics of a fan with a high blade angle may exhibit a region of discontinuity corresponding to stalling conditions on the blade airfoils. It is wise not to operate fans in this region, or at lower flow volumes.

Upstream guide vane fans tend to show more marked stalling characteristics, although developing higher pressures, than downstream guide vane fans. Contra-rotating fans develop the highest pressure and are the least effected by stalling conditions (Osborne, 1977).

Efficiencies of up to about 75% may be expected from non-guided vane fans, and up to 87% for large downstream guided vane fans (Osborne, 1977).

The purpose of a fan is to move air at the required volume flow rate, and to supply the total pressure loss (including the discharge velocity pressure) in the system to which it is supplied. The assumption is often made that the fan velocity pressure is very nearly equal to the system discharge velocity pressure. In calculating system pressure loss, the discharge velocity pressure is ignored and the resulting total taken as being the required fan static pressure (Osborne, 1977).

Bends, particularly at fan inlets, should be avoided. For the best performance out of a fan system the velocity distribution at the inlet side should be as uniform as possible. Where there is no duct connection to the fan inlet, is advisable to fit an entry flare: this can be a short cone of 60˚ total angle, having a length equal to about one-quarter of the fan inlet diameter (Osborne, 1977).

Fan pressure, fan power and system pressure loss will vary proportionately to the air density. One of the fan laws mentioned by Osborne (1977) is that the air volume flow at any operating point is independent of the air density change whilst fan pressure varies directly with air density. Density is indirectly proportional to temperature. When a fan is placed downstream from a heater the fan pressure and fan power will be lower, but the mass flow in the system will also be lower (Osborne, 1977).

When two or more fans are connected in series, the volume flow through each unit will be the same (since the air is regarded as being incompressible) whilst the overall total pressure will be the sum of the individual fan total pressures, less any losses in the interconnections. If series operation of fans is chosen for an application, identical units should be used since it is unlikely that efficient operation would result otherwise. It is preferable not to operate single impeller non-guide vane axial flow fans in series, unless these are widely spaced, since the rotational component of velocity in the air leaving the first impeller will modify operation of the second and succeeding fans (Osborne, 1977).

When two or more fans are connected in parallel there will be the same total pressure difference across each fan from the common connection point downstream to the common connection point upstream. The total volume flow will be the sum of the individual volumes flowing through each fan at the same effective fan total pressure, allowing for loss of total pressure due to the individual fan connections. If the cross section of the chamber were large

compared to the total fan discharge area of the parallel fan system the connection loss would be the same as for a sudden expansion. This means that there will be a pressure loss equal to the fan discharge velocity pressure. The effective total pressure across the common connections would be fan total pressure minus fan velocity pressure, which is fan static pressure (Osborne, 1977).

The total fan discharge area of a parallel fan system in a mango dryer is nearly equal to the cross section area formed between the false ceiling and the roof. This means that the connection loss would be much less than that formed by a sudden expansion in area.

Not all fans have the simple characteristic pressure/volume curve mentioned above when connected in a parallel-connected system. The characteristics of forward curved fans have points of contra-flexure, with the result that as many as three different volume flow rates are possible at certain values of fan total pressure. Thus six volume flow rates are possible for two identical fans in parallel. Probably the most serious effect of this situation is on the power consumption of the motors driving the individual fans. The desired operating point would be when both fans share the load equally. One can use the method developed by Hagen to determine if two fans connected in parallel would work well together and do not create excessive power consumption (Osborne, 1977).

If fans in parallel are started one at a time, it is desirable to fit automatic back-draught shutters to prevent air re-circulating through the fans not already running. This avoids reversed rotation of the impellers, which could lead to heavy starting currents and mechanical shock on starting (Osborne, 1977).

4.5.9 Fans modelled in Airpak 2.1

The main fan (630 mm in diameter, 8 blades at 14˚-blade-pitch) that circulates the air is placed on top of the false ceiling in the centre of the room (See Figure 4-14 and Figure 4-15). The walls and false ceiling are structurally reinforced by H-beams to support the weight of the fan. One has to be careful not to place the fan too far back as it will get some heat damage from the gas-burner flame. The main fan is driven via three fan belts by a 1.1 kW electric motor (supplied by fan manufacturer) that is placed on top of the roof (Donkin, 2009).

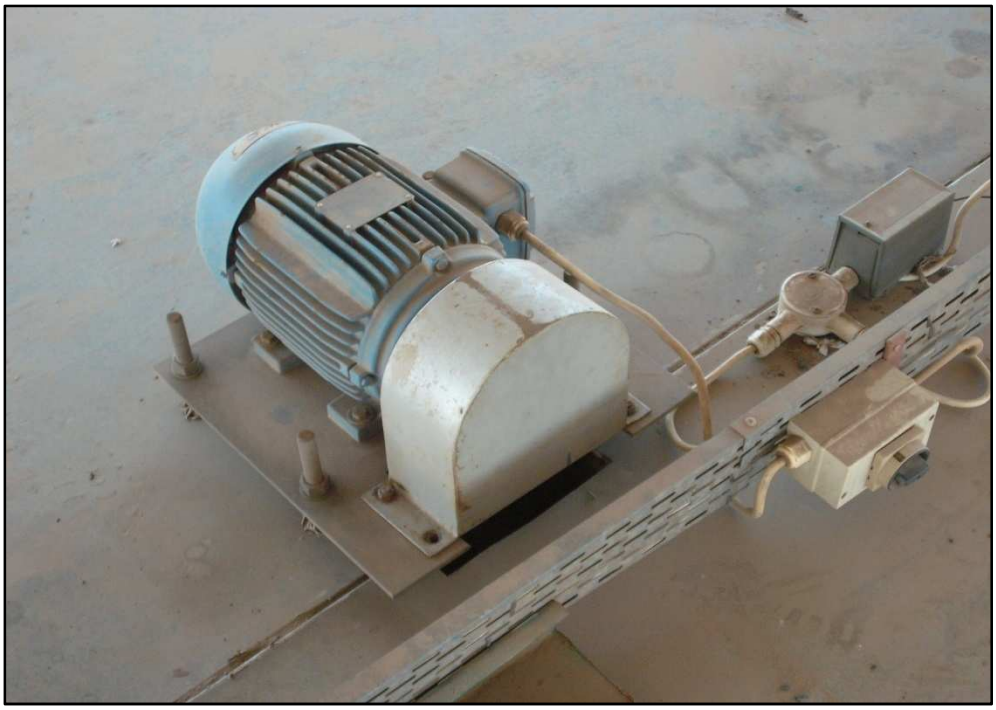

Figure 4-15 Electric motor of main fan (Fan-belts covered by steel box)

Source: M-Pak Musina

Figure 4-16 Main fan on support beams (Viewed from down-stream side)

Source: M-Pak Musina

The outlet fan (400 mm in diameter, 6 blades at 16°-blade-pitch) is placed on top of the roof near the gas burner tube. Its 0.37 kW electrical motor (supplied by the fan manufacturer) is directly coupled to the blades. Both the main and outlet fan contain internal hubs that are impervious to flow. Fans are modelled as two-dimensional circular objects. The direction of flow of both fans is shown in Figure 4-17. Airpak 2.1 requires the fan characteristic curve in terms of the static pressure plotted against the volume flow.

Figure 4-18 shows that as the volume flow decreases, the static pressure will increase. The outlet fan is defined as an exhaust fan and the main fan as an internal fan. The accuracy of the fan flow rate used by Airpak 2.1 is directly related to the accuracy with which the fan static pressure is computed. This in turn, depends on how accurately pressure losses in the entire system are modelled. Therefore care should be taken to model all features of the system that contribute to the overall nature of the pressure distribution in the system (Airpak 2.1 Documentation, 2002).

In order to simulate the swirl of the fan, the rotational speed of the fan is required. Airpak 2.1 allows the swirl factor to change as a function of the operating point on the fan curve. This is achieved by specifying the revolutions per minute (RPM) of the fan. Both fans are operating at 1440 r/min. The swirl magnitude (the ratio of the tangential velocity to the axial velocity) can then change as the fan operating point changes on the fan curve (Airpak 2.1 Documentation, 2002).

$$u_\theta(r) = \left[(RPM) \times \frac{2\pi}{60} \times r\right]\frac{1}{20}$$

Equation 4-18

where:

- $u_\theta(r)$ – The velocity in the direction of revolution
- r – The radial coordinate

It is assumed that only 5% of the maximum tangential velocity of the fan is transferred to the fluid.

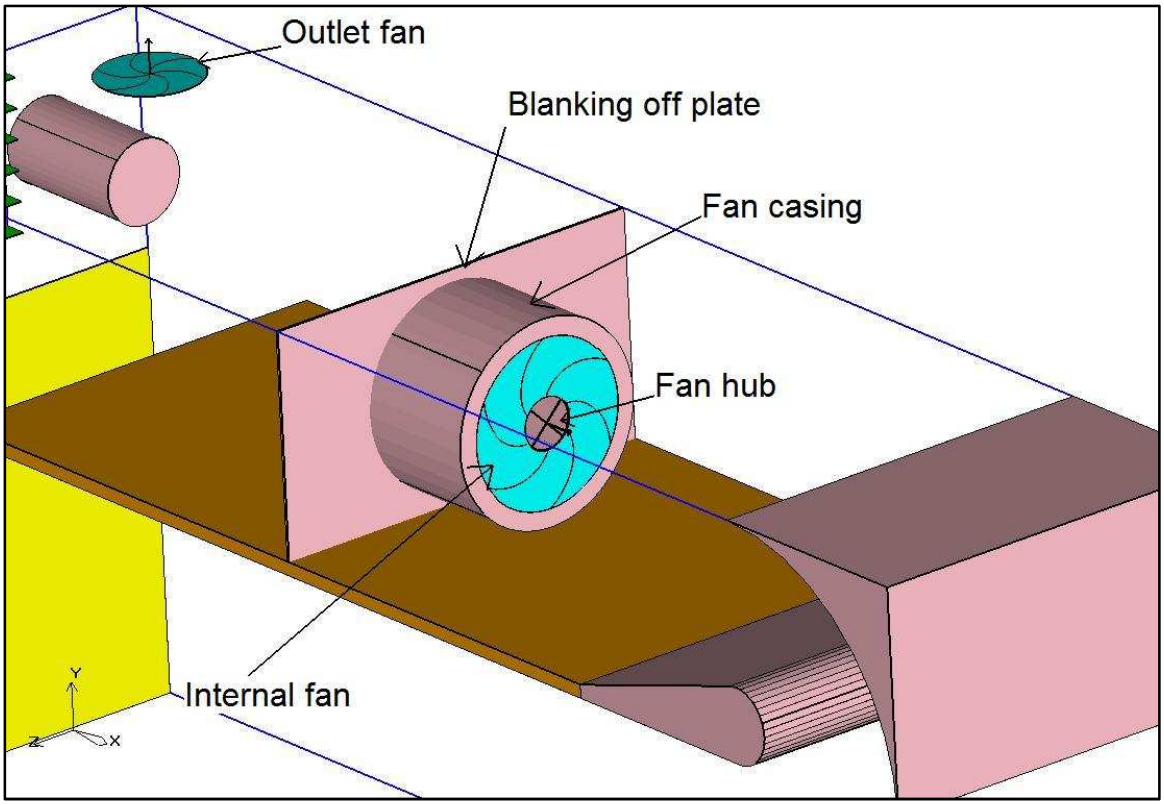

Figure 4-17 Main and Outlet Fan

A hollow block is used to define the fan casing and blanking off plate. Airpak 2.1 defines a hollow block as a three-dimensional region of the model for which only the side characteristics are important. Airpak 2.1 does not mesh or solve for the temperature or flow within the region bounded by the sides of the hollow block. The fan casing creates the three-dimensional aspect to the fan, thus presenting a more accurate model of the real world fan. The blanking off plate is there to stop the air from just circulating around the fan.

The relationship between volumetric flow rate and the pressure drop across the fan (static pressure) is described by the fan characteristic curve. The fan curves below show the static pressure versus the volume flow rate. This range of fans is ideally suited for moving large volumes of air against low and medium pressures (Donkin, 2009).

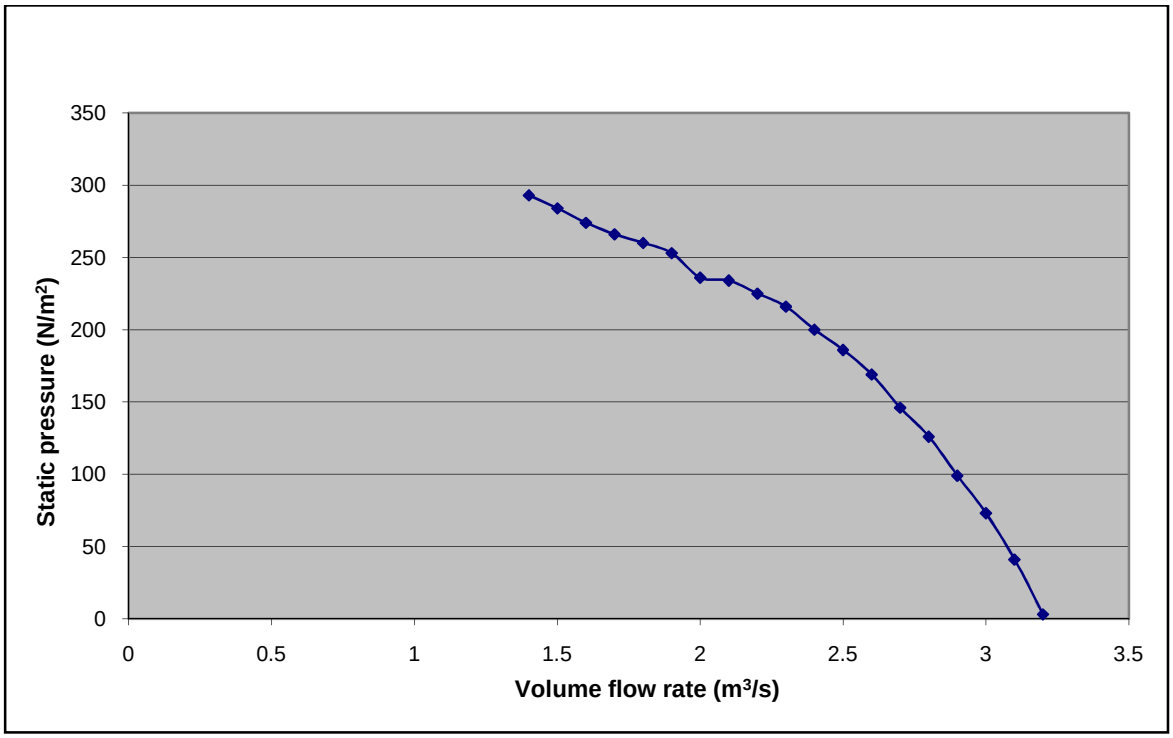

Figure 4-18 Characteristic fan curve of main fan

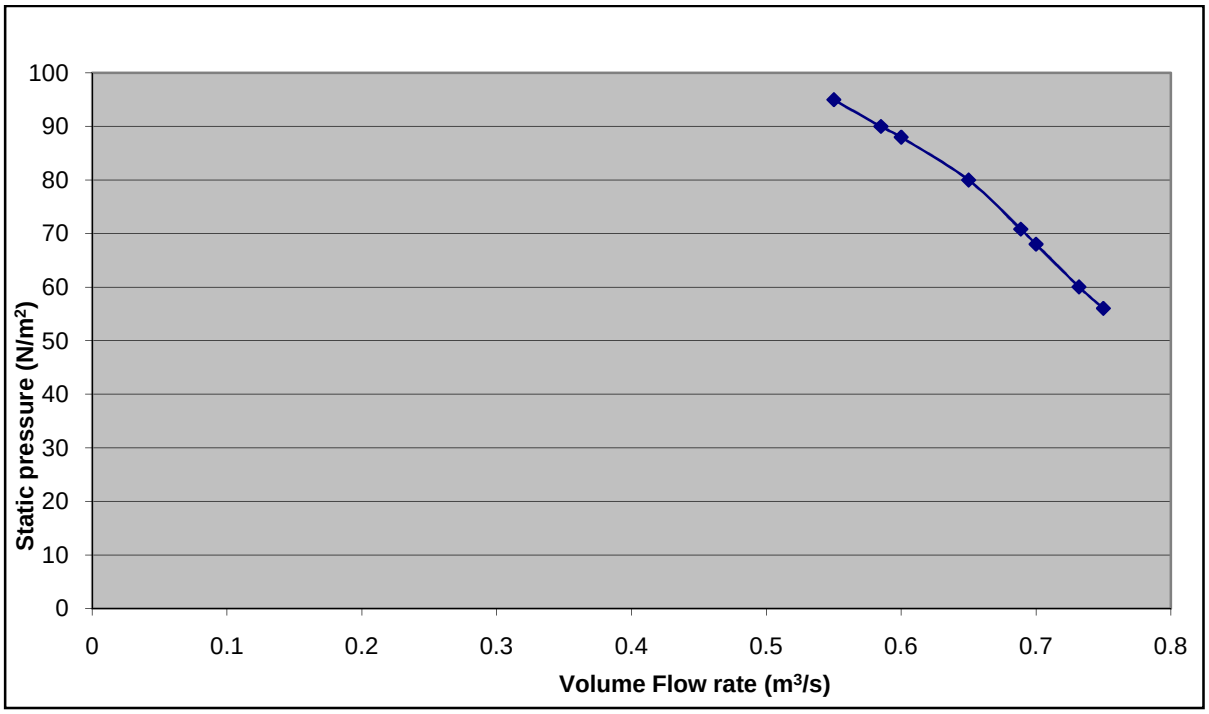

Figure 4-19 Characteristic fan curve of outlet fan

4.5.10 Turning vane and flow diverter

Turning vanes and flow diverters can be seen as some form of ducting to create a certain uniform flow pattern in the dryer.

'A vortex can be qualitatively described as circulatory flow about an axis. The centrifugal force acting radially on the particle must be countered by the pressure forces on it to remain at a constant radius with respect to the origin. When air flows around a bend, vortices with stream-wise axes are initiated by the sidewall boundary layers. The slow-moving air in the side–wall boundary layers, however, will not possess sufficient centrifugal force to balance the pressure gradient force imposed by the main stream, and will create secondary flow as illustrated in Figure 4-20' (Wallis, 1961, p. 78).

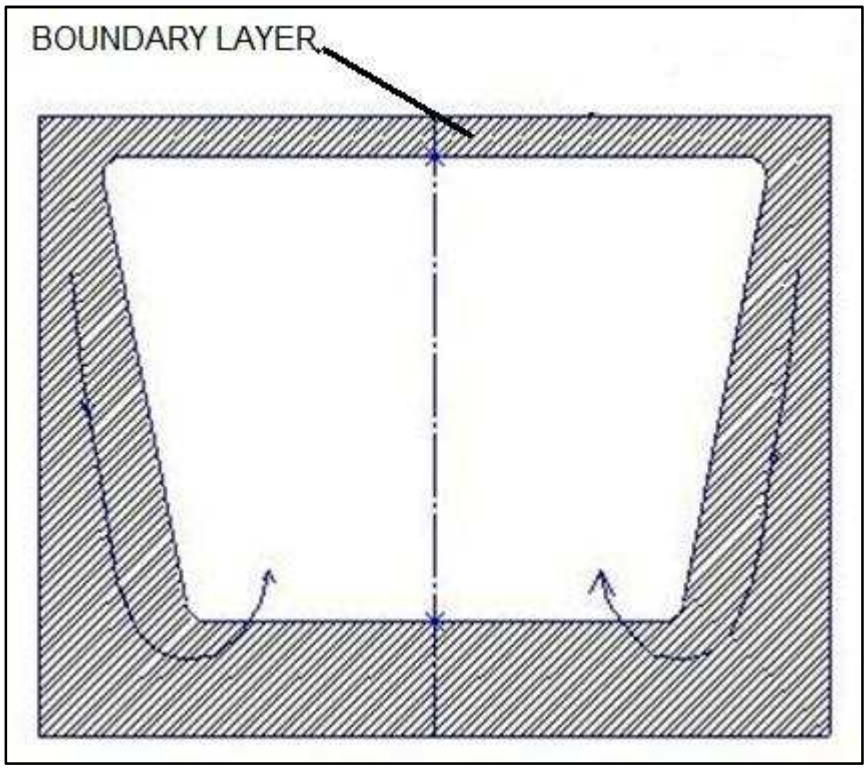

Figure 4-20 Secondary flow near the sides of the walls

Source: Wallis, 1961

'Turning vanes are frequently fitted to corners as a means of reducing the separation losses (See Figure 4-21). These vanes multiply the number of secondary flows present and reduce their individual magnitude. This creates a secondary flow problem, which is by no means negligible' (Wallis, 1961, p. 79).

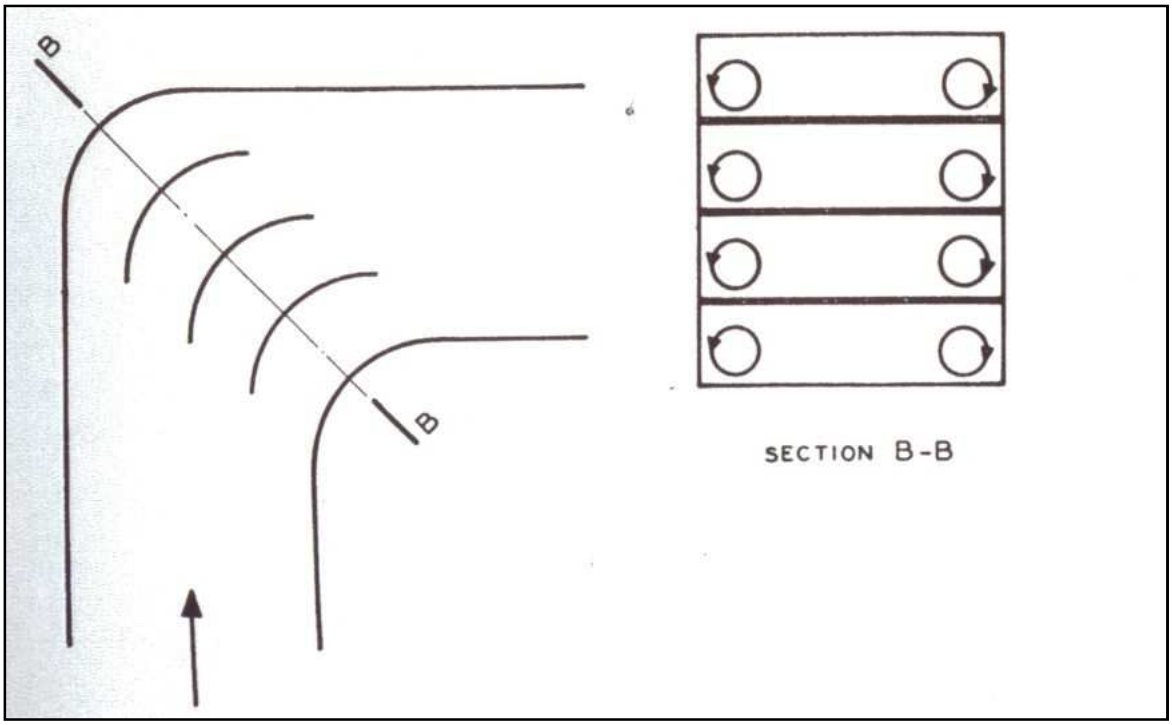

Figure 4-21 Secondary flow created by inserting vanes at a corner

Source: Wallis, 1961

A duct loss can be defined as the mean loss of the total head sustained by the stream in passing the specific item of ducting. The losses are due to the following factors (Wallis, 1961):

- Skin friction. This parameter determines the losses due to fluid shear stresses, when the boundary layer is attached to the duct walls.
- Eddying or separated flow. These losses have their origin in the random large-scale turbulence, which rapidly absorbs more and more of the free stream energy as the region of the separation expands.
- Secondary flow. Secondary flow leads to momentum losses. A portion of the stream wise momentum of the main flow is transferred to the secondary flow and finally dissipated as turbulence and heat.
- Discharge losses. In an open circuit duct system, the dynamic head of the air leaving the system is a loss, which the fan must overcome.
- Losses can result from poor joint connections; these may considerable proportions when insufficient care is taken in fabricating and assembling the duct.
- The main concern is with the loss of the total head in the stream wise direction.

‘Losses from 30-50% of the mean dynamic head downstream can occur in the duct when a sudden contraction is built in (See Figure 4-22). The free area ratio is the main variable, playing a role in these losses. Provided the flow is turbulent

upstream of the contraction, the variables of the inlet velocity distribution and Reynolds number have very little influence on the duct losses' (Wallis, 1961, p. 90).

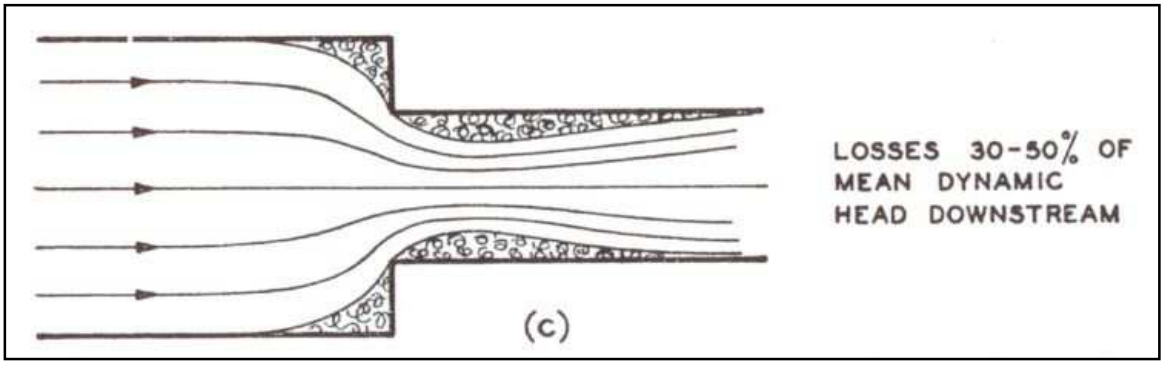

Figure 4-22 Losses due to sudden contraction

Source: Wallis, 1961

Losses from 60-70% of the mean dynamic head downstream at the inlet of a duct (fan inlet) can occur (See Figure 4-23). These losses can be contributed to the greater curvature of the inflowing streamlines, which leads to larger regions of separation. The second reason for the losses is the boundary layer, which is definitely laminar at the lip of the inlet. This results in a relatively large initial region of separation (Wallis, 1961).

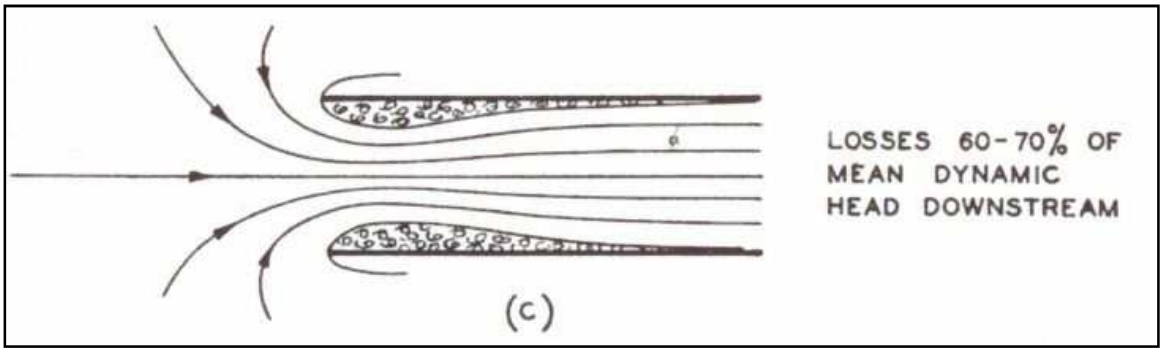

Figure 4-23 Losses that can occur at the inlet of a fan

Source: Wallis, 1961

'The flow in a corner will create streamlines at the inside corner which will first converge and then diverge. The opposite is happening at the outside corner. Since diverging streamlines signify flow retardation, the regions of rising pressure are self-evident. The presence of sidewalls produces secondary flow and the low energy air is swept from the sidewall boundary layers into the inner wall region of separation. When the sidewall boundary layers are thin, the out of balance between the centrifugal and pressure forces is confined to relatively small amount of the fluid and the secondary flows are at a minimum. Flow does not re-attach to the inside duct wall until it has progressed an appreciable distance

downstream of the 90° corner. Turning of the flow continues right up to this reattachment point. When however the inner and outer walls of the corner of a rectangular cross section are suitably shaped, the wall pressure gradients can be adjusted as to keep separated flow to minimum. Since the inner wall is the more critical, an increase in the radius of the curvature of this wall is beneficial' (Wallis, 1961, pp. 100-101).

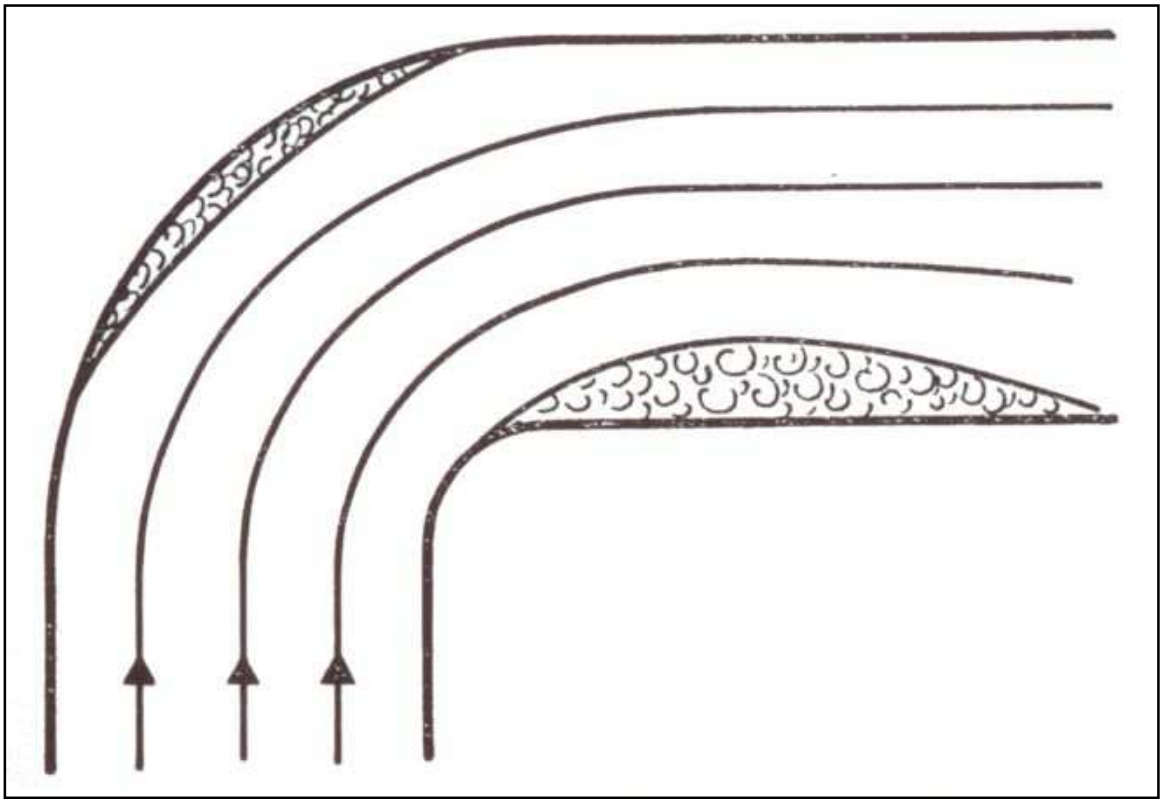

Figure 4-24 Region of separation in right-handed corner

Source: Wallis, 1961

With a non-uniform distribution of velocity at the inlet and with the higher velocity on the side adjoining the inner wall of the rectangular duct bend the losses are higher compared to a uniform velocity distribution entering the corner. This is due to the greater loss of total head in the region of separated flow (See Figure 4-24). Experiments have shown that the secondary motions initiated in a corner persist for large distances downstream. With the re-attachment of the flow to the surface just downstream of the outlet, the velocity distribution fairly rapidly reverts to approximately that normally found in uniform ducting (Wallis, 1961).

The aspect ratio is where the width of the duct is divided by the height of the duct. Higher aspect ratio in a rectangular duct decreases the secondary flow in strength and size. On the other hand, with increasing the aspect ratio, there is an increase in the ratio of wetted area to cross-sectional area and this leads to a rise in skin friction forces. Coupled to this definition is the radius ratio of a bend. This

is the mean radius of curvature, divided by the height of the duct. Experimental data obtained by Wallis (1961) show that low losses can be obtained with high aspect and radius ratios. For practical reasons it is not always possible to obtain these high values. When a sharp corner of small aspect ratio is unavoidable, vanes may be fitted as a means of reducing the corner loss. These can be considered either as highly cambered aerofoils that deflect the flow or as solid surfaces that divide the corner into a number of air passages possessing favourable aspect ratios. The performance of vanes can however be influenced where the angle of the flow relative to the leading edge of a corner edge could lead to losses due to the leading edge separation. Excessive number of vanes can lead to a large total drag force profile in the corner. When a set of corner vanes is to be designed, the aspect ratio of the passage at inlet should be at least six (Wallis, 1961). The aspect ratios of the various dryer configurations were calculated in Appendix 10.3.

With a non-uniform velocity distribution and the assumption that the inner portion of the bend is more critical, vanes distribution could be set closer at the inner region of the bend. This creates the best solution where the performance of the vanes is increased without increasing the number of vanes and thus the total drag force in the corner. The lowering of the loss in a corner system, could lead to a large increase in the mean duct velocity (Wallis, 1961).

4.5.11 Flow diverter and turning vane created in Airpak 2.1

The flow diverter is defined or modelled by using a hollow block to divert the flow around the sharp corner of the original false ceiling. It is made 0.6 mm Chromadek plate that is internally supported by struts to create its round shape at the corner (See Figure 4-25). One has to remember that walls and the false ceiling are built by attaching pre-manufactured insulation panels to each other. The manufacturer at the time could only build a panel with a maximum width of 0.865 m. The flow diverter's dimensions were chosen in such a way that a complete single unit could fit onto one panel. The angle of 13° between the flat sheet of the diverter and the false ceiling panel is based on the size of the flow diverter used by Adams and Thompson (1985) illustrated in Figure 2-6. This feature can easily be installed into already existing dryers.

The turning vane has a radius of 0.87 m. The vane is also manufactured of 0.6 mm Chromadek sheet that is hold in place by cover strips connected to the walls of the dryer (See Figure 4-26). The size or radius of the turning vane is based on the maximum available sheet width at the time of construction and the distance between the false ceiling and the roof.

Figure 4-25 Side view of flow diverter showing supporting struts

Source: M-Pak Musina

Figure 4-26 Turning vane (Viewed from downstream fan position)

Source: M-Pak Musina

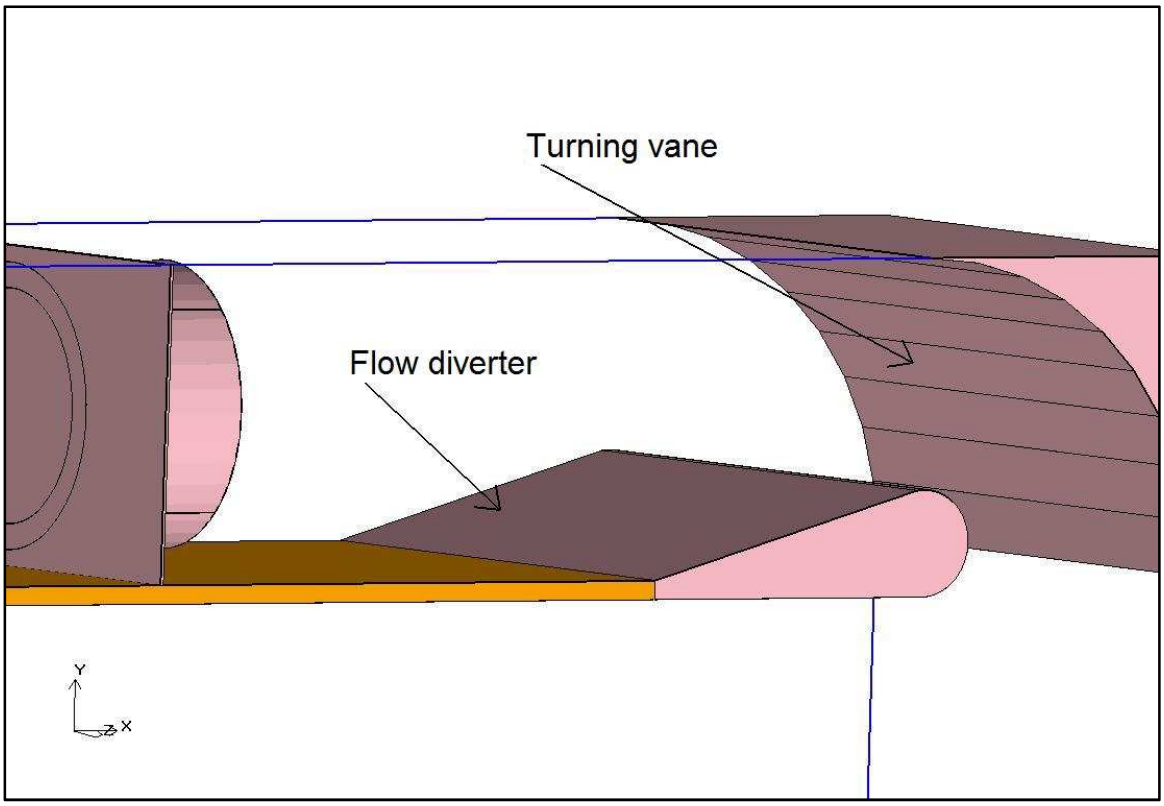

Figure 4-27 Flow diverter and turning vane placed on product inlet side

4.5.12 Trolleys and trays

Trolleys are steel frames on which the trays are placed. The trolleys used in the food drying industry are expensive relative to the other components that make up the whole drying process. For this reason the dimensions of the dryers built in Musina, were based on accommodating the old trolleys used in the previous dryers (See Figure 4-28). The dryer is built in such a way as to have the smallest gaps possible between the trolley, floor, false ceiling and side walls. One still has to consider the tolerances that must be allowed for the easiest and timeliest construction possible. The trolleys were modelled as hollow blocks in the Airpak 2.1 program. The wheels of the trolleys are modelled as square blocks. The is a valid assumption due to the fact that the mesh sizes created for this project are of such dimension that they would not in any case accurately capture the curvature of the wheels. In this case a refined grid around the wheels would put a large strain on the computational time without improving the quality of the results (See chapter 2.2.1). This square block wheels creates a better hex mesh, which in turns leads to more accurate results in the flow domain. Less time and computational effort is required in creating a simpler mesh. Keeping in mind that the main focus is the uniform velocity distribution over the entire drying domain,

the second simplification was to take out the sliding rails on which the trays rested.

Figure 4-28 Tray covered with a plastic net, placed on trolley slides

Source: M-Pak Musina

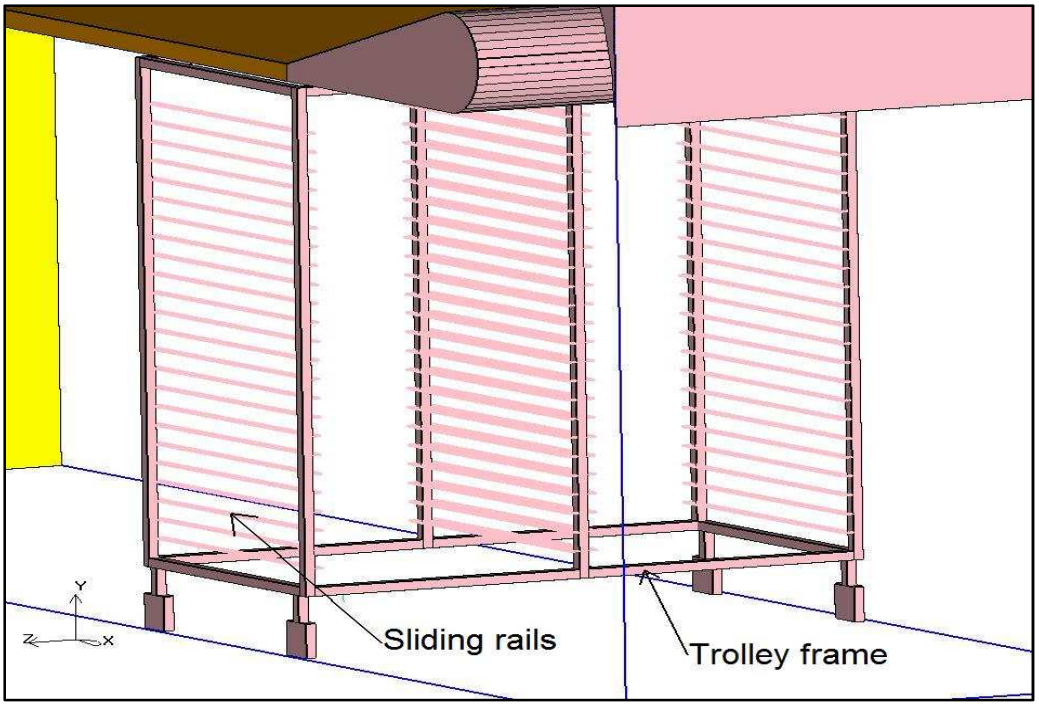

Figure 4-29 First trolley frame at product inlet side

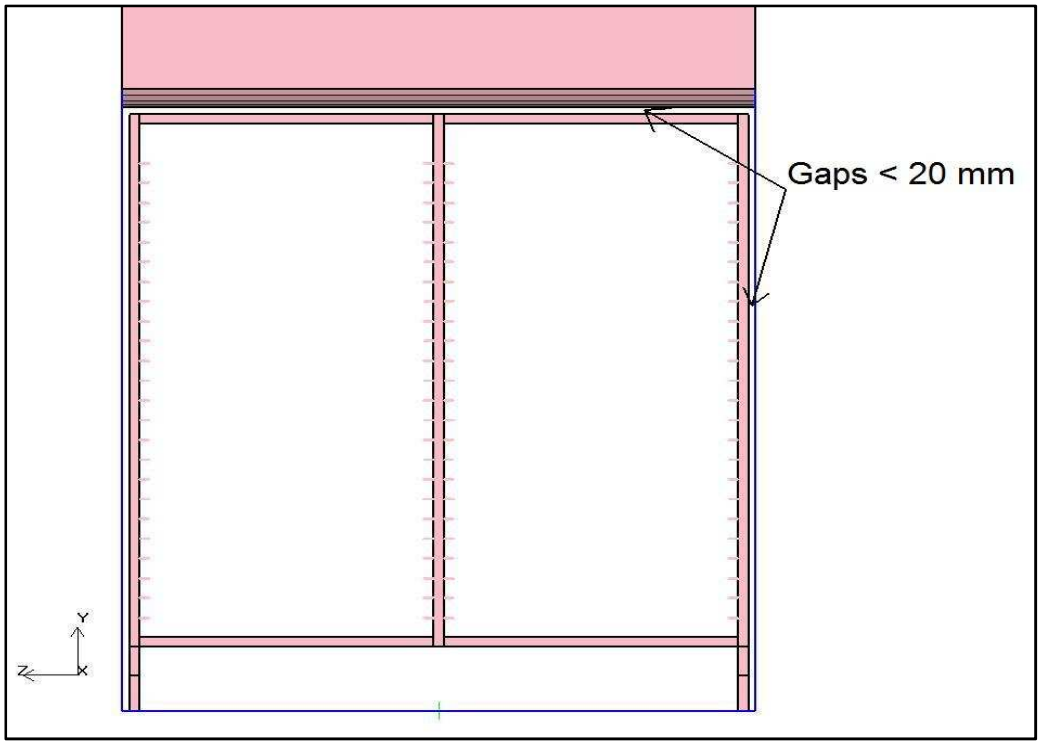

Figure 4-30 Gaps between trolleys, sidewalls and false ceiling was kept below 20 mm

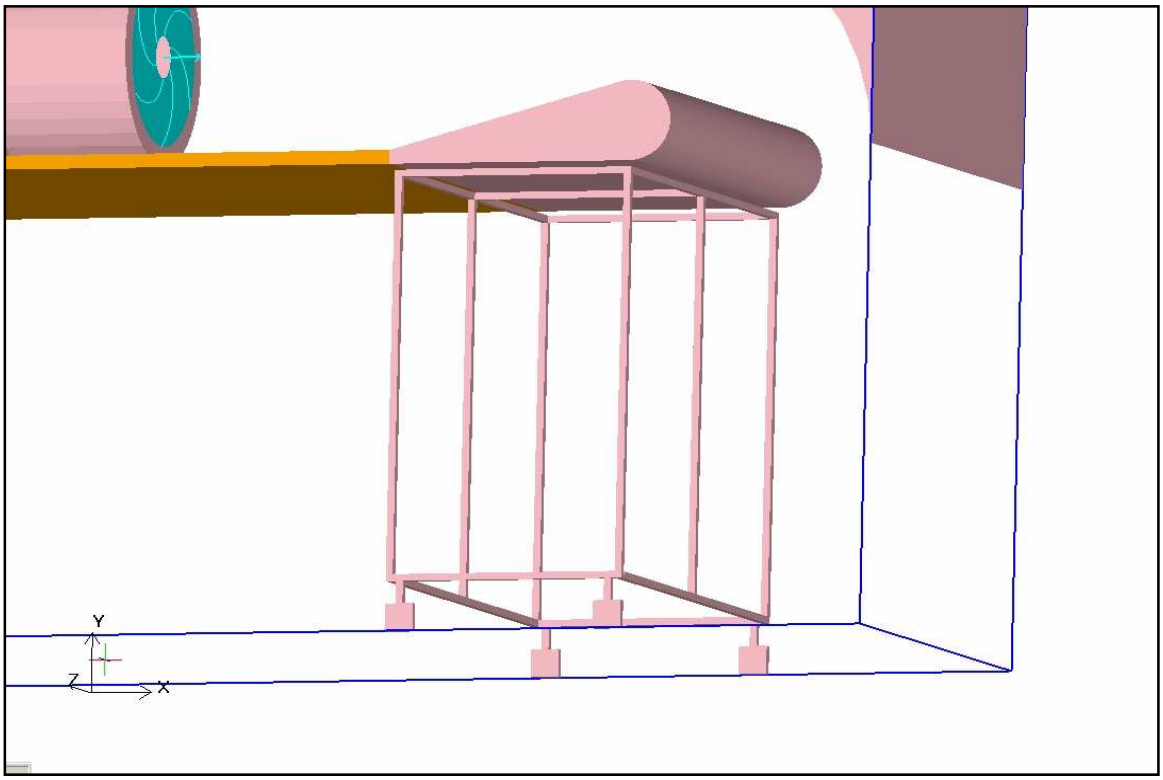

Figure 4-31 Simplified version of trolley used in CFD analysis

The trays are manufactured from rectangular stainless steel frames. Plastic nets are tightly pulled over the frames. The nets are made from hard polymer plastic strands, 2 mm in diameter. The strands forms 5 × 5 mm square holes with a free area ratio of 0.9. The nets are modelled as resistances. The trays are spaced 50 mm apart and rest on the sliding rails of the trolley frame. Once again the geometry of the trays was simplified to save in computational effort by leaving out the tray frames. This decreased the meshing elements around the trays considerably.

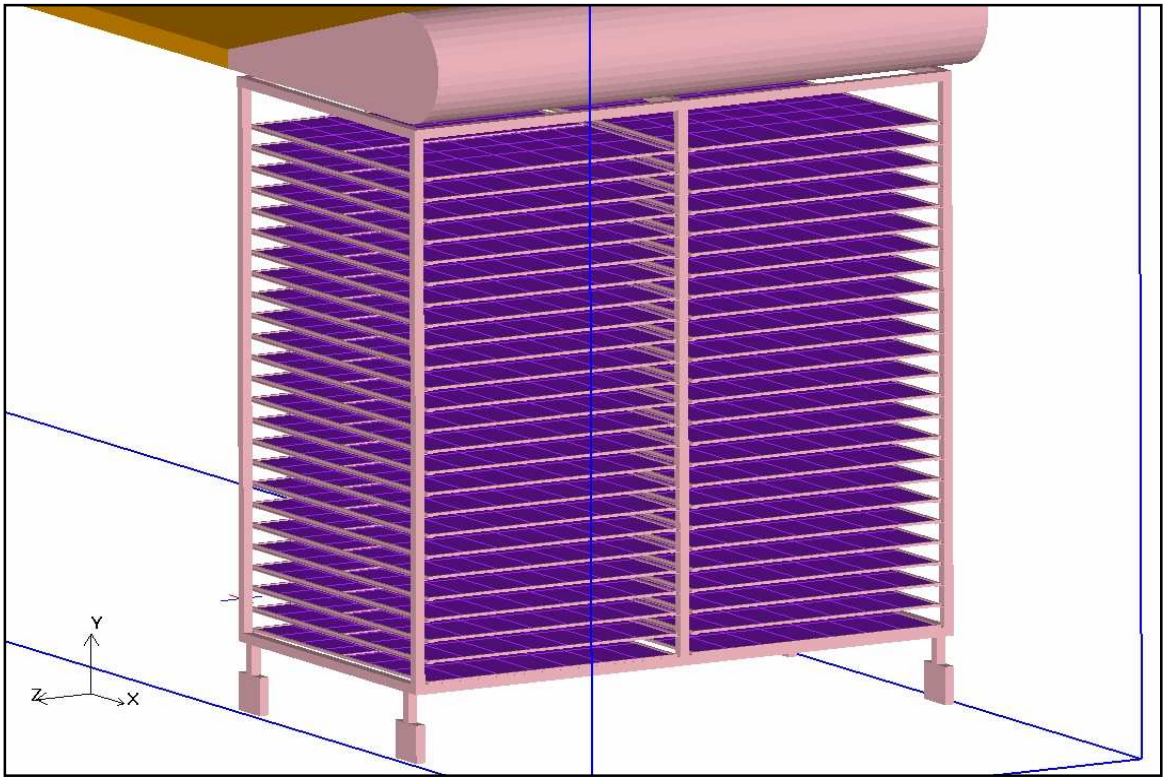

Figure 4-32 Complete trolley construction

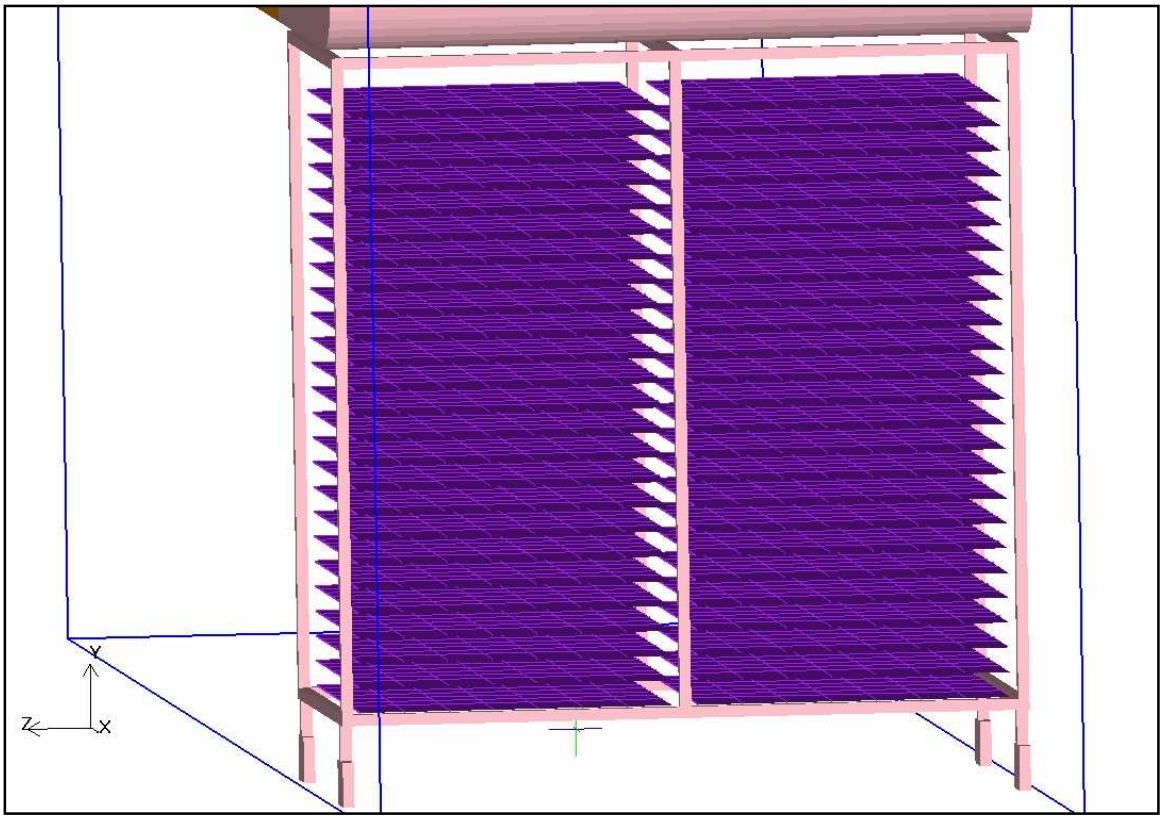

Figure 4-33 Simplified version of trolley construction used for CFD analysis

4.5.13 Mangoes

The average mango slice is about 100 mm in the length, 25 mm in width and height. The mango slices are preserved by chemical treatment, which stops any bacterial growth on the surfaces. Due to the high water content and the chemical treatment, the surface of the mango slices is very smooth and slippery. Roughly 5 kg of slices are evenly spread out per tray. The net surfaces are treated with a chemical that prevents the mangoes from sticking onto them. The nets of the trays on which the mangoes are placed sags in time. This results in the mango pieces sliding to the middle of the net. The mango slices can be simplified as hollow blocks on the trays. It would take considerable time and computational effort to model the mango slices, which varies in size, as individual parts. The purpose of this analysis is not to study the detailed turbulent flow over the mango slices but the uniform velocity distribution over the entire drying domain.

In discussions with Dr. Danie de Kock from Qfinsoft (Pty) Ltd (2005) and Michael Slack of Fluent Europe Ltd (2007), both mentioned that the mangoes, trays and trolleys could also be modelled as one three-dimensional resistance filling the entire drying domain.

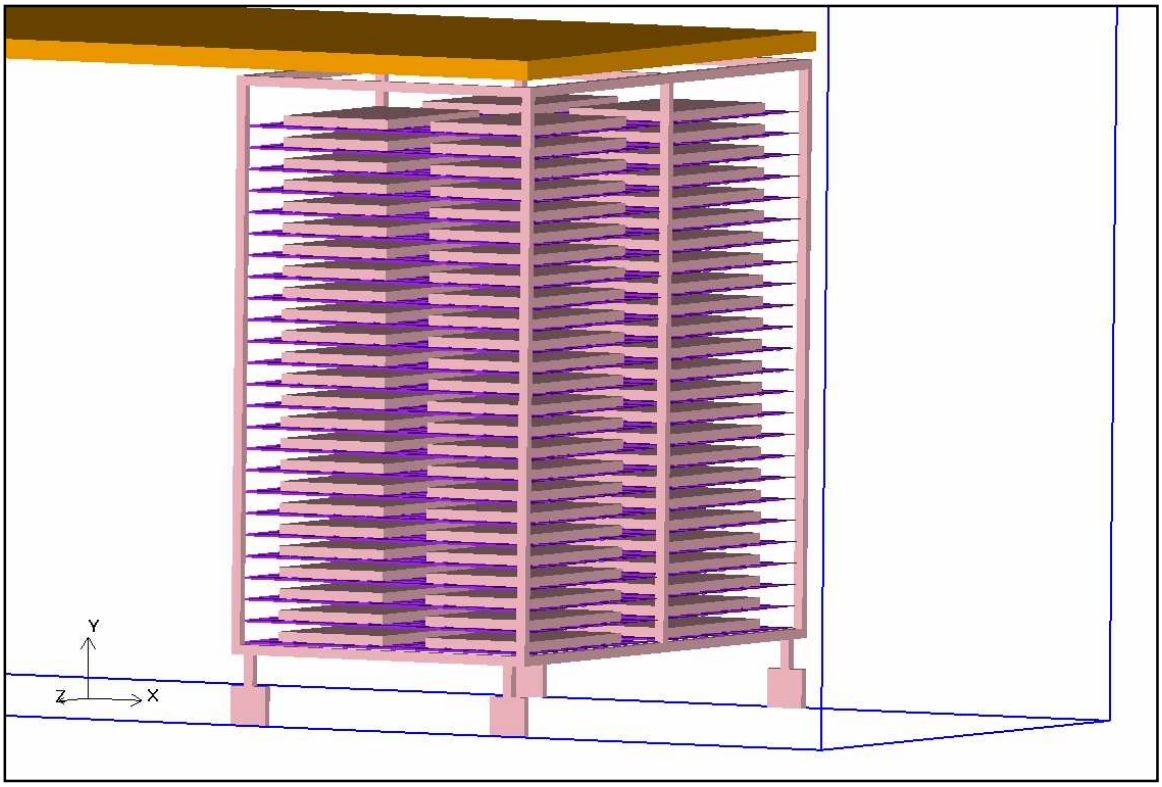

Figure 4-34 Displaying the mango blocks on the trays

In 2006 when M-Pak Musina was expanding their drying facilities, new trays that could be stacked like crates on each other were introduced. This was made of a hard plastic and the tray's structure was of such nature that no sagging occurred when the mango slices was put onto it. These trays were easily cleaned and maintained. The only question that remained was how it would influence the airflow over the mango slices.

4.6 Meshing, turbulence models and variables of CFD simulation

The mesh consists of discrete elements located throughout the computational domain. Within each element, the equations that govern the flow and the heat transfer are solved. A good quality mesh is one of the main factors that will result in an accurate solution. If the mesh is too coarse, the resulting solution may be inaccurate. One also has to guard against using an overall mesh that is too fine. This will result in a solution that takes up too much time and computational effort. If the mesh is too coarse in some areas and too fine in others, the solution may not converge at all (Airpak 2.1 Documentation, 2002).

Airpak 2.1 uses an automated mesh generation procedure. This has the advantage for design engineers that use this program on a normal desktop.

Without using too much computational effort, they can easily and in a timely manner create a suitable model. The drawback is that one has only got limited input in the parameters that control the mesh generation, compared to other meshing programs like Gambit.

Mesh elements must be small enough to capture the thermal and velocity gradients that usually occur near the boundaries of an object in a certain coordinate axis. Using the same free stream velocity (U) at the outlet of the fan of 16 m/s in section 4.2, the placement of the first grid point can be estimated by approximating the skin friction coefficient $\left(\overline{C_f}\right)$ (De Kock, 2004):

$$\overline{C_f}/2 \approx 0.039 Re_D^{-0.2}$$

Equation 4-19

The friction velocity (u_τ) is determined by:

$$u_\tau = U\sqrt{\overline{C_f}/2}$$

Equation 4-20

The backed out required distance from the wall can be determined by using the wall function (y_1):

$$y_1 = 50\,\nu/u_\tau$$

Equation 4-21

where:

$\boldsymbol{\nu}$ – The kinematic viscosity (m^2/s) (See Table 10-1)

It is good practice to have at least ten grid points in the log law region and to use stretched quadrilateral or hexahedral cells for economic purposes (De Kock, 2004). One has to remember that most of the $k-\varepsilon$ turbulence models are not valid in the near wall region. Near-wall functions are used to supply boundary conditions for turbulent flows.

4.6.1 Mesh quality

A good mesh requires proper resolution, smoothness, low skewness, and an appropriate number of elements (Airpak 2.1 Documentation, 2002). According to Airpak 2.1 the expansion ratio from one mesh element to the next should be kept in the range of between 2 and 5. Other CFD programs like CFX and Fluent use an aspect ratio of 1.2 in critical areas. It is better to use hexahedral compared to tetrahedral meshes in reducing computational effort and obtaining accurate results. Aligning faces that are nearly aligned can also lower the aspect ratio.

For any CFD project an iterative process is used in creating a suitable mesh. The first mesh is a coarse one, just to capture the necessary geometry and satisfy the minimum internal default meshing laws used by Airpak 2.1. It gives a rough guideline of where to refine the mesh in order to get accurate results. The mesh is refined until the results are independent of the grid count. The goal of the project determines if the results obtained from the simulation is accurate enough. There is no need to over refine the mesh near the mango blocks when the object of this exercise is to determine the velocity distribution over the entire drying region.

Airpak 2.1 evaluates the mesh quality in terms of three aspects:

- Element aspect ratio in terms of a hexahedral element is the ratio of its shortage edge length to its longest edge length. The best elements are those with an aspect ratio close to 1. An aspect ratio less than 0.15 indicate a distorted element.
- The face alignment index shows whether the faces of two elements are in alignment of each other. Adjacent mesh faces that are not aligned can result in long narrow elements. A value of 1 indicates perfect alignment. Values less than 0.15 indicates a severely distorted mesh.
- Extremely small elements (on the order of 10^{-12} or lower) can lead to problems in the Airpak 2.1 solver. It is therefore important to check the minimum volumes in your mesh.

4.6.2 Calculating the solution

Airpak 2.1 uses a control-volume-based technique to convert the governing equations to algebraic equations that can be solved numerically. This control volume technique consists of integrating the governing equations about each control volume, yielding discrete equations that conserve each quantity on a control-volume basis. The equations will, in general, be non-linear with respect to the variables that have to be solved. These equations are then linearised, resulting in a sparse coefficient matrix. For scalar equations, Airpak 2.1 solves this linear system using a point implicit (Gauss-Seidel) linear equation solver in

conjunction with an algebraic multigrid (AMG) method (Airpak 2.1 Documentation, 2002).

However, face values are required for the convection terms and must be interpolated from the cell centre values. This is accomplished using an upwind scheme. Upwinding means that the face value is derived from quantities in the cell upstream, or ``upwind,'' relative to the direction of the normal velocity. Airpak 2.1 allows you to choose from two upwind schemes: first-order upwind, and second-order upwind. These schemes are described below.

When first-order accuracy is desired, quantities at cell faces are determined by assuming that the cell-centre values of any field variable represent a cell-average value and hold throughout the entire cell; the face quantities are identical to the cell quantities (Airpak 2.1 Documentation, 2002).

When second-order accuracy is desired, quantities at cell faces are computed using a multidimensional linear reconstruction approach. In this approach, higher-order accuracy is achieved at cell faces through a Taylor series expansion of the cell-centred solution about the cell centroid (Airpak 2.1 Documentation, 2002).

The diffusion terms in the governing equations are central-differenced and are always second-order accurate (Airpak 2.1 Documentation, 2002).

Because of the non-linearity of the equation set being solved by Airpak 2.1, it is necessary to control the change of the variables (Pressure, momentum and viscosity values). This is typically achieved by under-relaxation, which reduces the change of the variables produced during iterations (Airpak 2.1 Documentation, 2002).

4.6.3 Turbulence models used in CFD project

Using one of the eddy–viscosity models (EVM) or Reynolds stress models (RSM) can solve the Reynolds-averaged Navier Stokes (RANS) equation (De Kock, 2004). All turbulence scales are modelled in the RANS models. The EVM uses the Boussinesq assumption whereby the Reynolds stresses are related to the mean flow by the turbulent viscosity (μ_t). It is assumed that the turbulent/eddy viscosity is isotropic when using the above assumption.

The first run of each CFD model was done by using the zero-equation indoor model to obtain results. The results were then used with the two-equation RNG $k-\varepsilon$ model to get more accurate final results. In all the cases using this method there was no need in decreasing the default relaxation parameters to obtain a solution that converges. Airpak 2.1 does not provide the option to obtain results using the more accurate Reynolds-Stress model, as it would be to

computationally expensive and time consuming for a design engineer using a modest computer. All of the final results were obtained by using a laptop computer with 1.86 GHz Intel Pentium(R) processor with 2GB of RAM. Each CFD run required about 10-12 hours solving time with all the residuals being below 10^{-3}.

The indoor zero-equation turbulence model was developed specifically for indoor airflow simulations. It addresses the need of engineers for a simple but reliable turbulence model that can be used with modest desktop computing resources. It uses the following relationship to calculate the turbulent viscosity (μ_t) (Airpak 2.1 Documentation, 2002):

$$\mu_t = 0.03874 \rho v L$$

Equation 4-22

Where:

- v – The local velocity magnitude (m/s)
- ρ – The fluid density (kg/m^3)
- L – Defined as the distance from the nearest wall (m)
- and 0.03874 is an empirical constant.

When using the Two-equation Eddy-Viscosity model to solve the RANS equation the turbulent viscosity is determined from the variables k and ε, where k are the turbulent kinetic energy and ε the dissipation rate of k. Therefore two extra partial differential transport equations have to be solved in order to obtain k and ε (De Kock, 2004).

The RNG $k-\varepsilon$ model was derived using a rigorous statistical technique (called renormalisation group theory). It is similar in form to the standard $k-\varepsilon$ model, but includes the following refinements (Airpak 2.1 Documentation, 2002):

- The RNG model has an additional term in its ε equation that significantly improves the accuracy for rapidly strained flows.
- The effect of swirl on turbulence is included in the RNG model, enhancing accuracy for swirling flows.
- The RNG theory provides an analytical equation for turbulent Prandtl numbers, while the standard $k-\varepsilon$ model uses user-specified, constant values.
- While the standard $k-\varepsilon$ model is a high-Reynolds-number model, the RNG theory provides an analytically derived differential formula for effective viscosity that accounts for low-Reynolds-number effects.

These features make the RNG $k-\varepsilon$ model more accurate and reliable for a wider class of flows than the standard $k-\varepsilon$ model. According to Danie de Kock this model is suitable for complex shear flows involving rapid strain, moderate

swirl, vortices and locally transitional flows. Therefore it is widely used in wide-angle diffusers and room ventilation (de Kock, 2004).

Due to the extra terms and functions in the governing equations and a greater degree of non-linearity, computations with the RNG $k-\varepsilon$ model tend to take 10-15% more CPU time than with the standard $k-\varepsilon$ model.

Aside from the time per iteration, the choice of turbulence model can affect the ability of Airpak 2.1 to obtain a converged solution. For example, the standard $k-\varepsilon$ model is known to be slightly over-diffusive in certain situations, while the RNG $k-\varepsilon$ model is designed such that the turbulent viscosity is reduced in response to high rates of strain. Since diffusion has a stabilising effect on the numerics, the RNG model is more likely to be susceptible to instability in steady-state solutions. However, this should not necessarily be seen as a disadvantage of the RNG model, since these characteristics make it more responsive to important physical instabilities such as time-dependent turbulent vortex shedding (Airpak 2.1 Documentation, 2002).

4.6.4 Definition of variables used in CFD analysis

A short definition of the variables used to evaluate the results is given below (Airpak 2.1 Documentation, 2002):

- Speed $|u|$ is the magnitude of the velocity vector $(\bar{u})$ and is available when flow is computed (m/s)
- Velocity $(\bar{u})$ is the vector quantity for flow velocity and is available when flow is computed (m/s)
- Vorticity $|\omega|$ is a derived scalar quantity representing the magnitude of vorticity $(\bar{\omega})$, which is computed from the velocity variable $(\bar{u})$:

$$\bar{\omega} = \nabla \times \bar{u}$$

Equation 4-23

  Vorticity is a measure of the rotation of a fluid element as it moves in the flow field (s^{-1}) (Fluent 6.3 User's Guide, 2006).
- Mass flow (M) is a derived scalar quantity computed from the velocity field. The flow rate can be computed only on the surface of model objects (typically, a fan, vent, or opening); it cannot be computed for plane cuts or iso-surfaces (kg/s).
- Volume flow (Q) is a derived scalar quantity computed from the velocity field. The flow rate can be computed only on the surface of model objects (typically, a fan, vent, or opening); it cannot be computed for plane cuts or iso-surfaces (m^3/s).

- Angular deviation (θ) is a derived scalar quantity computed from the velocity field. The angular deviation is computed as:

$$cos\theta = \frac{\bar{u} \cdot \bar{d}}{|u||d|}$$

Equation 4-24

Where $(\bar{u})$ is the local velocity vector, $(\bar{d})$ is a reference direction and the angular deviation is presented in degrees (°)

- Pressure (p) is the relative static pressure of the fluid and is available when flow is computed (N/m^2)
- TKE (k) is the turbulent kinetic energy (m^2/s^2)
- Epsilon (ε) is the turbulent dissipation rate (m^2/s^3)
- Viscosity ratio is the ratio of the turbulent (eddy) viscosity to the dynamic viscosity (A fluid property). The eddy viscosity (μ_t) has the same dimensions as dynamic viscosity (μ), but is not a fluid property, varying instead with flow conditions and the geometry (White, 1991)

5 Results of CFD simulation

Solving is an iterative process where the solution is refined until the required results are obtained. The first step would just be to create a simulation model with a coarse mesh, using a simple but robust indoor-zero turbulent equation and a first order discretisation scheme to solve the velocity field. A weighted body-force discretisation scheme was used in solving the pressure distribution. This will save time and computational effort but will not give accurate results. The focus will mainly be placed on the general flow pattern and where to refine the mesh locally near critical objects.

The second stage would be to run the model with the more accurate RNG $k-\varepsilon$ turbulent model. The mesh will globally be refined near all the objects surfaces to obtain the necessary grid points in the log law region (overlap layer). Using a first order scheme relatively quick and accurate results were obtained. With the computational resources available it would take much longer in solving the model using a second order discretisation scheme. The results obtained in using a second order discretisation scheme would not give a better picture or understanding in terms of the goal set for this project. With the two-equation turbulent model being so robust in terms of convergence, there was no need in the changing the default settings of the relaxation factors. During the second stage the first initial results (using the coarse mesh) were used as starting point. There were three principle ways in checking whether the solution converged:

- The first step was to check the solution residuals. Solution residuals measure the error or imbalance in the conservation equations that Airpak 2.1 solves. The residuals displayed by Airpak 2.1 are scaled using an appropriate scaling factor for the particular residual. When all applicable solution residuals (e.g. flow, energy, turbulence, species) are less than or equal to their specified convergence criteria, the solution will be considered converged (Airpak 2.1 Documentation, 2002). There are no universal metrics for judging convergence. Residual definitions that are useful for one class of problem are sometimes misleading for other for other classes of problems. For these models, the default convergence criterion is sufficient. This criterion requires that the scaled residuals decrease to 10^{-3} for all equations except the energy equation, for which the criterion is 10^{-6} (Airpak 2.1 Documentation, 2002). Other CFD packages like CFX suggest using a residual criterion of 10^{-4} for industrial problems.
- A second helpful way is to set up a point monitor to check the convergence or stabilising of a physical quantity or variable in a critical region. For example the velocity field in the vortex region near the false ceiling at the product inlet side.
- The overall momentum and mass balance. The difference between the mass in and out flow should be zero. Due to discretisation errors the CFD models' mass balance are very close to zero.

5.1 Results of unmodified dryer using a coarse mesh

The focus will be placed on where to refine the mesh for the more accurate second stage run of the model. The model has the same configuration as the dryer mentioned in paragraph 3.3 for the first experimental set up. The coarse mesh consisted of 547,276 elements and 576,747 nodes (See Figure 5-1). The purpose of this model is to indicate the regions to focus on in terms of where the most severe swirl is taking place.

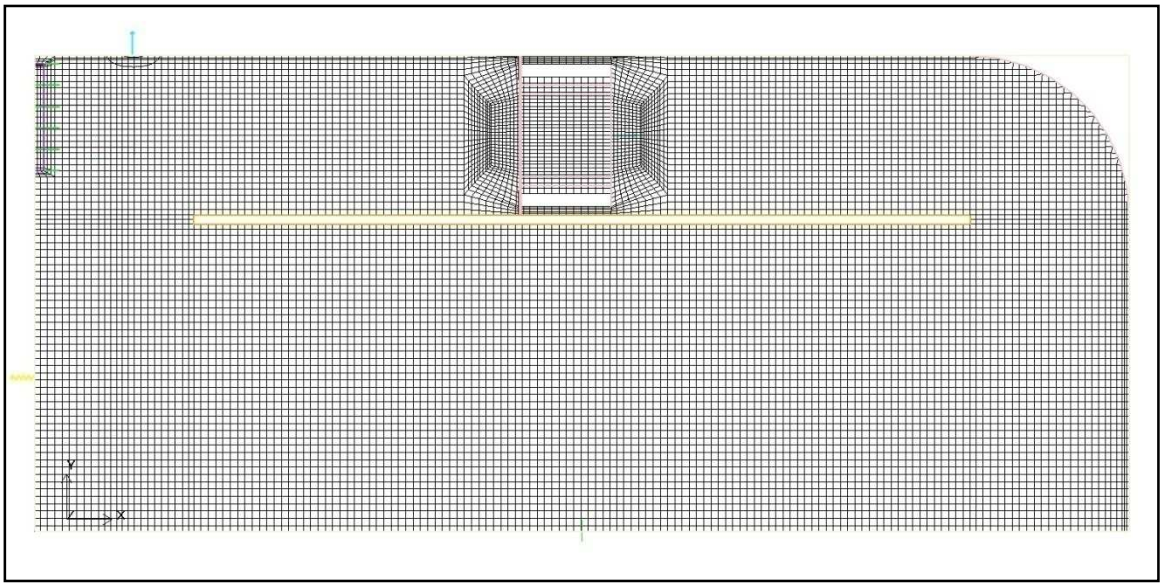

Figure 5-1 Coarse mesh used for first analysis on unmodified dryer (XY-plane)

In Figure 5-2 one can clearly detect the vortexes that are form at the tips of the false ceiling. Due to the vortexes, the vector path of the fluid is not parallel with the X-axis. This means that the angle of attack of the fluid on the different trolleys will vary along the drying chamber. The velocity increases from the false ceiling downwards to the floor. It shows why it will be necessary to test the theory of inserting a flow diverter at the end of the false ceiling. If the air path can be created in such a way not to form a vortex at the tip of the false ceiling the velocity distribution across the plane of the drying region would improve.

In Figure 5-3 the air forms a large vortex on the upstream side of the main fan. This is to be expected due to the sharp corner at the tip of the false ceiling. In the second more refined stage of running the Airpak 2.1 model the grid will first be refined between the roof and the false ceiling. This will create a better picture or understanding of the air movement between the inlet vent and the main fan.

Figure 5-4 show the two vortices formed on the downstream side of the main fan. It was found in previous dryers that have been built that the vortices in this region would add to the problem of the air just circulating around the main fan.

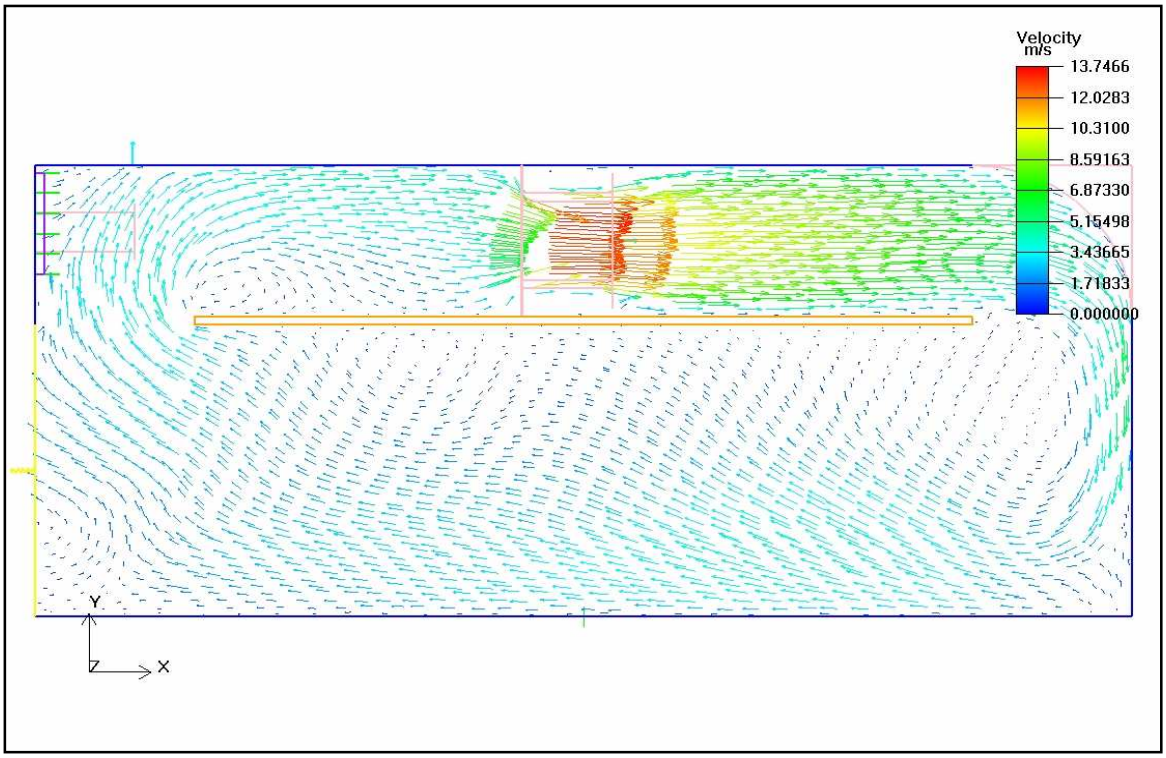

Figure 5-2 Velocity field at centre XY-plane

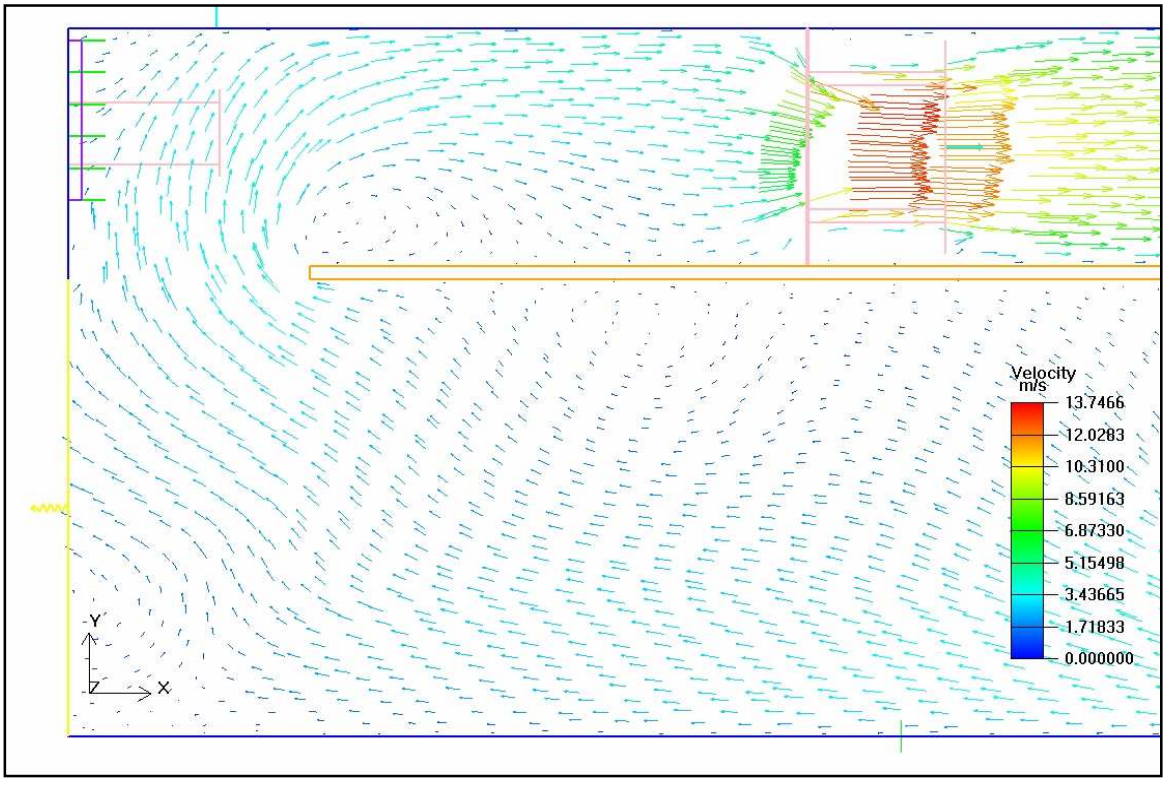

Figure 5-3 Detail of velocity field at product outlet side

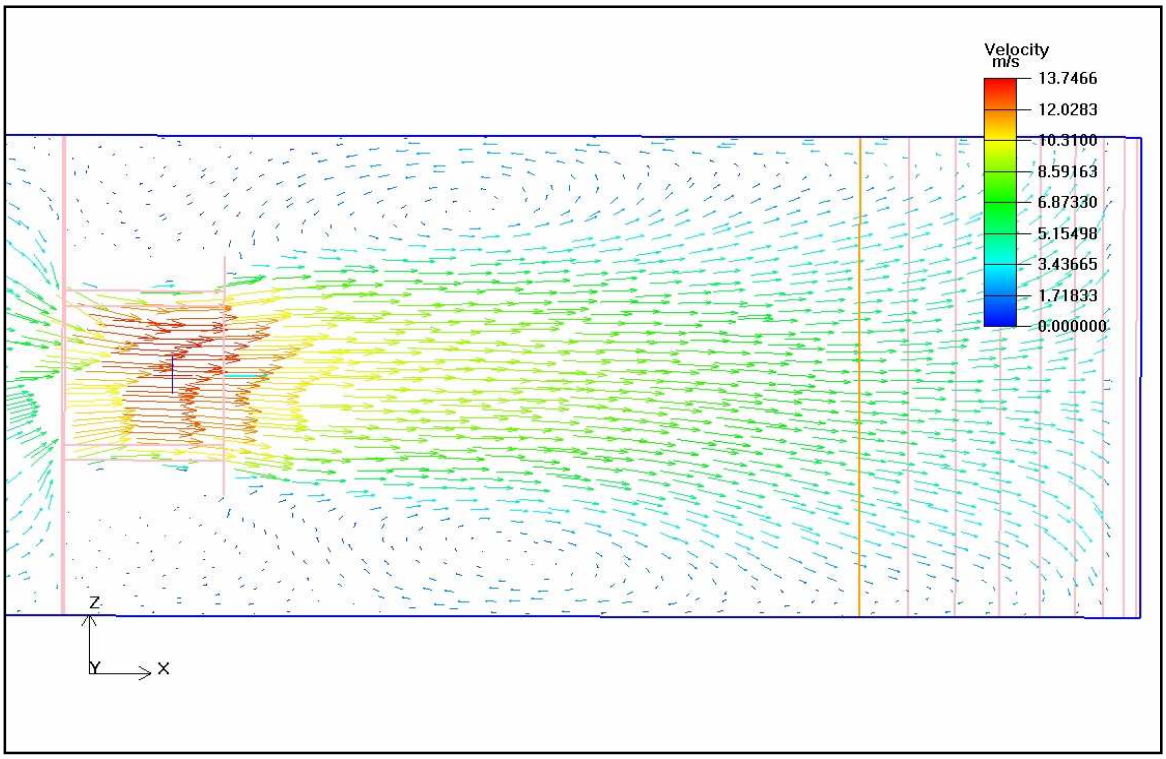

Figure 5-4 Detail of velocity field at fan centre in the ZX-plane

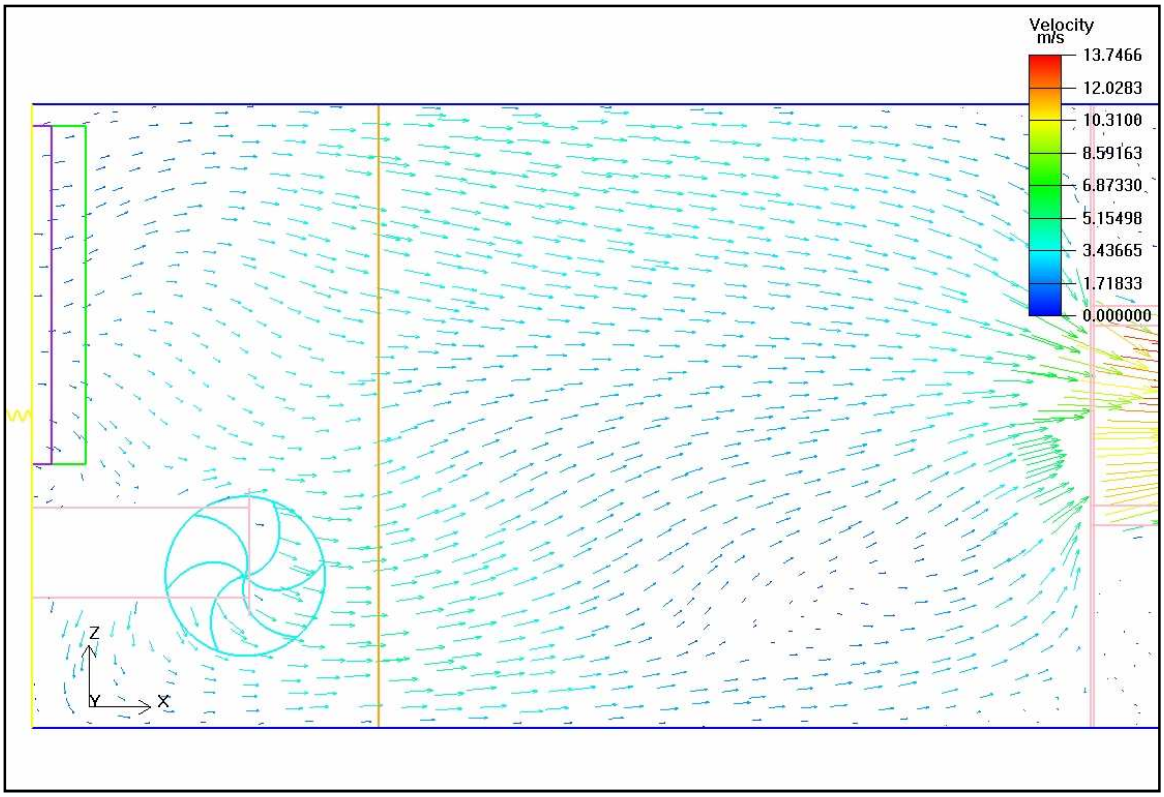

Figure 5-5 Detail of velocity field at fan centre in the ZX-plane

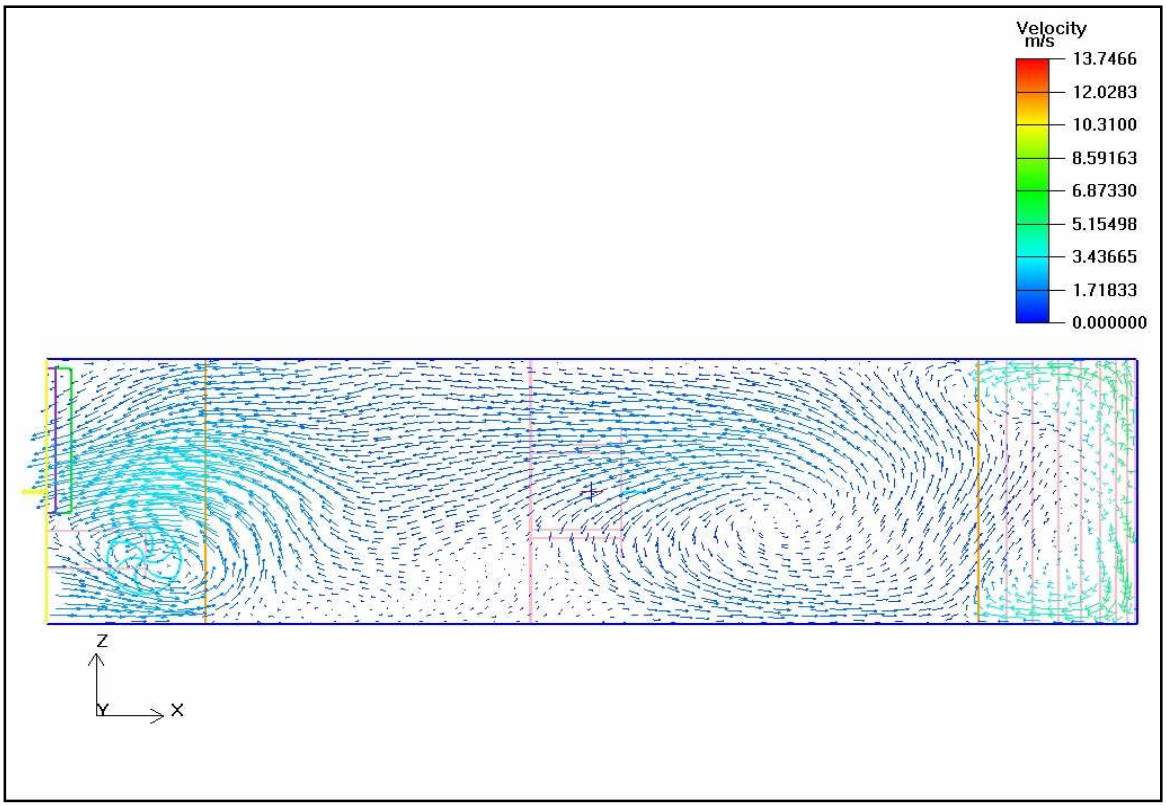

Figure 5-6 Velocity field 0.84 m from the floor in the ZX-plane

Figure 5-5 shows the asymmetric nature of the problem due to the placement of the inlet vent, gas burner tube and outlet fan on the upstream side of the main fan. The vector path gradient of the air entering or moving towards the main fan is more on the burner and outlet fan side than on the inlet vent side. This is also shown in Figure 5-6 where the swirl is more severe on the side of the gas burner.

None of the air entering at the inlet vent moves into the drying region before it has gone through the main fan (See Figure 5-7). One of the main concerns is the air movement around the gas burner. A large percentage of the air that has come into direct contact with the gas burner tube is directly expelled through the outlet vent without circulating through the entire drying domain. This increase the energy required heating up the air for the entire system (See Figure 5-8).

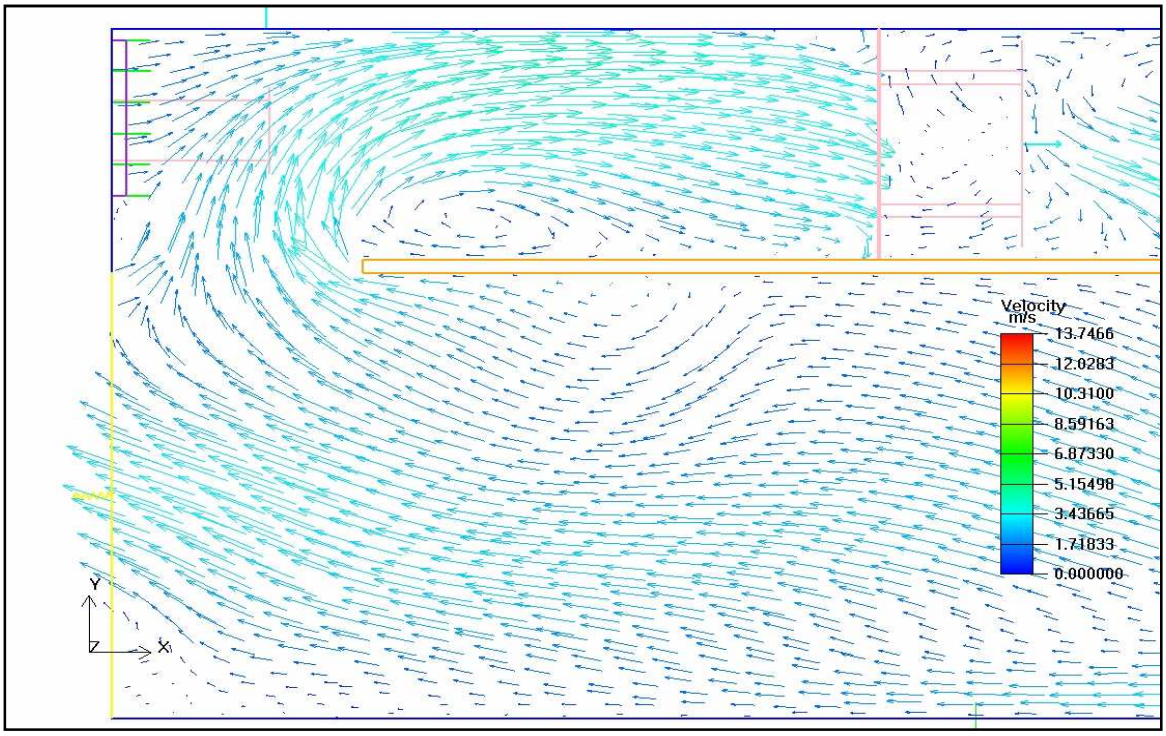

Figure 5-7 Detail of velocity field at centre of inlet vane in XY-plane

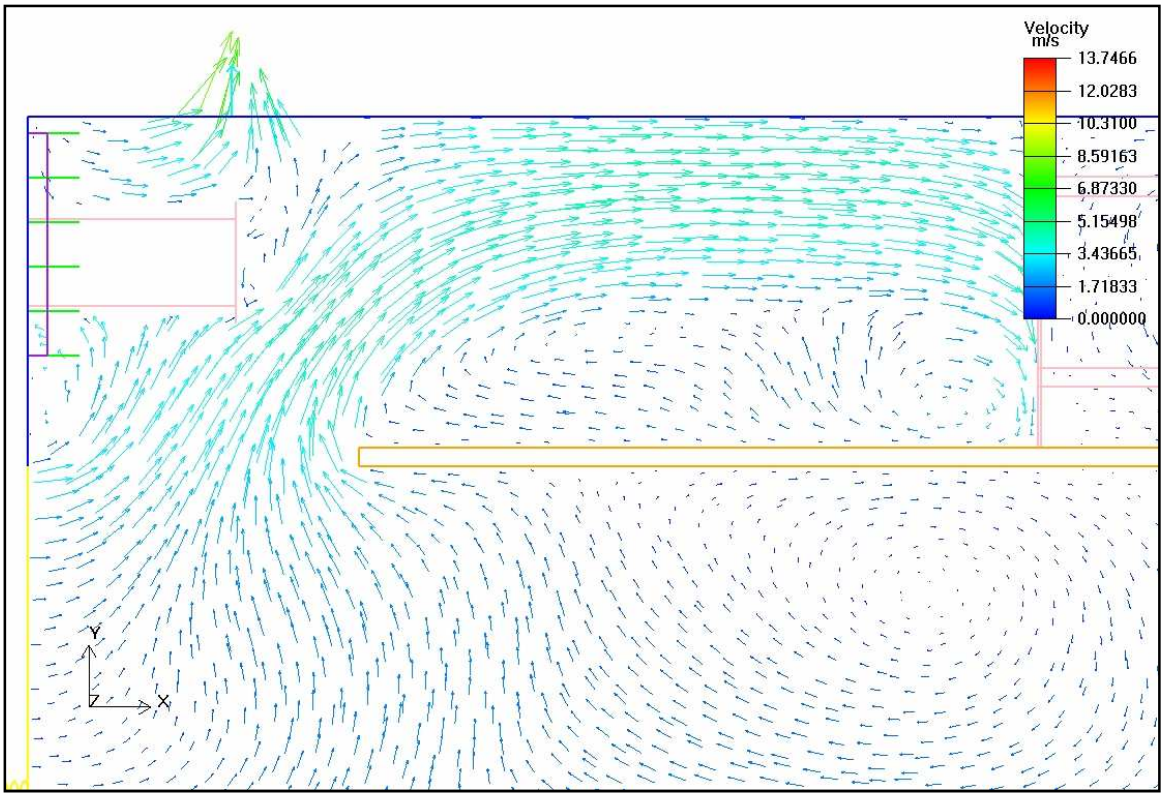

Figure 5-8 Detail of velocity field at centre of outlet fan in XY-plane

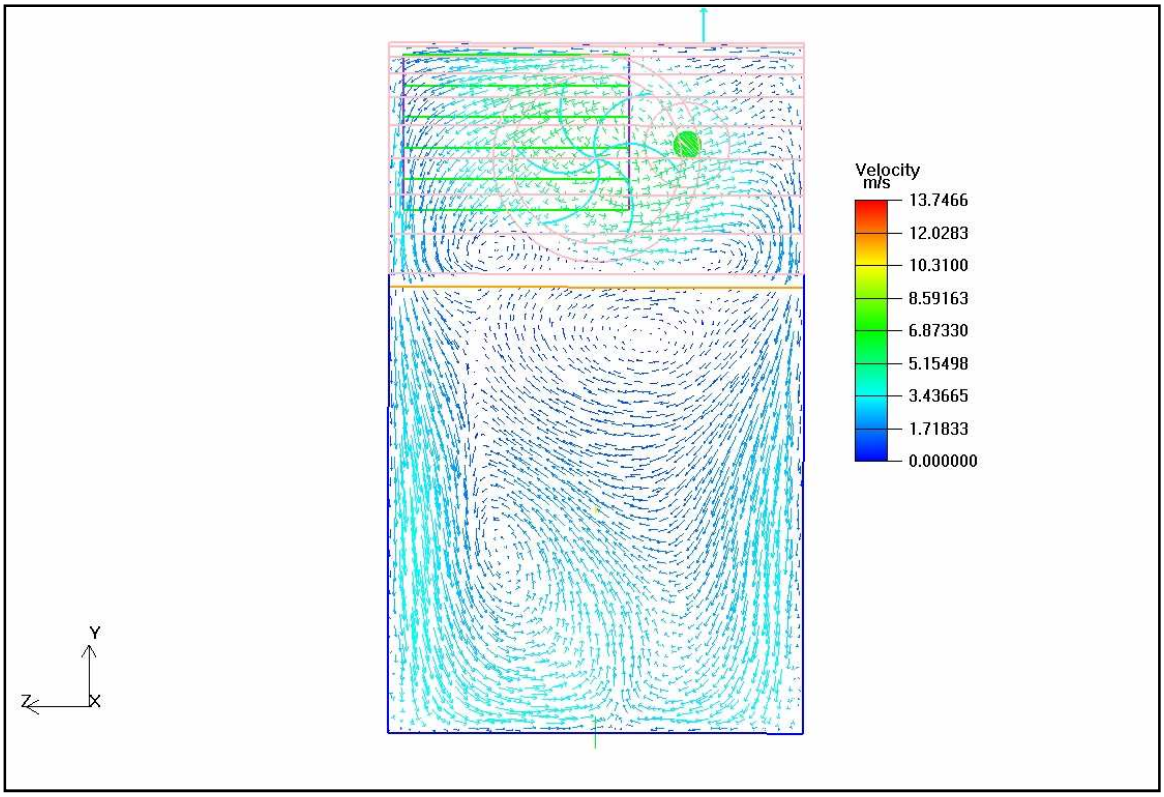

Figure 5-9 Detail of velocity field downstream of main fan in ZY-plane

The swirl action caused by the main fan is shown in Figure 5-9. The mesh is refined around this area in the second stage of the simulation runs. The swirl action is one of the main reasons why an uneven velocity distribution is formed in the drying region. In Figure 5-10 a massless particle is introduced to the dryer through the inlet vent. Particle traces provide information similar to that obtained by introducing dye or smoke into the fluid of a real model (Airpak 2.1 Documentation, 2002). This is merely an Eulerian tracking of the airflow compared to the Lagrangian way of tracking, where the forces, mass, energy and momentum equations are solved individually for each particle (Ansys CFX Release Notes 11.0, 2006). It shows the air entering through the inlet vent nearest to the outlet fan side is directly expelled. This once again increases the energy required to move or circulate the air through the entire region.

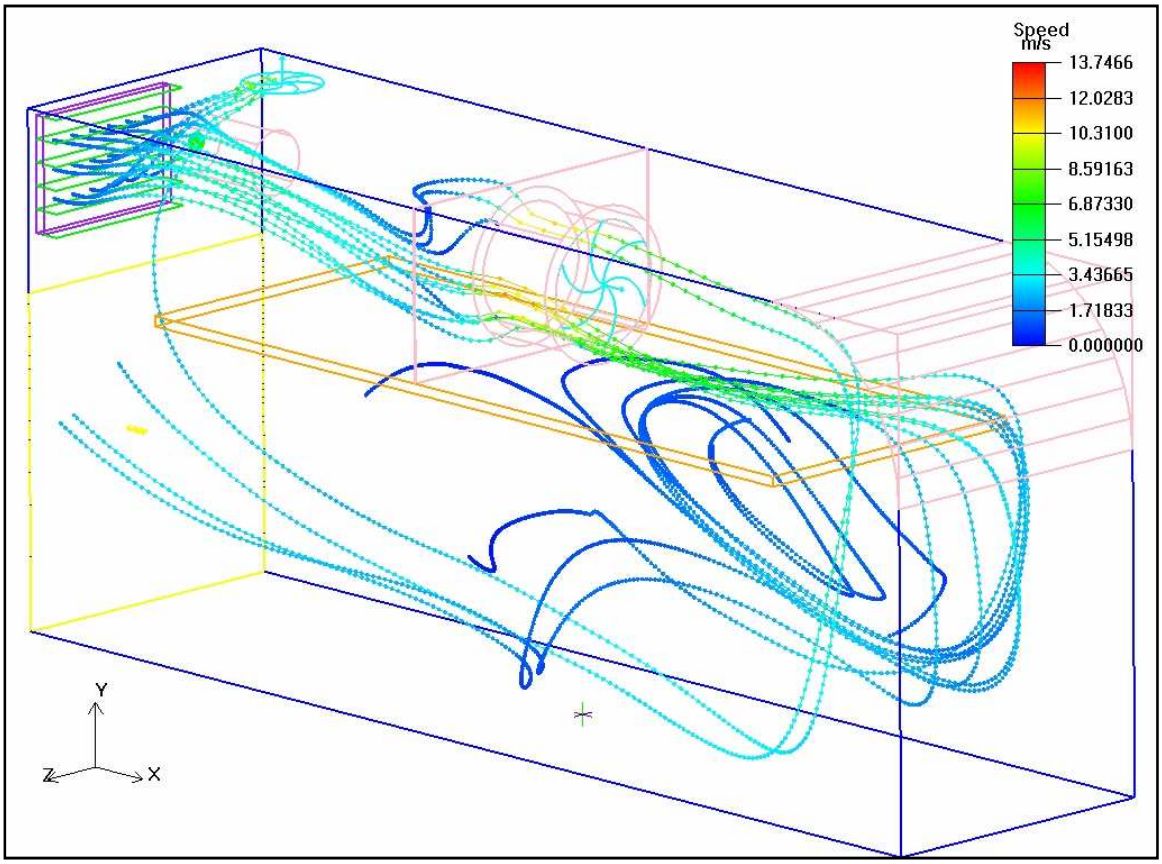

Figure 5-10 Particle tracking from the Inlet vane

5.2 Results of unmodified dryer using a refined mesh

The mesh around the main fan, outlet fan, inlet vent and gas burner is now greatly refined. The fine mesh consisted of 1,005,456 elements and 1,050,513 nodes (See Figure 5-11 and Figure 5-12). The unmodified dryer is based on the dryer set-up as in the first experiment where there was no flow diverter. The focus was to accurately capture the airflow pattern and velocity gradient in the region above the false ceiling. This set up was done to study the effect of the flow diverter alone without the influence of the mangoes and trolleys.

Figure 5-13, Figure 5-14 and Figure 5-15 show the velocity vector in three different XY-planes. The vortex or swirl moves more towards the front end of the false ceiling at the centre of the dryer, compared to the vortexes in the planes nearest to the sidewalls. Figure 5-13 and Figure 5-15 shows that the airflow is re-circulated at the fan tube as well as under the gas burner tube. A large vortex is formed at the upstream side of the fan above the false ceiling. The colour and size of the vectors used to describe the airflow pattern in the dryers is based on the magnitude of the velocity.

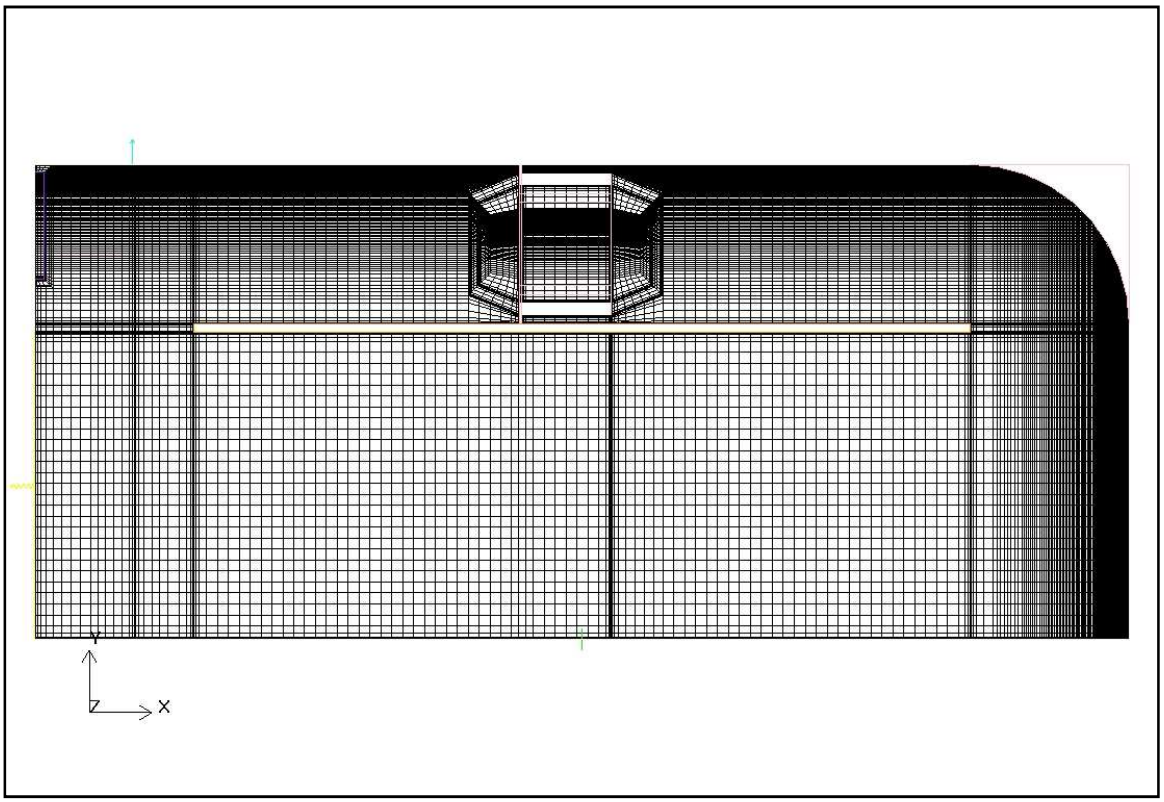

Figure 5-11 Refined mesh focusing on the upper part of the unmodified dryer

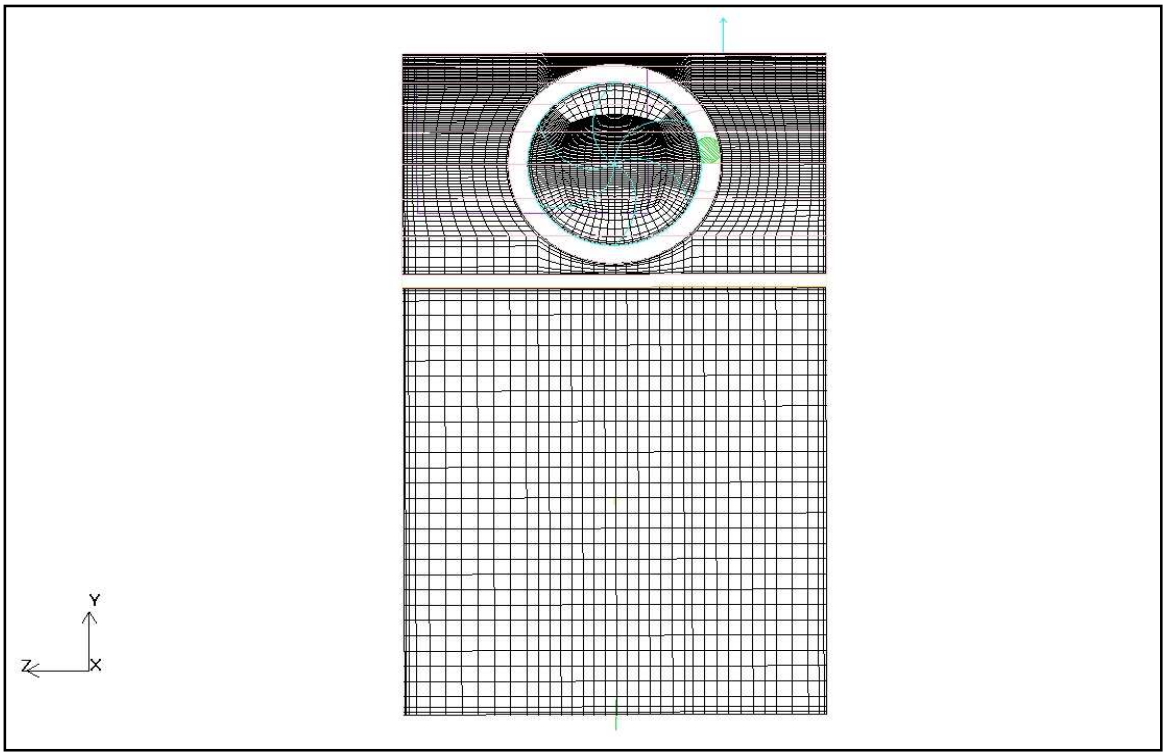

Figure 5-12 Detail of refined mesh in ZY-plane at the centre of the main fan

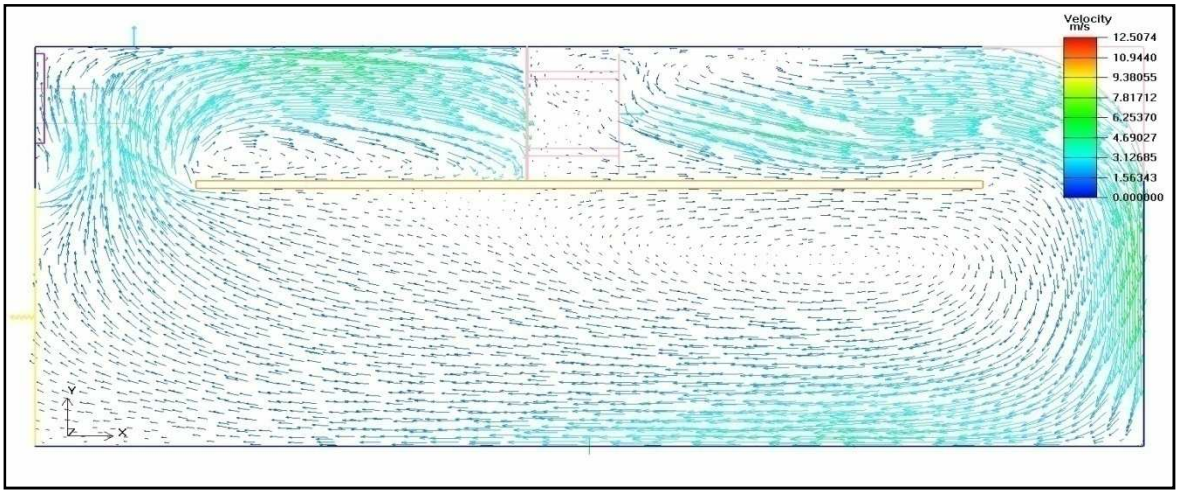

Figure 5-13 Velocity vector field at the centre of inlet vent in the YX-plane

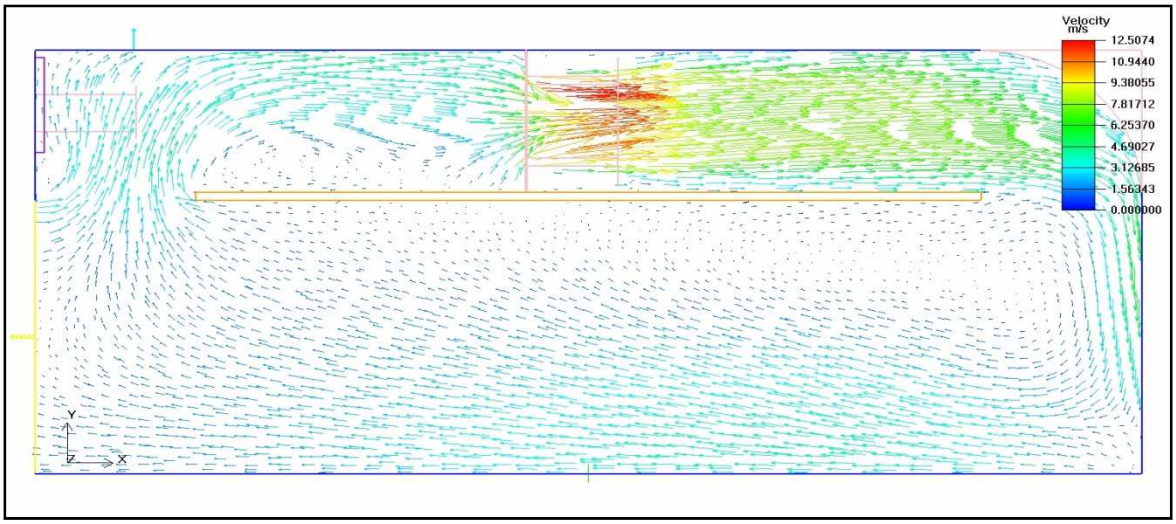

Figure 5-14 Velocity vector field at the centre of main fan in the YX-plane

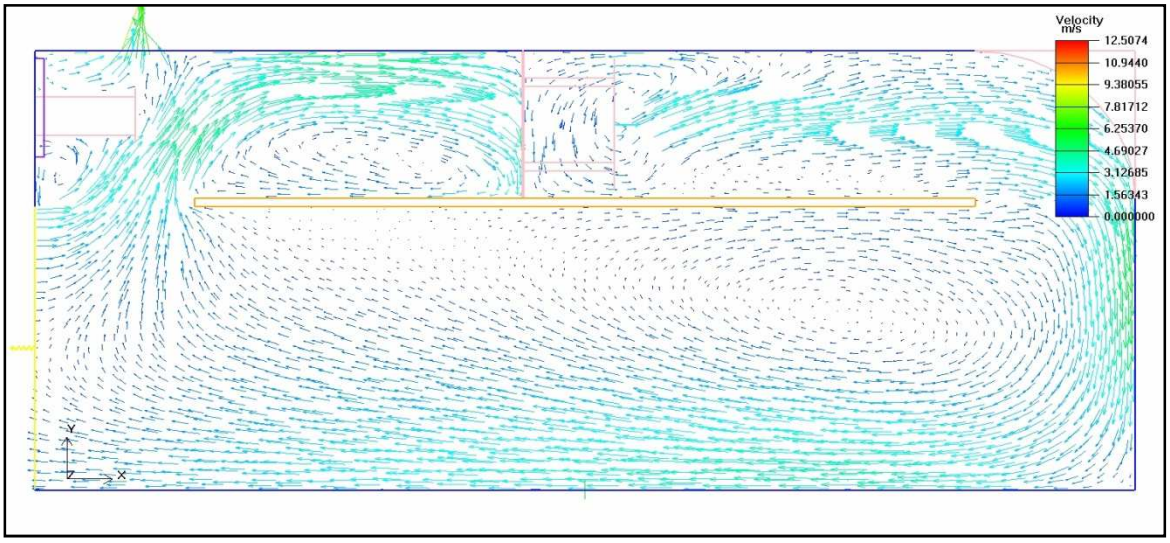

Figure 5-15 Velocity vector field at the centre of burner tube in the YX-plane

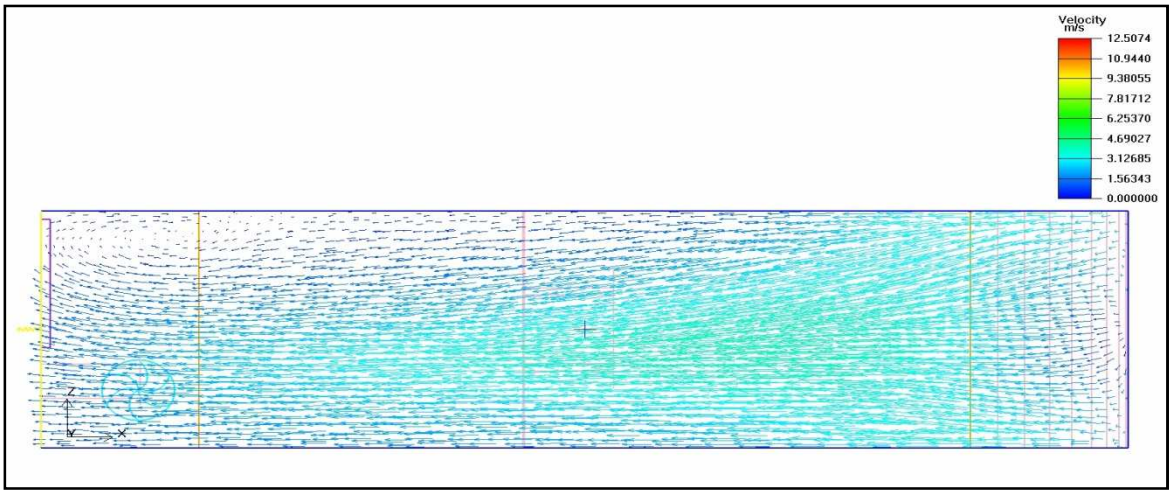

Figure 5-16 Velocity vector field, 0.28 m from the floor in the ZX-plane

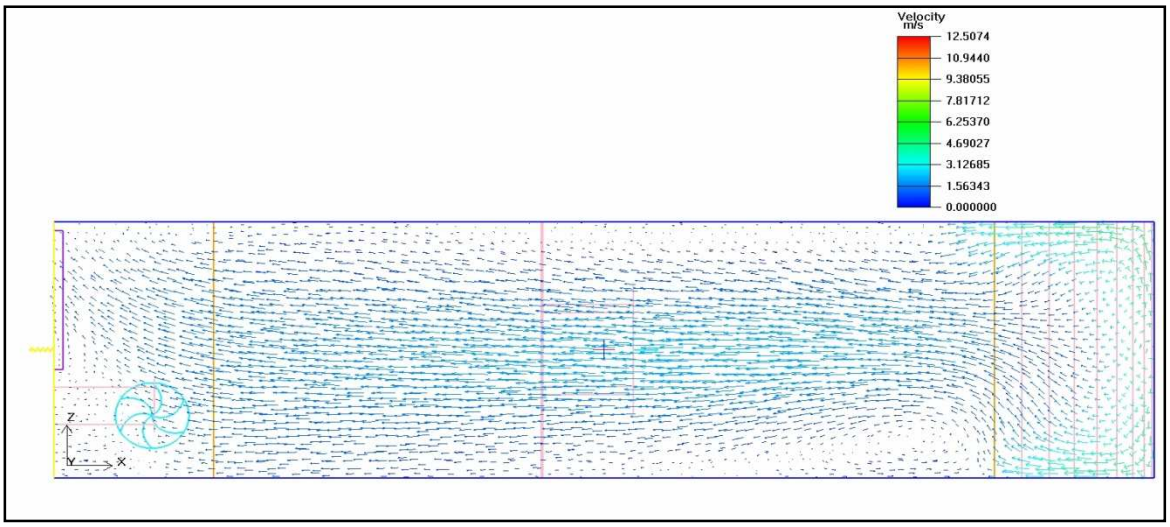

Figure 5-17 Velocity vector field, 0.84 m from the floor in the ZX-plane

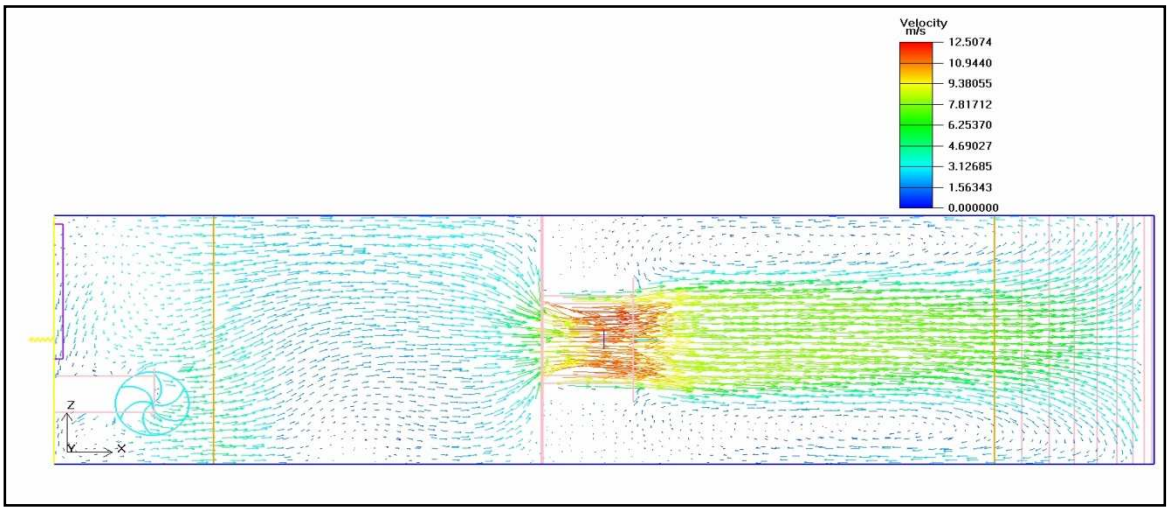

Figure 5-18 Velocity vector field, 2.1 m from the floor in the ZX-plane

No vortexes are form in the ZX-plane near the floor except at the top left hand corner near the outlet. This supports the fact that the airflow is higher and nearly uniform between at the lower part of the dryer and the floor.

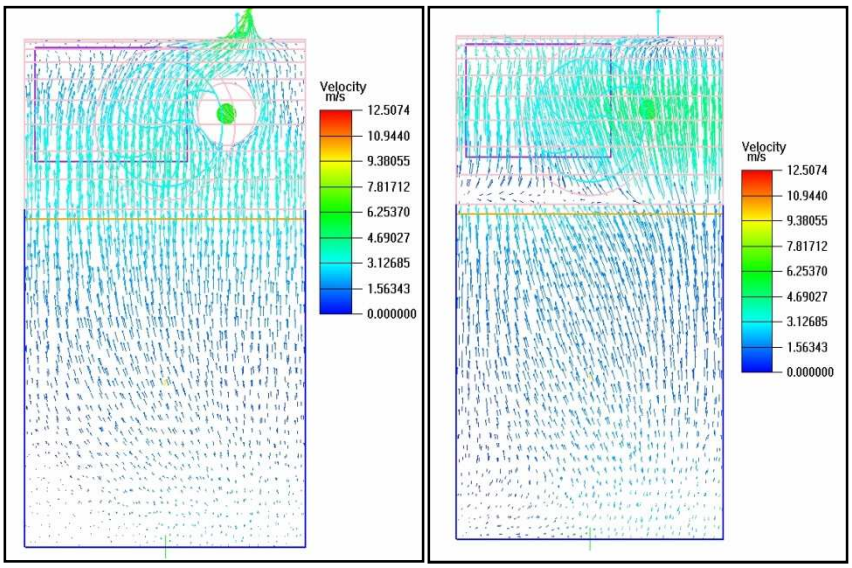

Figure 5-19 Midway between opening and section A (left), and viewing section A in the negative X-direction (right)

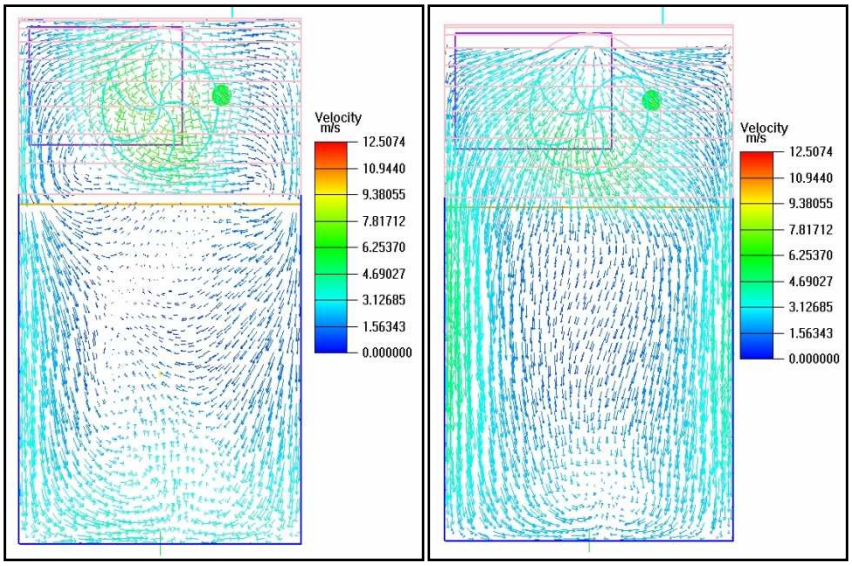

Figure 5-20 Velocity vector field of Section F (left) Midway between section F and the product inlet side (right)

In Figure 5-19 no swirl action is taking place in the upward flow from the floor towards the backend of the false ceiling. The flow is uniformly distributed around the gas burner tube and is extracted from the dryer before is circulated through the drying zone. The one concern is that a percentage of the heated airflow volume that comes directly from the gas burner tube gets expelled directly

through the outlet fan. Secondary flow is formed on the downstream side of the fan in the ZY-planes in the region between the false ceiling and inlet side (See Figure 5-20).

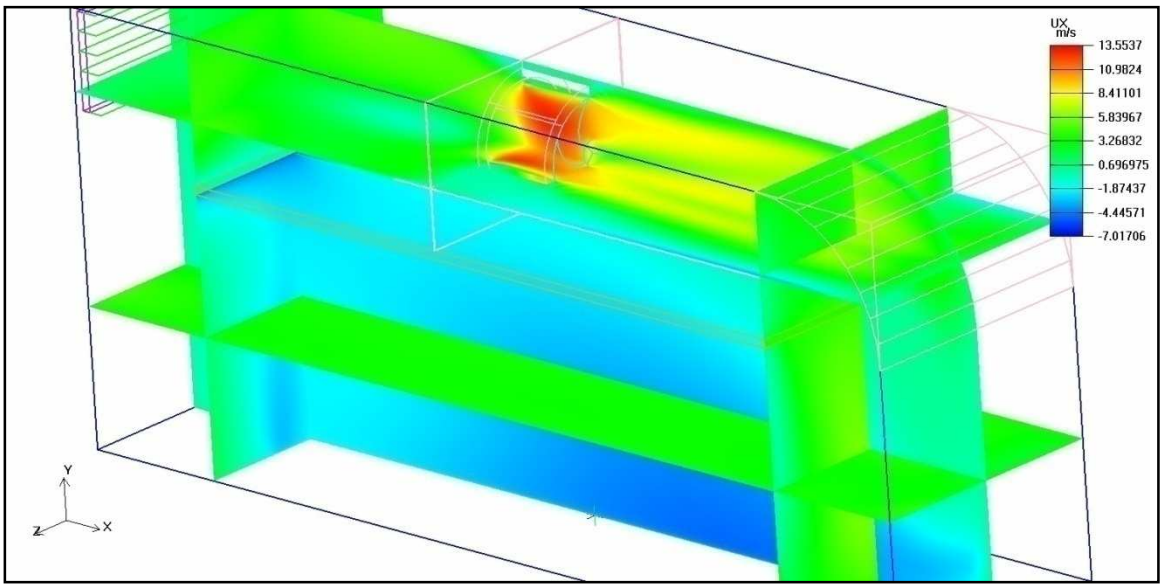

Figure 5-21 Velocity profiles on various planes

Figure 5-21 shows various contour velocities in the three main directions of the coordinate system. The YX-plane in the centre of the main fan shows the velocity contour in the X-direction. One can clearly see that the main focus should be placed on getting a uniform velocity distribution in the X-direction. It is also the direction in which the velocity range or profile is the largest compared to the velocity ranges in the Y-and Z-direction. The velocity contour in the X-direction of the ZX-plane in the centre of the main fan and in the ZY-plane at the end of the false ceiling underlines this statement. The velocity contour in the Z-direction in the ZX-plane 0.84 m above floor is uniform. The same goes for the velocity contour in the Y-direction in the ZX-plane at front end of the false ceiling.

Table 5-1 Mass, volume and pressure data on the main parts or sections of the dryer

Outlet Fan Operational point			
Volume Flow (m^3/s)	0.854		
Pressure Rise (N/m^2)	60.403		
Main Fan Operational point			
Volume Flow (m^3/s)	-2.994		
Pressure Rise (N/m^2)	72.277		
Objects	**Avg. Mass flow (kg/s)**	**Avg. Volume flow (m^3/s)**	**Avg. Pressure (N/m^2)**
Opening	1.0467	8.54E-01	-8.33E-01
Inlet Vent	N/A	N/A	N/A
Outlet Fan	-1.0461	-8.54E-01	-6.03E+01
Main Fan	3.667	2.994	-5.92E+01

Table 5-1 shows that the mass balance between the opening and the fan outlet differed by 0.05%. This is one of the ways to check if the solution of the model converged. Both fans' operational points are shown and correlates with the characteristic curves in Figure 4-18 and Figure 4-19. The average pressure mentioned in the right hand column is the average static pressure in the fluid on the 2D plane of the object, compared to the relative ambient pressure.

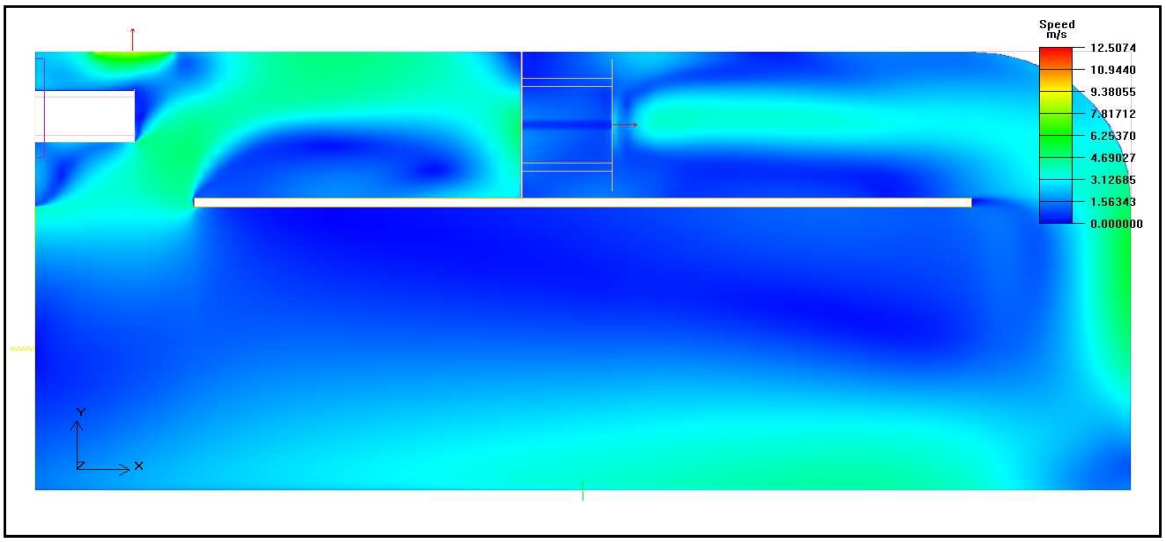

Figure 5-22 Speed contour in XY-plane in centre of burner tube

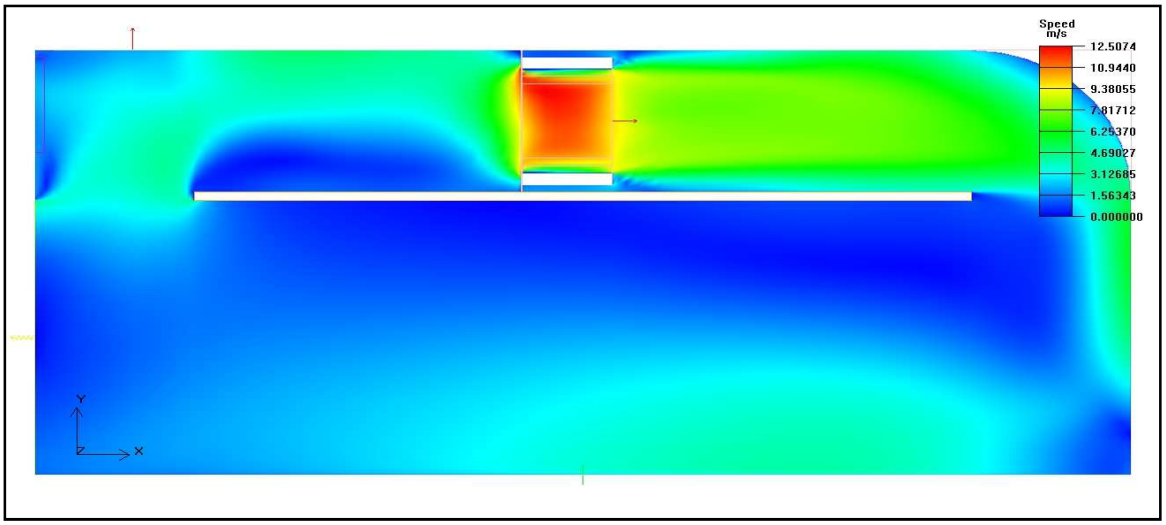

Figure 5-23 Speed contour in XY-plane in centre of main fan

The range of the speed contour in the XY-plane in the centre of the main fan is the largest compared to the speed contour ranges of the XY-planes at the centre of the gas burner tube and inlet vent (See Figure 5-22, Figure 5-23 and Figure 5-24. The speed profile in the drying zone of all three planes is very similar to each other. The speed gradient in the front drying zone is the largest at 0.28 to 0.84 m above the floor. There is as severe speed gradient at the tip of the false ceiling at both ends. The most uniform speed contour is found on the XY-plane at the centre of the inlet vent.

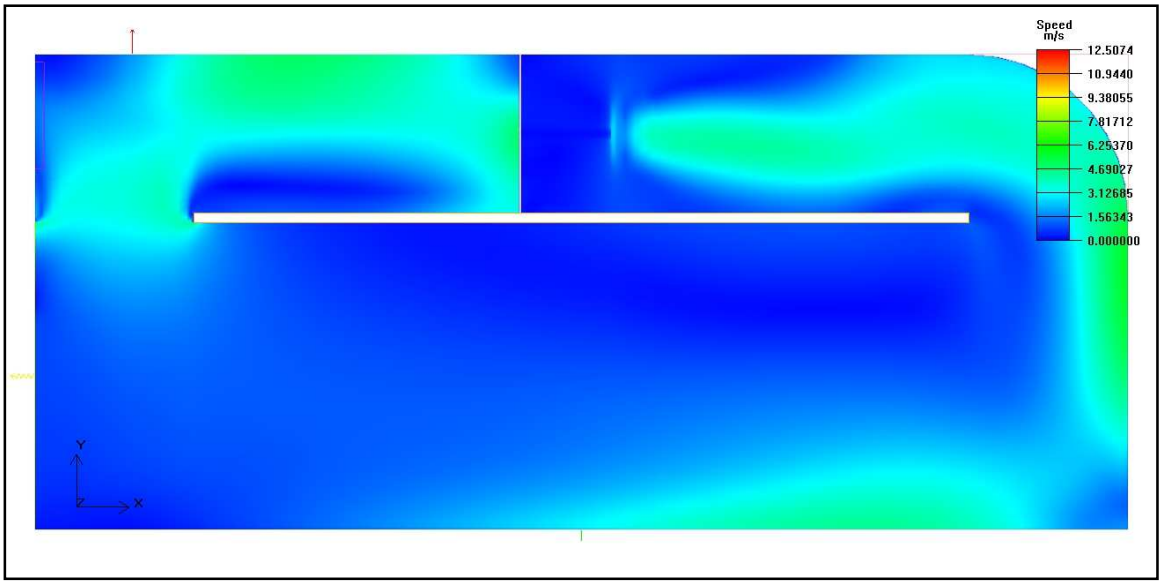

Figure 5-24 Speed contour in XY-plane in centre of inlet vent

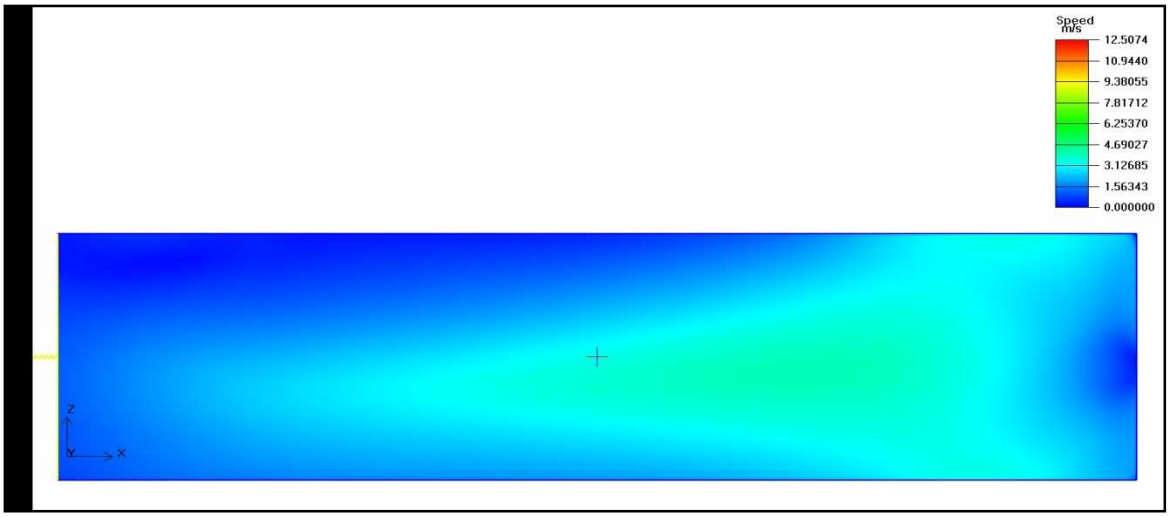

Figure 5-25 Speed contour in ZX-plane, 0.28 m from the floor.

The speed contour of the plane nearest to the floor Figure 5-25 has a larger range compared to the speed contours in the ZX-planes in Figure 5-26 and Figure 5-27. In Figure 5-25 the speed in the drying zone decreases as moves towards the back end of the dryer. The speed contour becomes more uniform from the floor upwards towards the false ceiling (See Figure 5-25 and Figure 5-26). The speed of the airflow decreases as it passes through the fan towards the turning vane; it then increases as the flow goes downwards and around the false ceiling (See Figure 5-23 and Figure 5-28).

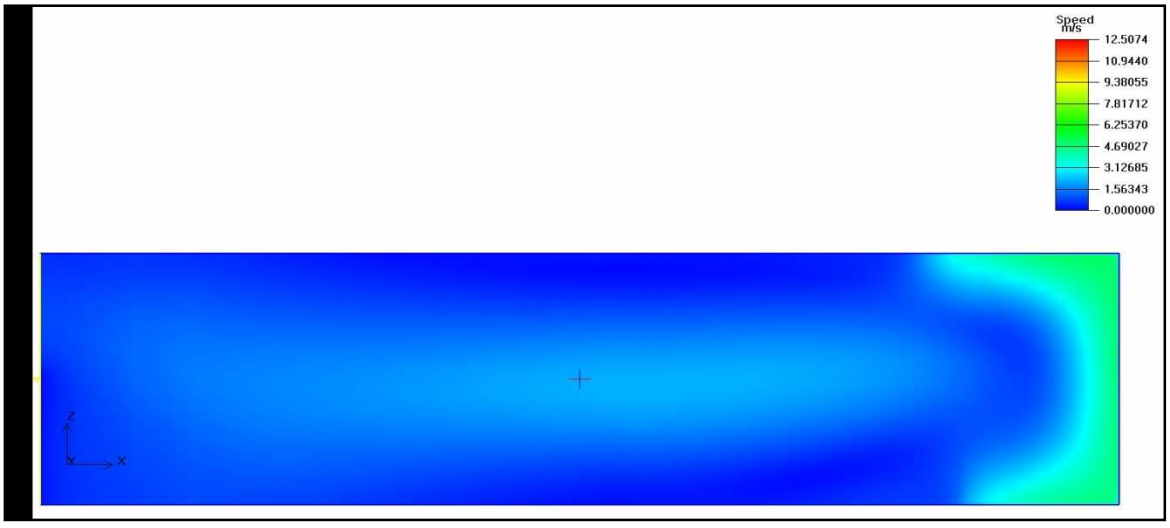

Figure 5-26 Speed contour in ZX-plane, 0.84 m from the floor.

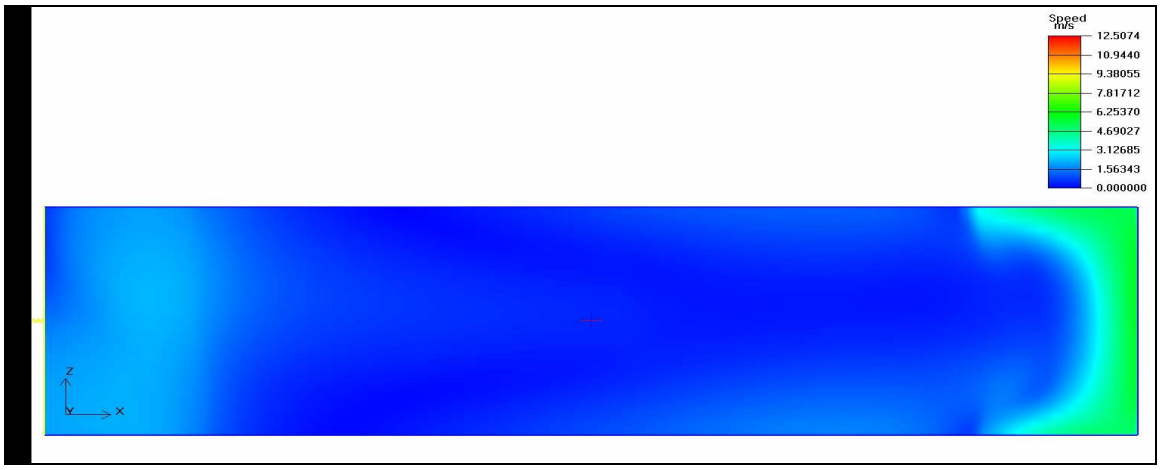

Figure 5-27 Speed contour in ZX-plane, 1.4 m from the floor

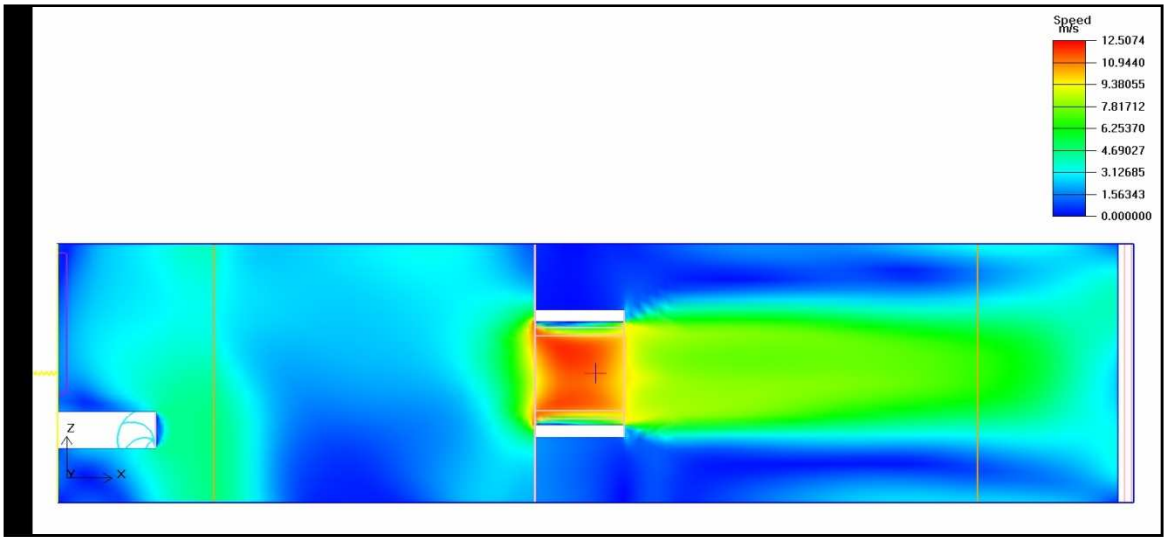

Figure 5-28 Speed contour in ZX-plane, 2.1 m from the floor

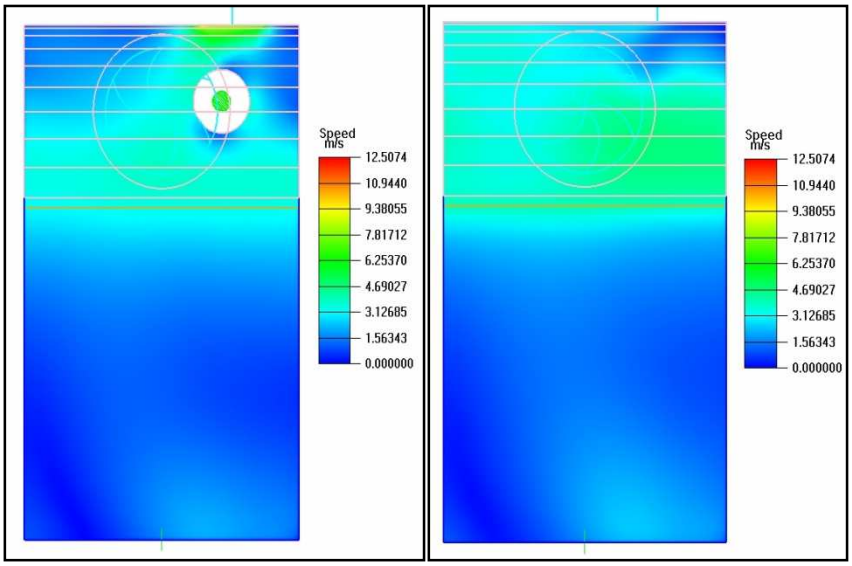

Figure 5-29 Midway between opening and section A (left), and viewing section A in the negative X-direction (right)

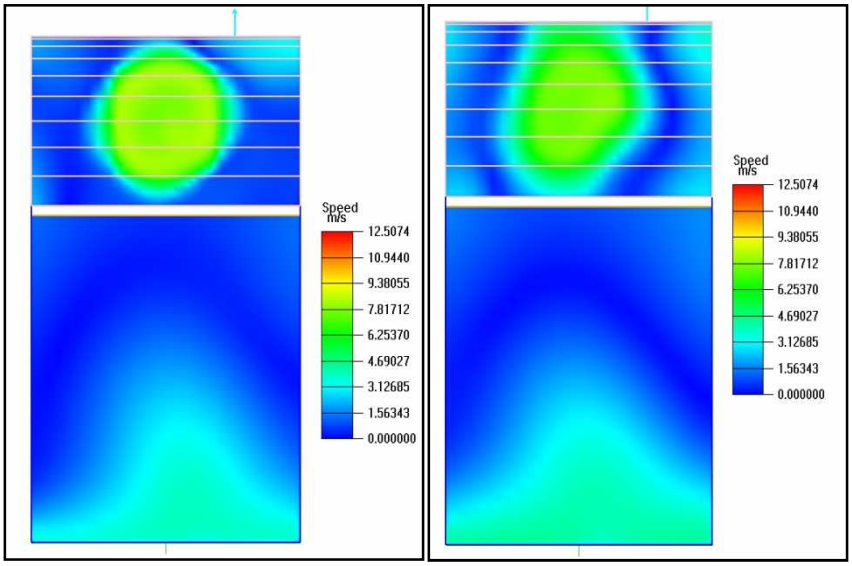

Figure 5-30 Speed contour of section D on the left and section E on the right in the ZY-plane

Figure 5-29 shows that as the air moved through the drying zone that the speed contour becomes more uniform. The speed of the airflow increases towards the outlet fan and as it goes around the back end of the false ceiling. In the middle of the drying zone the speed decreases from the floor upwards towards the false ceiling and towards the sidewalls (See Figure 5-30). The secondary flow at the front side of the false ceiling and turning vanes increases the speed in the ZY-plane, as can be seen in Figure 5-31.

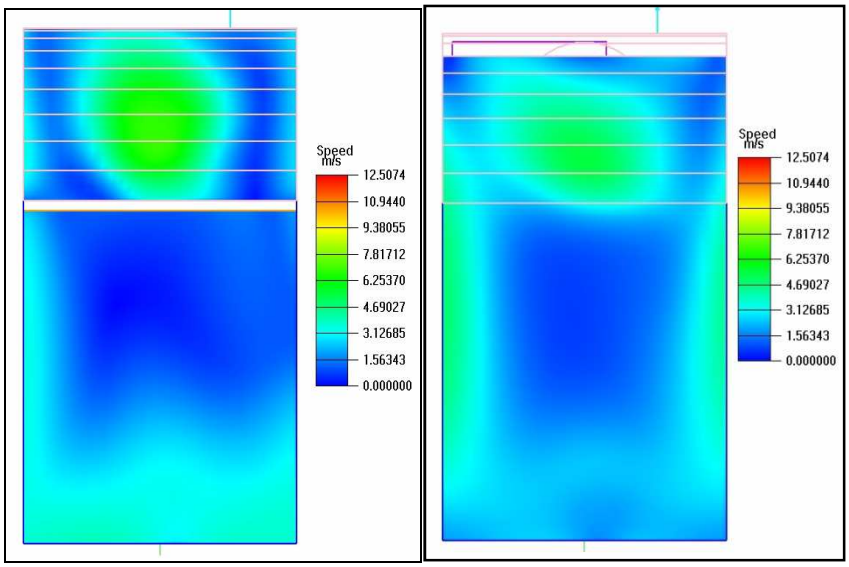

Figure 5-31 Speed contour of Section F (left) Midway between section F and the product inlet side (right)

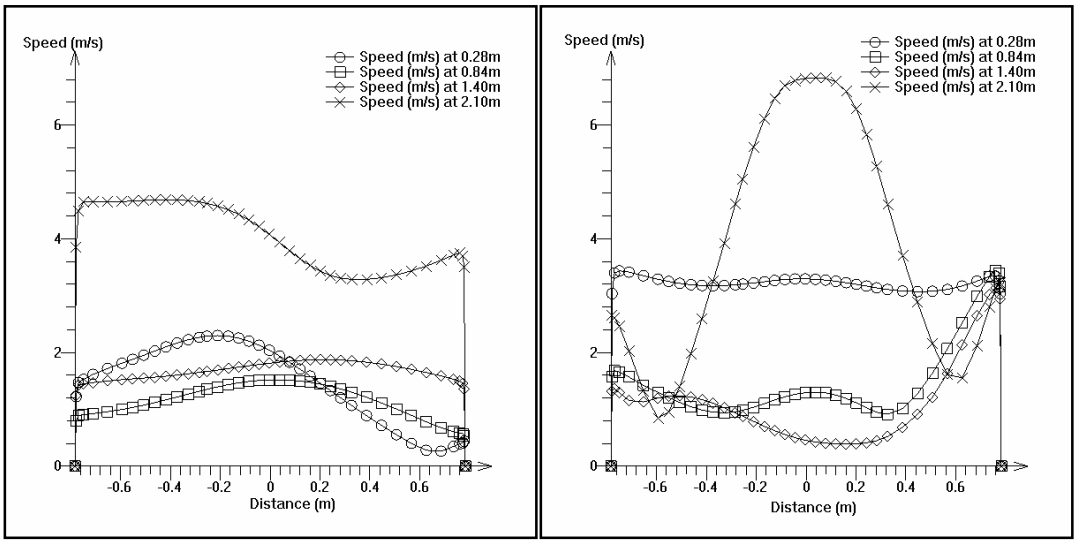

Figure 5-32 Variation speed plot at section A on the left and section F on the right

Figure 5-32 shows that the speed range in section A is more uniform than the speed range of section F. There is a large variation in the speed across the ZY-plane at section F downstream from the main fan (2.1 metres above the floor). The speed range in section A decreases from the floor towards the false ceiling, the opposite is happening in the drying zone of section F.

The pressure contour across the entire dryer was rather uniform except for the regions near the fans (See Figure 5-33).

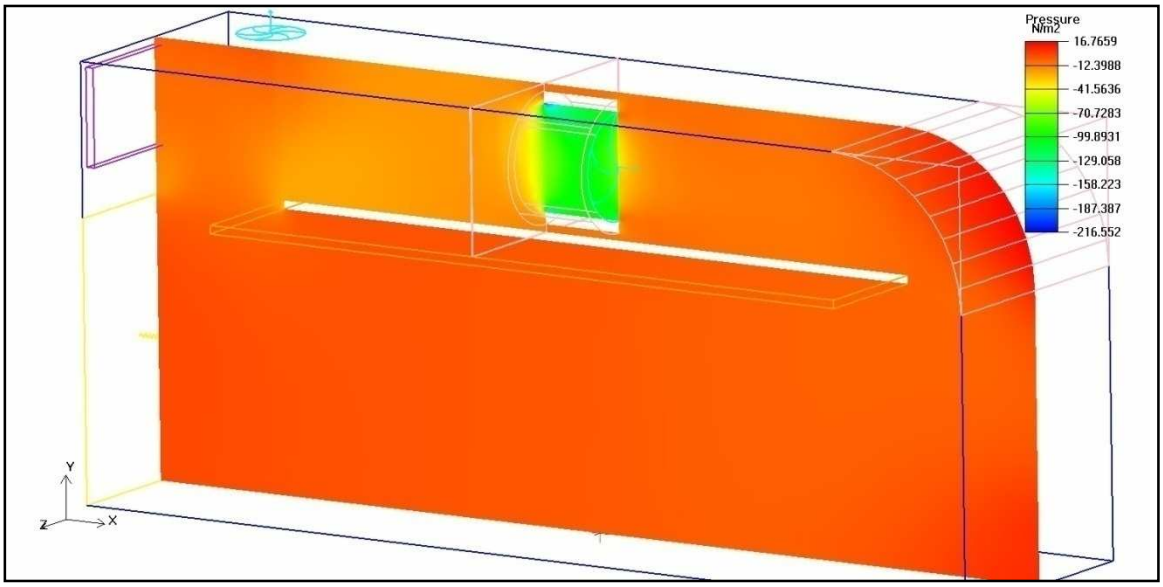

Figure 5-33 Pressure contour (XY-plane in centre of main fan)

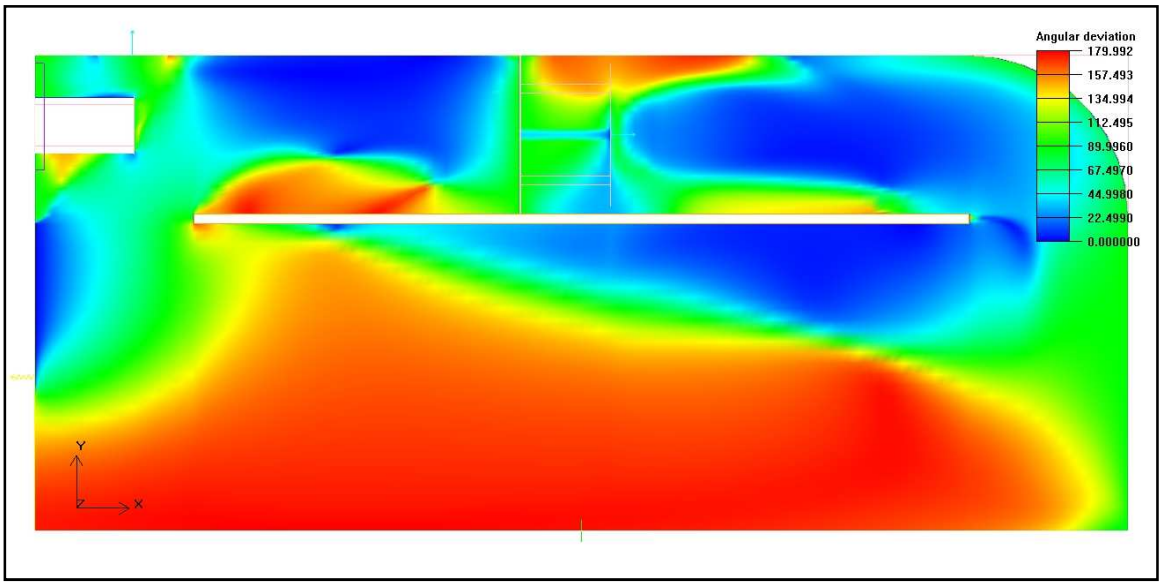

Figure 5-34 Angular deviation in the X-direction (XY-plane, centre of the burner tube)

A good way to visualise the vortex and reconnection zones in the dryer is through checking the angular deviation across a plane. Figure 5-34 shows clearly the vortex or swirl at the tips at both ends of the false ceiling.

The viscosity ratio is the most prevalent in the middle of the drying zone and decreases towards the walls of the dryer (See Figure 5-35).

The turbulent kinetic energy (k) and turbulent dissipation rate (ε) of the flow was found to be quite low and uniform throughout in the entire domain for all the analysis done on the dryer (See Figure 5-36 and Figure 5-37).

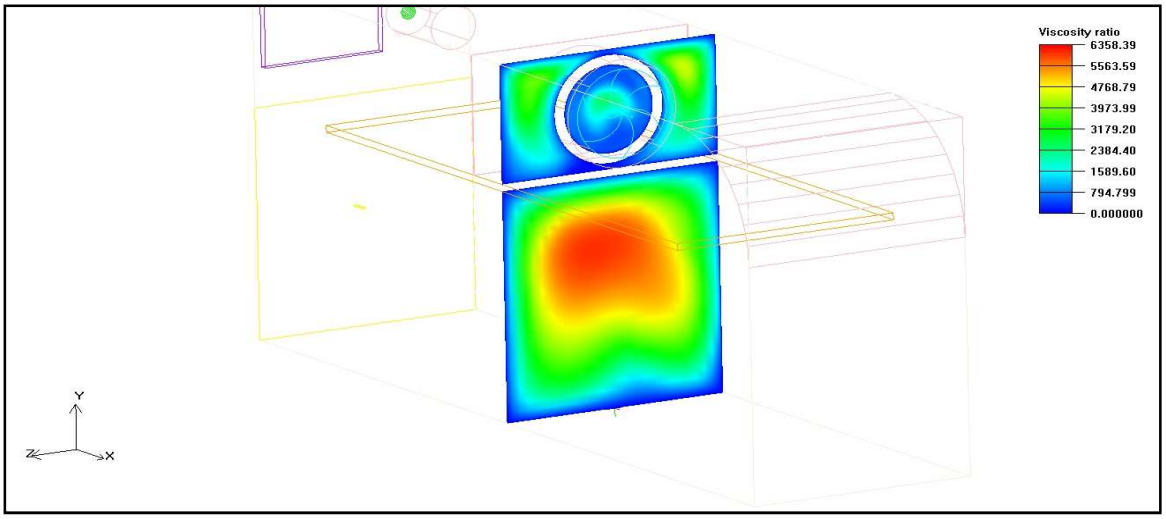

Figure 5-35 Viscosity ratio at section D

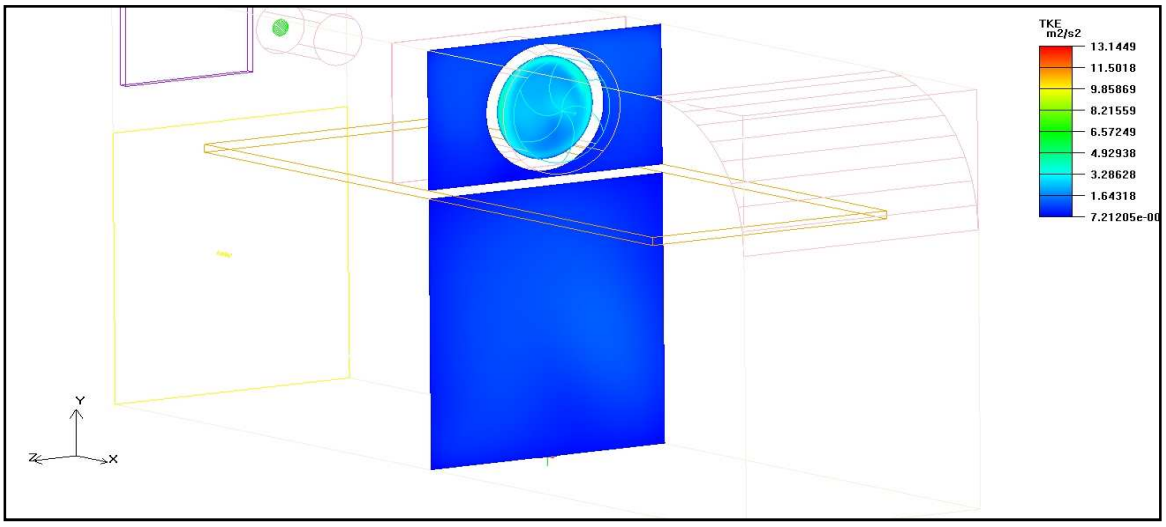

Figure 5-36 Turbulent Kinetic Energy at section D

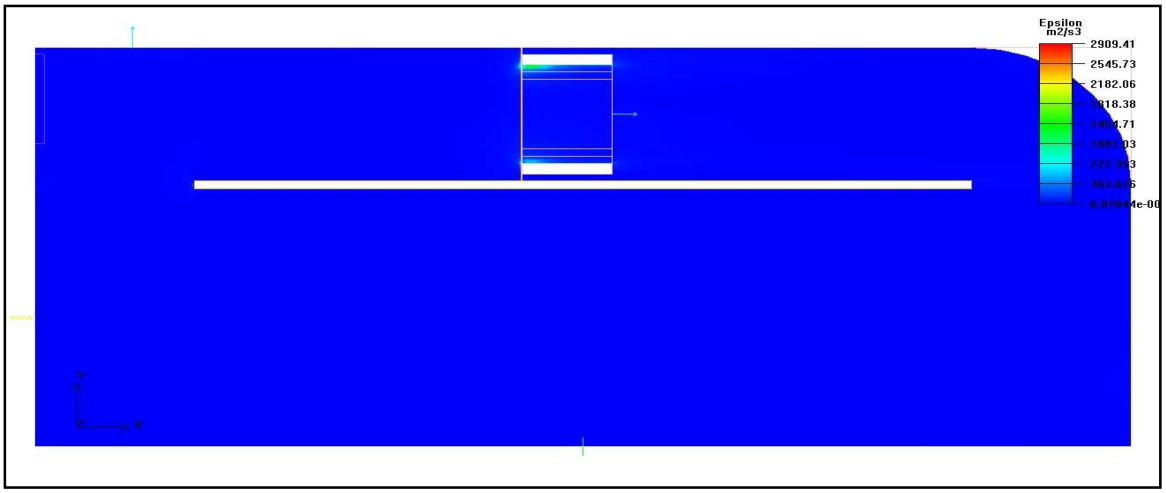

Figure 5-37 Turbulent dissipation rate (ε) at the YX-plane in the centre of the main fan

5.3 Data validation of CFD analysis of dryer without flow diverter

A validation was done on the CFD analysis of the dryer by comparing the speed contour on the same points that were evaluated in the experimental set up. It was found that the range of the speed contour of the CFD analysis was larger than the measured results.

The region of each section where the speed range was between 0 to 1 m/s was the same for both analyses. The region of where the highest speed was found did not compare well between the two analyses.

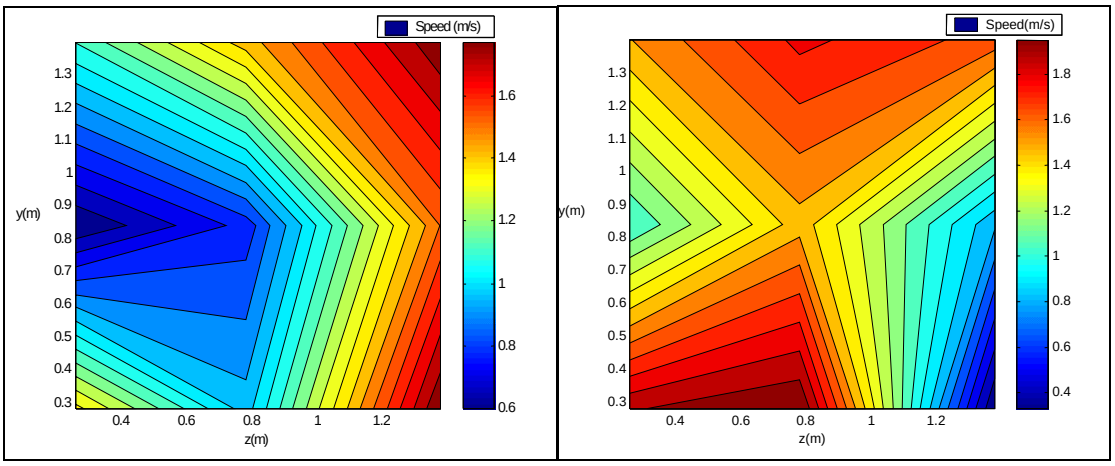

Section A

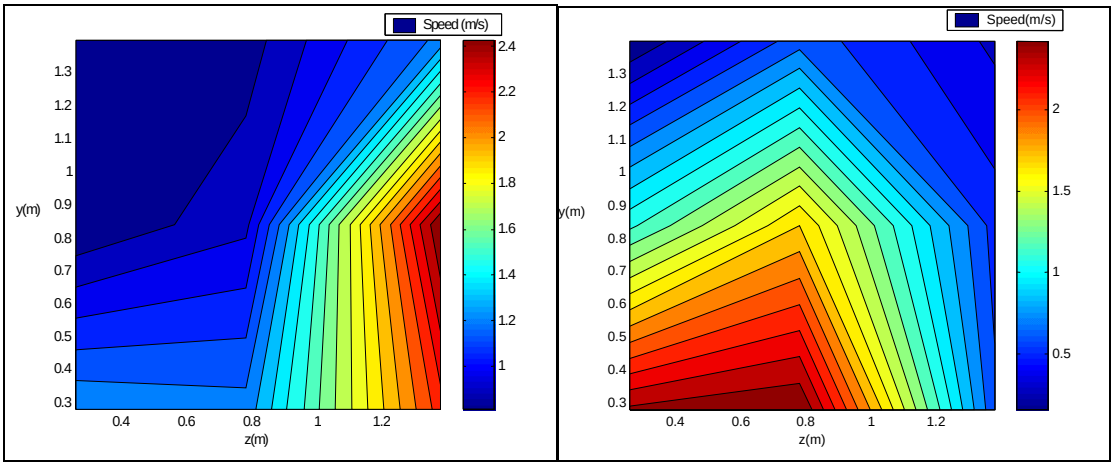

Section B

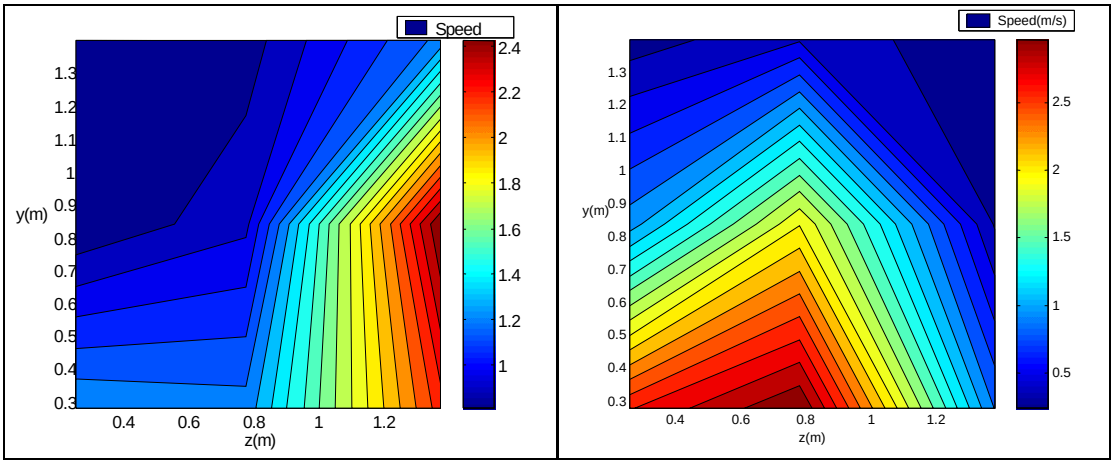

Section C

Figure 5-38 Comparison of the speed contours between the measured results (left) of the dryer without a flow diverter and the CFD analysis on the same sections (right)

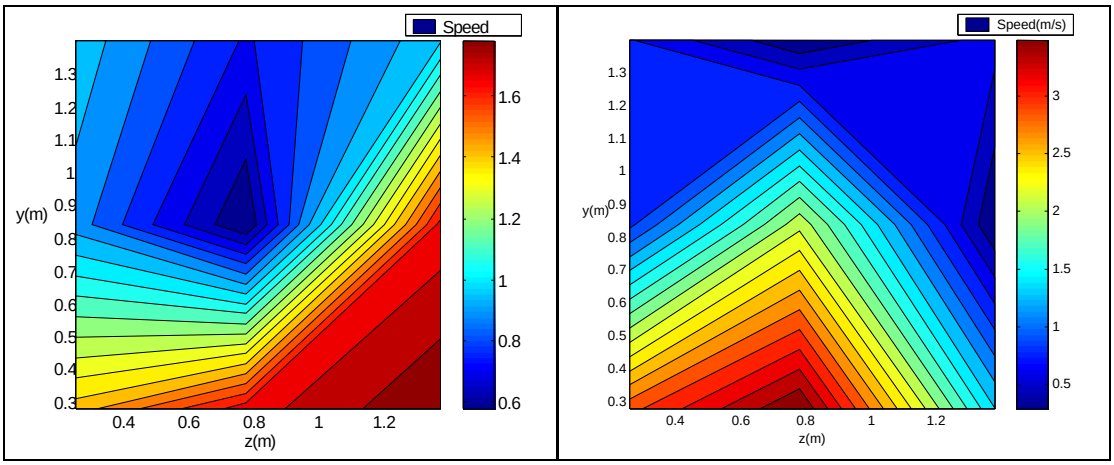

Section D

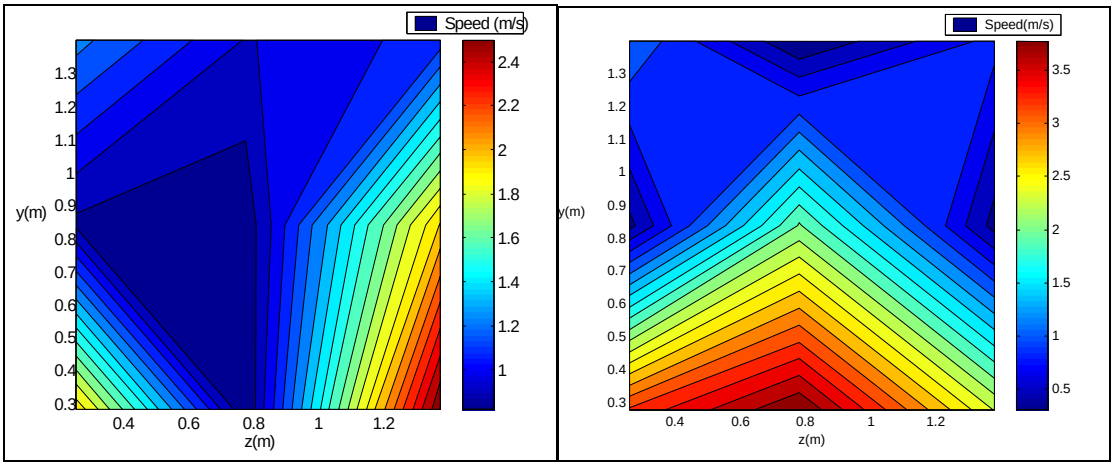

Section E

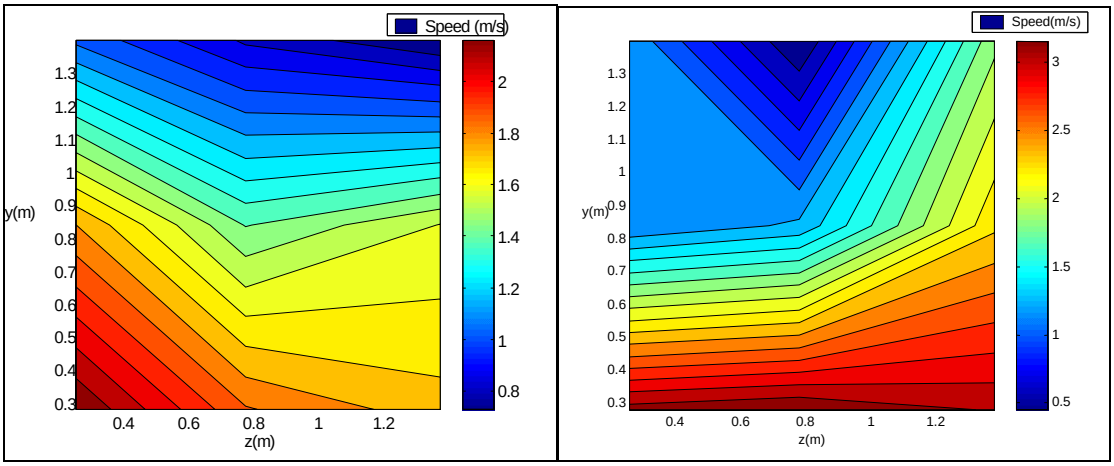

Section F

Figure 5-39 (Contd.) Comparison of the speed contours between the measured results (left) of the dryer without a flow diverter and the CFD analysis on the same sections (right)

5.4 CFD analysis of dryer with flow diverter

The mesh was mainly refined around the flow diverter. The fine mesh consisted of 1,433,722 elements and 1,494,033 nodes. The results of this analysis will be compared with the previous analysis of the dryer without the flow diverter. Only the planes with results that show the difference between the two analyses will be shown. The profile and range of some speed contours on planes did not differ that significantly from the previous analysis. The turbulent kinetic energy (k) and turbulent dissipation rate (ε) of all the analyses were constant over the entire region of the model and will thus not be shown in the following analyses.

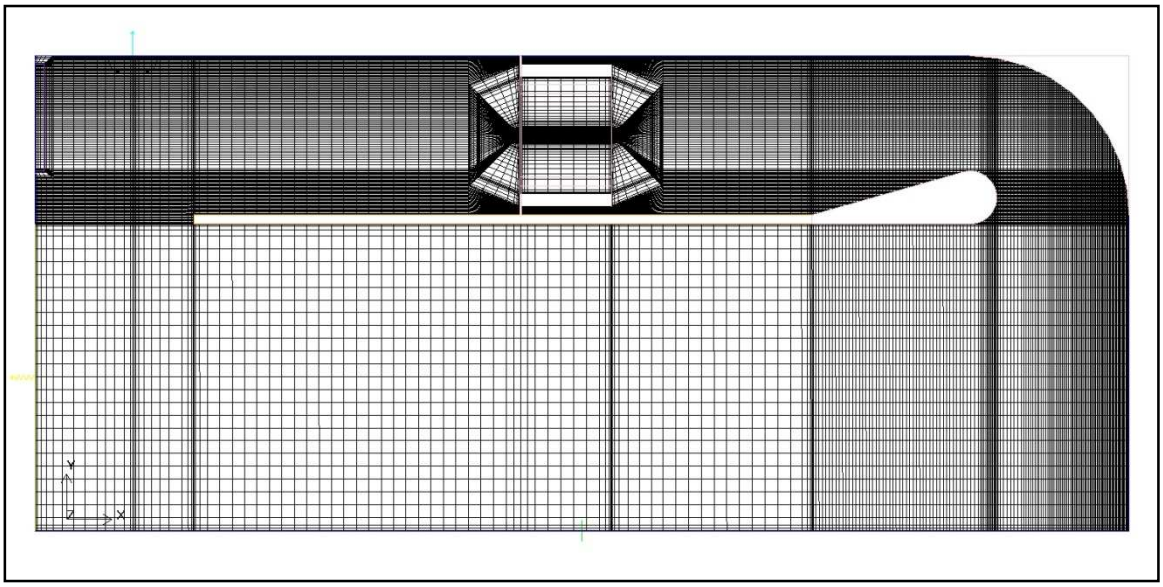

Figure 5-40 Detail of the mesh in the YX-plane in the centre of the main fan

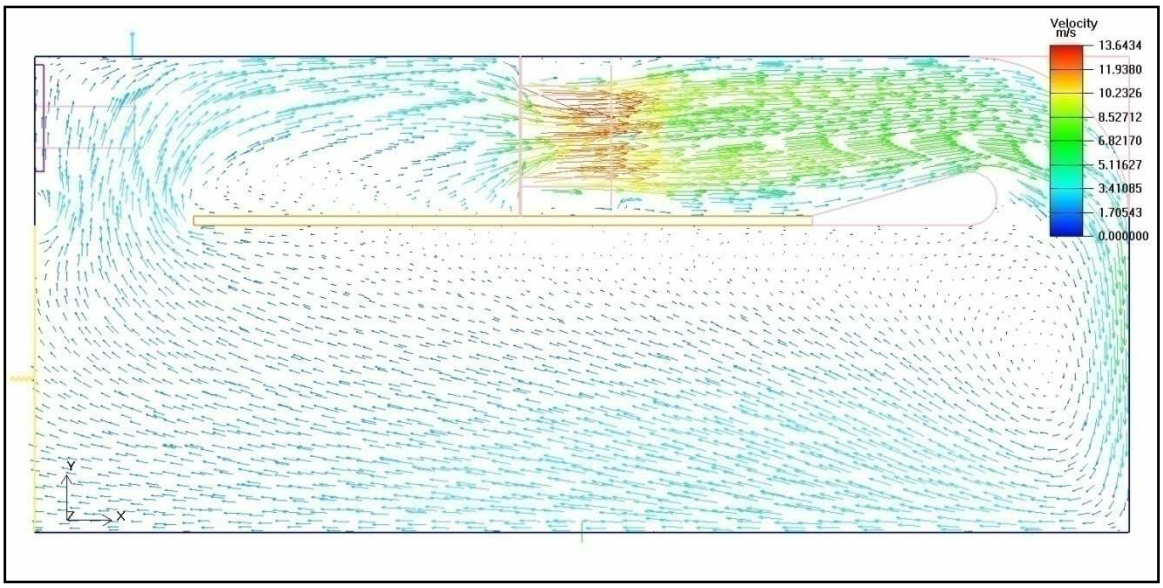

Figure 5-41 Velocity vector field at the centre of main fan in the YX-plane

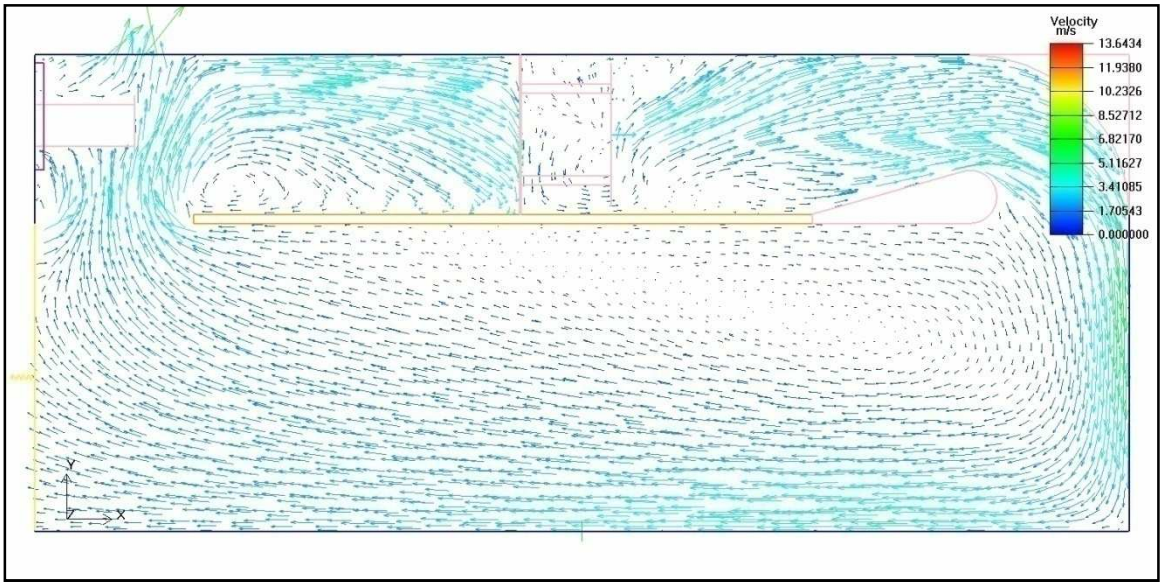

Figure 5-42 Velocity vector field at the centre of burner tube in the YX-plane

With the addition of the flow diverter the swirl region in the YX-plane in the centre of the fan moved more to the right of the front end of the false ceiling (See Figure 5-41), compared to the dryer without one (See Figure 5-14). The region of the swirl is the same in the YX-plane in the centre of the gas burner tube compared to the dryer without a flow diverter (Compare Figure 5-42 and Figure 5-15). The region of swirl is smaller in the dryer with the flow diverter at the front end of the false ceiling.

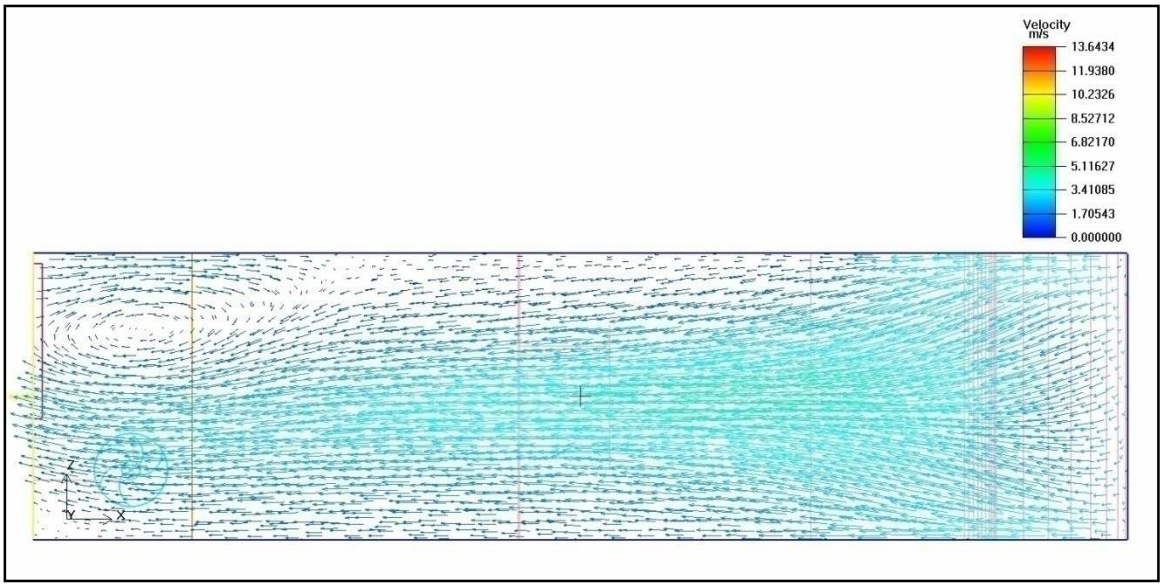

Figure 5-43 Velocity vector field, 0.28 m from the floor in the ZX-plane

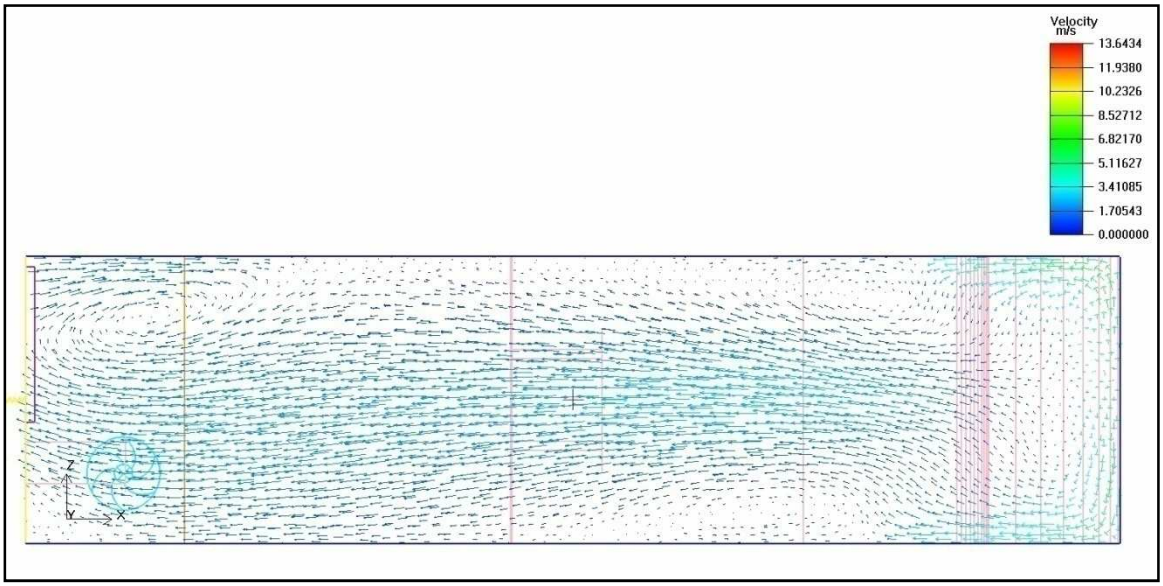

Figure 5-44 Velocity vector field, 0.84 m from the floor in the ZX-plane

The region of swirl is the same in the ZX-planes compared to the dryer without a flow diverter (Compare Figure 5-43, Figure 5-44 and Figure 5-45 to Figure 5-16, Figure 5-17 and Figure 5-18).

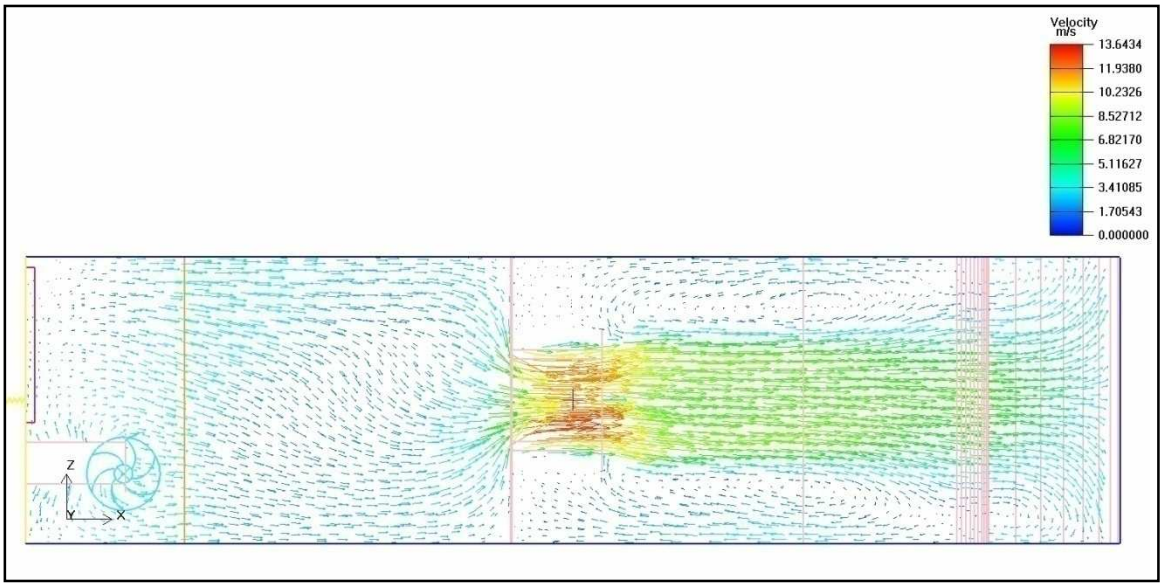

Figure 5-45 Velocity vector field, 2.1 m from the floor in the ZX-plane

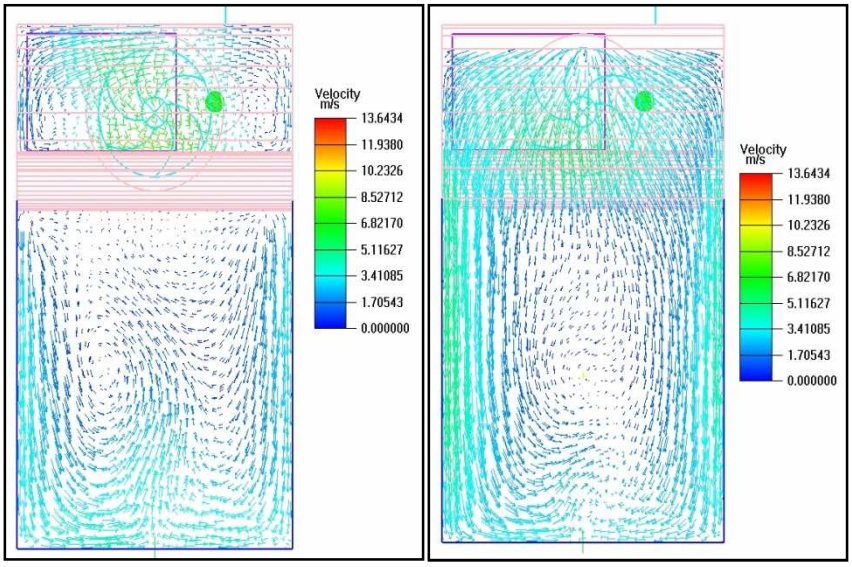

Figure 5-46 Velocity vector field of Section F (left) Midway between section F and the product inlet side (right)

Midway between section F and the product inlet side has more swirling taking place compared to the dryer without a flow diverter. This shows that swirl region moved more in front of the drying zone. There is still swirl action-taking place in section F but the swirl is less and takes up a smaller area (See Figure 5-46 and Figure 5-20).

The operational working pressure of the dryer with the flow diverter increased by 9.4% with a 1% decrease in volume flow (See Table 5-1 and Table 5-2). Although more torque and thus more input power would be required to operate at

this operational pressure point, the static pressure in the 2D fluid region at the main fan increased by 17%. Thus the efficiency of the dryer would be better due to fact that the average speed in the drying zone had increased.

Table 5-2 Mass, volume and pressure data on the main parts or sections of the dryer

Outlet Fan Operational point			
Volume Flow (m^3/s)	0.8246		
Pressure Rise (N/m^2)	60.8616		
Main Fan Operational point			
Volume Flow (m^3/s)	-2.9663		
Pressure Rise (N/m^2)	79.8113		
Objects	**Avg. Mass flow (kg/s)**	**Avg. Volume flow (m^3/s)**	**Avg. Pressure (N/m^2)**
Opening	1.0103	8.2461E-01	-8.7496E-01
Inlet Vent	N/A	N/A	N/A
Outlet Fan	-1.0101	-8.2461E-01	-6.0556E+01
Main Fan	3.6337	2.9663	-7.1433E+01

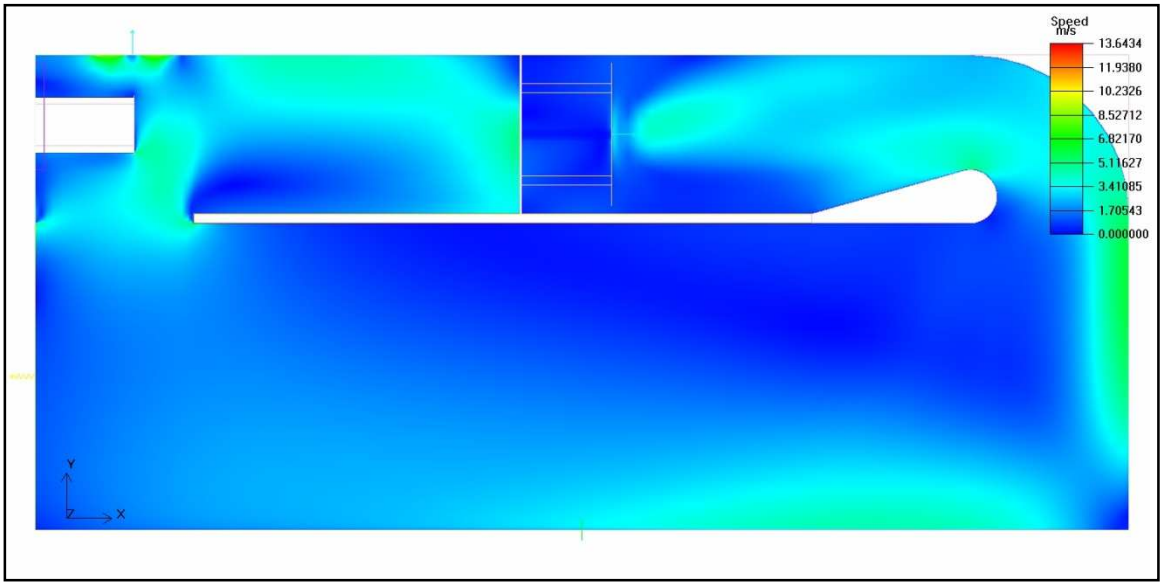

Figure 5-47 Speed contour in XY-plane in centre of burner tube

The profile of the speed contour of the dryer in this section was almost the same as the dryer without the flow diverter, although the maximum speed of this dryer increased by 8%. The speed gradient between the high-speed region 0.28 m and 0.84 m above the floor midway between the fan and the front of the false ceiling and the rest of the drying zone was less. The range of the overall drying zone was more, but the range was less in the middle region of the drying zone (Compare Figure 5-47, Figure 5-48 and Figure 5-49 to Figure 5-22, Figure 5-23 and Figure 5-24).

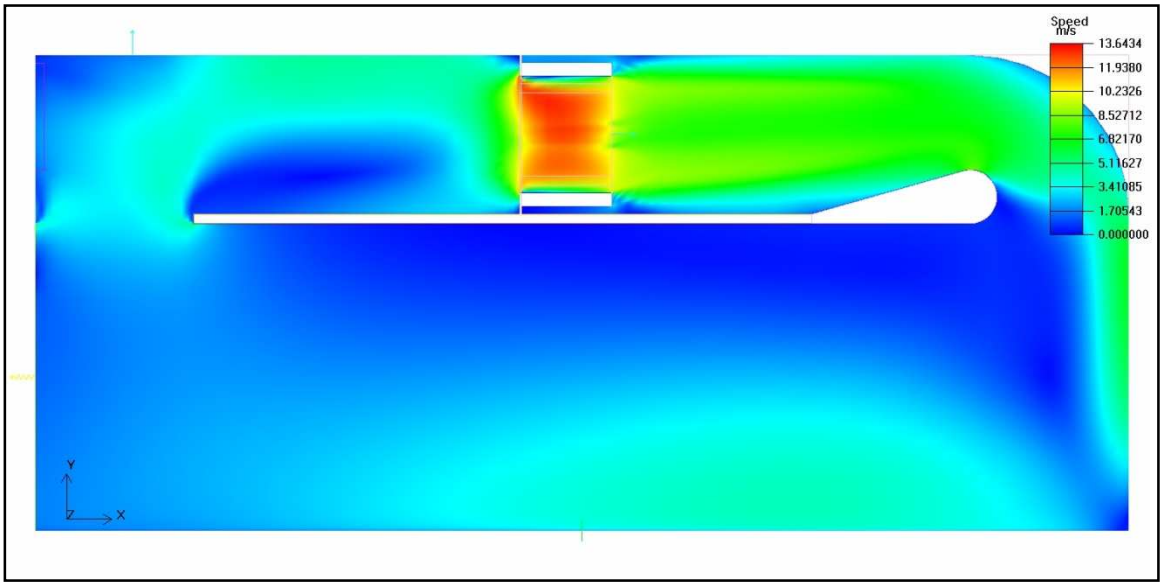

Figure 5-48 Speed contour in XY-plane in centre of main fan

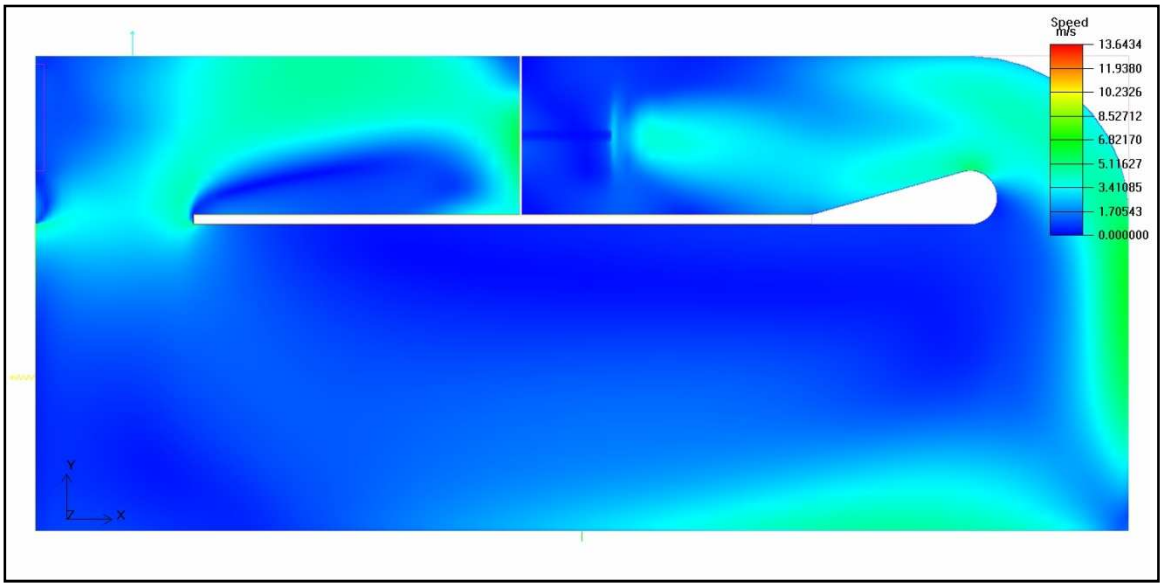

Figure 5-49 Speed contour in XY-plane in centre of inlet vent

In all the velocity contour profiles in the ZX-plane 0.28 m above the ground a sharp “spear” like speed contour is formed in the middle of the dryer. For this dryer the speed gradient between the edges of the “spear” contour and the rest of the drying zone was less than the dryer without the flow diverter (See Figure 5-50 and Figure 5-25).

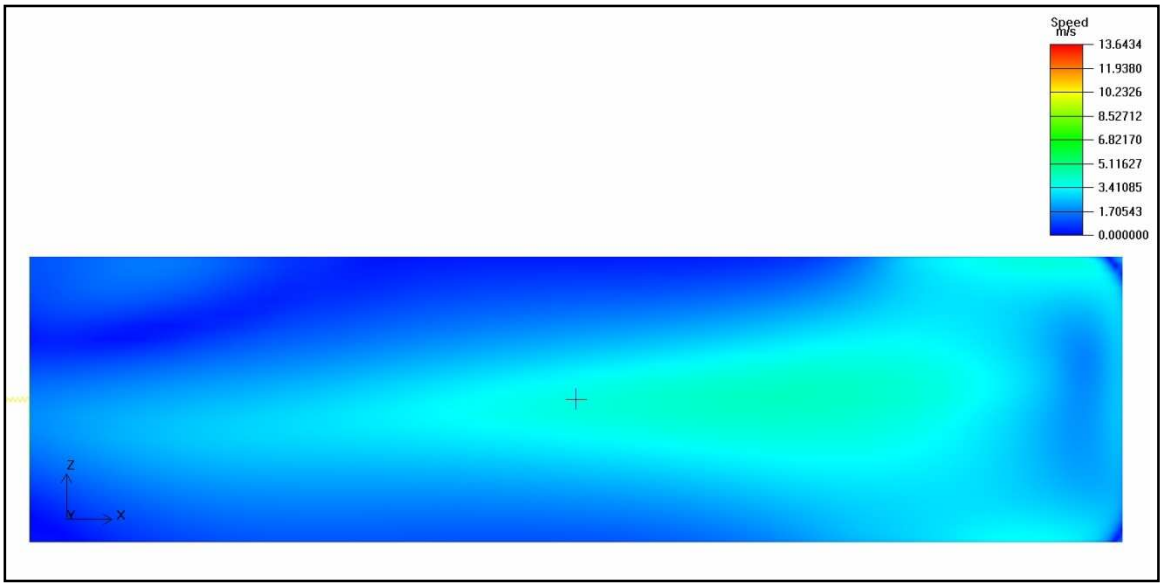

Figure 5-50 Speed contour in ZX-plane, 0.28 m from the floor.

The speed contour in Figure 5-51 did not differ from the speed contour in Figure 5-31 as was expected by inserting the flow diverter.

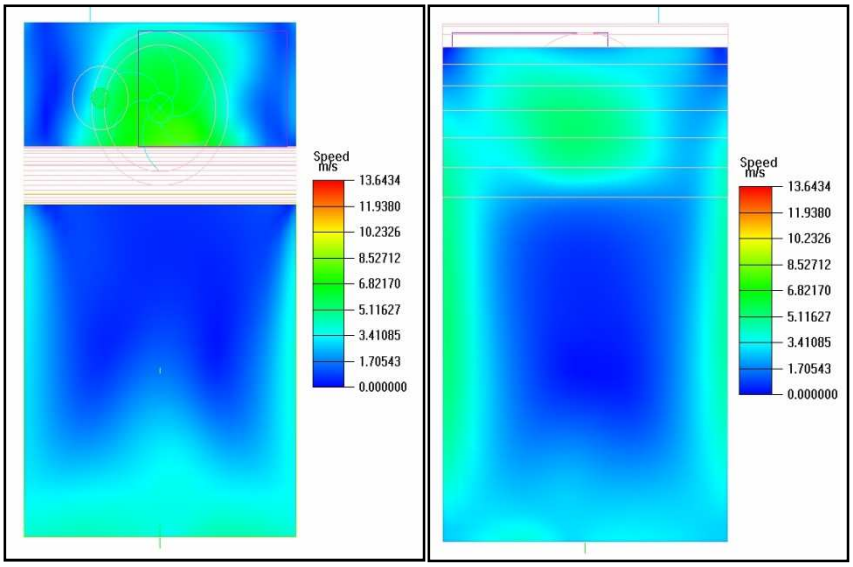

Figure 5-51 Speed contour of Section F (left) Midway between section F and the product inlet side (right)

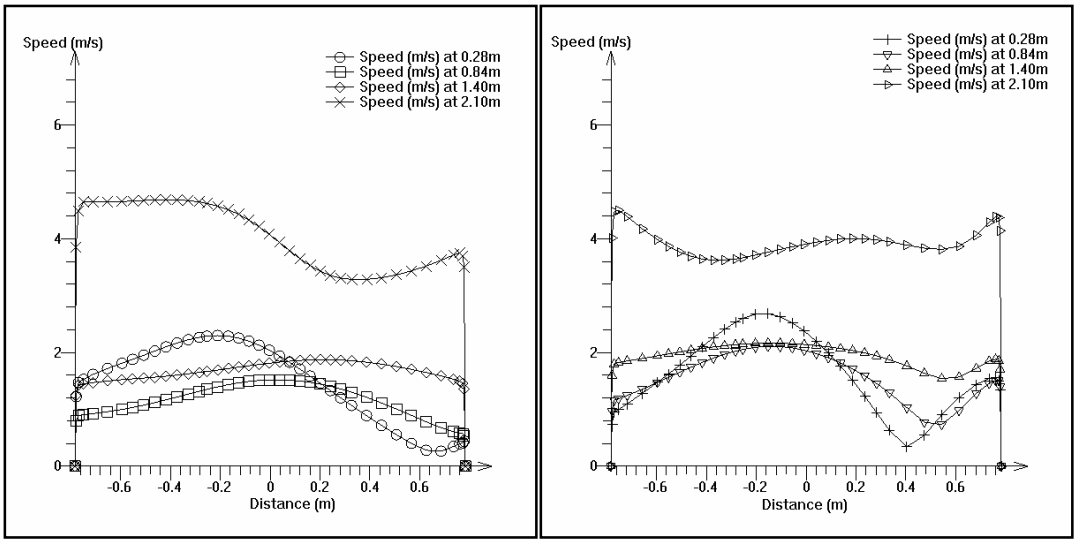

Figure 5-52 Variation speed plot at section A without flow diverter on the left and section A of dryer with flow diverter on the right

Figure 5-52 shows that the speed profile at 2.1 m across the Z-axis on the ZY-plane was more uniform with the flow diverter. In the drying zone itself it was less uniform than the dryer without a flow diverter. At 0.28 m and 1.4 m there was no difference at all.

Figure 5-53 the speed contour at 1.4 m was more uniform between –0.4 m and 0.4 m on the Z-axis with the flow diverter. For the rest of the heights the speed contour of the dryer without the flow diverter was more uniform.

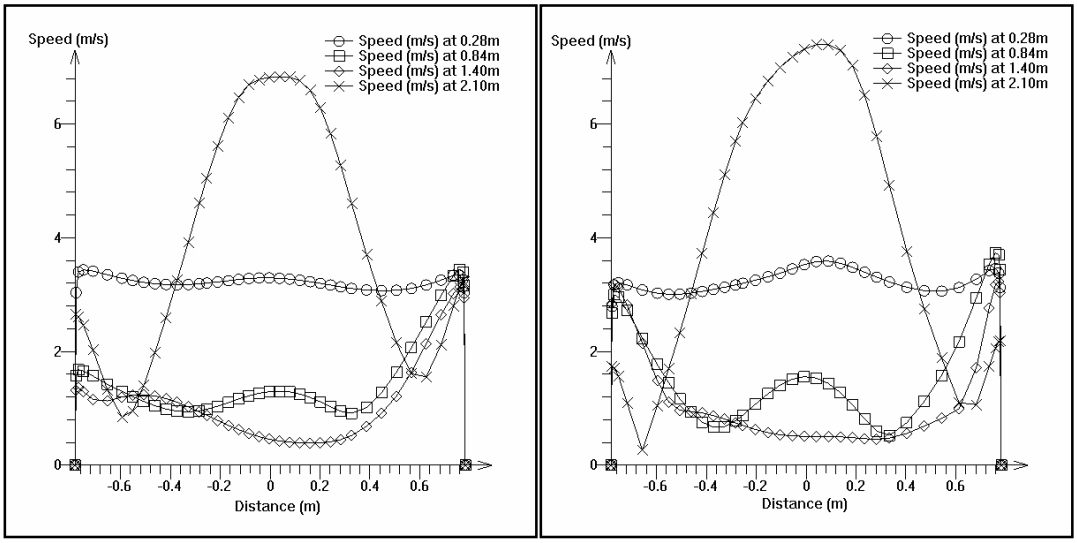

Figure 5-53 Variation speed plot at section F without flow diverter on the left and section F of dryer with flow diverter on the right

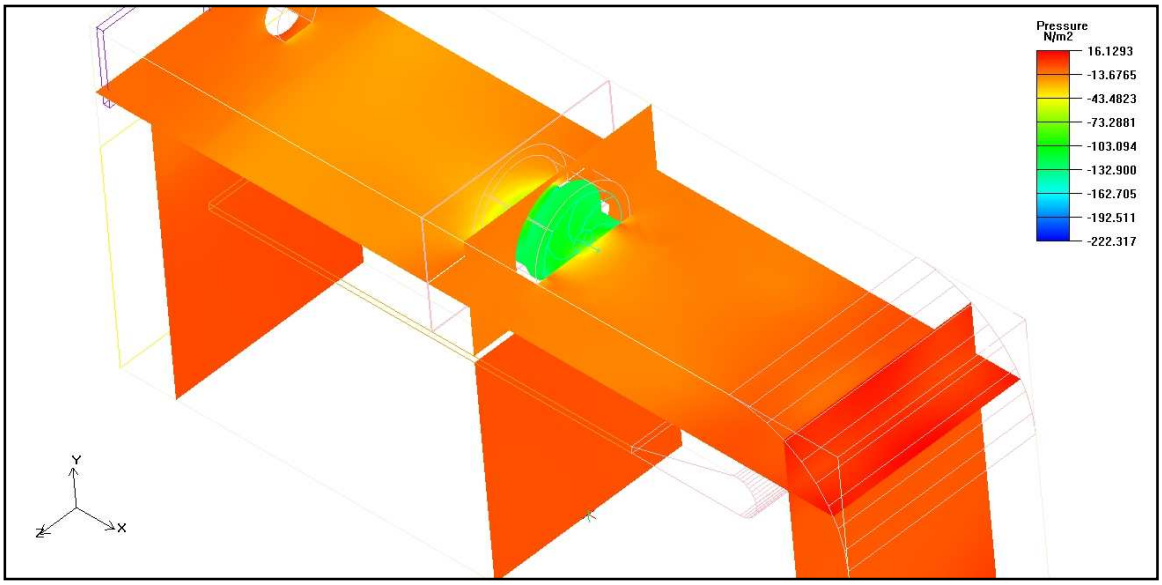

Figure 5-54 Pressure contours

Figure 5-54 will show once again that the pressure contour in the entire domain of the dryer was uniform except at the fan boundaries.

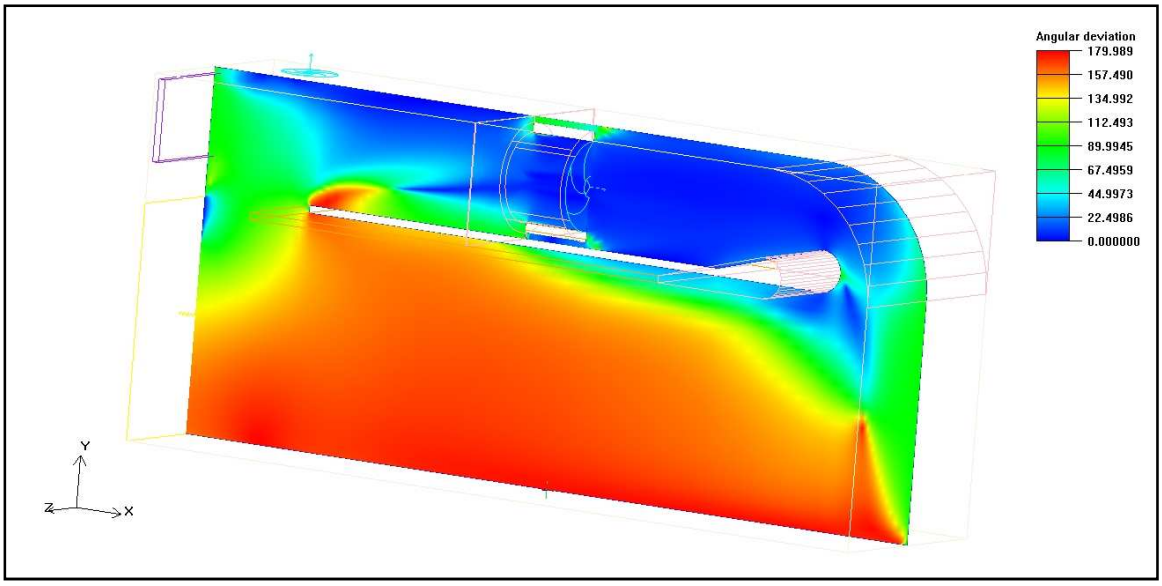

Figure 5-55 Angular deviation in the X-direction (XY-plane in the centre of the main fan)

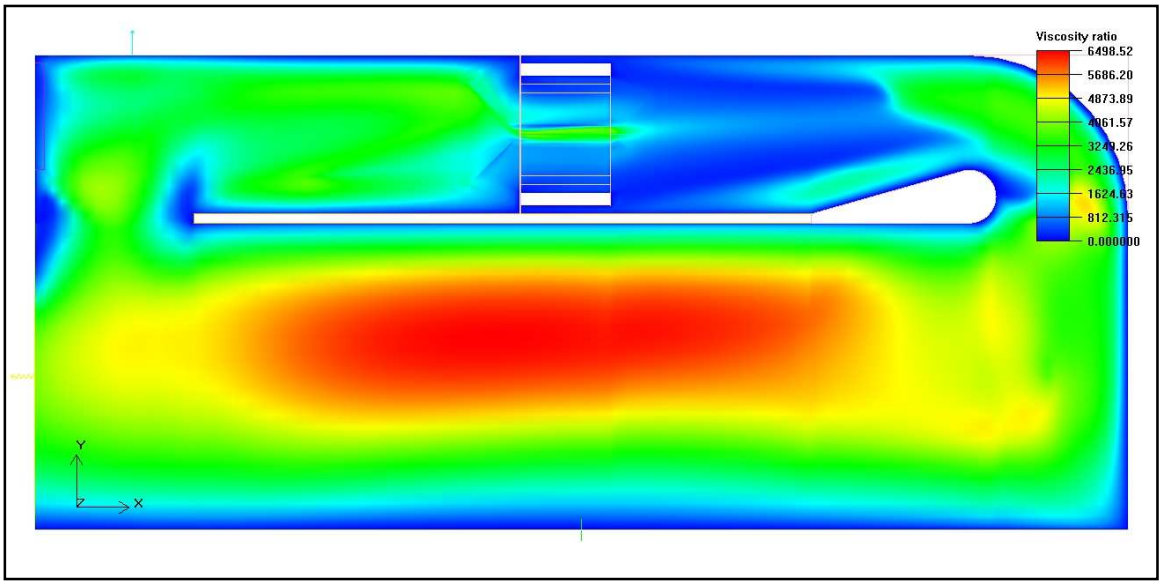

Figure 5-56 Viscosity ratio in XY-plane at the centre of the main fan

The angular deviation was much less at the front tip of the false ceiling compared to the dryer without the flow diverter. This shows that the swirl region is smaller with the flow diverter added (See Figure 5-55).

The viscosity ratio was the highest in the middle of the drying region. The viscosity ratio decreases dramatically near the walls and false ceiling of the dryer (See Figure 5-56).

5.5 Data validation of CFD analysis on dryer with flow diverter

It was found that the range of the speed contour of the CFD analysis was larger compared to the measured results of the same dryer. Overall the region where the range of the speed contour was between 0 and 1m/s agreed well with the experimental set up.

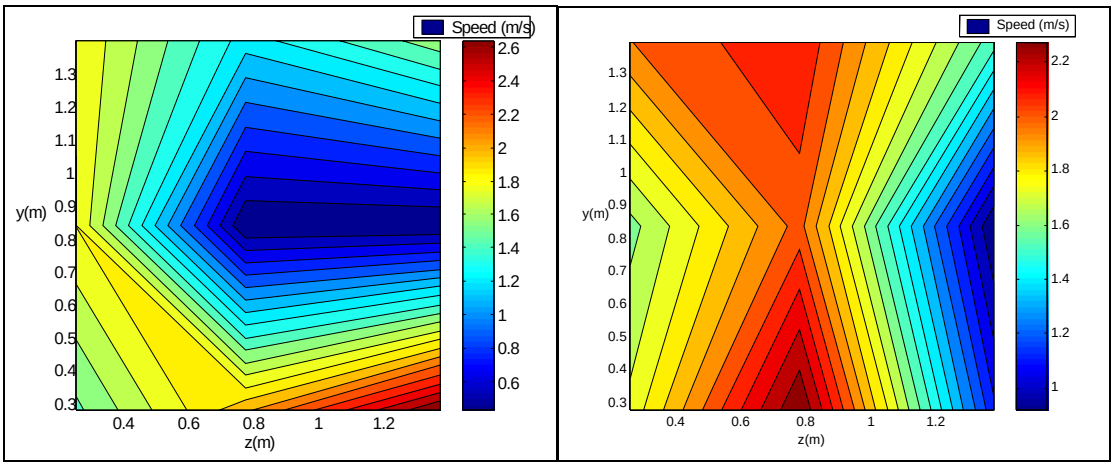

Section A

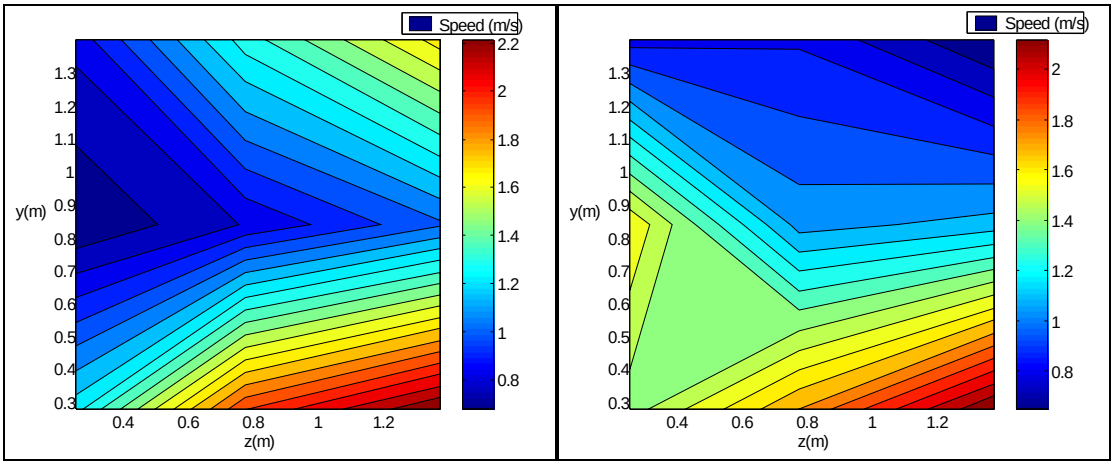

Section B

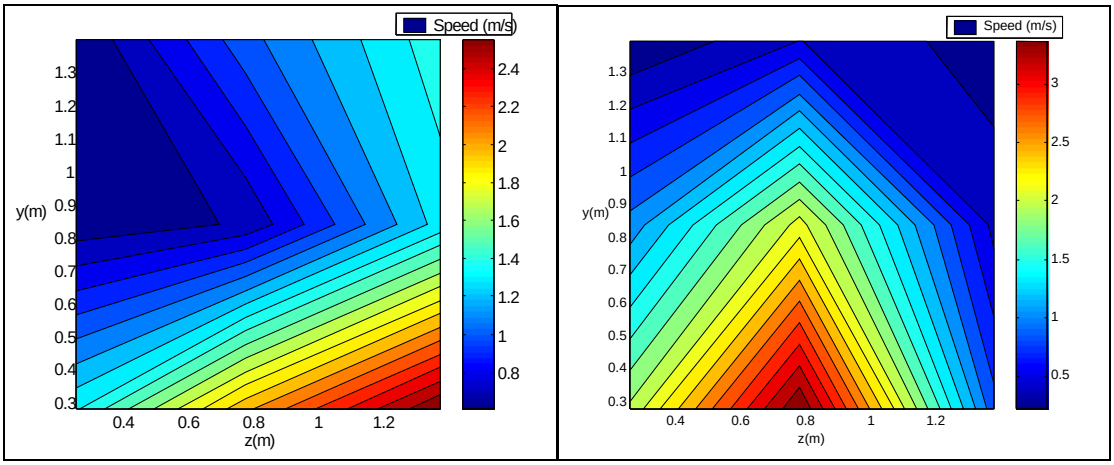

Section C

Figure 5-57 Comparison of the speed contours between the measured results (left) of the dryer with a flow diverter and the CFD analysis on the same sections (right).

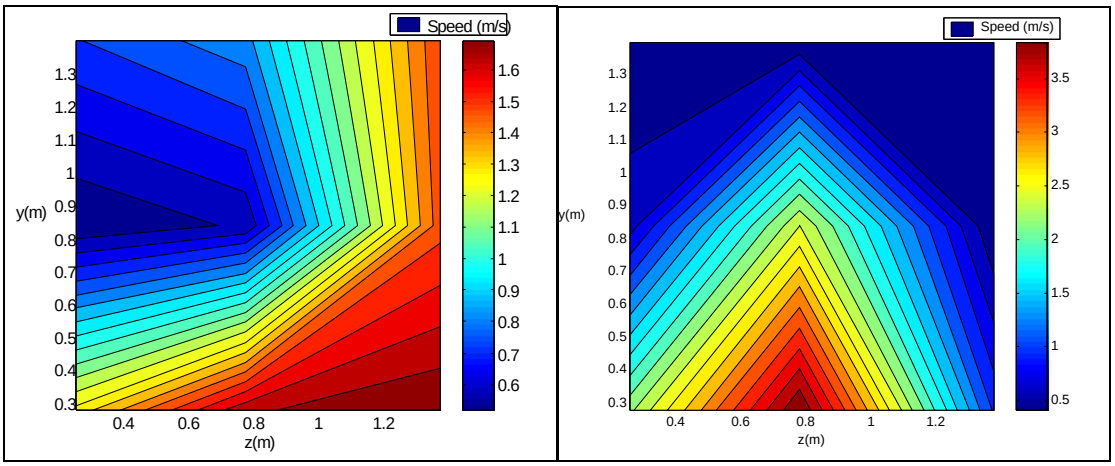

Section D

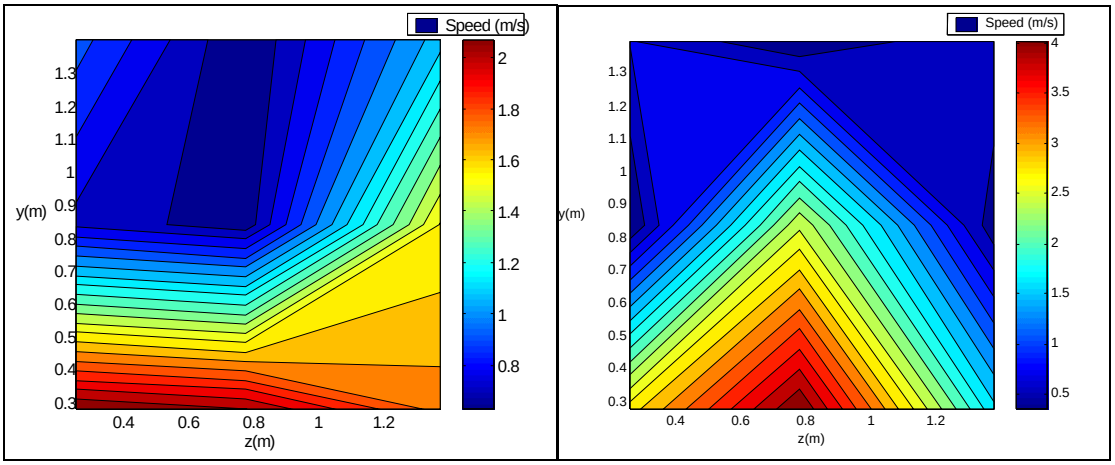

Section E

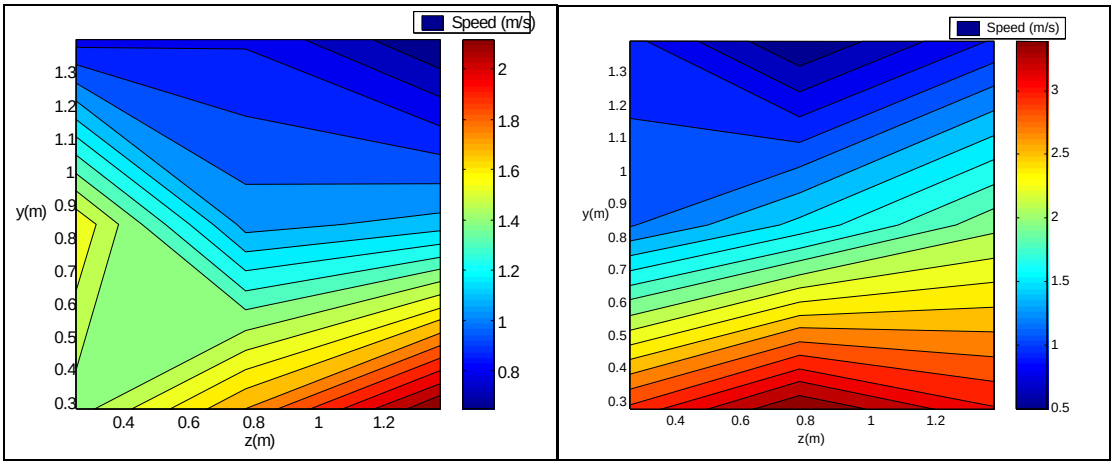

Section F

Figure 5-58 (Contd.) Comparison of the speed contours between the measured results (left) of the dryer with a flow diverter and the CFD analysis on the same sections (right).

5.6 CFD analysis of dryer with mango trolleys

The mesh was mainly refined around the flow diverter. The fine mesh consisted of 1,437,152 elements and 1,602,583 nodes. Taking in account the computing ability of the computer used to obtain the results, it was difficult to construct a more refined mesh with increased elements and nodes around the trolley and mango blocks. The trays' resistance has also been removed. The mango blocks cover 48% of one tray. The free-area ratio of the trays is 0.9, thus only 10% of 52% netting not covered, gives resistance to the airflow. Figure 5-61 shows an analysis done only on a single trolley with trays placed at the front end of the drying zone. It shows that the trays do have some straightening effect on the airflow through the trolleys but is not that significant compared to the mango blocks that have the largest effect on determining the airflow pattern.

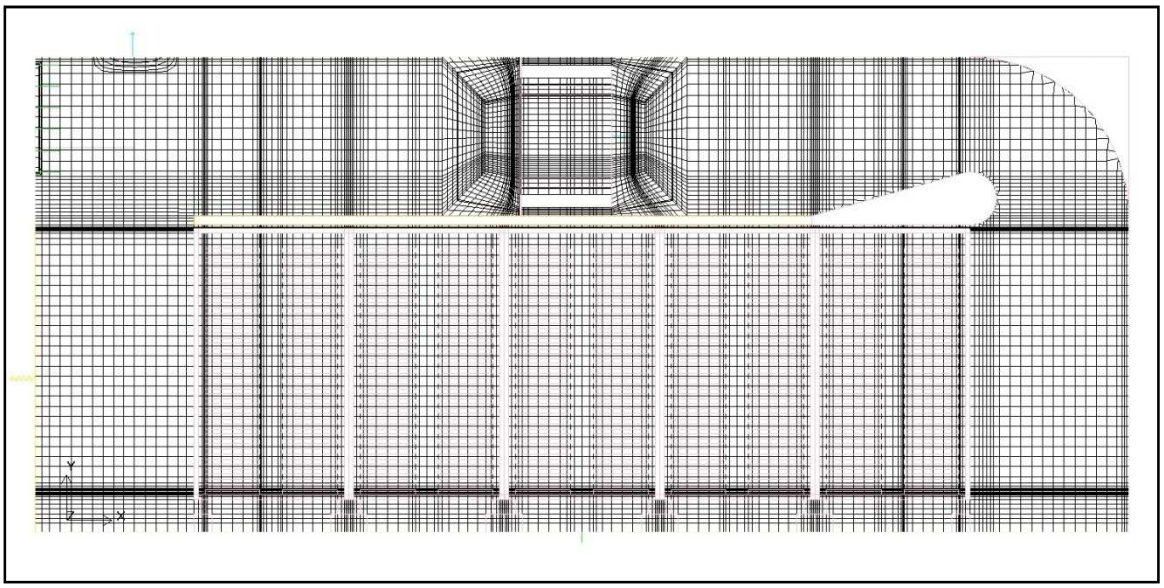

Figure 5-59 Detail of the mesh in the YX-plane in the centre of the main fan

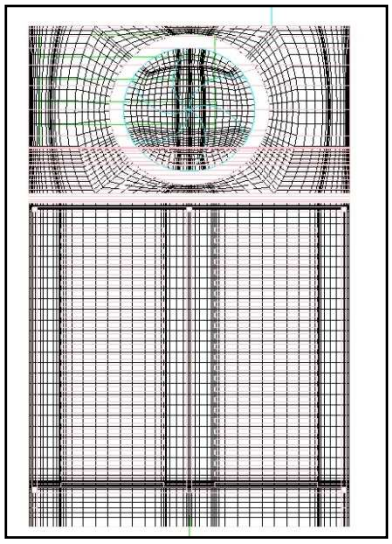

Figure 5-60 Detail of mesh in the ZY-plane the centre of the main fan

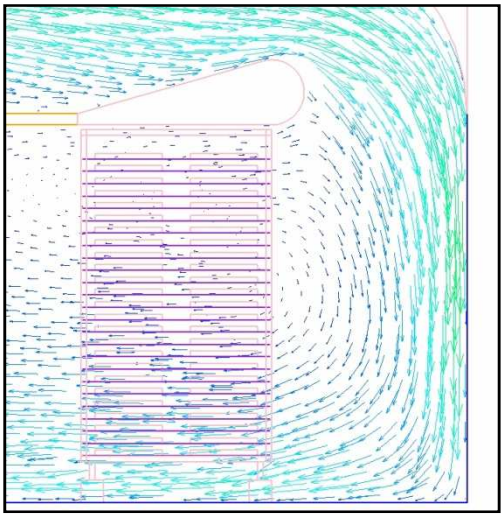

Figure 5-61 Velocity vector of trolley with trays included at the centre of the inlet vent in the XY-plane

Figure 5-62 shows that the swirl action has moved in front of the first trolley. The airflow pattern is straightened by the addition of the mango blocks and trolleys. A larger region of swirl is formed at the back end of the false ceiling compared to the dryer without the trolleys and flow diverter added (See Figure 5-62 and Figure 5-13). The swirl region in the middle of dryer is replaced with an airflow pattern where the air moves upward at a constant gradient from the floor at the beginning of the drying zone.

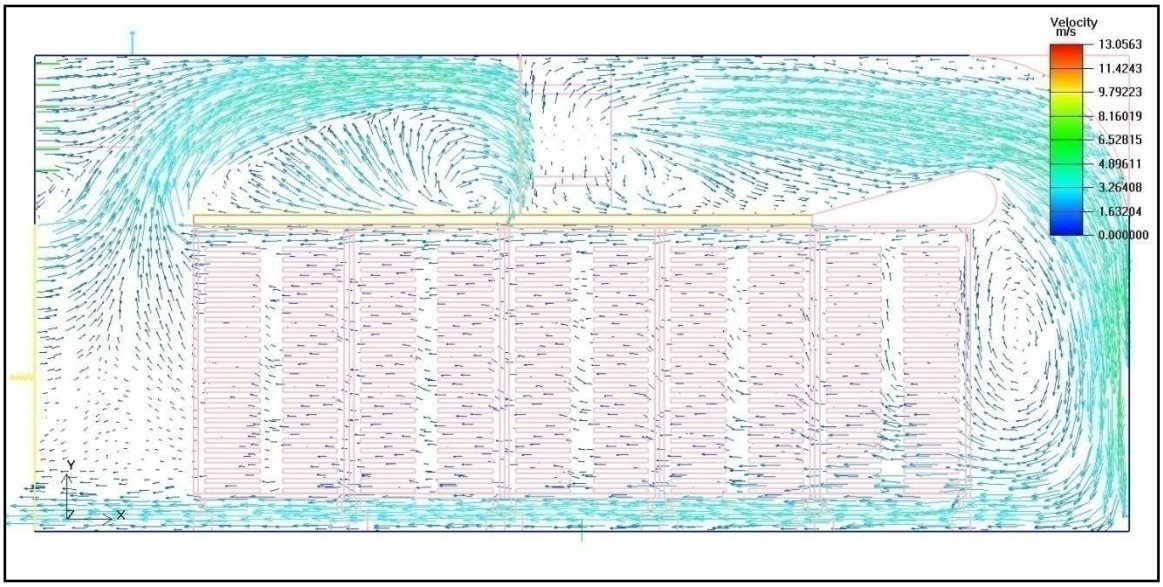

Figure 5-62 Velocity vector field at the centre of inlet vent in the YX-plane

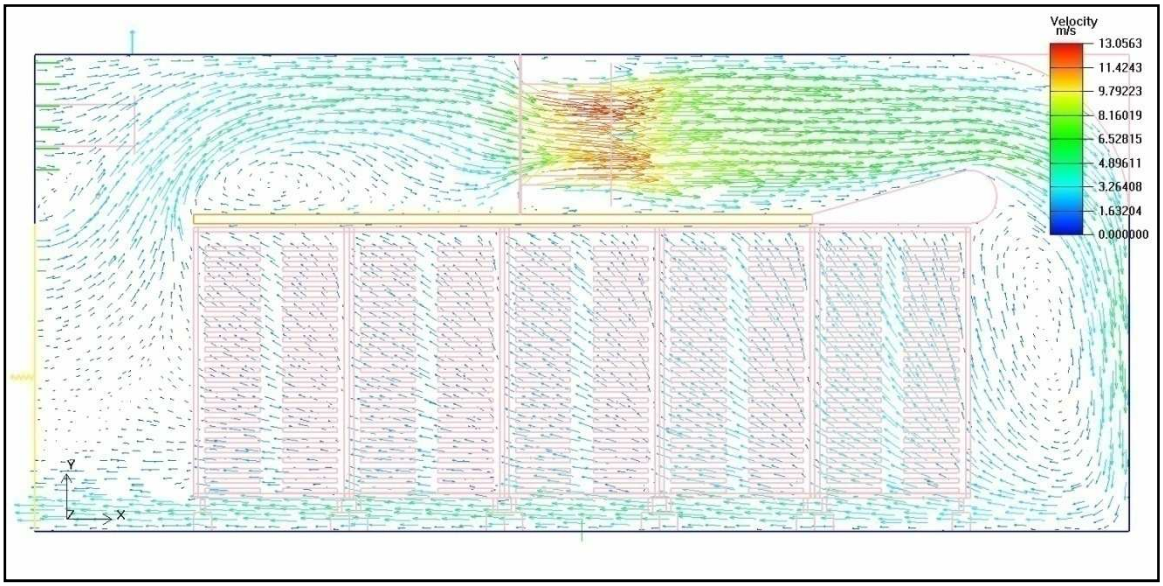

Figure 5-63 Velocity vector field at the centre of main fan in the YX-plane

In the centre of the drying zone where there is gap between the trays of the trolleys the air moves upwards at a greater gradient. The region of the swirl at the backend of the false ceiling is smaller. The swirl region is still in front the drying zone (See Figure 5-63).

The region of swirl at the backend of the false ceiling is smaller at the centre of the gas burner tube in the YX-plane compared to the region of swirl in Figure 5-62. The airflow from trolley two (from the front of the false ceiling) moves parallel with the X-axis.

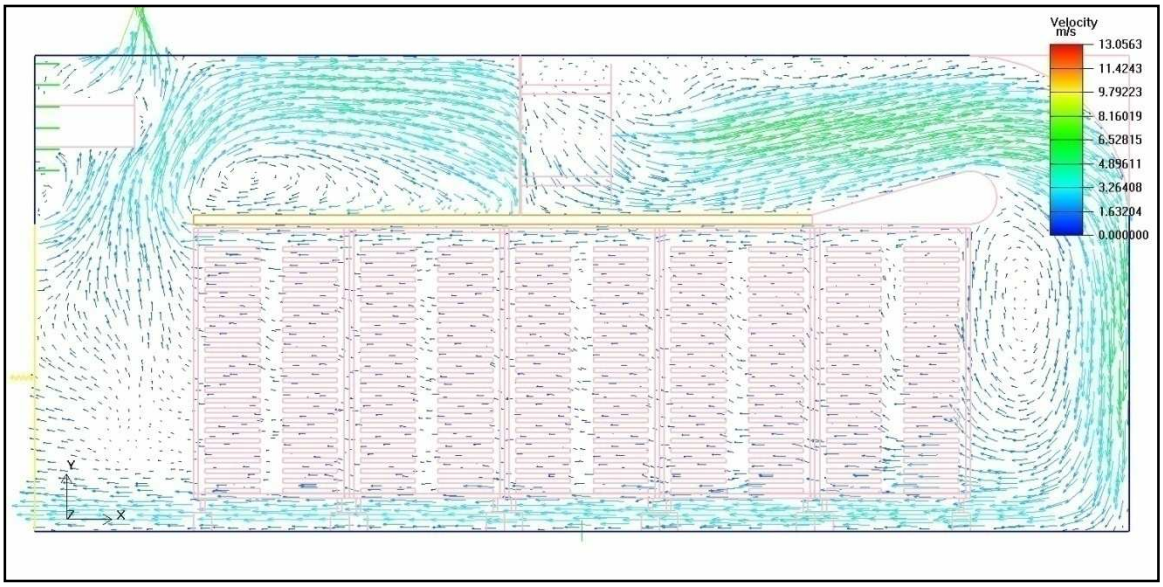

Figure 5-64 Velocity vector field at the centre of burner tube in the YX-plane

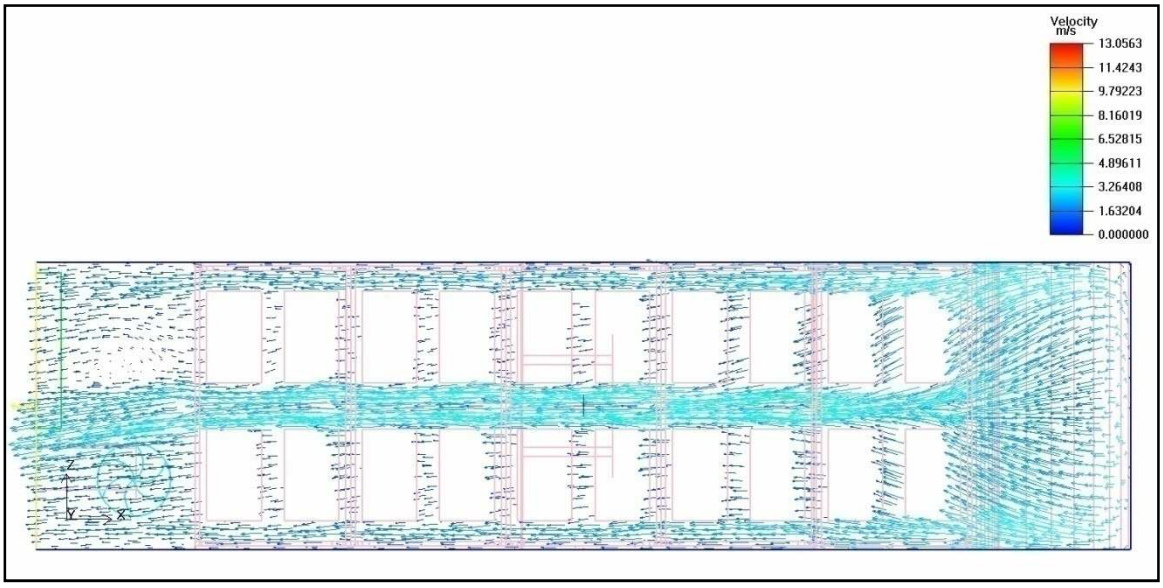

Figure 5-65 Velocity vector field, 0.28 m from the floor in the ZX-plane

No region of swirl is present in the ZX-plane at 0.28 m from the floor (See Figure 5-65). The air is forced between the middle gap of the trolleys and between the walls and the trolleys.

The gaps between the sidewalls, floor, false ceiling and trolleys caused the air to form a circulation flow pattern around the mangoes in the upper half of the drying zone (See Figure 5-66).

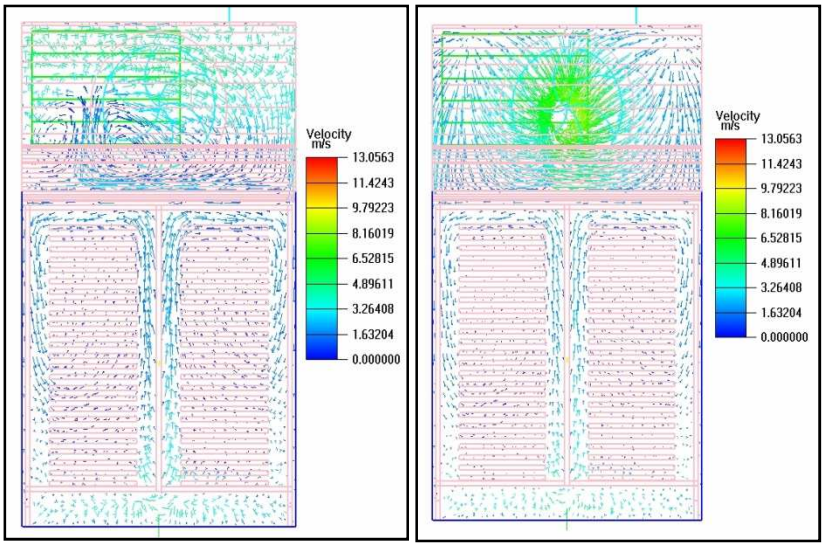

Figure 5-66 Velocity vector field at section D (left) and E (right) in the ZY-plane

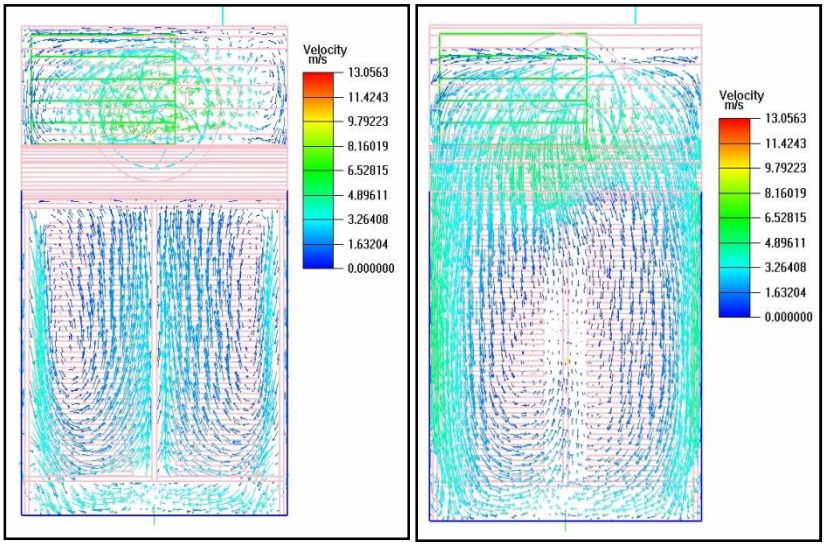

Figure 5-67 Velocity vector field of Section F (left) Midway between section F and the product inlet side (right)

A large region of swirl is formed before the air enters the drying zone (See Figure 5-67).

Table 5-3 Mass, volume and pressure data on the main parts or sections of the dryer

Outlet Fan Operational point			
Volume Flow (m^3/s)	0.8755		
Pressure Rise (N/m^2)	59.2563		
Main Fan Operational point			
Volume Flow (m^3/s)	-3.0229		
Pressure Rise (N/m^2)	72.3158		
Objects	**Avg. Mass flow (kg/s)**	**Avg. Volume flow (m^3/s)**	**Avg. Pressure (N/m^2)**
Opening	1.0372E-02	8.4675E-03	-6.1870E-01
Inlet Vent	1.0619E+00	8.6680E-01	-6.6378E+00
Outlet Fan	-1.0725E+00	-8.7558E-01	-5.5160E+01
Main Fan	3.7031E+00	3.0229E+00	-5.0870E+01
Mass Balance of In & Outlets	-2.2800E-04		

The mass balance between the different in-and-outlets is close to zero, showing that CFD analysis converged to a suitable solution. The pressure rise of the main fan's operational point dropped by 7.5% compared to the dryer without the trolleys and mangoes included, with the volume flow increasing by 1.8%. (See Table 5-2 and Table 5-3). The pressure in the 2D region at the main fan decreased by 38.5%, meaning there is a large pressure drop over the drying zone now containing the mangoes and trolleys.

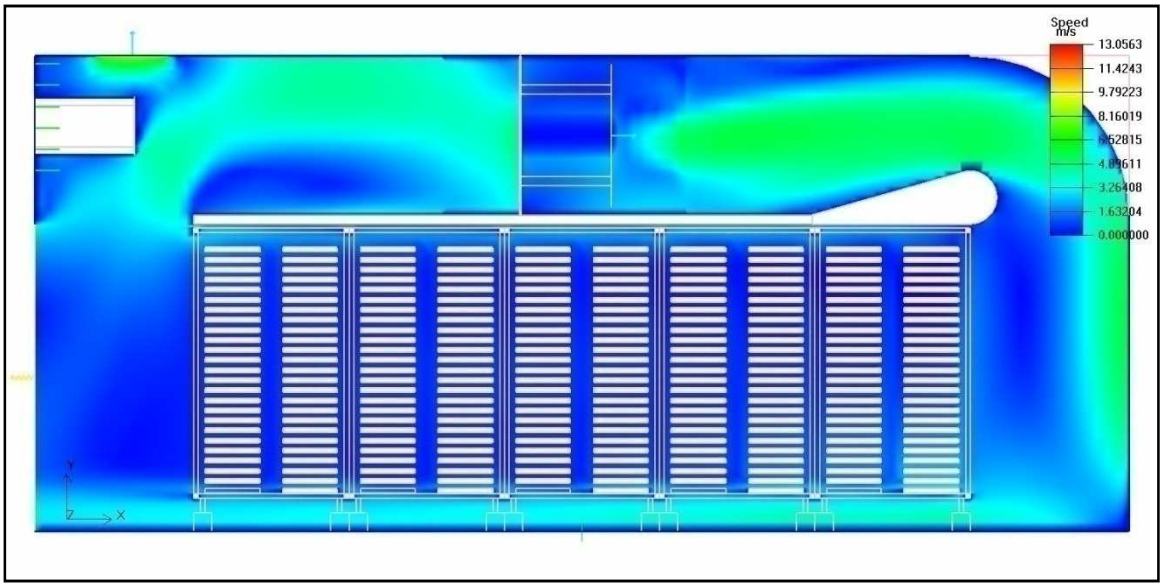

Figure 5-68 Speed contour in XY-plane in centre of burner tube

The range of the speed contour is uniform over the trays and mangoes, but there is large increase in speed in the gap between the floor and the trolleys. The

range of the speed contour at the region in front of the first trolley near the flow diverter is almost the same as in the drying zone (See Figure 5-68).

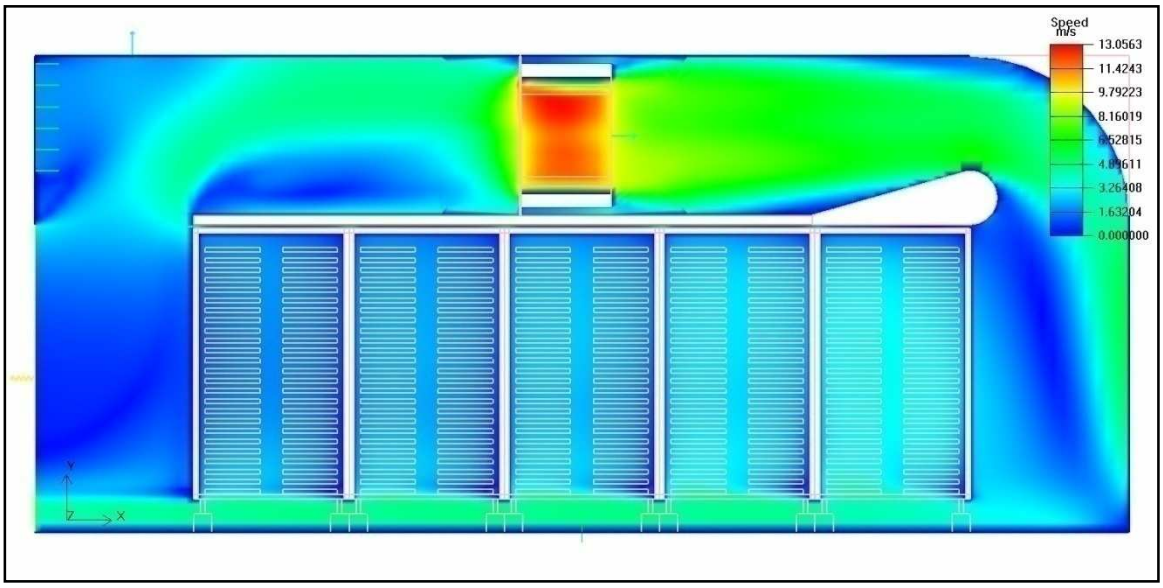

Figure 5-69 Speed contour in XY-plane in centre of main fan

There is large increase in speed in the gap between the trays of the trolleys. The range of the speed contour over the first two trolleys is uniform. The speed goes down as the air flows down the drying zone (See Figure 5-69).

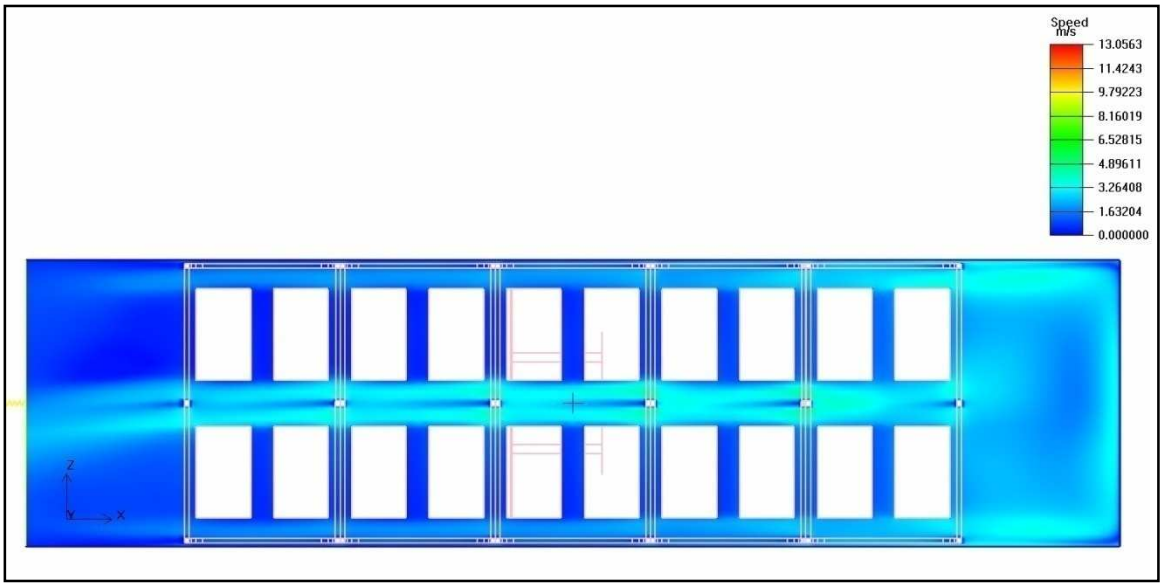

Figure 5-70 Speed contour in ZX-plane, 0.28 m from the floor

The speed decreases from the floor upwards towards the ceiling. The range of the speed contour decreases in the positive Y-axis (See Figure 5-70 and Figure 5-71).

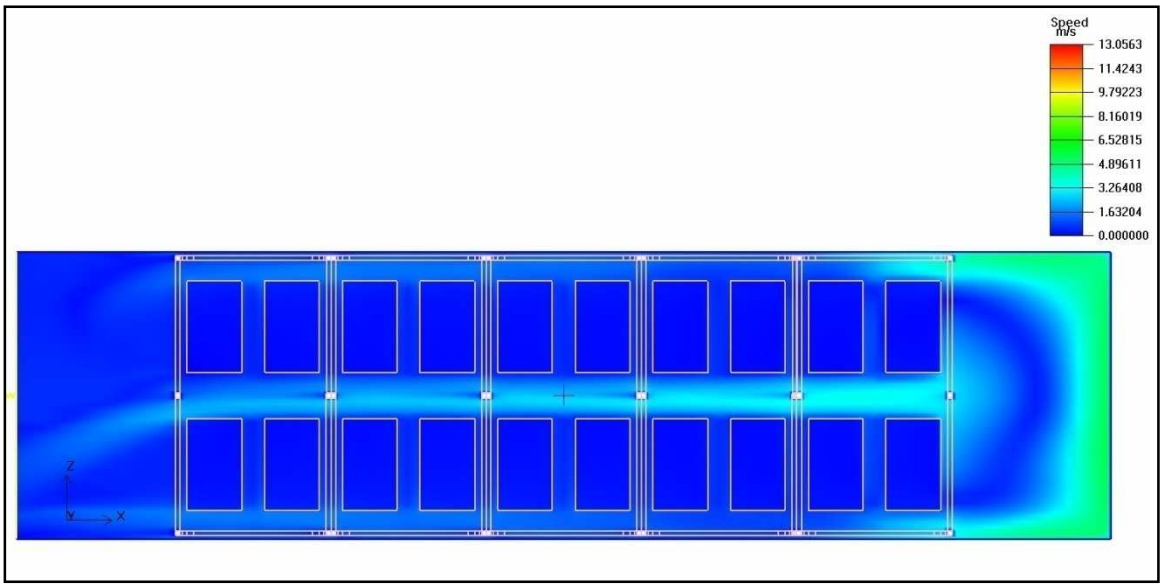

Figure 5-71 Speed contour in ZX-plane, 0.84 m from the floor

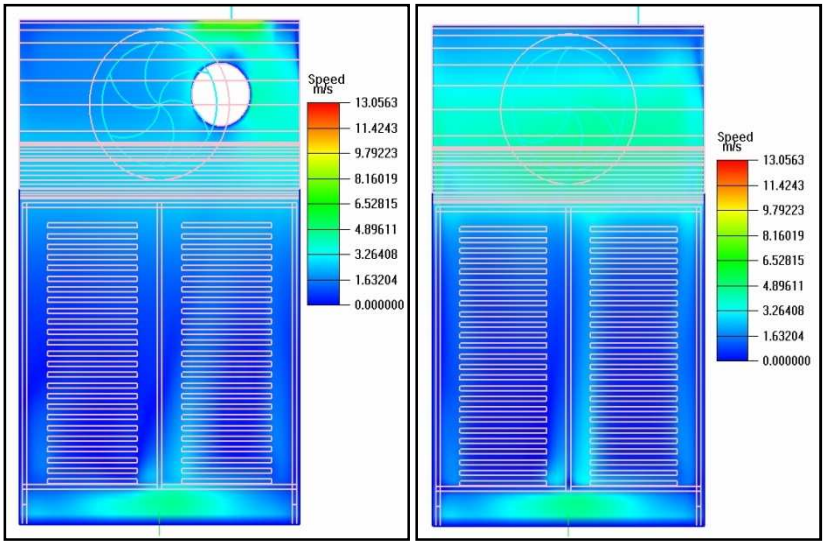

Figure 5-72 Midway between opening and section A (left), and viewing section A in the negative X direction (right)

The range of the speed contour is uniform over most of the region at the back of the last trolley. The largest speed hike is in the middle gap of the trolleys near the floor (See Figure 5-72). By comparing Figure 5-73 to Figure 5-72 one can see that the range of the speed contour decreases, even in the middle gap of the trolleys as the air moves along in the negative X-axis.

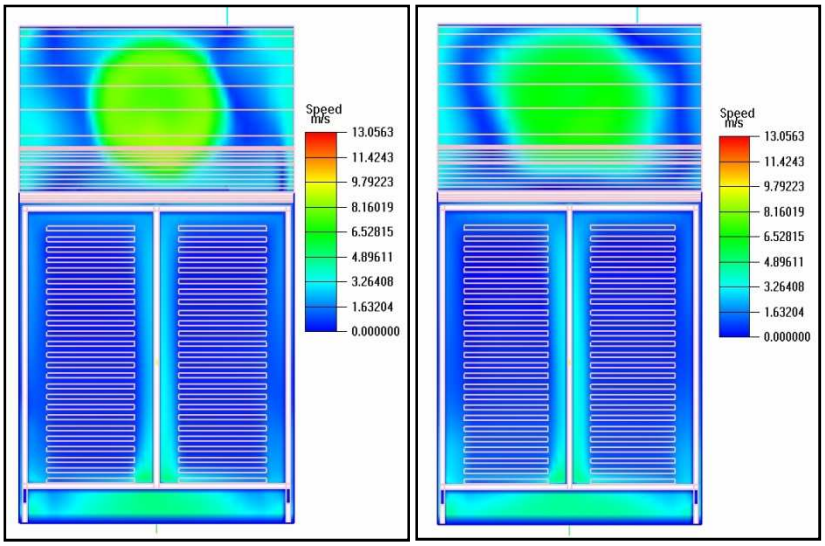

Figure 5-73 Speed contour of section D on the left and section E on the right in the ZY-plane

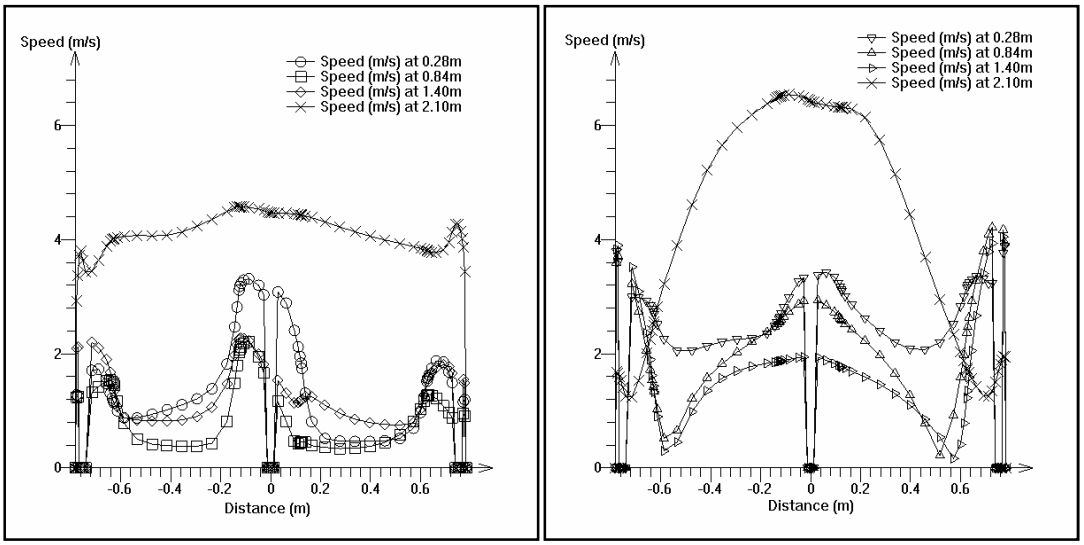

Figure 5-74 Variation speed plot at section A on the left and section F on the right

The speed at the 0 m point on the Z-axis goes to zero on the ZY-plane at both sections (See Figure 5-74). The section goes across the entire drying zone and this is where it intersects with the frame of the trolleys. The speed is still increasing towards the middle of the drying zone in the region of the gap between the trolleys. This figure once again shows that the speed between the gaps created between the walls and trolleys increases. On the wall, due to the no-slip theory, the speed is zero. At section F the mango slices that lie 0.6 m to 0.7825 m from the centre of the dryer experience a sharp increase in speed. This increase in speed is less in section F at the points mentioned above.

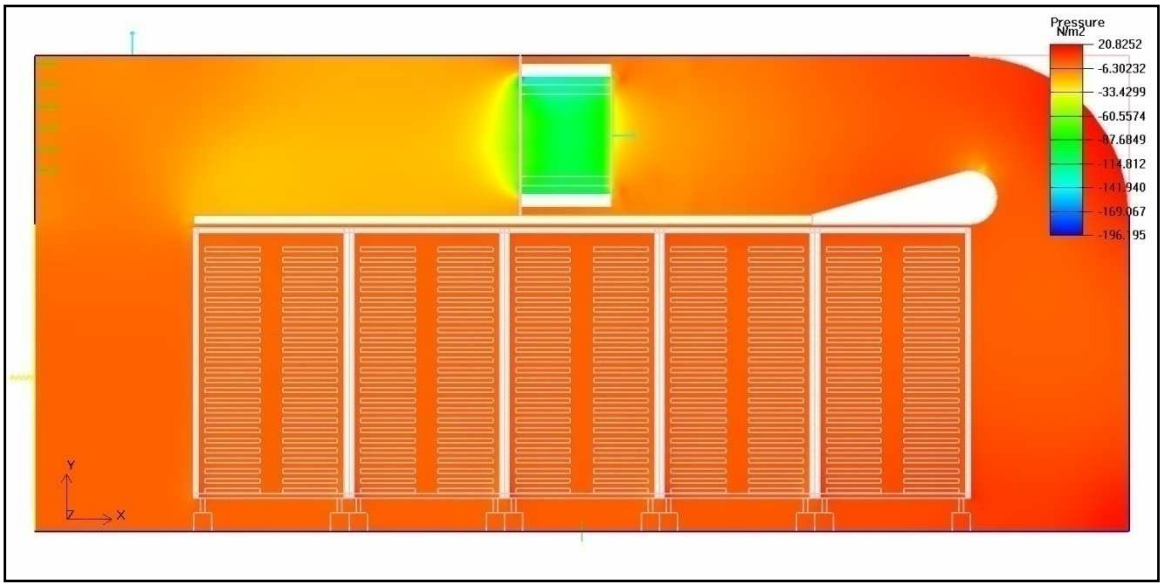

Figure 5-75 Pressure contour at the centre of the main fan at the YX-plane

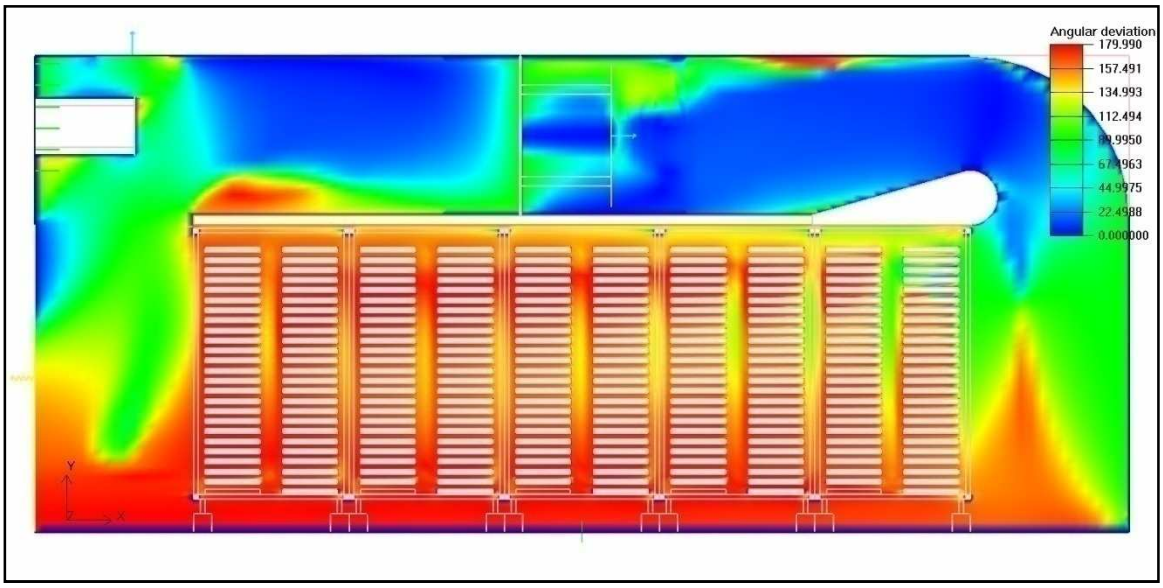

Figure 5-76 Angular deviation in the X-direction (XY-plane in the centre of the gas burner tube)

The pressure drop over the drying zone is uniform (See Figure 5-75). The angular deviation in the X-direction at the front end of the false ceiling shows that the region of swirl is has moved outside the drying zone. There is a very small region of swirl at the first top trays of the front trolley. In the rest of the drying zone the flow is parallel over the mango blocks. With the addition of the trolleys and trays the region of swirl at the back end of the false ceiling decreased (See Figure 5-76, Figure 5-55 and Figure 5-34).

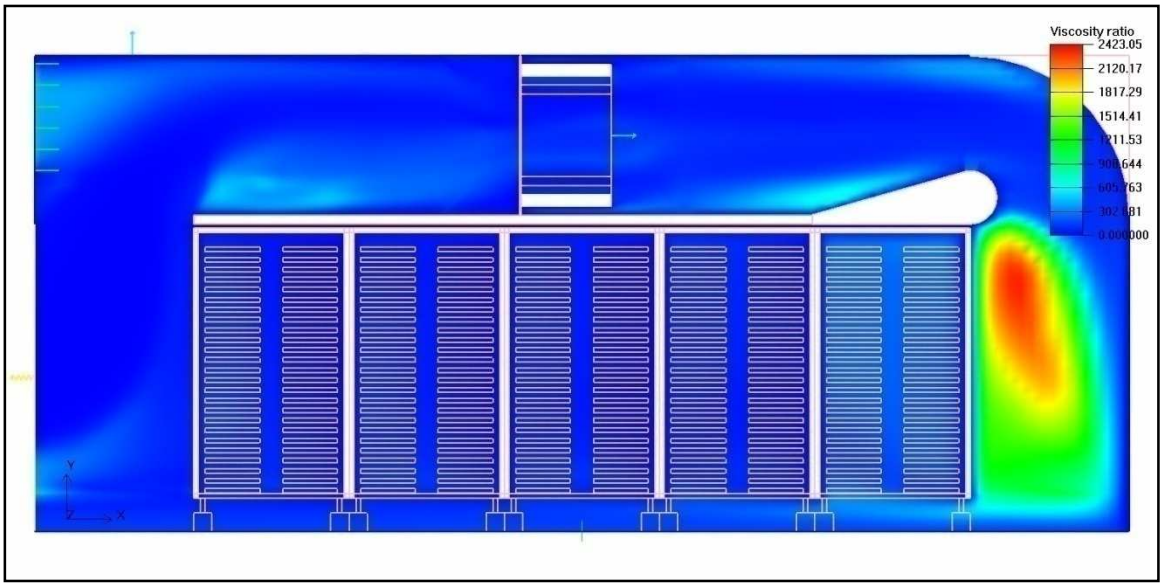

Figure 5-77 Viscosity ratio at the centre of the main fan in the XY-plane

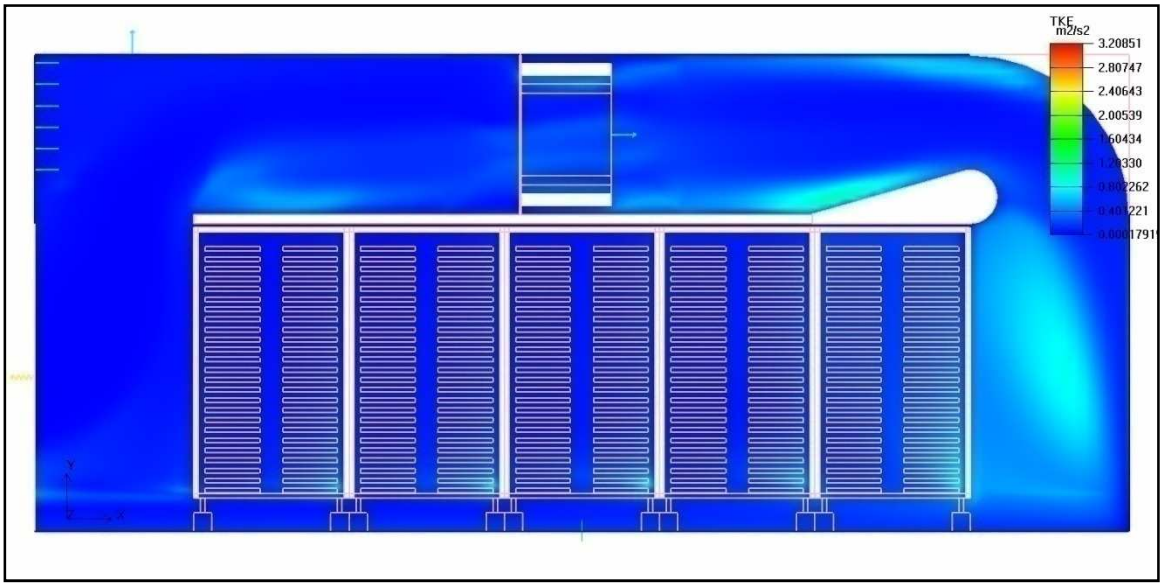

Figure 5-78 Turbulent kinetic energy at the centre of the main fan in the XY-plane

The viscosity ratio became more uniform in the drying zone of the dryer with the mango trolleys (See Figure 5-77). The region in front of the first trolley has the largest viscosity ratio. The turbulent kinetic energy also increased in the region in front of the first trolley. In the drying zone the TKE (k) is uniform just like the dryers without the trolleys (See Figure 5-78).

5.7 CFD Data validation of dryer with flow diverter, mangoes and trolleys

The profile of the speed contours for the CFD simulation and the experimental set-up differed from the dryers without the trolleys added. There is now two separate regions divided by the gap between the trolleys where the speed range is 0-1m/s. These regions compared well between the CFD analysis and the test results. The maximum speed of each section of the CFD analysis is still on average 1m/s higher compared to the region of the test results.

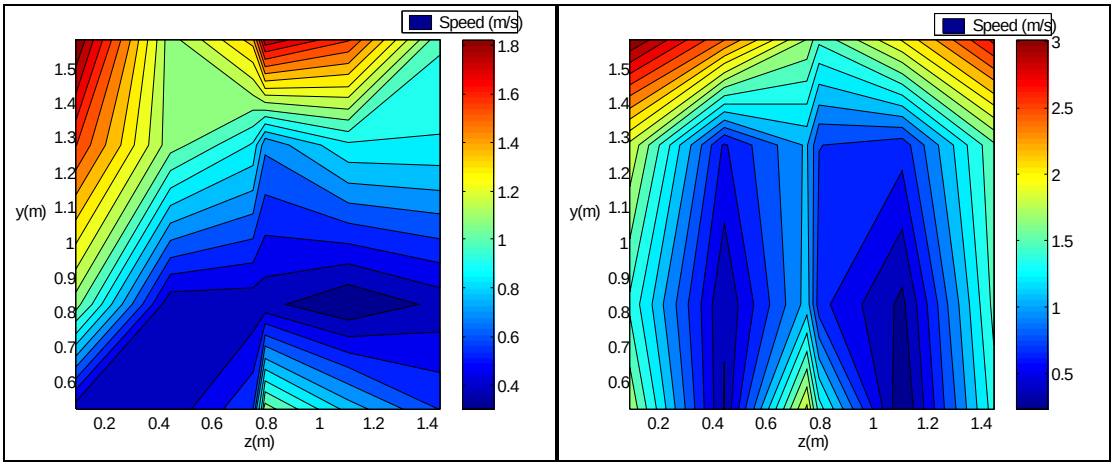

Section A

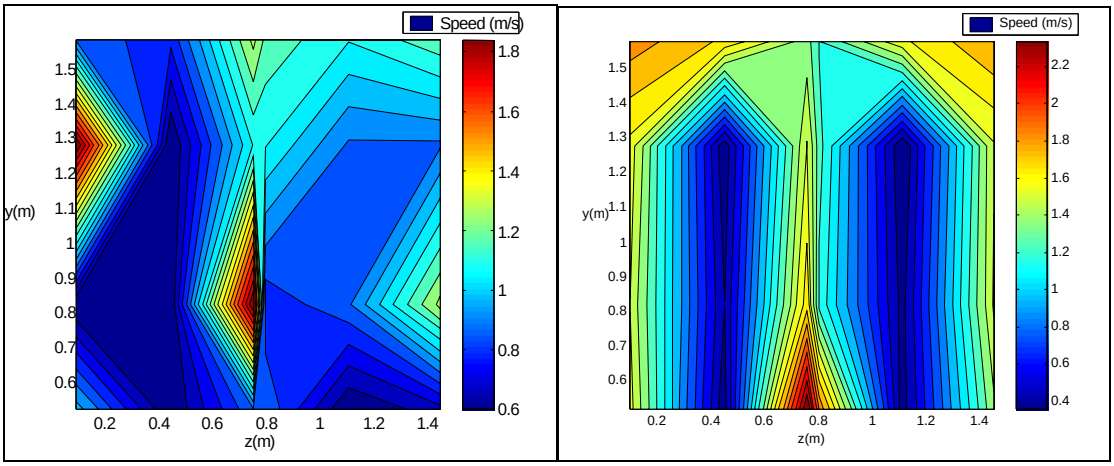

Section B

Figure 5-79 Comparison of the speed contours between the measured results (left) of the dryer with a flow diverter and the CFD analysis on the same sections (right).

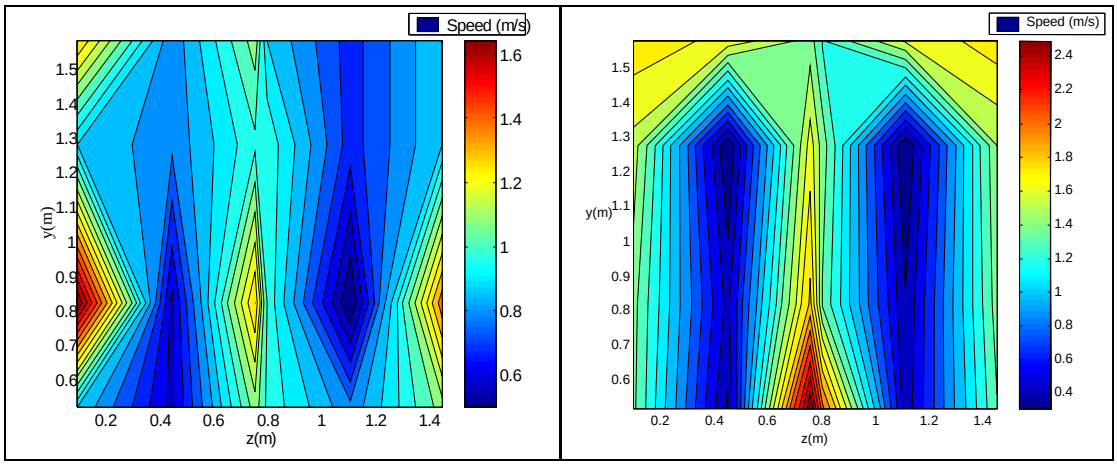

Section C

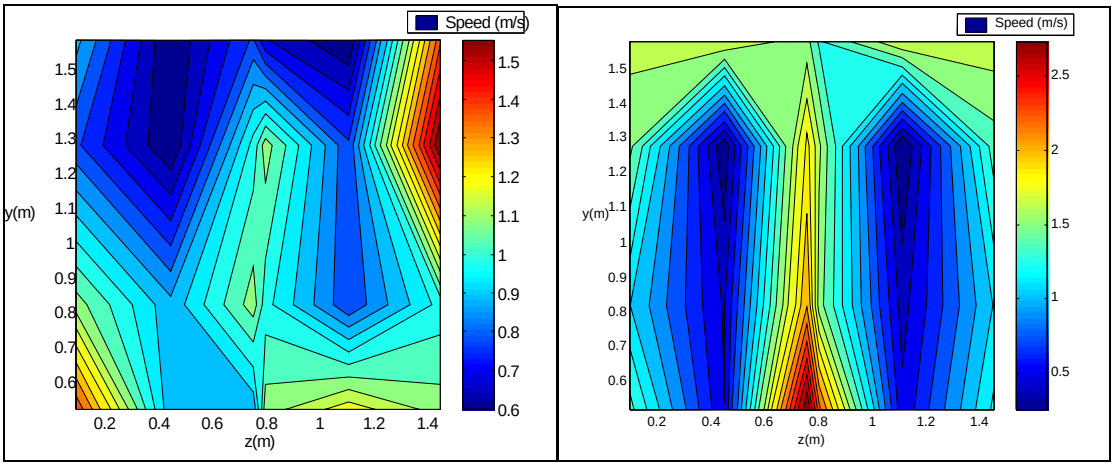

Section D

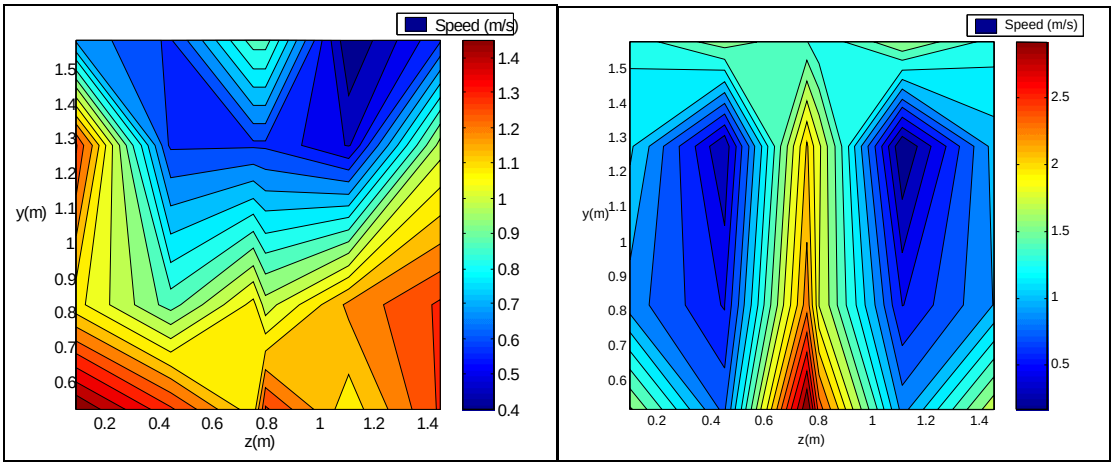

Section E

Figure 5-79 (Contd.) Comparison of the speed contours between the measured results (left) of the dryer with a flow diverter and the CFD analysis on the same sections (right).

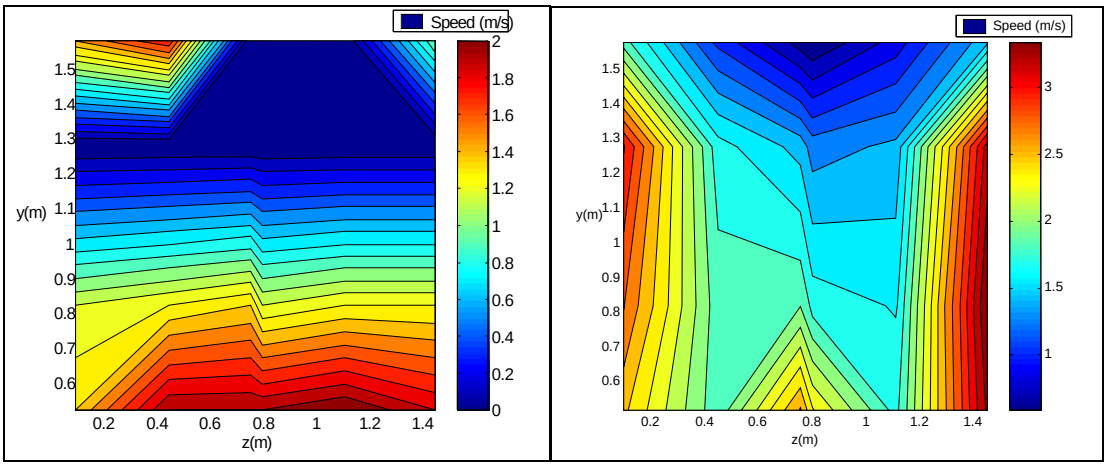

Section F

Figure 5-79 (Contd.) Comparison of the speed contours between the measured results (left) of the dryer with a flow diverter and the CFD analysis on the same sections (right).

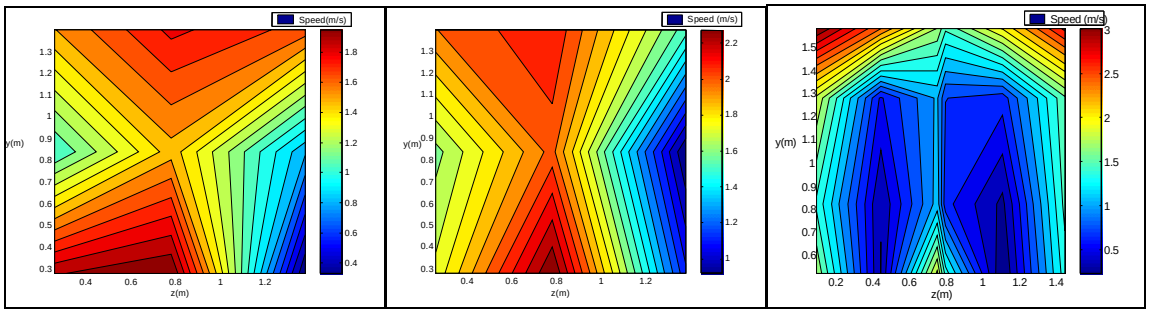

Section A

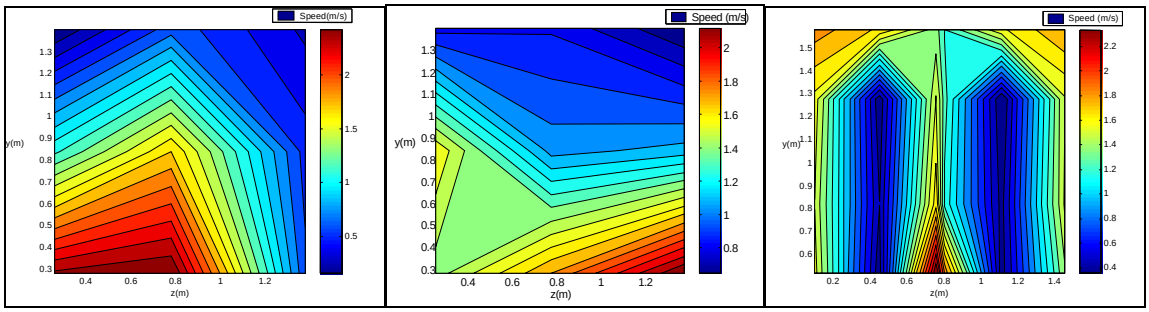

Section B

Figure 5-80 Comparison of the speed contours between the CFD results of the dryer without a flow diverter (left), the dryer with the flow diverter (middle) and the one with the flow diverter and the trolleys added (right).

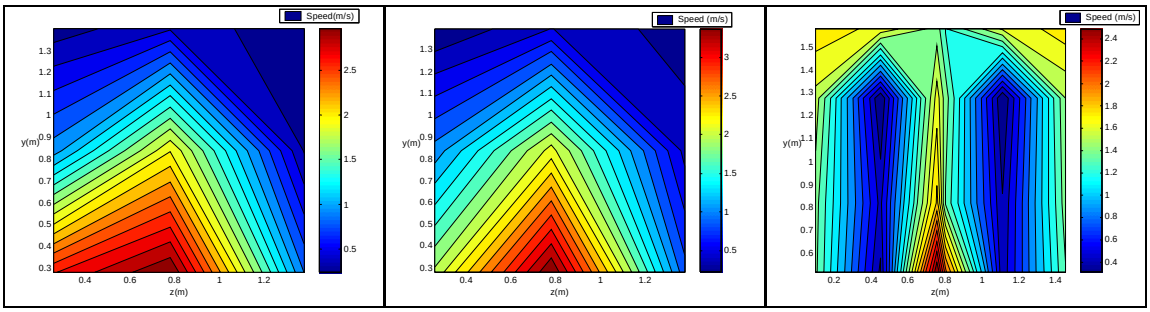

Section C

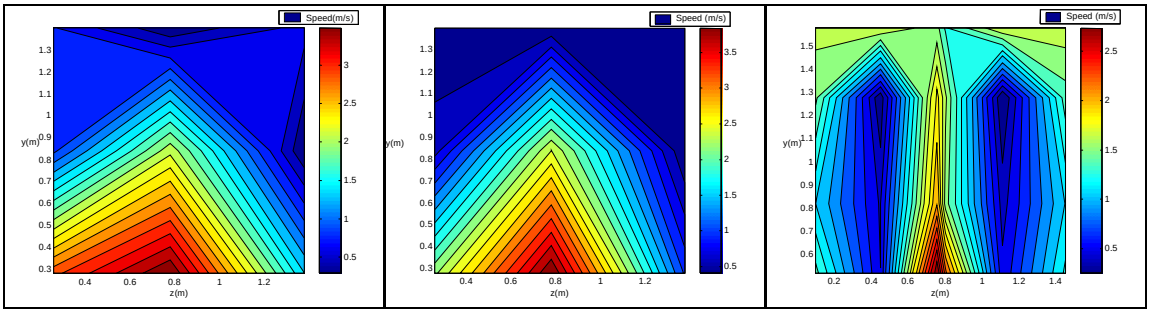

Section D

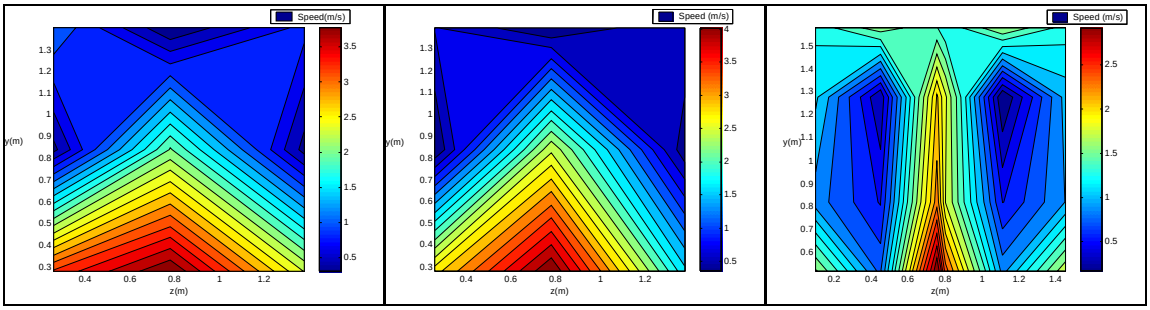

Section E

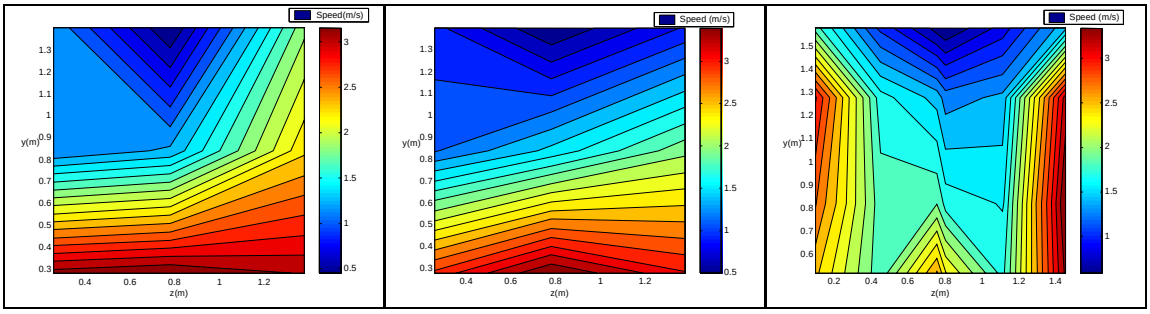

Section F

Figure 5-81 (Contd.) Comparison of the speed contours between the CFD results of the dryer without a flow diverter (left), the dryer with the flow diverter (middle) and the one with the flow diverter and the trolleys added (right).

Figure 5-81 shows that the speed range over the region that contained the trolleys is smaller and more uniform, compared to the dryers without the trolleys added.

5.8 The comparison of the average speed in each section

The arithmetic mean of each section's velocity was taken. This was done for the measured results and the CFD analysis. A standard deviation was taken on each section, which is a sample of the speed in the drying zone. The standard deviation is a measure of how widely values are dispersed from the average mean value (statistics.com, 2009). The sample was taken in the fully turbulent region of the velocity profile over the section in the drying zone. The region near the wall where the no-slip theory was applied (velocity is zero at the wall) was not part of the sample points to calculate the average speed over the sections.

Table 5-4 The average speed of each section for the dryer without a flow diverter

Section	Exp.1 Speed Avg.	RNG Speed Avg.	ABS. % Diff.	Stdev of Exp1	Stdev of RNG
A	1.28	1.41	10.32	0.43	0.56
B	1.31	1.14	12.68	0.48	0.89
C	1.33	1.23	7.51	0.62	1.09
D	1.21	1.46	20.52	0.46	1.20
E	1.38	1.65	19.28	0.64	1.33
F	1.48	2.00	34.43	0.50	1.05
Total Avg.	1.33	1.48	17.46	0.52	1.02
Stdev of Section A-F	0.09	0.31			
% Diff between Total Avg. of Exp1 and RNG			11.16		

The total average speed of all the sections for the CFD analysis was 11.2% higher than the measured results (See Table 5-4). The average speed of the D, E and F sections differed 20% and higher compared to measured results.

Table 5-5 The average speed of each section for the dryer with a flow diverter

Section	Exp.2 Speed Avg.	RNG Speed Avg.	ABS. % Diff.	Stdev of Exp2	Stdev of RNG
A	1.53	1.72	12.64	0.75	0.47
B	1.33	1.27	4.75	0.55	0.86
C	1.32	1.25	5.56	0.68	1.11
D	1.16	1.37	17.72	0.48	1.27
E	1.29	1.53	18.59	0.60	1.38
F	1.28	1.87	46.95	0.50	1.10
Total Avg.	1.32	1.50	17.70	0.59	1.03
Stdev of Section A-F	0.12	0.26			
% Diff between Total Avg. of Exp1 and RNG			13.92		

The total average speed of all the sections for the CFD analysis done on the dryer with the flow diverter configuration, were 14% higher than the measured results (See Table 5-5).

Table 5-6 The average speed of each section for the dryer with a flow diverter and trolleys

Section	Exp.3 Speed Avg.	RNG Speed Avg.	ABS. % Diff.	Stdev of Exp3	Stdev of RNG
A	1.02	1.53	50.04	0.56	1.11
B	1.11	1.35	21.53	0.49	0.59
C	1.05	1.38	31.23	0.38	0.62
D	1.04	1.41	35.66	0.31	0.67
E	1.01	1.47	45.55	0.34	0.70
F	0.94	2.05	118.46	0.83	0.81
Total Avg.	1.03	1.53	50.41	0.49	0.75
Stdev of Section A-F	0.06	0.26			
% Diff between Total Avg. of Exp1 and RNG			48.91		

The average speed of the CFD analysis in Table 5-6 was 49% higher compared to the test results. The absolute difference was taken to make sure that sections with lower average speed do not cancel out with sections with high average speeds. The configuration of the dryer with flow diverter and mango trolleys has a stabilising effect on the uniform flow of air through the drying zone.

Table 5-7 Average speed of the CFD analysis on the dryer without a flow diverter but with the mango trolleys included

Section	RNG Speed Avg.	Stdev of RNG
A	1.53	0.82
B	1.41	0.65
C	1.40	0.74
D	1.40	0.85
E	1.33	0.92
F	1.82	0.94
Total Avg.	1.48	0.82
Stdev of Section A-F	0.18	

No measured results were taken on the dryer without a flow diverter and mango trolleys configuration. The coefficient of variation (*CV*) is the ratio of the standard deviation (*STDEV*) to the arithmetic mean (statistics.com, 2009). This can be used to compare the amount of variance between populations with different means. The standard deviation mentioned in Table 5-8 is calculated from the sample points within the drying zone from section A to F. The *CV* value according to the CFD results (RNG) for the dryer with the flow diverter and mango trolleys included (Table 5-6) was lower compared the dryer without the flow diverter (Table 5-7). Without the mango trolleys in the drying zone which are

a factor that influence the uniform velocity, there was no difference in the CFD *CV* values of Table 5-4 and Table 5-5. The *CV* value of test results from the dryer without flow diverter and mango trolleys (Table 5-4) are lower compared to the dryer referenced in Table 5-5.

Table 5-8 Comparison of the CV values of the various dryer configurations

Ref.	Table 5-4		Table 5-5		Table 5-6		Table 5-7
Results	Exp. 1	RNG	Exp. 2	RNG	Exp. 3	RNG	RNG
MEAN	1.33	1.48	1.31	1.50	1.03	1.53	1.48
STDEV	0.51	1.04	0.58	1.05	0.51	0.80	0.82
CV	0.38	0.70	0.44	0.70	0.49	0.52	0.55

One should not conclude by just looking at Table 5-8 that it is unnecessary to include a flow diverter in the dryer construction due to the small differences between *CV* values. Consideration should be given to the error of the measured results between the different experimental set-ups. Secondly this standard deviation values were calculated for the complete drying zone, showing that the non-uniform velocity distribution do even out as the air flows through to the zone.

Table 5-9 shows the *CV* values of section E and F of Table 5-6 and Table 5-7. These are the sections nearest to the flow diverter (Table 5-6) or where the air enters the drying zone after it passed through the main fan (Table 5-7). It is in these sections where the largest non-uniform velocity distribution occurred. The *CV* value of the dryer with the flow diverter (Table 5-6) is 25% lower compared to the dryer without one (Table 5-7). This is an indication along with the other statistical, experimental and CFD results that the flow diverter in a drier in the industrial environment (Doors closed and trolleys stacked with mangos), produces a more uniform velocity distribution in the drying zone.

Table 5-9 Comparison of the CV values for section E-F of the various dryer configurations

Ref.	Table 5-6	Table 5-7
Results	RNG	RNG
MEAN	1.75	1.58
STDEV	0.80	0.95
CV	0.45	0.60

It is difficult to compare or evaluate the results with previous findings of studies that used CFD analysis, because of the various factors that change for each analysis. A cooler with similar dimensions, geometry and air velocity was simulated using a standard $k-\varepsilon$ model by Nahor, Hoang, Verboven, Baelmans and Nicolai in 2004. The CFD results of their study also showed an over and

under estimation (up to 50%) of the air velocity in region near the floor and on the upper part of the cooling zone. The average speed in the planes of the CFD analysis compared well with measured results. Their standard deviation for their model was much lower at 23.5 %. One of the reasons given for the difference of the CFD analysis compared to the measured results is the error of the experimental set up (See Chapter 10.2). The direction of the airflow is not known, thus the correct placement and direction of the velocity sensor to accurately capture the flow is difficult (Nahor et al., 2004). In section 3.2 it was mentioned that the two different anemometers that was used to measure the speed, differed by 30% of each other at the same point. The difference in the measurements of results could also be attributed to the fact that anemometers should be used for specified applications. The large fan anemometer (AV6) should be used for turbulent flow in between the trolleys with mangos and the Testo 451 anemometer for open volumes when the trolleys are removed from the drying zone (See Chapter 10.2.1)

The average flow results should be evaluated with the contour and velocity flow vectors to give real insight into the uniform velocity distribution in the drying zone. All the previous studies showed that the speed contours and swirl region of the CFD analysis compared well with the measured results. With all three ways of evaluating the problem taken into account, then one can say if some structural changes improved the uniform velocity distribution.

5.9 Dryer results with doors closed

In section 5 the validation of the CFD analysis compared to the experimental set up were done. This was done due to the fact that it is difficult to measure the flow results when the dryer is in full operation under working conditions. For the measured results the back door was open and the trolleys were moved backwards so that one can get in between trolleys to measure the speed. This section gives the CFD results of the different dryer configurations under real working conditions.

5.9.1 Dryer without flow diverter

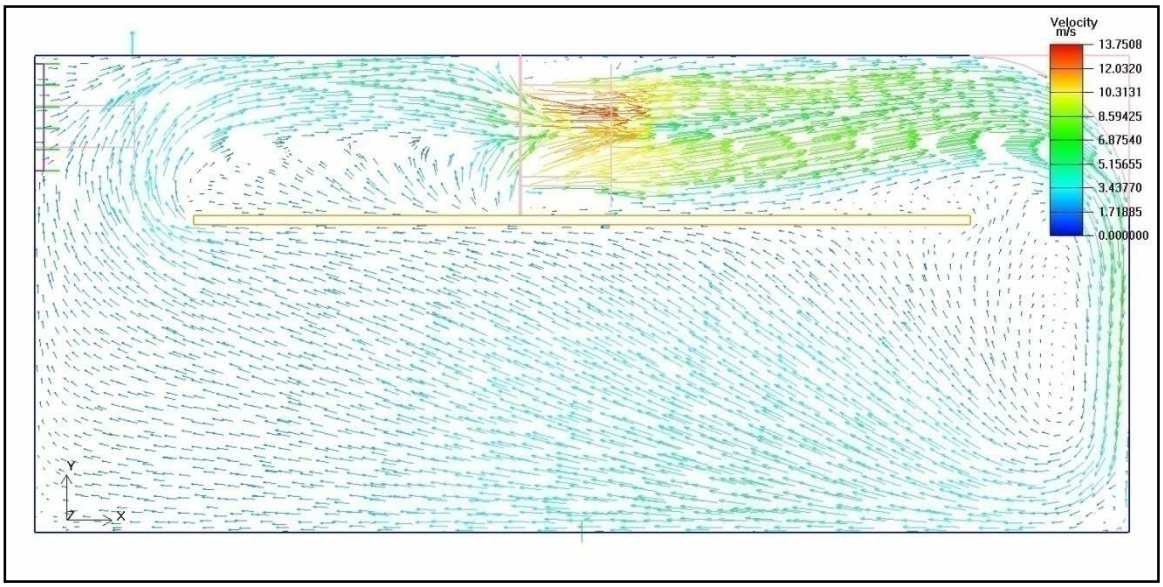

Figure 5-82 Velocity vector field at the centre of main fan in the YX-plane

The swirl region at the front side of the false ceiling is more towards the right of the drying zone and occupies a smaller area. The region of swirl at the back end of the false ceiling is larger compared to the dryer with the back door open (Compare Figure 5-82 and Figure 5-14).

In Figure 5-83 the region of swirl in the drying zone is larger compared to the one in Figure 5-13. One has to take notice of the region of swirl forming on the topside of the false ceiling downstream of the main fan.

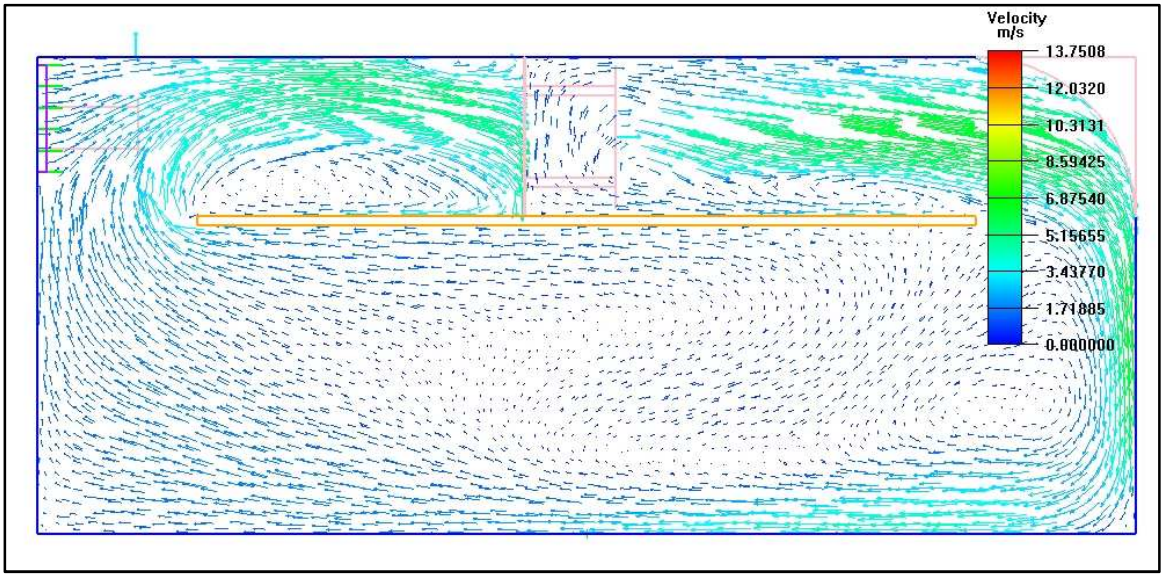

Figure 5-83 Velocity vector field at the centre of the inlet vent in the YX-plane

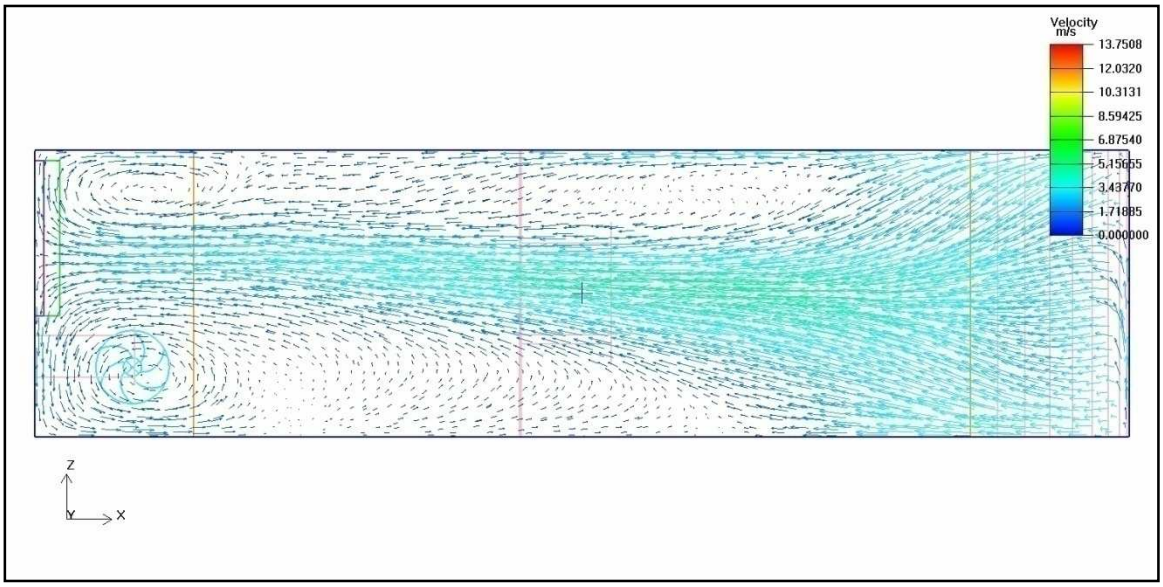

Figure 5-84 Velocity vector field, 0.28 m from the floor in the ZX-plane

The region of swirl in Figure 5-84 at the back end of the tunnel is much larger compared to the same swirl region in the ZX-plane in Figure 5-16.

The range of the speed contour (Figure 5-85) in the drying zone is higher compared the range in Figure 5-23. The region of where the speed profile is between 1.5 and 3 m/s is larger compared to the dryer where the back door was open.

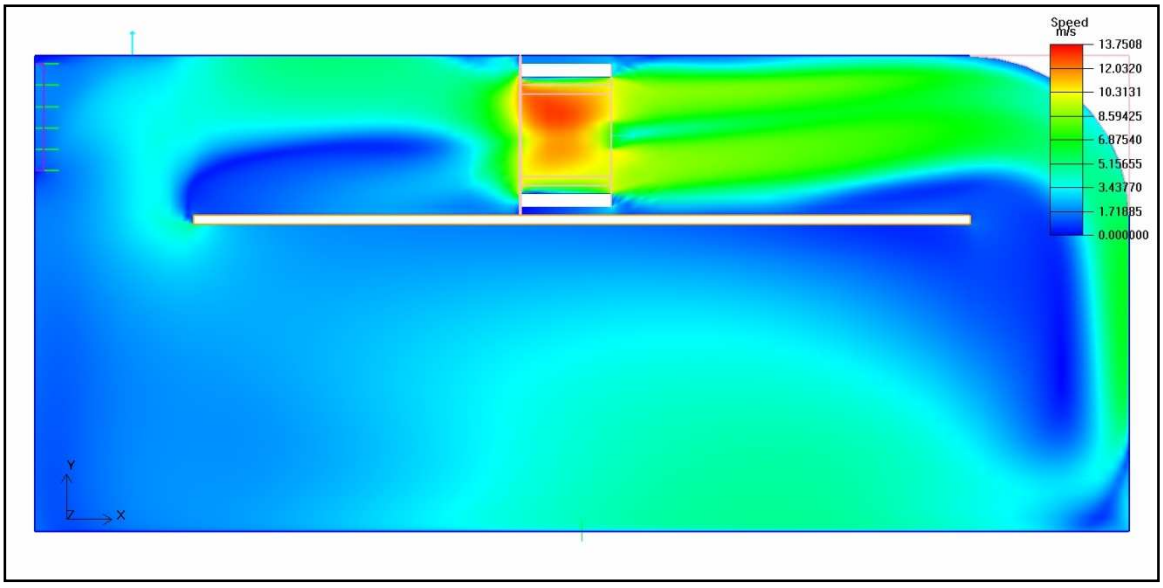

Figure 5-85 Speed contour in XY-plane in centre of main fan

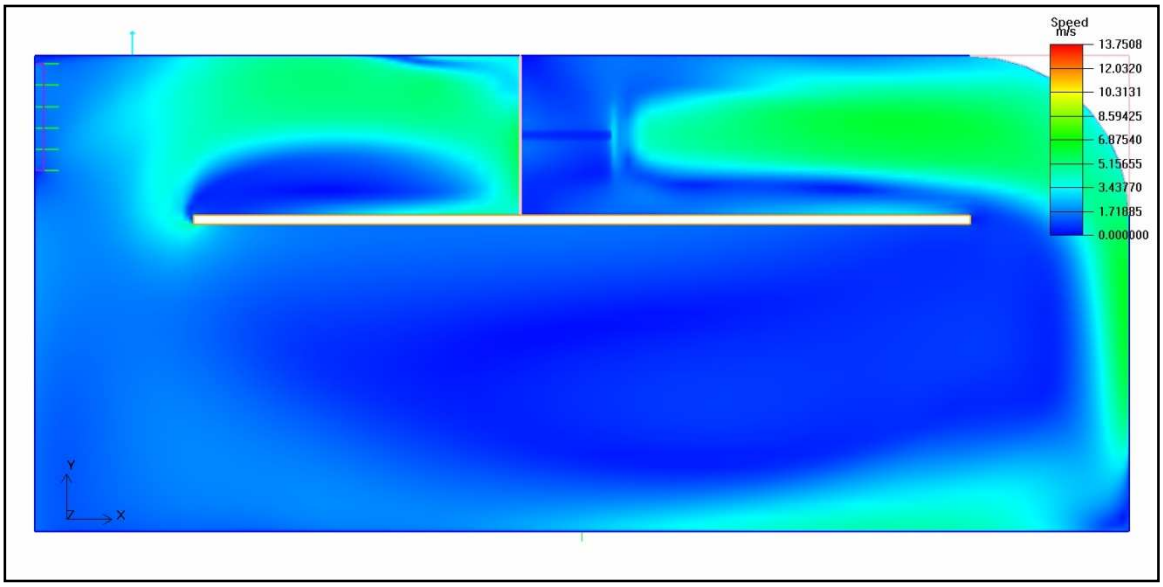

Figure 5-86 Speed contour in XY-plane in centre of inlet vent

The profile of the speed contour is more uniform in the YX-plane situated in the centre of the inlet vent (Compare Figure 5-86 to Figure 5-24). The profile or area covered where the speed range is between 1.5-3 m/s of the speed contour 0.28 m (Figure 5-87) from the floor is smaller in comparison to dryer displayed in Figure 5-25.

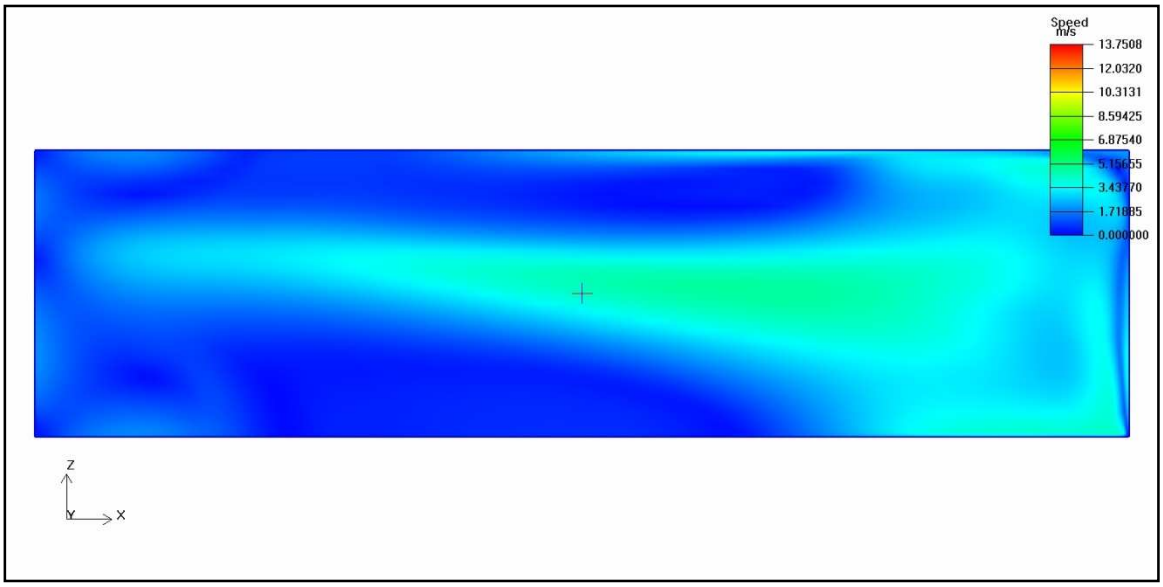

Figure 5-87 Speed contour 0.28 m from the floor in the ZX-plane

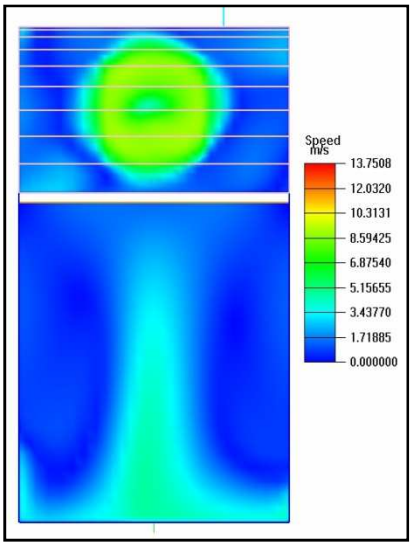

Figure 5-88 Speed contour of section D in the ZY-plane

In section D there is an increase in the speed in the middle of the dryer towards from the floor towards the ceiling. The regions next to this speed hike are more uniform if one compares the speed contour of Figure 5-88 and Figure 5-30.

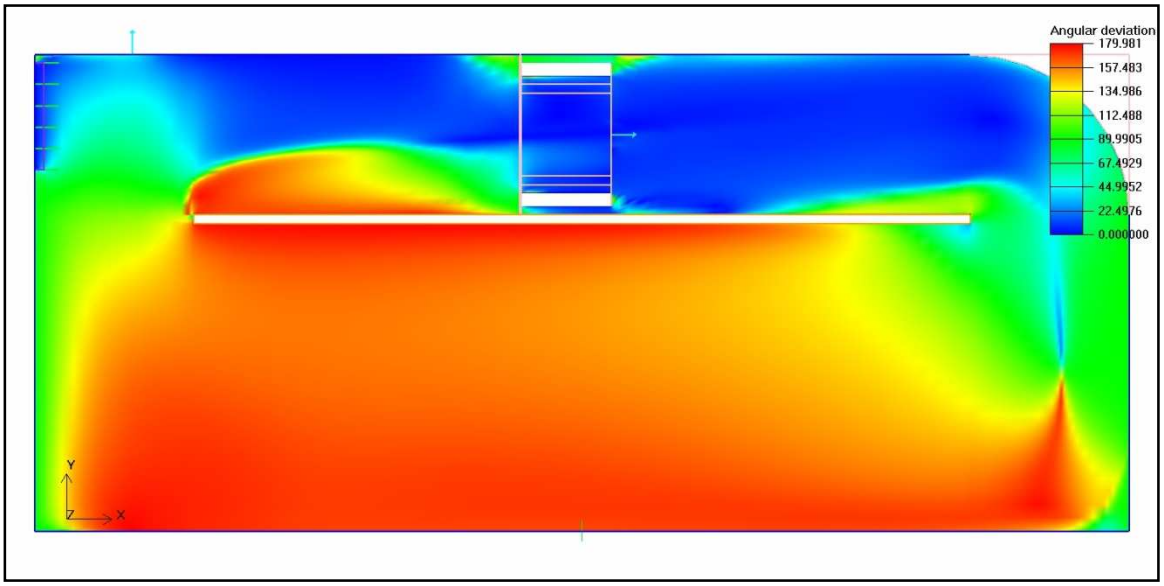

Figure 5-89 Angular deviation in the X-direction (XY-plane in the centre of the main fan)

The angular deviation shows that the swirl region at the front of the false is considerably smaller compared to the dryer with back door open in Figure 5-34. The real working configuration actually shows how the air is moving around the back end of the false ceiling. There is still a large region of swirl taking place on the top surface at the back end of the false ceiling.

5.9.2 Dryer with flow diverter

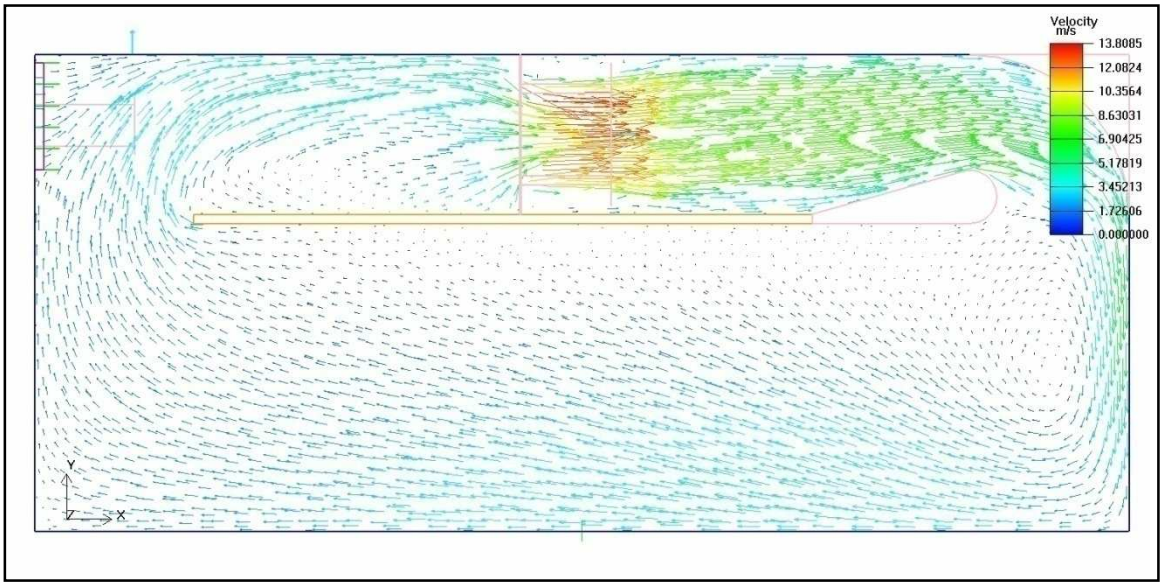

Figure 5-90 Velocity vector field at the centre of main fan in the YX-plane

The gradient of the velocity vector (Figure 5-90) field moving upwards from the floor towards the false ceiling is less compared to the dryer without the flow diverter (See Figure 5-82). The region of swirl at the front of the false is more or less in the same place or region. The region of swirl at the back end on the top surface of the false ceiling is smaller.

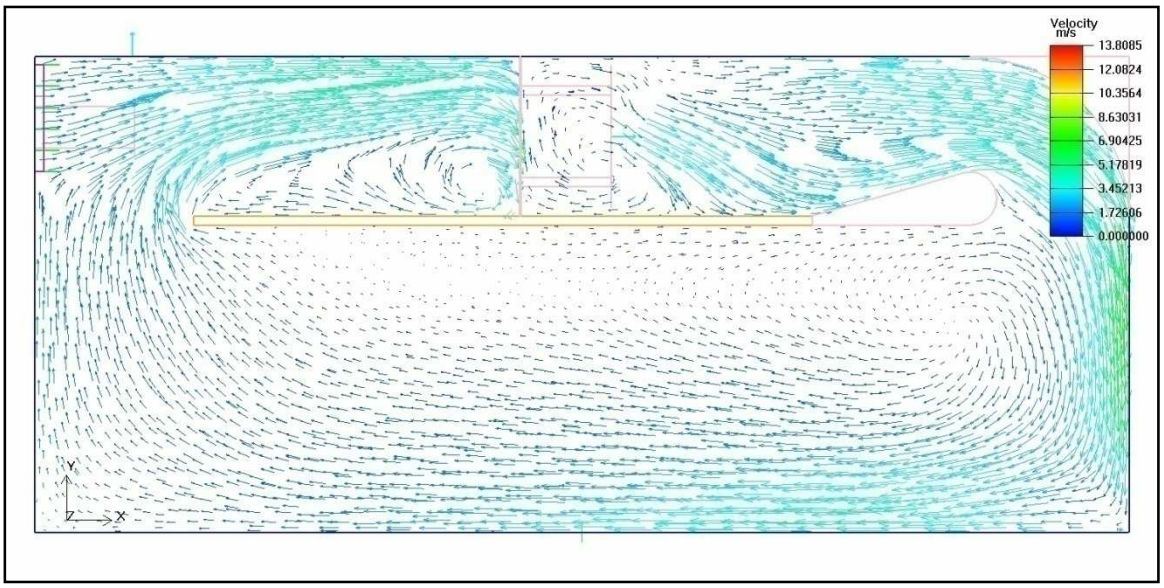

Figure 5-91 Velocity vector field at the centre of the inlet vent in the YX-plane

The airflow is more in tangent with the negative X-direction compared to the same plane in the dryer without a flow diverter (See Figure 5-83). The region of swirl is smaller at the back of the dryer (Compare Figure 5-92 with Figure 5-87).

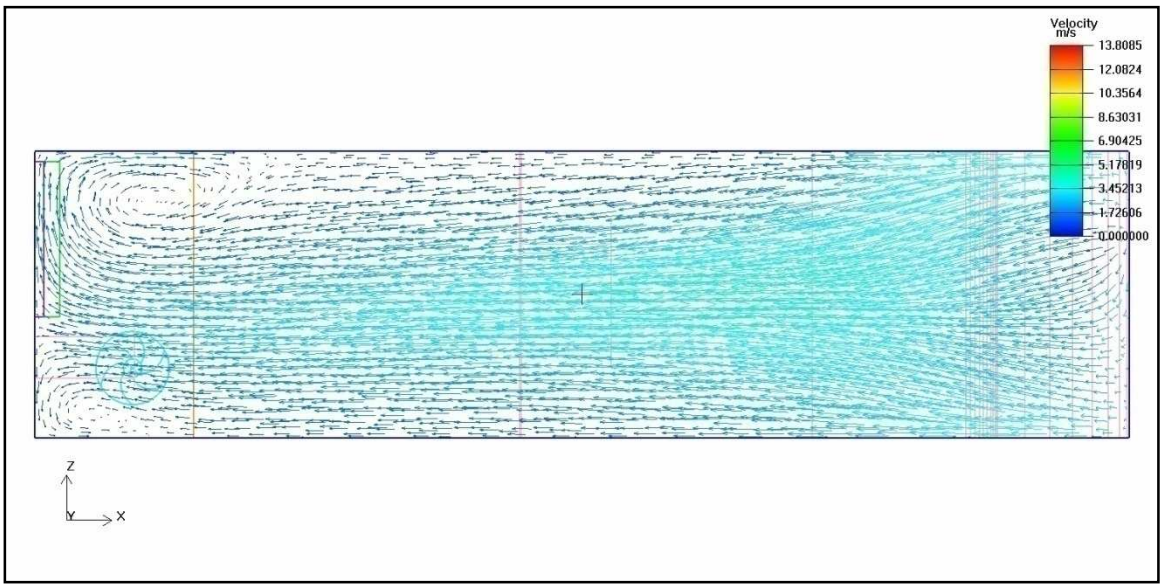

Figure 5-92 Velocity vector field, 0.28 m from the floor in the ZX-plane

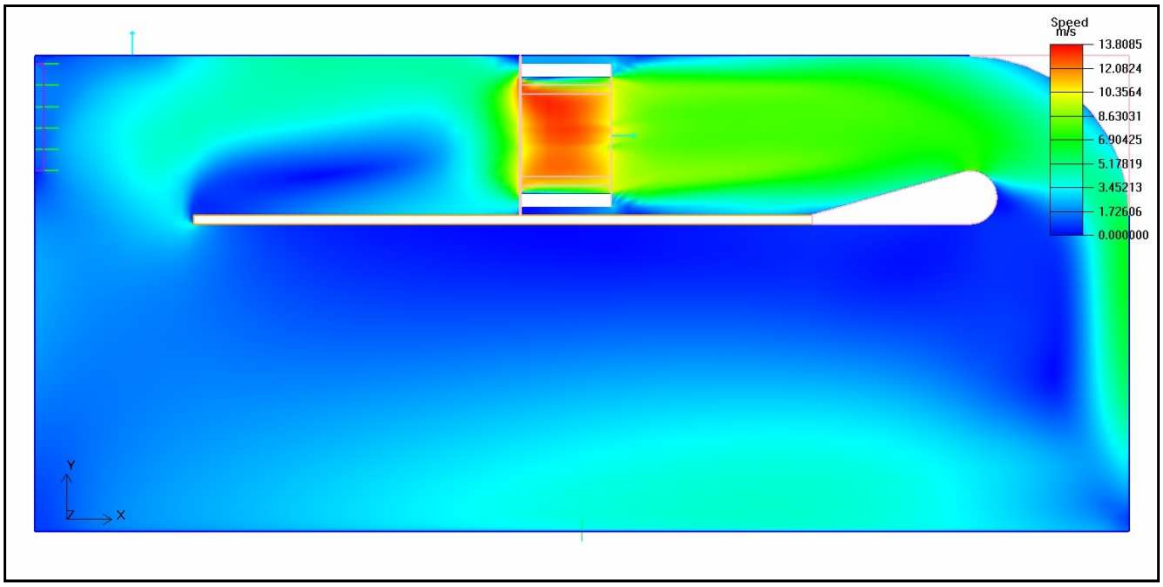

Figure 5-93 Speed contour in XY-plane in centre of main fan

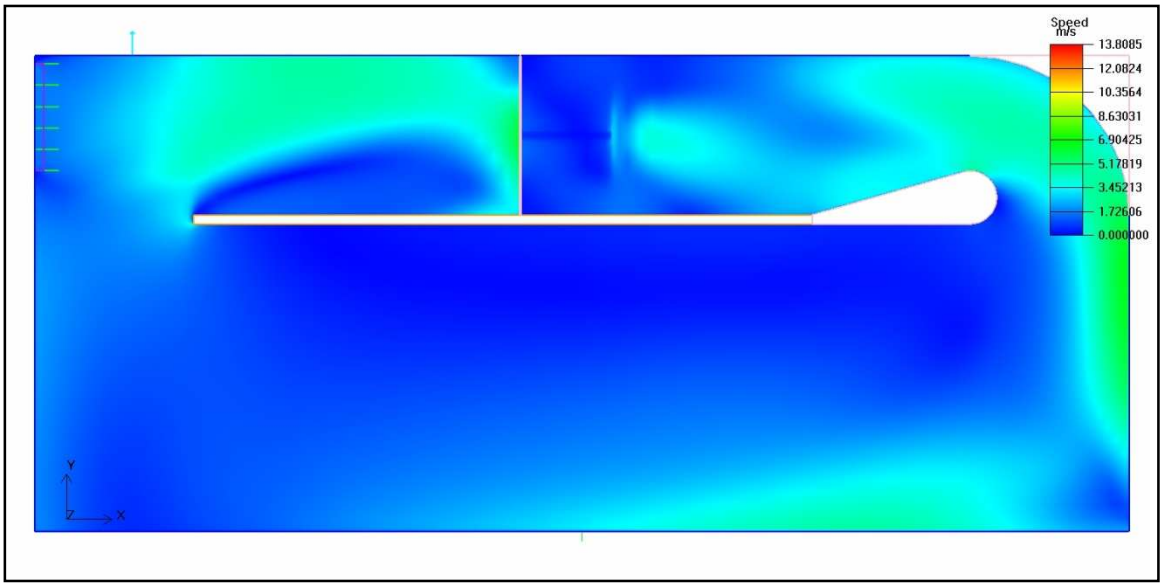

Figure 5-94 Speed contour in XY-plane in centre of inlet vent

Figure 5-93 and Figure 5-94 shows that the region that contains the speed range between 1.5-3 m/s is smaller compared to Figure 5-85 and Figure 5-86.

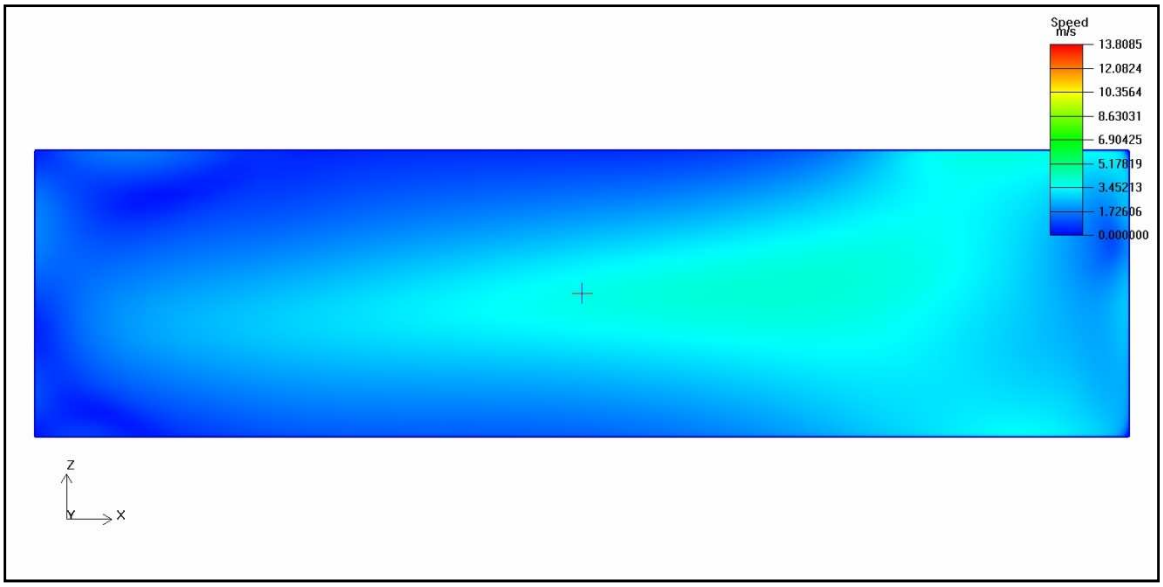

Figure 5-95 Speed contour 0.28 m from the floor in the ZX-plane

The speed gradient of where the speed region goes from 1 m/s to 3 m/s is less for the dryer with the flow diverter (Compare Figure 5-95 to Figure 5-87).

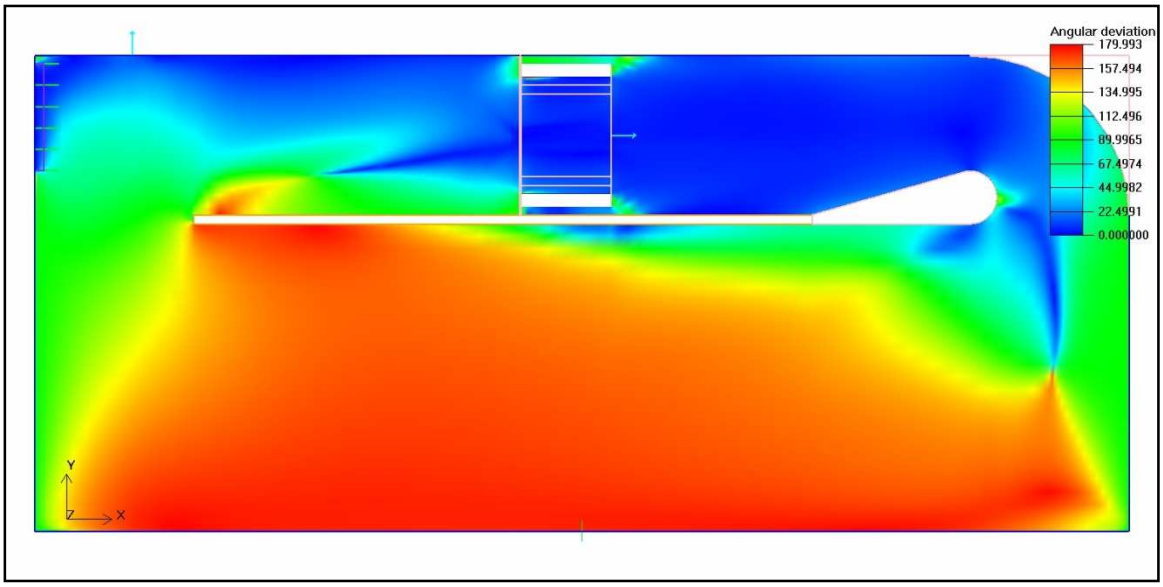

Figure 5-96 Angular deviation in the X-direction (XY-plane in the centre of the main fan)

There is still a region is swirl created in the drying at the first trolley. The angle of where the airflow is between 90° to 113° is extende d more into the drying zone than the dryer without the flow diverter. However this region is not extended so far downwards as in Figure 5-89. There is second region of swirl formed at the bottom side of the false ceiling near the main fan. This is between the gap of the top tray and the false ceiling. The region of swirl is decreased at the topside of the back end of the false ceiling.

5.9.3 Dryer with trolleys

Only two trolleys were added at the front of the drying zone. It is clear from previous analyses that the flow is straightened by the addition of the mangoes and trolleys. This created a smaller mesh count and the focus was only placed on the front part of the drying zone. It is apparent from Figure 5-97 and Figure 5-98 that with the addition of the flow diverter the region of swirl is moved outside the drying zone. The mango and the trolleys straighten the flow. The speed contour is uniform in the drying zone. There is still a speed increase between the gap of the floor and the bottom trays (See Figure 5-99).

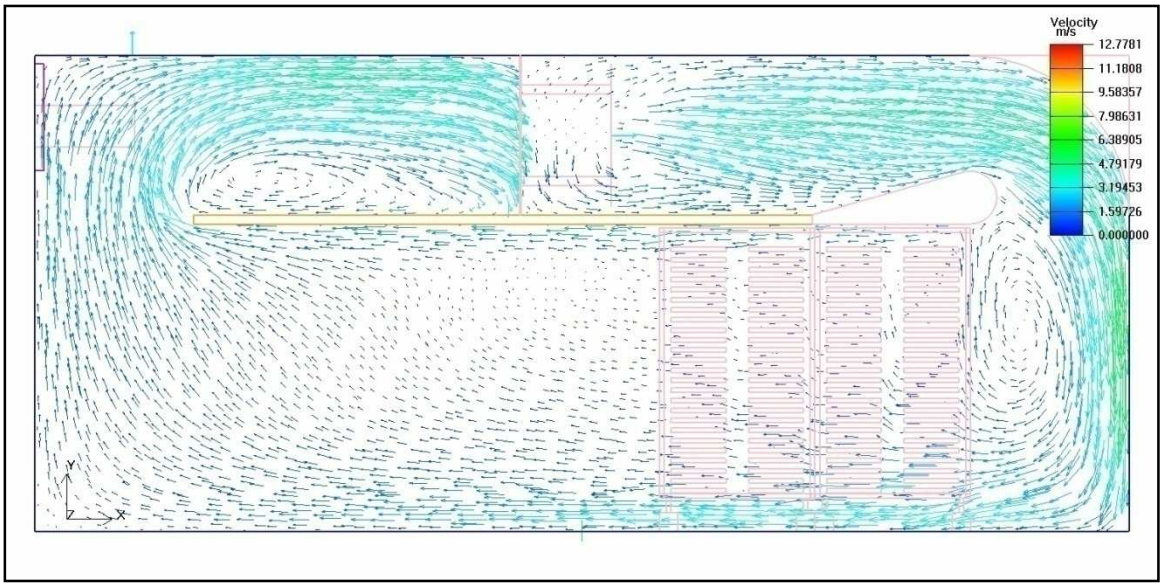

Figure 5-97 Velocity vector field at the centre of the inlet vent in the YX-plane

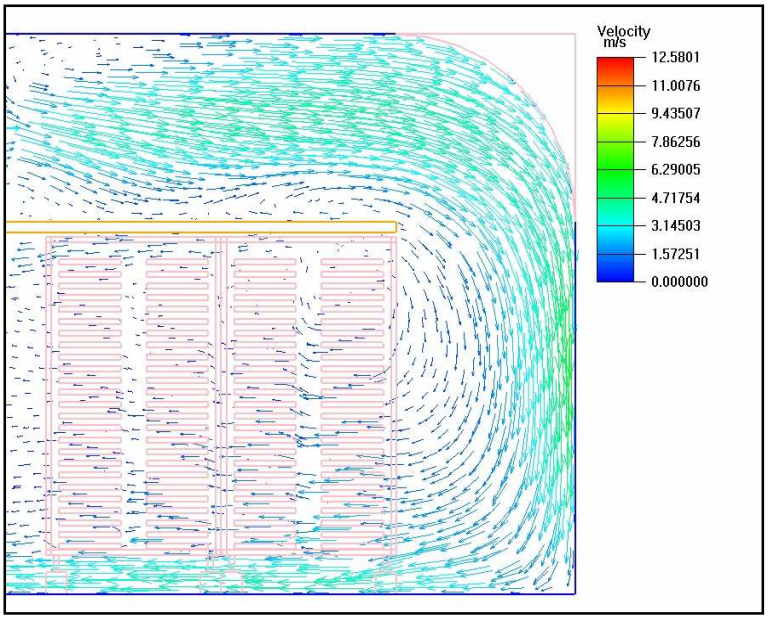

Figure 5-98 Velocity vector field at the centre of the inlet vent in the YX-plane

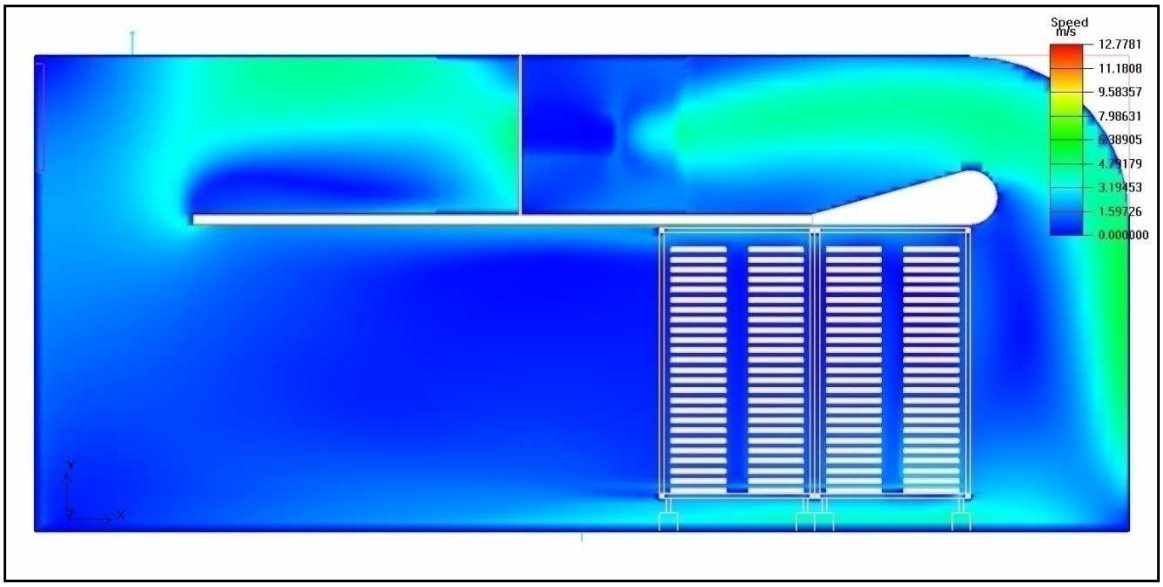

Figure 5-99 Speed contour in XY-plane in centre of inlet vent

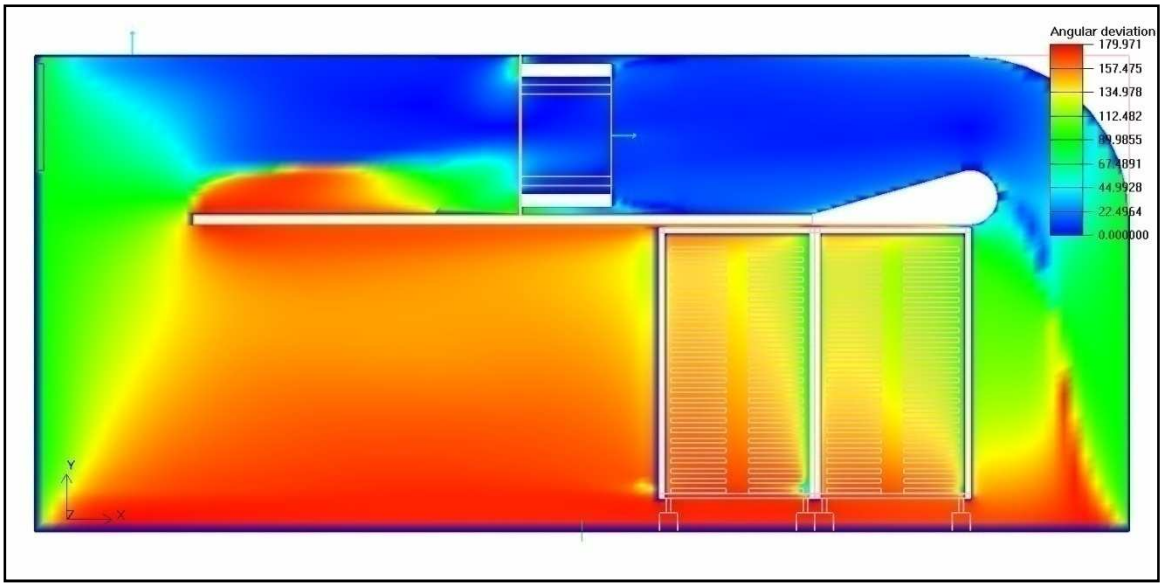

Figure 5-100 Angular deviation in the X-direction (XY-plane in the centre of the inlet vent)

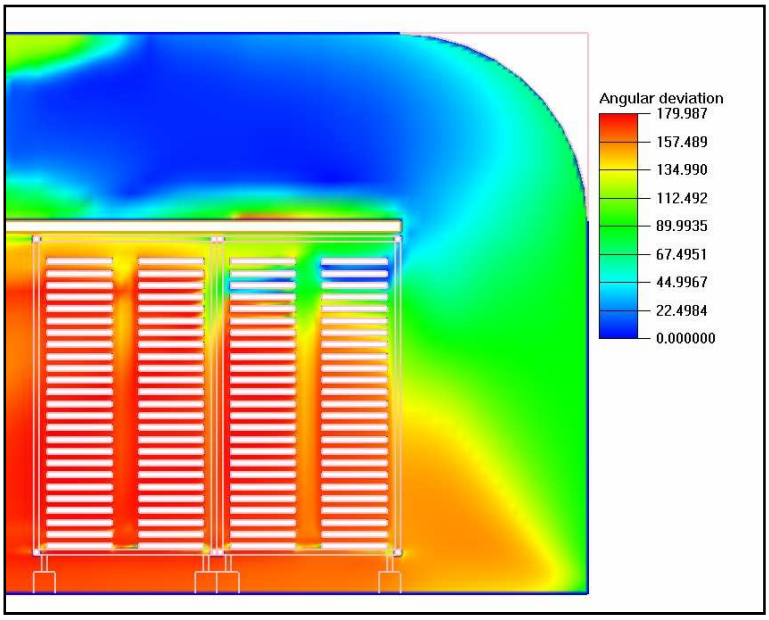

Figure 5-101 Angular deviation in the X-direction (XY-plane in the centre of the inlet vent)

Figure 5-100 and Figure 5-101 illustrates that there is small region of swirl around the top three layers of mango slices without the addition of a flow diverter. The region of 90-113° is larger in the dryer with a flow diverter, but the section moving into the region of 130-150° is more gradual.

6 Improvements made to various dryer configurations

The advantage of using CFD analysis is that changes in the model can be quickly updated by changing the parameters of the simulation. Various drying configurations were modelled and compared to the existing dryers that were tested.

6.1 Flow diverters only placed in front of drying zone of the dryer

The engineering department of the Hans Merensky Holdings in 2003 designed a flow diverter that was placed adjacent to the drying zone for a batch dryer system (See Figure 10-1 for technical drawing). This design could be converted for a continuous produce dryer where the trolleys enter from the side. This can be achieved by converting a normal trolley by removing the trays and inserting flow diverters. The radius of the flow diverters increases towards the floor of the dryer. This is simulated by the configuration illustrated in Figure 6-1. The idea or concept is to reduce the swirl region at the front end of the drying zone, especially at the region towards the front of the false ceiling.

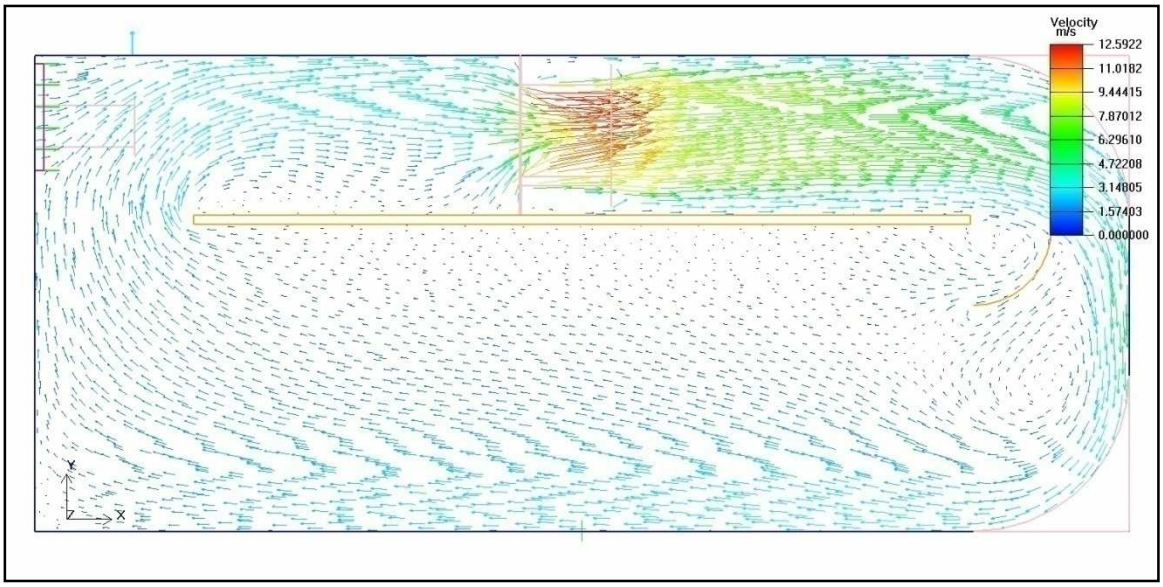

Figure 6-1 Velocity vector field at the centre of the main fan in the YX-plane

The first flow diverter begins level with the bottom side of the false ceiling. The trolley on which it is mounted can still easily be removed to insert other trolleys with produce on it. The second flow diverter is situated near the floor and helps to move the air more easily around into the drying zone.

The diverter decreased the region of swirl but created more swirl or separation behind the first flow diverter from the false ceiling. The flow is however more parallel with the X-axis in the drying zone.

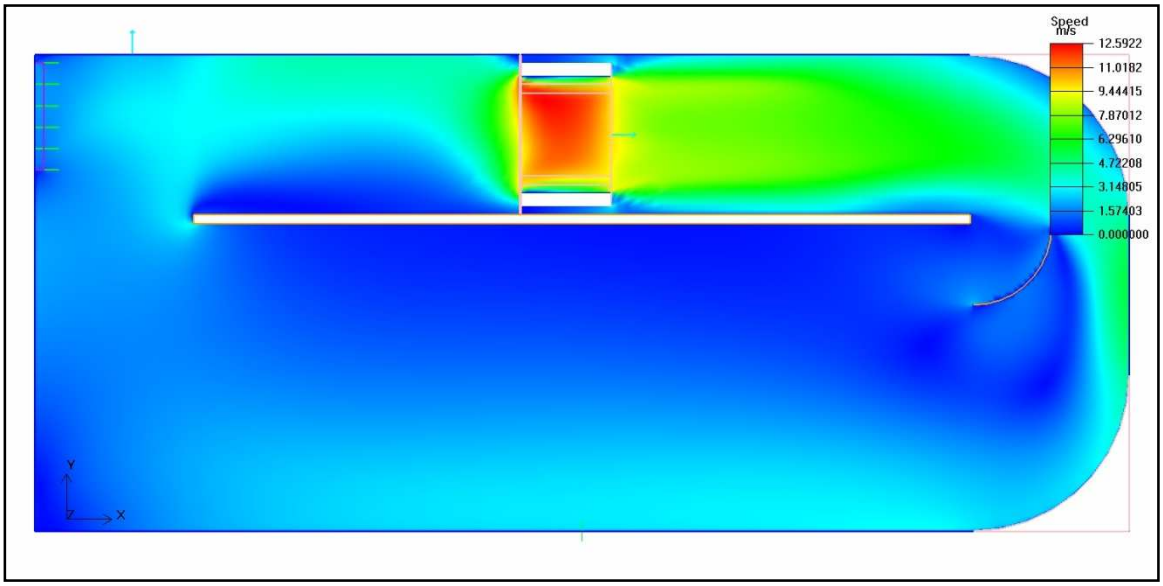

Figure 6-2 Speed contour in XY-plane in centre of main fan

The speed contour is more uniform compared to the same plane in Figure 5-85. The range, especially at the region between the floor and 0.28m upwards has decreased.

6.2 Flow diverters placed above false ceiling and before the drying zone

The same configuration was analysed for the dryer with the flow diverter. The same flow pattern was created at the first flow diverter. The range of the speed contour even increased by a small margin compared to the dryer without a flow diverter in section 6.1. This cannot be seen as an improvement on the original design.

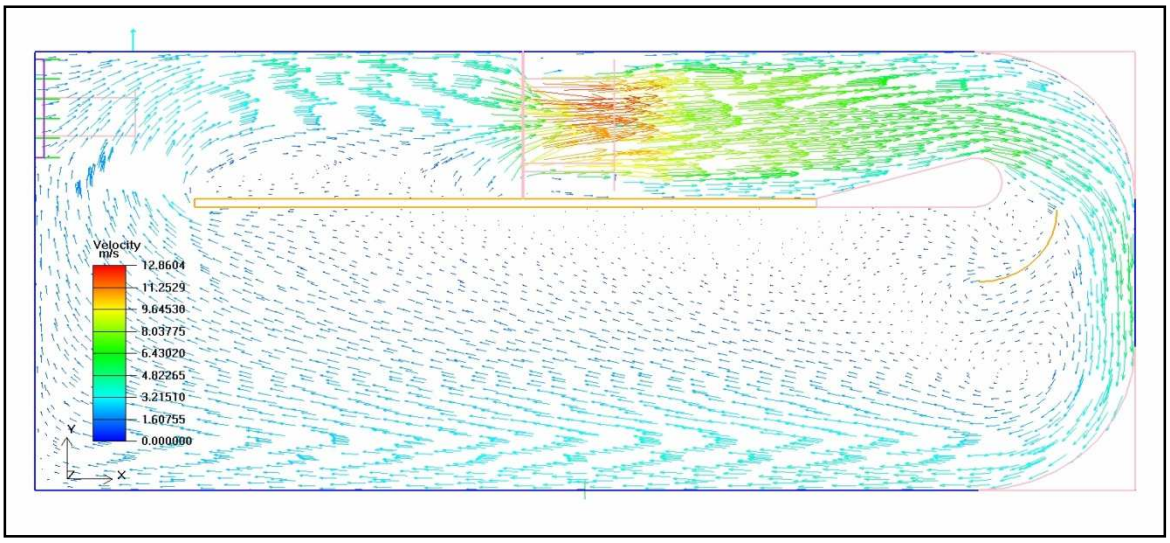

Figure 6-3 Velocity vector field at the centre of the main fan in the YX-plane

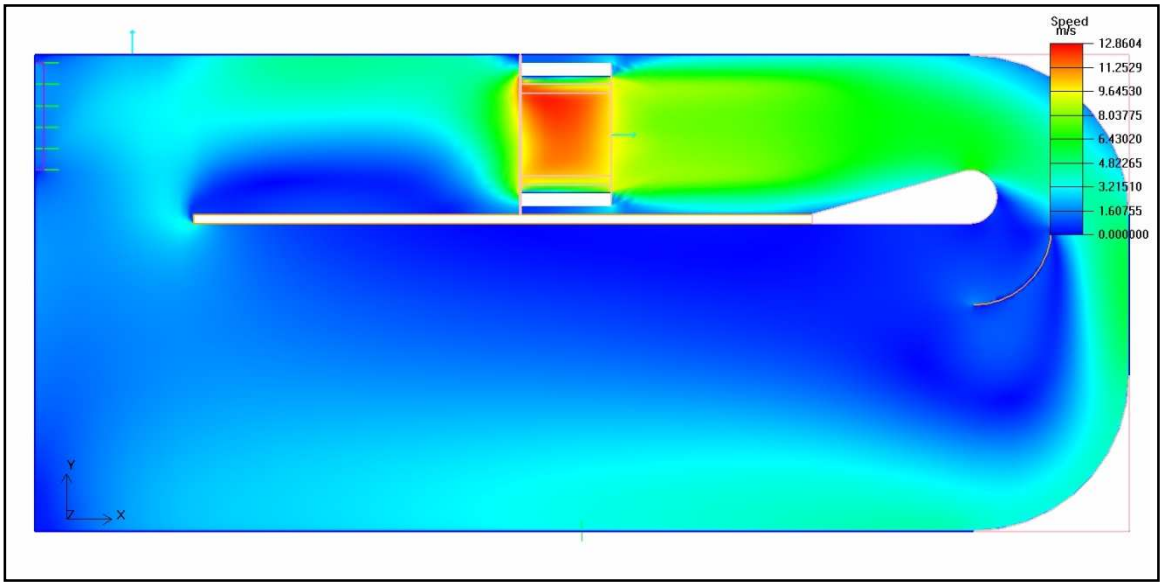

Figure 6-4 Speed contour in XY-plane in centre of main fan

6.3 Inserting Blanking off plates in front of the first and last trolley

At M-Pak Musina and Bavaria Packers the production staff put blanking off plates at each end of the first and last trolley to decrease the velocity range found between the underside of the trolleys and floor (See Figure 6-5 and Figure 6-6).

Figure 6-5 Blanking off plate placed before first trolley

Source: M-Pak Musina

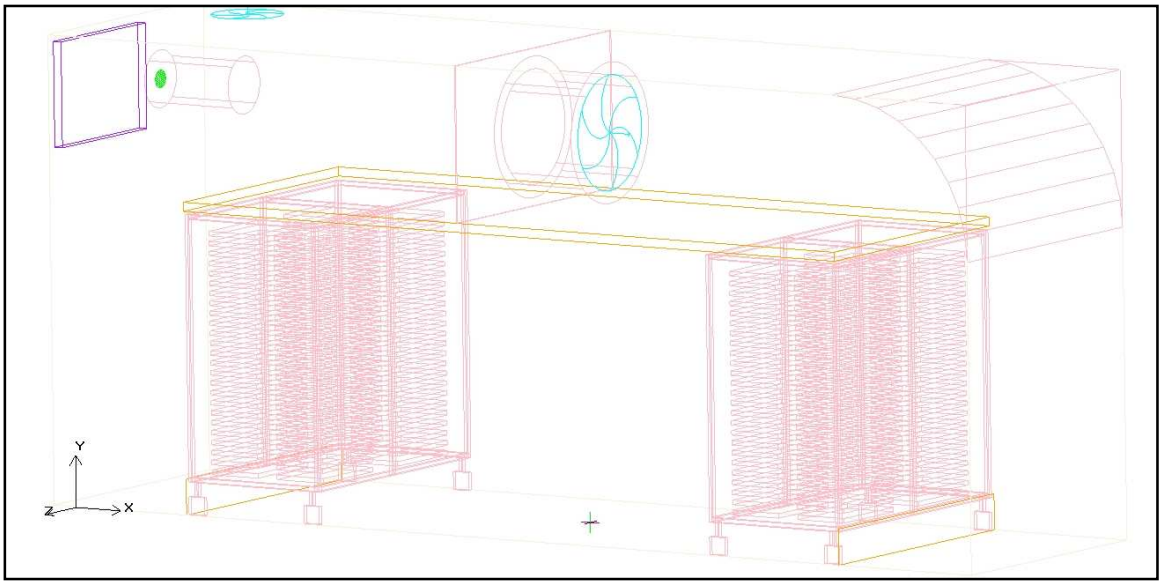

Figure 6-6 Blanking off plates

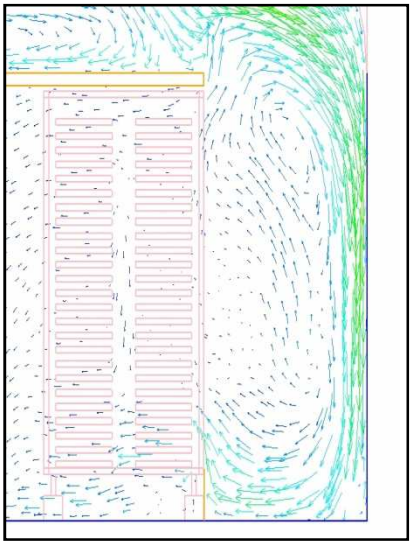

Figure 6-7 Velocity vector field at the centre of the inlet vent in the YX-plane

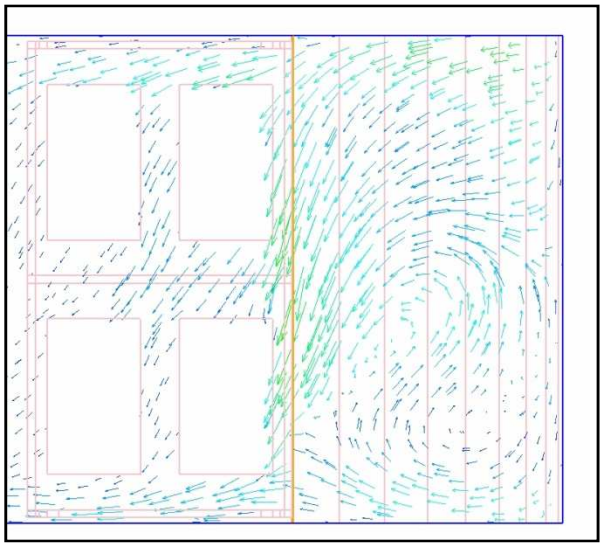

Figure 6-8 Velocity vector at 0.28 m from the floor in the ZX-plane

Figure 6-9 Detail view of the speed contour in the YX-plane at the centre of the inlet vent

This created a larger region of swirl in front the first trolley (See Figure 6-7 and Figure 6-8). Behind the blanking off plate a small region of swirl was created in the drying zone at the floor. It did decrease the range of the velocity in the gap between the floor and the first trays on the trolleys.

6.4 Flow diverters placed up-and-downstream of main fan

In order to decrease the region of swirl at the false ceiling and behind the first flow diverter of the modified trolley, more flow diverters were added. Secondly a flow diverter and modified trolley was placed at the back end of the false ceiling and the drying zone. A duct was placed up and down stream of the main fan. This was done to decrease the re-circulation found around the main fan's tube.

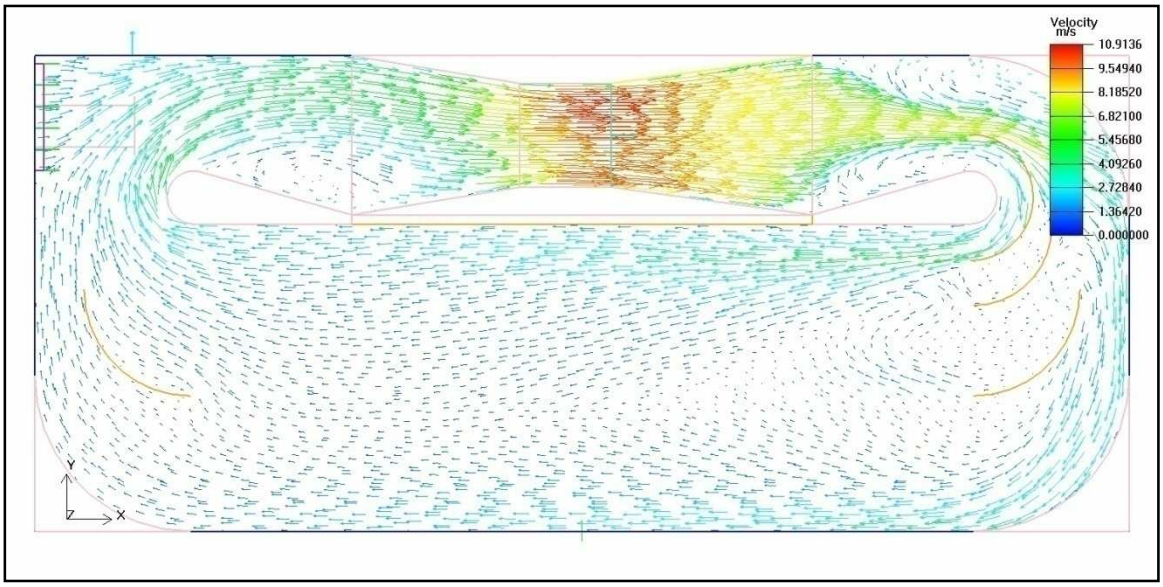

Figure 6-10 Velocity vector field at the centre of the main fan in the YX-plane

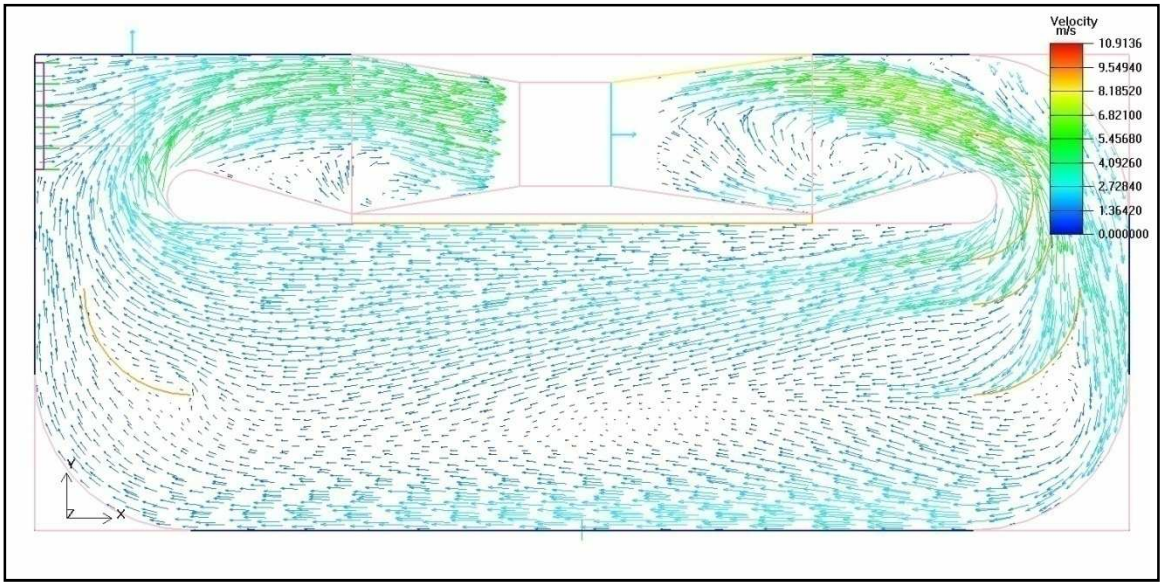

Figure 6-11 Velocity vector field at the centre of the inlet vent in the YX-plane

Figure 6-10 and Figure 6-11 show that the region of swirl is decreased behind the first flow diverter. The flow is more parallel or tangent with the X-axis. There is no region of swirl in the front of the drying zone. There is however a region of swirl formed between the end of the downstream duct and the beginning of the flow diverter. The same goes for the upstream duct and the back-end flow diverter.

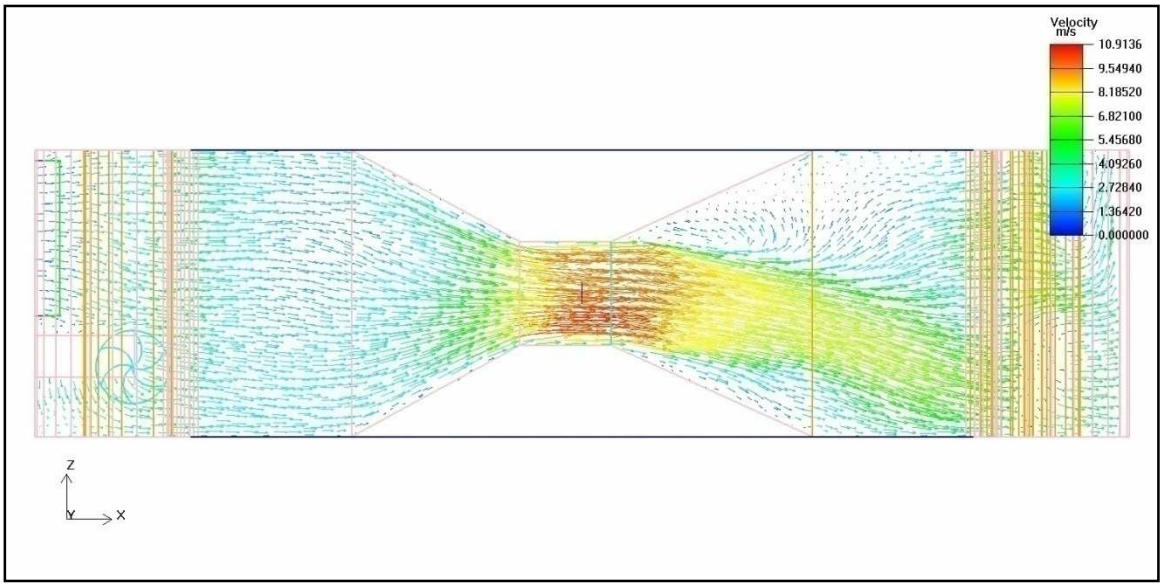

Figure 6-12 Velocity vector in the ZX-plane in the centre of the main fan

The re-circulation is cancelled out upstream from the main fan and the general flow pattern is improved. The downstream is however still problematic. (Compare Figure 6-12 and Figure 5-45)

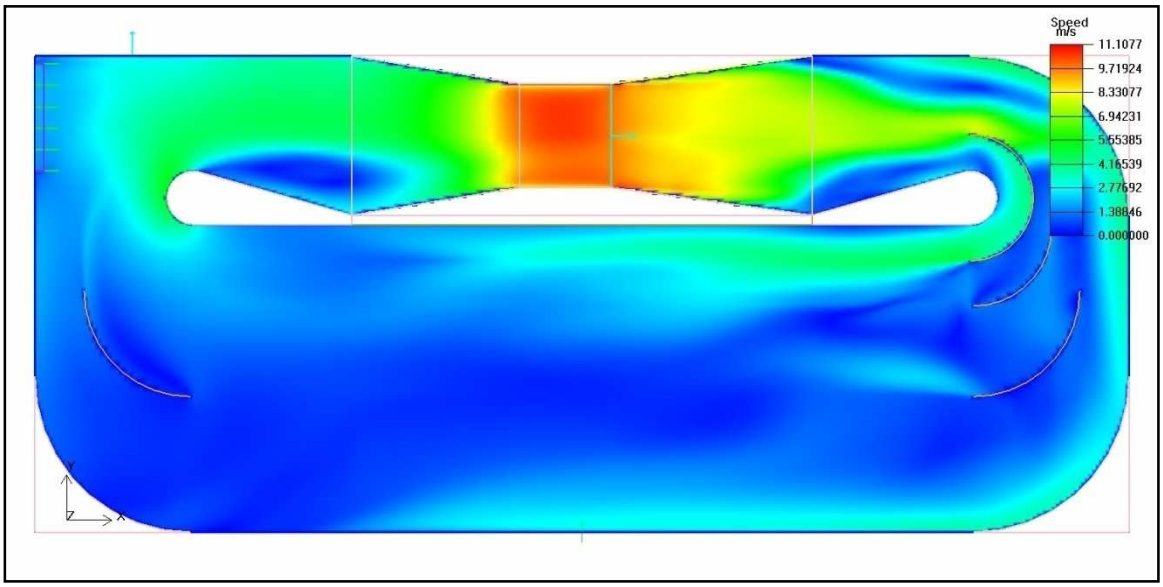

Figure 6-13 Speed contour in XY-plane in centre of main fan

Manufacturing a flow diverter that goes completely around the down-stream flow diverter increases the range of the speed contour. The configuration in paragraph 6.2 should be kept with the additional flow diverters added underneath the flow diverter that stops level with the bottom surface of the false ceiling (Compare Figure 6-13 and Figure 6-4). The region at the floor where the range of the speed

varied more compared to the speed range in the rest of the drying zone, is decreased.

Table 6-1 Average speed of CFD analysis

Section	RNG Speed Avg.	Stdev of RNG
A	1.38	0.63
B	1.22	0.49
C	1.28	0.76
D	1.30	1.01
E	1.74	1.06
F	1.71	0.81
Total Avg.	1.44	0.79
Stdev of Section A-F	0.23	
Coefficient of variance	0.54	= 0.79 ÷ 1.44

Compared to the CFD coefficient of variance *(CV)* value of 0.7 for the dryer with just the flow diverter at the downstream section of the main fan (See Table 5-5 and Table 5-8), the results showed a decrease of 16 %.

6.5 Double fan configuration

Some dryers at the M-Pak production facility are used for a high capacity application. The dryers are fitted with a second main fan. These dryers are utilised for drying mango fruit rolls and removing moisture from mango slices at a more rapid rate.

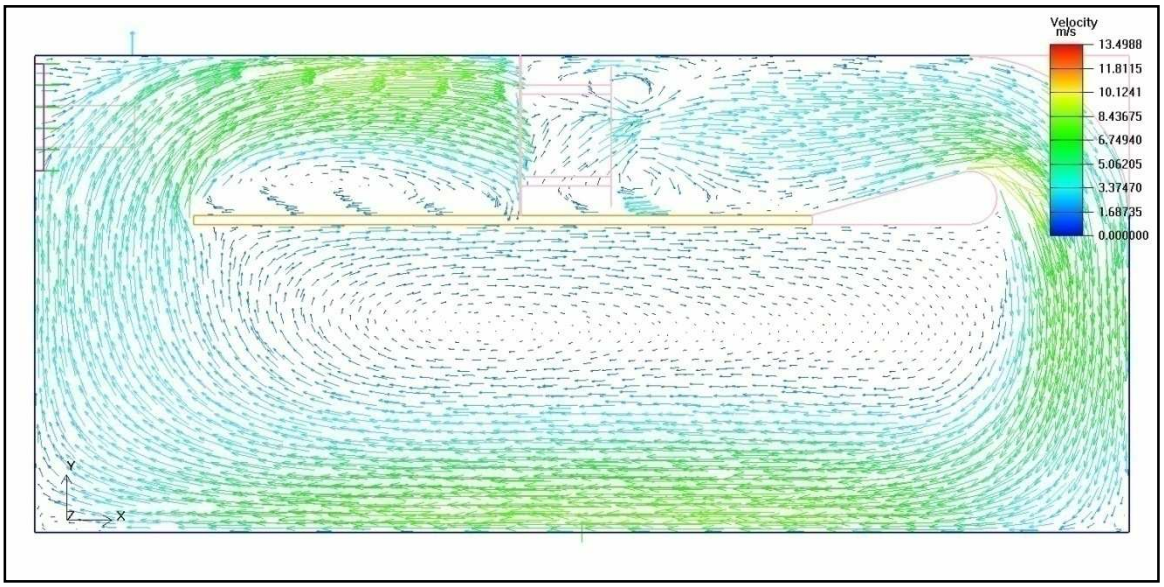

Figure 6-14 Velocity vector field in the middle of the two main fans in the YX-plane

A large region of swirl is created in the drying zone (See Figure 6-14). The re-circulation is cancelled out with the addition of the second main fan (See Figure 6-15). Figure 6-16 shows that the secondary flow created at the front of the drying zone or first trolley using is decreased when compared to a dryer configuration with one main fan.

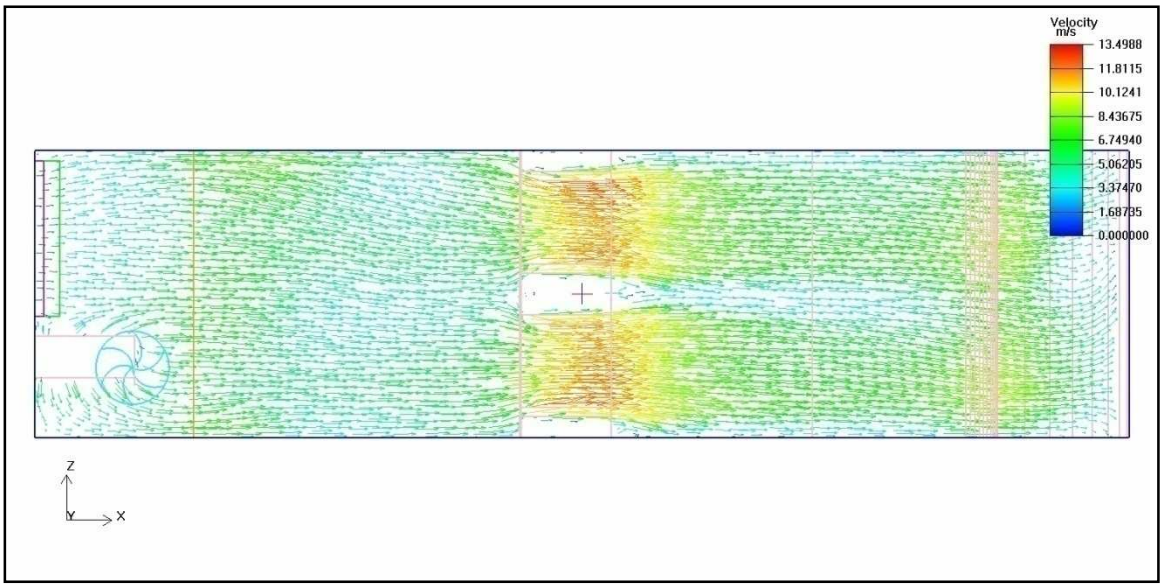

Figure 6-15 Velocity vector in the ZX-plane in the centre of the main fan

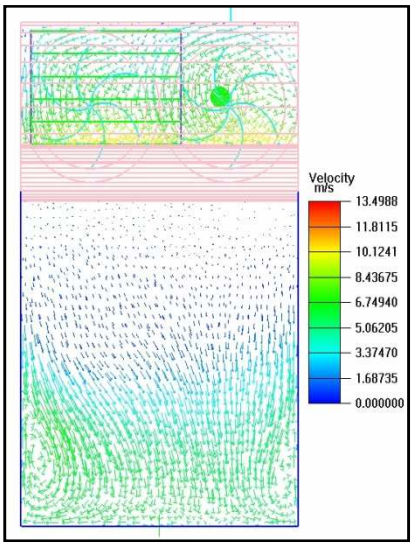

Figure 6-16 Velocity vector in the ZY-plane at section F

The range of the speed contour in the drying zone is increased. The region near the floor has a speed increase of 2 m/s compared to dryers with one main fan (Compare Figure 6-17 and Figure 5-94).

The angular deviation of the plane illustrated in Figure 6-18 shows the large region of swirl created underneath the false ceiling. The area covered by the region of swirl at the topside of the false on the upstream side of the main fans is smaller (See Figure 6-18).

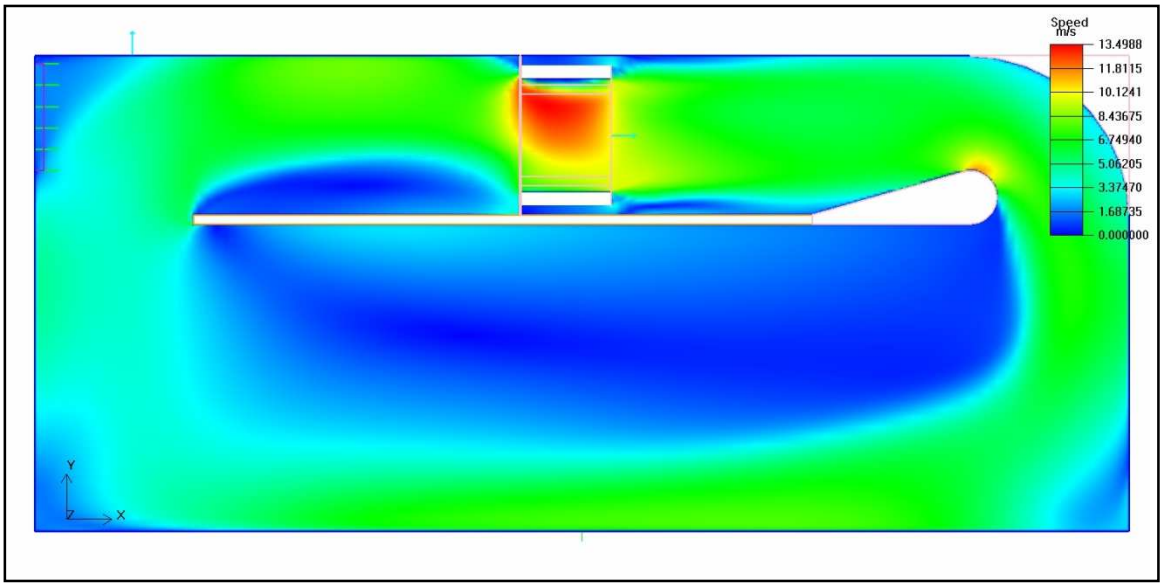

Figure 6-17 Speed contour in XY-plane in centre of the inlet vent

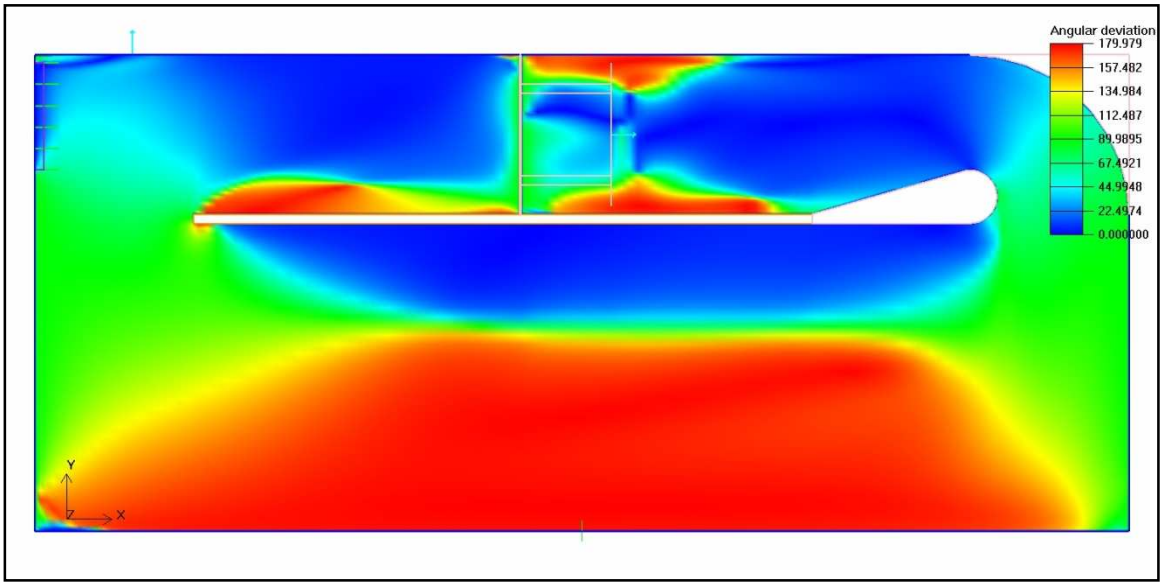

Figure 6-18 Angular deviation in the X-direction (XY-plane in the centre of the inlet vent)

6.6 Changing the drying zone configuration with mango-trolleys included

Conventional air-dryers are used in the industry due the high adaptability; easy maintenance and low initial start up cost. Teeboonma (2003) however suggests that using heat pump dryers would lower the energy consumption, the relative humidity and temperature in the drying chamber. Heat pump dryers are where the heating and fan unit are separated from the drying chamber. The air velocity, relative humidity and temperature can be better and more accurately regulated. It was found that it improves the colour and aroma qualities of the dried fruit. According to Teeboonma (2003) studies done by Meyer and Greyvenstein (1992) showed that in the overall life cycle of the dryer it was more economical than conventional hot air dryers.

One of the main concerns with the conventional dryers is airflow around the false ceiling. With the addition of flow diverters and turning vanes there is still a non-uniform velocity profile in the drying zone. With the heat pump separated, a chamber can be implemented where air flows direct from an inlet over the produce. This configuration illustrated below in Figure 6-19 shows the advantage of using a CFD package to analyse the design of a different configuration that is normally used in the mango drying industry.

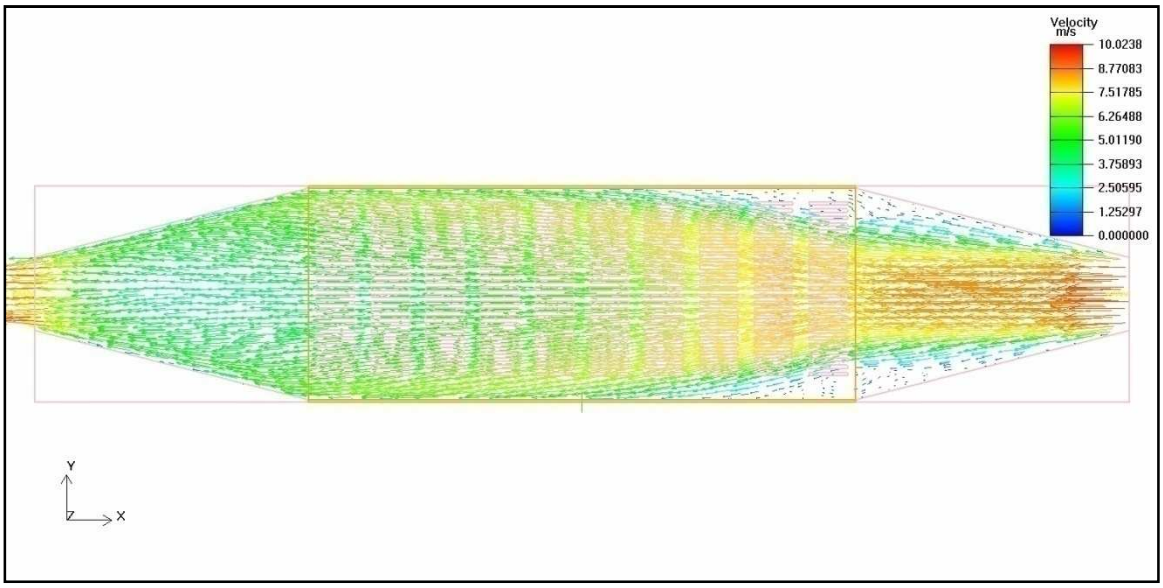

Figure 6-19 Velocity vector in the YX-plane in the centre of the main fan

Using this configuration the mango is inserted from one of the sidewalls like in the Batch system used at the Bavaria Packers drying plant. The trolleys can still be periodically moved from one to side to the other, so that continuous flow system can be implemented. The advantage of a continuous flow system is that all the trolleys and thus the mango slices are exposed to the full and different profile across the drying zone of the airflow pattern. The same volume flow was implemented at the inlet as what was produced by the main fan in the

conventional dryers. Airpak 2.1 can create a combination in-and-outlet-boundary to make sure that all the heat and flow properties of the air are kept intact.

Figure 6-19 and Figure 6-20 still shows that a region of swirl is created in the front section of the drying zone, but this is much less compared to the configuration with the false ceiling. The airflow is almost flowing completely tangent with the X-axis, although there is still airflow from the gap between trolleys and the walls that moves towards the middle of the drying zone in-between the mango slices. Figure 6-20 is the same YX-plane that is used to describe the velocity vector flow in the YX-plane situated in the centre of the inlet vent of the conventional dryers.

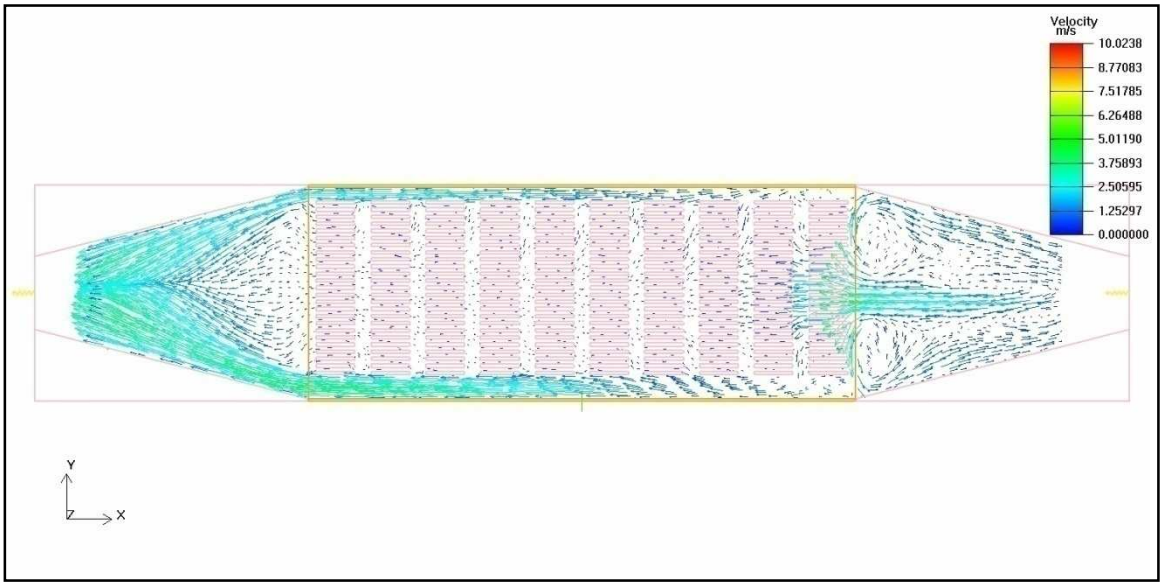

Figure 6-20 Velocity vector 0.39125 m (Z-axis) from the mid YX-plane

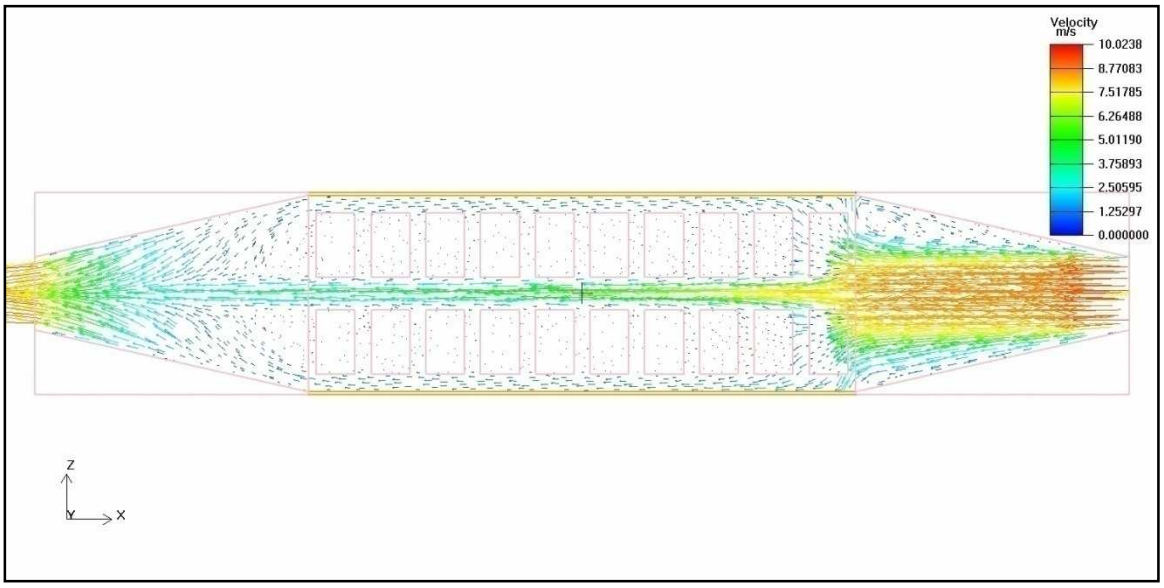

Figure 6-21 Velocity vector 0.84 m from the floor in the ZX-plane

The region of swirl is greatly reduced before and especially after the drying zone in the ZX-plane (See Figure 6-21). There is still however some degree of secondary flow before the air enters the drying zone (See Figure 6-22).

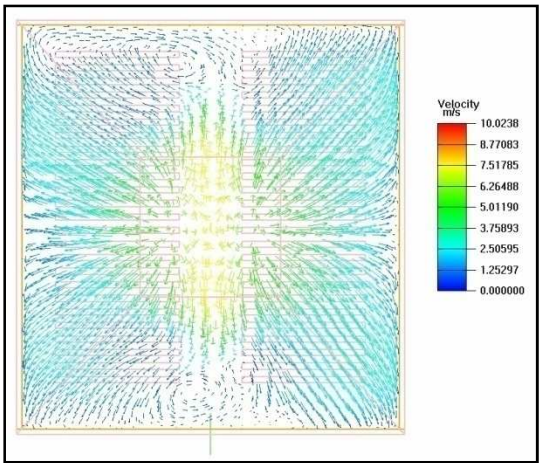

Figure 6-22 Velocity vector in section F (ZY-plane)

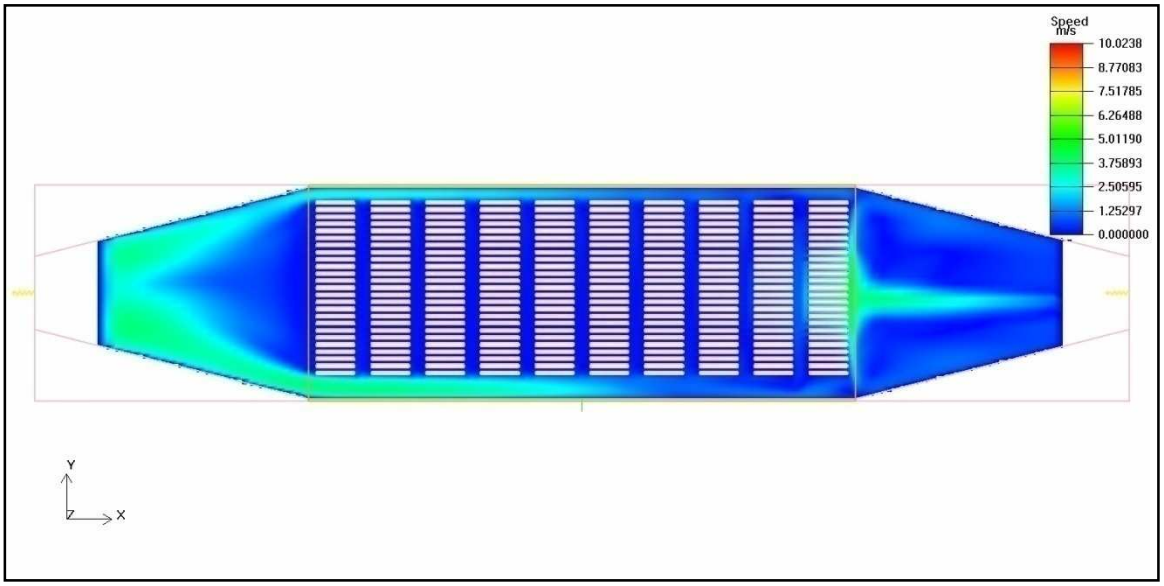

Figure 6-23 Speed contour 0.39125 m (pos. Z-axis) from the mid YX-plane

The speed contour over the middle of the mango slices in the YX-plane is uniform. The speed of the air is more or less the same as for the false ceiling dryers. Figure 6-23 still shows the speed increase in the gap between the floor and the first trays on the trolleys. In front of the first trolley the range of the speed contour increases, but quickly dissipates over the first column of mango slices.

One of the main concerns is still the speed increase in the middle gap between the trolleys. (See Figure 6-24 and Figure 6-25)

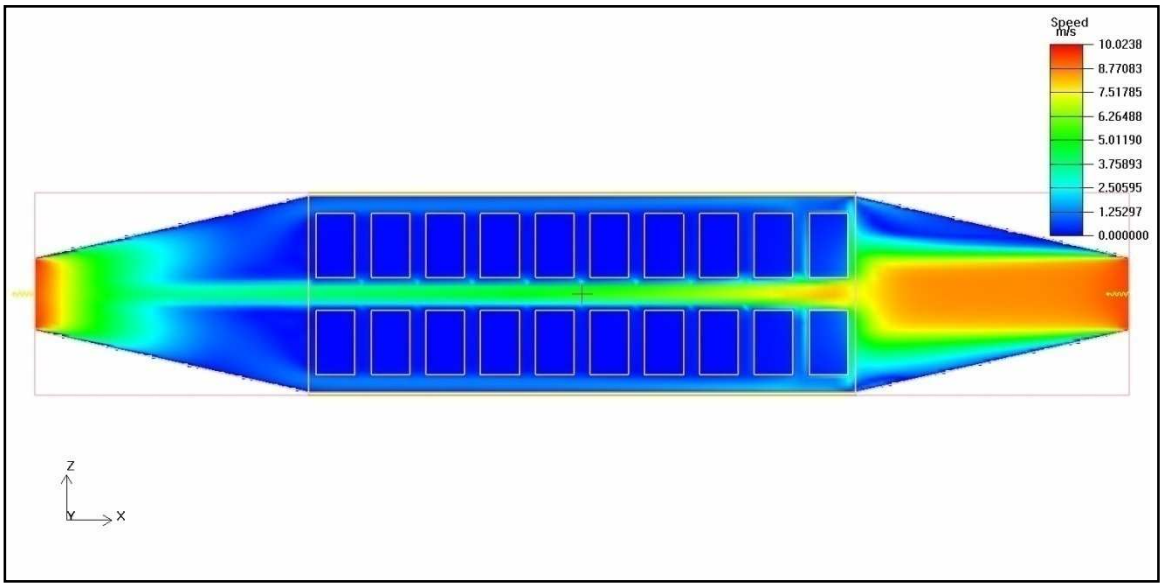

Figure 6-24 Speed contour 0.84 m from the floor in the ZX-plane

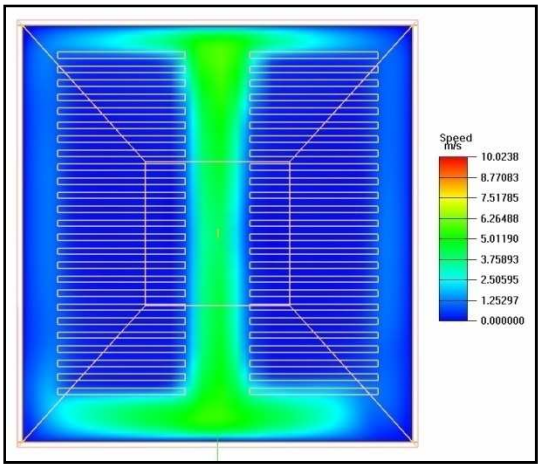

Figure 6-25 Speed contour at section A in the ZY-plane

The pressure drop with this configuration is less and more uniform over the drying zone than the conventional dryer (See Figure 6-26). Thus more energy is saved and the efficiency of the dryer is increased.

The angular deviation is not that uniform compared to the conventional dryer, but the only region of swirl is very small and at the beginning of the drying zone near the top and floor region (See Figure 6-27).

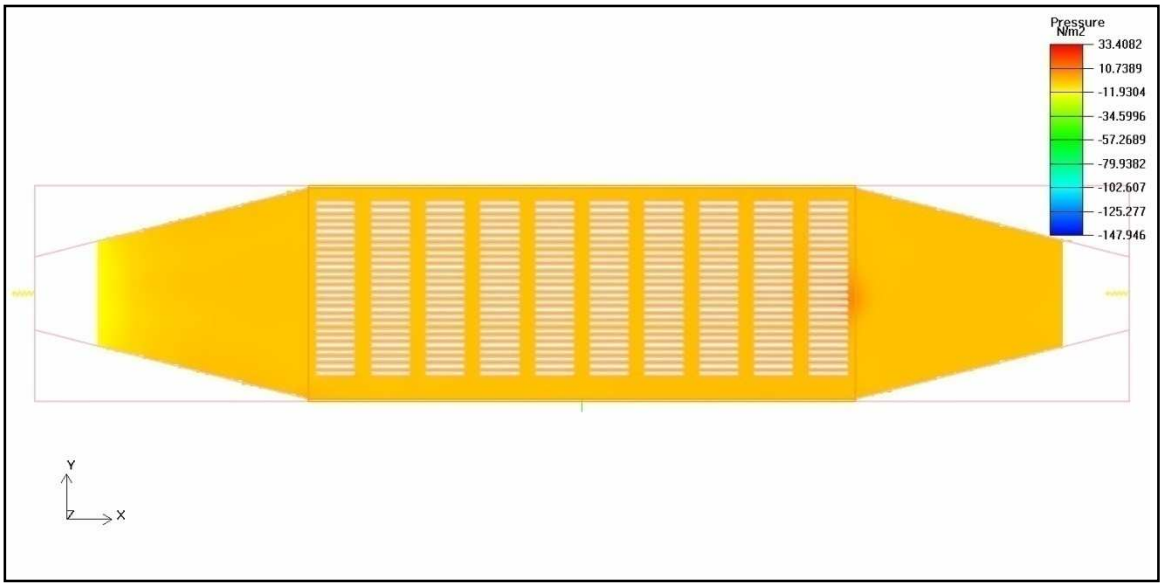

Figure 6-26 Pressure contour in the centre of the dryer in the YX-plane

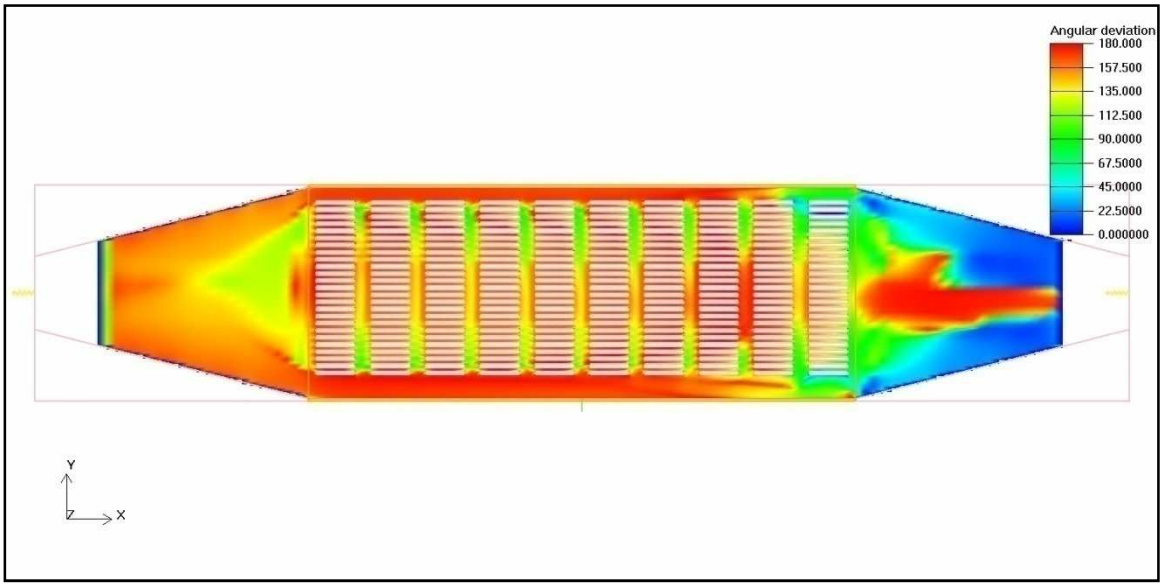

Figure 6-27 Angular deviation 0.39125 m (Z-axis) from the mid YX-plane

Table 6-2 Average speed of CFD analysis

Section	RNG Speed Avg.	Stdev of RNG
A	1.95	1.85
B	2.28	2.10
C	2.35	2.24
D	2.41	2.41
E	2.40	2.75
F	3.06	2.28
Total Avg.	2.41	2.27
Stdev of Section A-F	0.36	

The standard deviation of the dryer is high compared to the conventional dryers in the previous sections. This due to the high velocities created in the gap between the trays. The range of the speed in each section is higher as well. This does not mean that the dryer is less effective in accomplishing a uniform velocity distribution in the drying zone. The conventional trays create the non-uniform velocity distribution with the large gap between the mango slices.

7 Conclusion

The first objective was to see whether a CFD analysis was prudent to investigate the non-uniform velocity distribution in industrial tray air-dryers. The drying industry could say with certainty that the conventional dryer had this problem by just evaluating the non-uniformed dried produce. The problem was the difficulty in measuring the velocity field in the drying zone under real working circumstances.

The CFD analysis determined where and to what extent the swirl region was formed inside the drying zone. The results from the analysis could be used to make informed decisions whether the structural changes made any difference in improving the non-uniform velocity field in the dryer.

The second objective was to determine if the results of the CFD analysis gave an accurate presentation of what is actually happening inside the dryer. The data or results of the CFD analysis were validated against the measured results. The first test was on the dryer with no flow diverter. The average speed of the CFD analysis in each section of the drying zone was 17% higher compared the measured results (Table 5-4). The standard deviation of the speed in each section related to the total average speed in the drying zone is 0.31 for the CFD analysis compared to the 0.09 for the measured results. The standard deviation of the CFD analysis compared to the measured results is quite high, especially in the regions of swirl taking place (Section D, E and F). It was difficult to get accurate measurements in these zones.

The configuration of the dryer with the flow diverter, mango slices and trolleys showed a decrease in the non-uniformity of the velocity profile. Table 5-8 showed that the *CV* value obtained through CFD results of the average speed was 3% lower. This is where the CFD simulation gave valuable insight if the addition of flow diverters really improved the uniformity of the velocity profile under real working conditions. The fact must not be overlooked that the main reason why the flow is more uniform in the drying zone is that the trays, mango slices and trolley rails helps in reducing the swirl of the airflow.

The addition of converted trolleys with additional flow diverters improved the uniform velocity distribution, reducing the relative humidity in the upper region of the drying zone. This is the most cost effective and convenient way of improving existing dryers.

The main drawback of the conventional dryer is that it will always produce a non-uniform velocity distribution in the drying zone. The space or volume where the air has to flow from the fan, around the false ceiling and into the drying zone is too small to create an airflow pattern that stabilizes into flow along the X-axis without swirl taking place before it reaches the first trolley. All these changes, which are mentioned above can all be changed within the certain limits. It would

create a situation where the increase in initial building cost to enlarge the volume in that region would outweigh the gains made by improving the airflow over the produce.

The dryer in paragraph 6.6 showed that when the drying zone is separated from the heating and fan unit that the swirl region is greatly reduced in the area of the trolleys. There is still a region of swirl formed at the front of the dryer. The velocity range in the drying zone, implementing the conventional trolleys, is still larger compared to the dryers that are currently in use.

8 Recommendations

The cost of manufacturing a simple vane and a flow diverter for an existing dryer comprises 4% of the initial building costs (excluding the initial cost of the trolleys). If one considers that the overall drying uniformity of the produce is improved by 7% according to CFD analysis, and the average life cycle of a dryer is 15 years, it justifies this improvement.

The cost of running a dryer should be looked at in two ways. The first one is the actual running cost of the dryer. This is the amount of heat (gas) that is required to heat up the air in the drying zone and the electricity required for running the fans. If the airflow is more uniform over the produce, then so is the convective heat transfer. The efficiency of the fans is increased due to the fact that the pressure required moving the same volume of air trough the drying zone is less.

The second cost factor is the re-drying of the wet produce. Labour costs will be lower if less time is required in sorting out the wet slices from the dried product. Resources are taken up (dryers and trolleys) that could have been used in increasing the production rate of the plant. A cost analysis (please see paragraph 10.3.1) in terms of the energy requirement for various water evaporation rates showed that the dryer with the flow diverter was 6% less expensive to run on an annual basis.

The gap between the trolleys, sidewalls, false ceiling and floor should be decreased as much as practically possible using the current construction methods. The gap between trays on the same level should also be decreased. Mango slices should be spread out to cover as much of the net area on the tray as possible. If conventional trolleys are to be used with the existing dryers, blanking off plates should be installed in front of the trolleys. These reduce the high velocity range at the lower trays on the trolleys. A vortex is still created behind the blanking off plate but the region it covers is small relative to the large volume of the drying zone.

The placement of the outlet fan is another concern. A percentage of the air is flowing directly from the inlet vent to the outlet fan, reducing the overall efficiency of the dryer. The heated air from the gas burner tube is expelled directly through the outlet fan before it goes through circulation (through the dying zone), wasting the energy input in heating that volume of air. The outlet fan should be placed as far back as possible in the corner, opposite from the inlet vent. It should be outfitted with a one-way butterfly valve that only opens when the fan is on. The tube of the gas burner can be extended as far possible within the geometric constraints of the upstream volume before the main fan. This would create a flow-volume that offers the most resistance for the air to move directly from the inlet vent to the outlet fan. This would also help protect the surrounding structure from the direct heat of the flame.

Further investigation is required in designing a trolley with trays that would reduce the high velocity range of the dryer in paragraph 6.6. The swirl region could be greatly reduced in the front section of the dryer by installing flat horizontal vanes in front of the first trolley. It should be kept in mind that the space or volume in front of the first trolley must be cleaned on a continuous basis according to the health and safety standards of food manufacturing. The volume should thus be easily accessible. Due to the fact that this type of dryer could be used in the same way as a batch dryer, the floor can be made as a sunken step, so that the first tray at the bottom of the trolley is level with the ducting system at the front of the dryer. The addition of blanking off plates is thus eliminated.

9 References

Adams, R.L. & J.F. Thompson, 1985. Improving Drying Uniformity in Concurrent Flow Tunnel Dehydrators. Transactions of the ASAE, Vol. 28(3): May-June, 1985, pp. 890-893.

Ansys Inc. Ansys CFX Release Notes 11.0, 2006. www.ansys.com

Batty, J.C. & S.L. Folkman, 1983. Food Engineering Fundamentals. John Wiley, New York, U.S.A. pp.169-177 and 200-209

BSRIA Instrument Solution, 2002. Product Data Sheet, viewed 25 November 2009, http://www.bis.fm/assets/documents/faxdatasheets/AV6%20Vane%20Anemometer.PDF

Chadwick, A., J. Morfett, 1998. Hydraulics in Civil and Environmental Engineering. E & FN Spon, 11 New Fetter Lane, London EC4P 4EE (ISBN 0-419-22580-3)

Charm, S.E. (1978). The Fundamentals of Food Engineering. AVI Publishing Company.

De Beer, R.W. & J.H. Muller, 2003. Heat and mass transfer phenomena related to the dehydration of deciduous and subtropical fruit in the Western Cape and Limpopo. 2nd International Conference on Heat Transfer, Fluid Mechanics and Thermodynamics, 24-26 June 2003, Victoria Falls, Zambia, Paper number: DR2

De Kock, D. (2004). Turbulence Modelling in CFD. Class notes of MSM 732, University of Pretoria.

De Kock, D. (2005). Personal Communication. South African branch of Qfinsoft (Pty) Ltd

Donkin, (2009). Majax-2 General specification, viewed 25 November 2009, http://www.donkin.co.za/Majax-2%20Brochure.pdf

Fluent Inc. Airpak 2.1 Documentation, 2002. www.fluentusers.com

Fluent Inc. Fluent 6.3 User's Guide, 2006. www.fluentusers.com

F.B.R Gas Burners Series X, 2009, viewed 25 November 2009, www.fbr.it/SchedulePdf/pdf_popup_Download.asp?iddownloads=43

Jones, F.E. (1977). The Air Density Equation and the Transfer of the Mass Unit. Institute for Basic Standards. National Bureau of Standards Washington , D.C. 20234 (NBSIR 77-1278)

Ku, H (1966). Notes on the Use of Propagation of Error Formulas, J Research of National Bureau of Standards-C. Engineering and Instrumentation, Vol. 70C, No.4, pp. 263-273.

Lange Gas, 2009. Technical Features of LPG or propane gas, viewed 25 November 2009, http://www.langegas.de/alte_daten/gasle.htm

Mathioulakis, E., V.T. Karathanos, V.G. Belessiotis, 1998. Simulation of Air Movement in a Dryer by Computational Fluid Dynamics: Application for the Drying of Fruits. Journal of Food Engineering 36 (1998) 183-200

Mills, A.F. (1999) Basic Heat and Mass Transfer 2nd Edition. Prentice Hall, Inc. Upper Saddle River, New Jersey

Nahor, H.B., M.L. Hoang, P. Verboven, M. Baelmans, B.M. Nicolai, 2004. CFD model of the airflow, heat and mass transfer in cool stores. International journal of refrigeration 28 (2005) 368-380

Nel, J. (2006) Personal communication, M-Pak Musina, 4 January 2006

NIST/SEMATECH e-Handbook of Statistical Methods, viewed 25 November 2009, http://www.itl.nist.gov/div898/handbook/, 2006

Osborne, W.C. (1977) Fans 2nd Edition (in SI/Metric Units). Pergamon Press Ltd.

Precool, 2009. Insulated doors: Sliding doors, viewed 25 November 2009, http://www.precool.co.za/main.html

Rajkumar, P., R. Kailappan, R. Viswanathan, K. Parvathi, G. Raghaven, V. Orsat, 2007. Thin Layer Drying Study on Foamed Mango Pulp. Agricultural Engineering International: the CIGR Ejournal Manuscript. FP 06 024. Vol IX. March, 2007

Reddek, G.W. (1973) Laboratory simulation of a commercial dehydration tunnel. Division of Agricultural Engineering at Stellenbosch University. Division of Agricultural Engineering at the Fruit and Fruit Technology Research Institute (FFTRI), Stellenboch

Slack, M. of Fluent Europe Ltd, Personal Communication. Solidcad office, November 2007

Sonntag, R.E., C. Borgnakke, G.J. van Wylen, 1998. Fundamentals of Thermodynamics Fifth Edition. John Wiley & Sons, Inc.

Southern African Weather Service, 2009. Climate data Musina, viewed 25 November 2009, http://www.weathersa.co.za/Climat/Climatstas/MusinaStats.jsp

Statistics. Com, 2009. Statistical Glossary – Coefficient of variation, viewed 25 November 2009, http://www.statistics.com/resources/glossary/c/coeffvar.php

Suwapanich, R., M. Haesungcharoen, 2006. Application of Thermal Properties to Predict Chilling Injury of Mango Fruits. Journal of Agricultural and Social Sciences 1813-2235/2006/02-4-225-226

Teeboonma, U., J. Tiansuwan, S. Soponronnarit, 2002. Optimization of heat pump fruit dryers. Journal of Food Engineering 59 (2003) 369-377

Testo, ll/2008. Measuring Instruments For Velocity, viewed 25 November 2009, http://www.testo-international.com/online/embedded/Sites/INT/SharedDocuments/ProductBrochures/MeasurementParameters_velocity_en.pdf

The Engineering Toolbox, 2009. Air Pressure and Altitude above Sea level, viewed 25 November 2009, http://www.engineeringtoolbox.com/air-altitude-pressure_462.html

The Engineering Toolbox, 2009. Colebrook equation, viewed 25 November 2009, http://www.engineeringtoolbox.com/colebrook-equation-d_1031.html

The Engineering Toolbox, 2009. Moody-diagram, viewed 25 November 2009, http://www.engineeringtoolbox.com/moody-diagram-d_618.html

The Engineering Toolbox, 2009. Roughness and surface coefficients of Ventilation Ducts, viewed 25 November 2009, http://www.engineeringtoolbox.com/surface-roughness-ventilation-ducts-d_209.html

Trox Technik, 2004. Washable Primary Filter. www.troxsa.co.za

Ventrite, 2009. Stormline: Inlet and Outlet louvers, viewed 25 November 2009, http:www.ventrite.co.za/Stormline%20suggested%20applications.htm

Vertex Technology Corp., 2009. VT30 Series Fuzzy Enhanced Programmable Controllers Instruction Manual, viewed 25 November 2009, http://www.vertex-tw.com/english/downloads.htm

Wallis, R.A. (1961) Axial Flow Fans Design and Practice. George Newnes Limited. London

White, F.M. (1991) Viscous fluid flow 2nd Edition. McGraw-Hill, Inc.

Wills, R.H.H., T.H. Lee, D. Graham, W.B. McGlasson, E.G. Hall, 1981. Postharvets: An Introduction to the Physiology and Handling of Fruit and Vegetables. Granada Publishing 1981

10 Appendix

10.1 Data points used for validation purposes

Table 10-1

Calculation of various factors relative to first run		
Air properties at 340K	**Value**	**Units**
Thermal conductivity	0.0294	W/m-K
Density	1.042	kg/m^3
Dynamic viscosity	2.01E-05	kg/m s
Kinematic viscosity	1.93E-05	m^2/s
Free stream velocity	16	m/s
Diameter of fan (D)	0.63	m
Length of Fan Tube (X)	0.5	m
Reynolds Stress number (D)	5.22E+05	
Reynolds Stress number (X)	4.14E+05	
Skin friction coefficient/2	2.80E-03	
Friction velocity	8.47E-01	m/s
Wall function	1.14E-03	m
Turbulent intensity	3.086273595	%
Boundary layer thickness	4.80E-03	m
Turbulent length scale	2.40E-03	m
Source of Thermal Air properties: Mills (1999)		

Table 10-2 Points used for data validation and creation of speed contours

Section A: No flow diverter and trolleys					
Point	**Exp.1 Speed (m/s)**	**RNG Speed (m/s)**	**X-axis (m)**	**Y-axis (m)**	**Z-axis (m)**
1	1.13	1.54	0	1.4	0.261
2	1.45	1.81	0	1.4	0.783
3	1.82	1.67	0	1.4	1.381
4	0.6	1.06	0	0.84	0.261
5	0.8	1.51	0	0.84	0.783
6	1.54	0.83	0	0.84	1.381
7	1.38	1.94	0	0.28	0.261
8	0.98	2.03	0	0.28	0.783
9	1.83	0.33	0	0.28	1.381

Table 10-3 Points used for data validation and creation of speed contours

Section B: No flow diverter and trolleys					
Point	Exp.1 Speed (m/s)	RNG Speed (m/s)	X-axis (m)	Y-axis (m)	Z-axis (m)
1	0.6	0.16	0.85	1.4	0.261
2	1.1	0.68	0.85	1.4	0.783
3	1.6	0.36	0.85	1.4	1.381
4	0.82	1.15	0.85	0.84	0.261
5	1.07	1.74	0.85	0.84	0.783
6	2.2	0.56	0.85	0.84	1.381
7	1.31	2.44	0.85	0.28	0.261
8	1.35	2.53	0.85	0.28	0.783
9	1.7	0.64	0.85	0.28	1.381

Table 10-4 Points used for data validation and creation of speed contours

Section C: No flow diverter and trolleys					
Point	Exp.1 Speed (m/s)	RNG Speed (m/s)	X-axis (m)	Y-axis (m)	Z-axis (m)
1	0.85	0.3	1.7	1.4	0.261
2	0.85	0.5	1.7	1.4	0.783
3	1.24	0.24	1.7	1.4	1.381
4	0.81	0.99	1.7	0.84	0.261
5	0.95	2	1.7	0.84	0.783
6	2.51	0.36	1.7	0.84	1.381
7	1.29	2.68	1.7	0.28	0.261
8	1.25	3.1	1.7	0.28	0.783
9	2.23	0.91	1.7	0.28	1.381

Table 10-5 Points used for data validation and creation of speed contours

Section D: No flow diverter and trolleys					
Point	Exp.1 Speed (m/s)	RNG Speed (m/s)	X-axis (m)	Y-axis (m)	Z-axis (m)
1	0.98	0.78	2.55	1.4	0.261
2	0.75	0.32	2.55	1.4	0.783
3	0.99	0.67	2.55	1.4	1.381
4	0.91	0.89	2.55	0.84	0.261
5	0.58	2.15	2.55	0.84	0.783
6	1.68	0.29	2.55	0.84	1.381
7	1.45	2.95	2.55	0.28	0.261
8	1.69	3.64	2.55	0.28	0.783
9	1.84	1.41	2.55	0.28	1.381

Table 10-6 Points used for data validation and creation of speed contours

Section E: No flow diverter and trolleys					
Point	Exp.1 Speed (m/s)	RNG Speed (m/s)	X-axis (m)	Y-axis (m)	Z-axis (m)
1	1.27	1.16	3.4	1.4	0.261
2	0.98	0.31	3.4	1.4	0.783
3	1.11	0.89	3.4	1.4	1.381
4	0.88	0.43	3.4	0.84	0.261
5	0.84	2.06	3.4	0.84	0.783
6	2	0.41	3.4	0.84	1.381
7	1.97	3.28	3.4	0.28	0.261
8	0.82	3.94	3.4	0.28	0.783
9	2.58	2.37	3.4	0.28	1.381

Table 10-7 Points used for data validation and creation of speed contours

Section F: No flow diverter and trolleys					
Point	Exp.1 Speed (m/s)	RNG Speed (m/s)	X-axis (m)	Y-axis (m)	Z-axis (m)
1	1.07	1.23	4.25	1.4	0.261
2	0.86	0.45	4.25	1.4	0.783
3	0.73	1.9	4.25	1.4	1.381
4	1.8	1.13	4.25	0.84	0.261
5	1.44	1.29	4.25	0.84	0.783
6	1.59	2.31	4.25	0.84	1.381
7	2.23	3.22	4.25	0.28	0.261
8	1.88	3.29	4.25	0.28	0.783
9	1.76	3.14	4.25	0.28	1.381

Table 10-8 Points used for data validation and creation of speed contours

Upstream of fan: No flow diverter and trolleys					
Point	Exp.1 Speed (m/s)	RNG Speed (m/s)	X-axis (m)	Y-axis (m)	Z-axis (m)
1	3.2	4.67	0	2.1	0.261
2	3.7	4.06	0	2.1	0.783
3	3.78	3.481	0	2.1	1.381
Downstream of fan: No flow diverter and trolleys					
Point	Exp.1 Speed (m/s)	RNG Speed (m/s)	X-axis (m)	Y-axis (m)	Z-axis (m)
1	0.9	1.34	4.25	2.1	0.261
2	1.57	6.82	4.25	2.1	0.783
3	2.17	1.58	4.25	2.1	1.381

Table 10-9 Points used for data validation and creation of speed contours

Section A: With flow diverter (No trolleys)					
Point	Exp.2 Speed (m/s)	RNG Speed (m/s)	X-axis (m)	Y-axis (m)	Z-axis (m)
1	1.86	2	0	1.4	0.261
2	1.26	2.13	0	1.4	0.783
3	1.6	1.56	0	1.4	1.381
4	1.87	1.64	0	0.84	0.261
5	0.43	2.03	0	0.84	0.783
6	0.43	0.92	0	0.84	1.381
7	1.51	1.75	0	0.28	0.261
8	2.06	2.34	0	0.28	0.783
9	2.75	1.14	0	0.28	1.381

Table 10-10 Points used for data validation and creation of speed contours

Section B: With flow diverter (No trolleys)					
Point	Exp.2 Speed (m/s)	RNG Speed (m/s)	X-axis (m)	Y-axis (m)	Z-axis (m)
1	0.86	0.76	0.85	1.4	0.261
2	1.33	0.83	0.85	1.4	0.783
3	1.71	0.34	0.85	1.4	1.381
4	0.68	1.45	0.85	0.84	0.261
5	0.84	1.99	0.85	0.84	0.783
6	1.05	0.67	0.85	0.84	1.381
7	1.26	1.94	0.85	0.28	0.261
8	1.98	2.9	0.85	0.28	0.783
9	2.29	0.55	0.85	0.28	1.381

Table 10-11 Points used for data validation and creation of speed contours

Section C: With flow diverter (No trolleys)					
Point	Exp.2 Speed (m/s)	RNG Speed (m/s)	X-axis (m)	Y-axis (m)	Z-axis (m)
1	0.61	0.22	1.7	1.4	0.261
2	1.06	0.54	1.7	1.4	0.783
3	1.45	0.29	1.7	1.4	1.381
4	0.64	1.07	1.7	0.84	0.261
5	0.72	2.18	1.7	0.84	0.783
6	1.33	0.48	1.7	0.84	1.381
7	1.37	1.99	1.7	0.28	0.261
8	2.04	3.53	1.7	0.28	0.783
9	2.65	0.91	1.7	0.28	1.381

Table 10-12 Points used for data validation and creation of speed contours

Section D: With flow diverter (No trolleys)					
Point	Exp.2 Speed (m/s)	RNG Speed (m/s)	X-axis (m)	Y-axis (m)	Z-axis (m)
1	0.75	0.43	2.55	1.4	0.261
2	0.85	0.45	2.55	1.4	0.783
3	1.51	0.53	2.55	1.4	1.381
4	0.52	0.68	2.55	0.84	0.261
5	0.59	2.47	2.55	0.84	0.783
6	1.49	0.41	2.55	0.84	1.381
7	1.3	2.25	2.55	0.28	0.261
8	1.68	4.01	2.55	0.28	0.783
9	1.75	1.06	2.55	0.28	1.381

Table 10-13 Points used for data validation and creation of speed contours

Section E: With flow diverter (No trolleys)					
Point	Exp.2 Speed (m/s)	RNG Speed (m/s)	X-axis (m)	Y-axis (m)	Z-axis (m)
1	0.95	0.73	3.4	1.4	0.261
2	0.63	0.36	3.4	1.4	0.783
3	1.1	0.71	3.4	1.4	1.381
4	0.75	0.35	3.4	0.84	0.261
5	0.66	2.51	3.4	0.84	0.783
6	1.57	0.4	3.4	0.84	1.381
7	2.14	2.83	3.4	0.28	0.261
8	2.07	4.2	3.4	0.28	0.783
9	1.75	1.69	3.4	0.28	1.381

Table 10-14 Points used for data validation and creation of speed contours

Section F: With flow diverter (No trolleys)					
Point	Exp.2 Speed (m/s)	RNG Speed (m/s)	X-axis (m)	Y-axis (m)	Z-axis (m)
1	0.84	0.98	4.25	1.4	0.261
2	0.86	0.5	4.25	1.4	0.783
3	0.65	0.95	4.25	1.4	1.381
4	1.59	1.21	4.25	0.84	0.261
5	1.06	1.55	4.25	0.84	0.783
6	1.12	2.04	4.25	0.84	1.381
7	1.42	3	4.25	0.28	0.261
8	1.75	3.53	4.25	0.28	0.783
9	2.19	3.11	4.25	0.28	1.381

Table 10-15 Points used for data validation and creation of speed contours

Upstream of fan: With flow diverter (No trolleys)					
Point	Exp.2 Speed (m/s)	RNG Speed (m/s)	X-axis (m)	Y-axis (m)	Z-axis (m)
1	3.2	3.78	0	2.1	0.261
2	3.7	3.9	0	2.1	0.783
3	3.78	3.85	0	2.1	1.381
Downstream of fan: With flow diverter (No trolleys)					
Point	Exp.2 Speed (m/s)	RNG Speed (m/s)	X-axis (m)	Y-axis (m)	Z-axis (m)
1	1.82	2.24	4.25	2.1	0.261
2	2.5	7.33	4.25	2.1	0.783
3	3.75	1.26	4.25	2.1	1.381

Table 10-16 Points used for data validation and creation of speed contours

Section A: With flow diverter and trolleys					
Point	Exp.3 Speed (m/s)	RNG Speed (m/s)	X-axis (m)	Y-axis (m)	Z-axis (m)
1	1.9	3.15	0	1.58	0.1
2	1.1	2.46	0	1.58	0.45
3	1.4	1.74	0	1.58	0.76
4	1.8	1.51	0	1.58	0.805
5	1.6	2.05	0	1.58	1.115
6	1	2.77	0	1.58	1.456
7	1.6	1.87	0	1.28	0.1
8	1.1	0.63	0	1.28	0.45
9	0.9	1.09	0	1.28	0.76
10	0.7	0.79	0	1.28	0.805
11	0.9	0.71	0	1.28	1.115
12	0.9	1.6	0	1.28	1.456
13	1.1	1.45	0	0.82	0.1
14	0.4	0.38	0	0.82	0.45
15	0.4	1.12	0	0.82	0.76
16	0.4	0.7	0	0.82	0.805
17	0.3	0.33	0	0.82	1.115
18	0.4	1.52	0	0.82	1.456
19	0.4	1.73	0	0.52	0.1
20	0.4	0.36	0	0.52	0.45
21	0.6	1.93	0	0.52	0.76
22	1.1	1.41	0	0.52	0.805
23	0.8	0.23	0	0.52	1.115
24	0.6	1.42	0	0.52	1.456
25	1.9	1.76	0	0.22	0.261
26	2.2	5.7	0	0.22	0.783
27	1.7	1	0	0.22	1.381

Table 10-17 Points used for data validation and creation of speed contours

Section B: With flow diverter and trolleys					
Point	Exp.3 Speed (m/s)	RNG Speed (m/s)	X-axis (m)	Y-axis (m)	Z-axis (m)
1	0.9	1.89	0.85	1.58	0.1
2	0.8	1.72	0.85	1.58	0.45
3	1.3	1.39	0.85	1.58	0.76
4	1.2	1.24	0.85	1.58	0.805
5	1.1	1.62	0.85	1.58	1.115
6	1.2	1.84	0.85	1.28	1.456
7	1.9	1.61	0.85	1.28	0.1
8	0.6	0.39	0.85	1.28	0.45
9	1.1	1.55	0.85	1.28	0.76
10	1.1	1.29	0.85	1.28	0.805
11	0.9	0.36	0.85	1.28	1.115
12	0.9	1.53	0.85	1.28	1.456
13	0.6	1.54	0.85	0.82	0.1
14	0.6	0.46	0.85	0.82	0.45
15	1.9	1.7	0.85	0.82	0.76
16	0.8	1.22	0.85	0.82	0.805
17	0.9	0.42	0.85	0.82	1.115
18	1.3	1.56	0.85	0.82	1.456
19	1	1.58	0.85	0.52	0.1
20	0.6	0.39	0.85	0.52	0.45
21	0.9	2.43	0.85	0.52	0.76
22	0.9	1.93	0.85	0.52	0.805
23	0.6	0.41	0.85	0.52	1.115
24	0.7	1.42	0.85	0.52	1.456
25	2.2	1.59	0.85	0.22	0.261
26	2.2	2.37	0.85	0.22	0.783
27	1.9	1.13	0.85	0.22	1.381

Table 10-18 Points used for data validation and creation of speed contours

Section C: With flow diverter and trolleys					
Point	Exp.3 Speed (m/s)	RNG Speed (m/s)	X-axis (m)	Y-axis (m)	Z-axis (m)
1	1.3	1.8	1.7	1.58	0.1
2	0.8	1.69	1.7	1.58	0.45
3	1.1	1.46	1.7	1.58	0.76
4	0.9	1.28	1.7	1.58	0.805
5	0.7	1.63	1.7	1.58	1.115
6	0.9	1.79	1.7	1.28	1.456
7	0.9	1.58	1.7	1.28	0.1
8	0.8	0.32	1.7	1.28	0.45
9	1	1.67	1.7	1.28	0.76
10	1	1.46	1.7	1.28	0.805
11	0.7	0.31	1.7	1.28	1.115
12	0.9	1.51	1.7	1.28	1.456
13	1.7	1.44	1.7	0.82	0.1
14	0.6	0.49	1.7	0.82	0.45
15	1.3	1.87	1.7	0.82	0.76
16	1	1.39	1.7	0.82	0.805
17	0.5	0.43	1.7	0.82	1.115
18	1.4	1.46	1.7	0.82	1.456
19	0.9	1.42	1.7	0.52	0.1
20	0.6	0.4	1.7	0.52	0.45
21	1.1	2.6	1.7	0.52	0.76
22	1	2.09	1.7	0.52	0.805
23	0.8	0.46	1.7	0.52	1.115
24	1.1	1.39	1.7	0.52	1.456
25	1.7	1.609	1.7	0.22	0.261
26	2.1	2.54	1.7	0.22	0.783
27	1.6	1.18	1.7	0.22	1.381

Table 10-19 Points used for data validation and creation of speed contours

Section D: With flow diverter and trolleys					
Point	Exp.3 Speed (m/s)	RNG Speed (m/s)	X-axis (m)	Y-axis (m)	Z-axis (m)
1	0.9	1.66	2.55	1.58	0.1
2	0.6	1.73	2.55	1.58	0.45
3	0.8	1.54	2.55	1.58	0.76
4	0.7	1.35	2.55	1.58	0.805
5	0.6	1.72	2.55	1.58	1.115
6	1.4	1.69	2.55	1.28	1.456
7	0.8	1.52	2.55	1.28	0.1
8	0.6	0.28	2.55	1.28	0.45
9	1	1.91	2.55	1.28	0.76
10	1.1	1.64	2.55	1.28	0.805
11	0.8	0.25	2.55	1.28	1.115
12	1.6	1.43	2.55	1.28	1.456
13	1.1	1.12	2.55	0.82	0.1
14	0.9	0.48	2.55	0.82	0.45
15	1.1	2.1	2.55	0.82	0.76
16	1	1.56	2.55	0.82	0.805
17	0.8	0.45	2.55	0.82	1.115
18	1	1.13	2.55	0.82	1.456
19	1.4	1.41	2.55	0.52	0.1
20	0.9	0.5	2.55	0.52	0.45
21	0.9	2.86	2.55	0.52	0.76
22	1.1	2.28	2.55	0.52	0.805
23	1.2	0.53	2.55	0.52	1.115
24	1.1	1.27	2.55	0.52	1.456
25	1.5	1.81	2.55	0.22	0.261
26	1.6	2.55	2.55	0.22	0.783
27	1.6	1.35	2.55	0.22	1.381

Table 10-20 Points used for data validation and creation of speed contours

Section E: With flow diverter and trolleys					
Point	Exp.3 Speed (m/s)	RNG Speed (m/s)	X-axis (m)	Y-axis (m)	Z-axis (m)
1	0.7	1.31	3.4	1.58	0.1
2	0.6	1.63	3.4	1.58	0.45
3	0.9	1.42	3.4	1.58	0.76
4	0.9	1.29	3.4	1.58	0.805
5	0.4	1.68	3.4	1.58	1.115
6	0.6	1.34	3.4	1.28	1.456
7	1.3	1.16	3.4	1.28	0.1
8	0.6	0.32	3.4	1.28	0.45
9	0.6	2.12	3.4	1.28	0.76
10	0.6	1.85	3.4	1.28	0.805
11	0.5	0.17	3.4	1.28	1.115
12	1	1.05	3.4	1.28	1.456
13	1.1	0.93	3.4	0.82	0.1
14	0.9	0.57	3.4	0.82	0.45
15	1.1	2.31	3.4	0.82	0.76
16	1	1.82	3.4	0.82	0.805
17	1.2	0.58	3.4	0.82	1.115
18	1.3	1	3.4	0.82	1.456
19	1.5	1.7	3.4	0.52	0.1
20	1.3	0.82	3.4	0.52	0.45
21	1.1	3.06	3.4	0.52	0.76
22	1.3	2.44	3.4	0.52	0.805
23	1.1	0.94	3.4	0.52	1.115
24	1.3	1.79	3.4	0.52	1.456
25	1.6	2.22	3.4	0.22	0.261
26	1.2	2.41	3.4	0.22	0.783
27	1.5	1.66	3.4	0.22	1.381

Table 10-21 Points used for data validation and creation of speed contours

Section F: With flow diverter and trolleys					
Point	Exp.3 Speed (m/s)	RNG Speed (m/s)	X-axis (m)	Y-axis (m)	Z-axis (m)
1	1.5	1.89	4.25	1.58	0.1
2	1.8	1.1	4.25	1.58	0.45
3	0	0.67	4.25	1.58	0.76
4	0	0.59	4.25	1.58	0.805
5	0	0.93	4.25	1.58	1.115
6	1	1.52	4.25	1.28	1.456
7	0	3.08	4.25	1.28	0.1
8	0	1.75	4.25	1.28	0.45
9	0	1.5	4.25	1.28	0.76
10	0	1.35	4.25	1.28	0.805
11	0	1.45	4.25	1.28	1.115
12	0	3.27	4.25	1.28	1.456
13	1.2	2.8	4.25	0.82	0.1
14	1.3	1.9	4.25	0.82	0.45
15	1.4	1.96	4.25	0.82	0.76
16	1.2	1.77	4.25	0.82	0.805
17	1.3	1.68	4.25	0.82	1.115
18	1.3	3.48	4.25	0.82	1.456
19	1.4	2.55	4.25	0.52	0.1
20	2	1.87	4.25	0.52	0.45
21	2	2.67	4.25	0.52	0.76
22	2	2.39	4.25	0.52	0.805
23	2.1	1.78	4.25	0.52	1.115
24	1.9	3.38	4.25	0.52	1.456
25	1.9	2.53	4.25	0.22	0.261
26	0	2.69	4.25	0.22	0.783
27	0	2.72	4.25	0.22	1.381

Table 10-22 Points used for data validation and creation of speed contours

Upstream of fan: With flow diverter and trolleys					
Point	Exp.3 Speed (m/s)	RNG Speed (m/s)	X-axis (m)	Y-axis (m)	Z-axis (m)
1	3.57	4.07	0	2.1	0.261
2	7.2	4.47	0	2.1	0.783
3	3	3.94	0	2.1	1.381
Downstream of fan: With flow diverter and trolleys					
Point	Exp.3 Speed (m/s)	RNG Speed (m/s)	X-axis (m)	Y-axis (m)	Z-axis (m)
1	2.3	4.16	4.25	2.1	0.261
2	2.2	6.42	4.25	2.1	0.783
3	2.8	3.01	4.25	2.1	1.381

10.2 Uncertainty analysis

According to NIST/SEMATECH (2006) the International Organisation for Standardisation (ISO) and the International Vocabulary of Basic and General Terms in Metrology defines uncertainty as:

> "parameter, associated with the result of measurement, that characterises the dispersion of the values that could be reasonable be attributed to the measurand"

This definition is consistent with the concept of Eisenhart that the uncertainty statement assigns credible limits to the accuracy of a reported value, stating to what extent that value may differ from its reference value. The estimation of the possible discrepancy takes into account random errors and bias in the measurement process. Random errors cannot be corrected, whereby biases can theoretically at least be corrected or eliminated from the measurement result. Precision and bias are properties of a measurement method, while uncertainty is a property of a specific result for a single test item that depends on a specific measurement process (NIST/SEMATECH, 2006).

The steps to determine the uncertainty of the measurements is based on the ISO approached described in NIST/SEMATECH e-Handbook of Statistical Methods updated in 2006. The ISO approach is based on the following rules:

- Each uncertainty component is quantified by a standard deviation.
- All biases are assumed to be corrected and any uncertainty is the uncertainty of the correction.
- Zero corrections are allowed if the bias cannot be corrected and an uncertainty is assessed.
- All uncertainty intervals are symmetric

The ISO approach is to classify the sources of error. Components are grouped together into two major categories depending on the source of the data and not the type of error (NIST/SEMATECH, 2006). The categories are:

- Type A – components evaluated by statistical methods
- Type B – components evaluated by other means

In the computation of the final uncertainty it makes no difference how the components are classified because the ISO guidelines treat the type A and type B evaluations in the same manner. All uncertainty components (standard deviations) are combined by root-sum-squares (quadrature) to arrive at a 'standard uncertainty', u, which is the standard deviation of the reported value, taking into account all sources of error, both random and systematic, that effect the measurement result. If the purpose of the uncertainty statement is to provide

coverage with a high level of confidence, an expanded uncertainty is computed as:

$$U = ku$$

Equation 10-1

Where k is chosen to be the $t_{\alpha/2}(\nu)$ critical value from the t-table for ν degrees of freedom. The table can be found at:
http://itl.nist.gov/div898/handbook/mpc/section3/mpc3652.htm

For large degrees of freedom, it is suggested to use $k = 2$ to approximate 95% coverage.

The first step is to define the result for the test item for which an uncertainty is required. The number of repetitions on the test item, the range of environmental and operational conditions and sources of error (such as calibration uncertainties) influences the computation of the standard deviation. If the value for the test item is calculated from measurements on secondary quantities, the equation for combining the various quantities must be defined. Steps for an uncertainty analysis involving one quantity are (NIST/SEMATECH, 2006):

- Compute a standard deviation for the random sources of error defined as type A
- Make sure that the collected data and analysis cover all sources of random error and bias
- Compute standard deviation for each type B component of uncertainty
- Combine type A and type B standard deviation into a standard uncertainty for the reported result using sensitivity factors
- Compute an expanded uncertainty

Type A evaluations can apply to both random error and bias. The only requirement is that the calculation of the uncertainty component be based on a statistical analysis of data. Uncertainties associated with the instrument's calibration are reported as type B evaluations. Instruments should agree within the calibration uncertainties. Sources of uncertainty that lead to type B evaluations are (NIST/SEMATECH, 2006):

- Reference standards calibrated by another laboratory
- Physical constants used in the calculation of the reported value
- Environmental effects that cannot be sampled
- Possible configuration or geometry misalignment in the instrument
- Lack of resolution of the instrument

The uncertainty for all the experiments done for this dissertation will be considered as type B evaluations. The reason for this is that anemometers were

handheld devices, so misalignment of the instruments played a large role in determining the accuracy of the results. Other factors were the environmental effects that could not be replicated again for each experiment and the devices were calibrated by the manufactures of the products. The measurements were not repeated over an extended period so type-A statistical methods could not be applied to determine the uncertainty components.

Documented sources of uncertainty, such as calibration reports for reference standards or published reports of uncertainties for physical constants are usually given as an expanded uncertainty, U, which is converted to the standard uncertainty (NIST/SEMATECH, 2006):

$$u = U/k$$

Equation 10-2

If the k factor is not known or documented, it is conservative to assume that $k = 2$.

Sources of uncertainty that are local to the measurement process but which cannot be adequately sampled to allow a statistical analysis require type B evaluations. One technique is to estimate the worst-case effect, a , for the source of interest, from

- Experience
- Scientific judgement
- Scant data

A standard deviation, assuming that the effect is two-sided, can then be computed based on a uniform, triangular or normal distribution of possible effects. For type B evaluation the ISO approach is to assign infinite degrees of freedom to the standard deviations derived in this manner (NIST/SEMATECH, 2006).

The ISO guidelines do not allow worst-case estimates of bias to be added to the other components, but require they in some way be converted to equivalent standard deviations. The approach is to consider that any error or bias, for the situation at hand, is a random draw from a known statistical distribution. Then the standard deviation is calculated from known (or assumed) characteristics of the distribution. The uniform distribution leads to the most conservative estimate of uncertainty. It gives the largest standard deviation. The calculation of the standard deviation is based on the assumption that the end points, $\pm a$, of the distribution are known. It also embodies the assumption that all effects on the reported value, between $-a$ and $+a$, are equally likely for the particular source of uncertainty (NIST/SEMATECH, 2006).

$$S_{source} = \frac{1}{\sqrt{3}} a$$

Equation 10-3

The way of determining the uncertainty components from estimating it directly from direct repetitions of the measurement result is called the top-down approach (As in Equation 10-3). The second alternative approach is the propagation of error. The estimates from the individual auxiliary measurements are combined. The approximate formula is to compute the standard deviation of each variable and then to combine into a standard deviation, ignoring the possible covariance between the variables (NIST/SEMATECH, 2006).

Each approach mentioned above contains a sensitivity coefficient. The sensitivity coefficient shows the relationship of the individual uncertainty component to the standard deviation of the reported value of the test item. The sensitivity coefficient relates to the result that is being reported and not to the method of estimating uncertainty components where the uncertainty, u, is

$$u = \sqrt{\sum_{i=1}^{R} {a_i}^2 {s_i}^2}$$

Equation 10-4

Given R components:

- a_i – sensitivity coefficient
- s_i – standard deviation

The majority of sensitivity coefficients for type B evaluations will be one with a few exceptions. The sensitivity coefficient for the type B uncertainty of a reference standard is the nominal value of the test item divided by the nominal value of the reference standard. When applying a propagation of error approach the partial derivatives are the sensitivity coefficients for the associated components (NIST/SEMATECH, 2006).

The expanded uncertainty (See Equation 10-1) is such that the true unknown value of the measurement of interest is so that for any measurement results, Y ,

$$Y - U \leq True\ value \leq Y + U$$

Equation 10-5

10.2.1 Expanded uncertainty for experiments

The equations mentioned in the paragraph above will be implemented to determine the expanded uncertainty of experiments. The application of the equations are shown for experiment one. The uniform distribution method (Equation 10-3) will be used in determining the uncertainty component due to the calibration of the instrument. The most conservative approach is used due the fact that the maintenance history of the instrument is not known by the author. The handheld anemometer Testo 451 series was used to determine the velocity magnitude in the drying zone of experiments one and two. This device was also used in determining the temperature and humidity of all the experiments. The table below (Table 10-23) gives the accuracy and the range of the device. Table 10-25 gives the accuracy of the AV6 anemometer that was used for experiment three.

Table 10-23 Accuracy of handheld anemometer (Testo 451)

Testo 451 series	Measured range	Accuracy
Vane probe (5 mm) (0635 range)	0 to + 20 m/s	± (0.03 m/s + 5% of mean value
Temperature/Humidity Probe (0636 range)	-20 to +70℃ 0 to + 100% RH	± 0.4℃ (-10 to + 50℃) ± 0.5℃ (remaining range) ±2 %RH (+2 to +98 %RH)

Source: (Testo, 2008)

Table 10-24 Accuracy of handheld anemometer (AV6 Vane Anemometer)

AV6 (100 mm vane)	Measured range	Accuracy
Vane probe (0.01 m/s resolution)	0.25 to + 30 m/s	± 1% of reading ± 1Digit
Temperature (0.1 ℃ resolution)	0 to 80℃	± 1℃ + 1 Digit

Source: (BSRIA Instrument Solutions, 2002)

Large diameters (Ø 60 mm, Ø 100 mm) are suitable for the measurement of turbulent flows (e.g. at outlet ducts) at smaller and medium velocities. Small diameters are more suitable for the measurement in ducts, in which case the duct cross-section must be 100 times bigger than the probe cross section be impacted (Testo, 2008).

Point 9 in section E (See Table 10-6) produced the largest endpoint in experiment one, a:

$$a_{exp1} = \left|2.58 - (2.58 + 0.03 + \frac{5}{100} \times 2.58)\right| = 0.16$$

The standard deviation for the calibration component is:

$$S_{exp1} = \frac{1}{\sqrt{3}} a_{exp1} = 0.09$$

In order to calculate the sensitivity coefficient, a_{sc1}, the nominal (average) value, Y_{exp1}, of the 54 (N) data measurement points , X, in the drying zone was used.

$$Y_{exp1} = 1.33$$

$$a_{sc1} = \frac{1.33}{2.58} = 0.52$$

The propagation of error method was used in determining the standard deviation for the uncertainty component of the measurements, X, taken in the drying zone. The average value, Y_{exp1}, is a function of only one variable, namely,X.

$$Y_{exp1} = \bar{X}$$

where, $\bar{X}$, is an average of , N, measurements. NIST/SEMATECH (2006) used the formulas of H.Ku (1966) in order to determine the standard deviation of Y_{exp1}:

$$S_{Y_{exp1}} = \frac{1}{\sqrt{N}} S_x$$

Where:

$S_x = standard\ deviation\ of\ X$

$$S_{Y_{exp1}} = \frac{1}{\sqrt{54}} \times 0.511 = 0.069$$

The sensitivity coefficient for this propagation of error method is 1 (The partial derivative of $Y_{exp1} = \bar{X}$).

The combined standard coefficient, u_{exp1}, for the experiment is:

$$u_{exp1} = \sqrt{(S_{exp1} a_{sc1})^2 + (S_{Y_{exp1}})^2} = 0.08$$

The expanded uncertainty, U, for experiment 1, with infinite degrees of freedom (DF) is:

$$U = u_{exp1} \times 2 = 0.17$$

This relates to a relative error compared to Y_{exp1} of 12.65%.

All the equations mentioned above were applied to the data points of experiments two and three. The results are tabulated and compared to the values of experiment one in the table below (See Table 10-25).

Table 10-25 Uncertainty analysis for experiments

Components	Exp. 1	Exp. 2	Exp.3
a	0.16 m/s	0.12 m/s	0.03 m/s
S_{exp}	0.09	0.07	0.02
$Y_{\exp}$	1.33	1.31	1.02
a_{sc}	0.52	0.71	0.47
S_x	0.511	0.583	0.513
N	54	54	162
$S_{Y_{\exp}}$	0.069	0.079	0.040
$\frac{\partial Y_{exp}}{\partial X}$	1	1	1
u_{exp}	0.08 m/s	0.09 m/s	0.04 m/s
k	2	2	2
U	0.17 m/s	0.19 m/s	0.08 m/s
% relative error	12.65	14.27	8.02

Technical drawing of the flow-diverters designed by the engineering section of the Hans Merensky group:

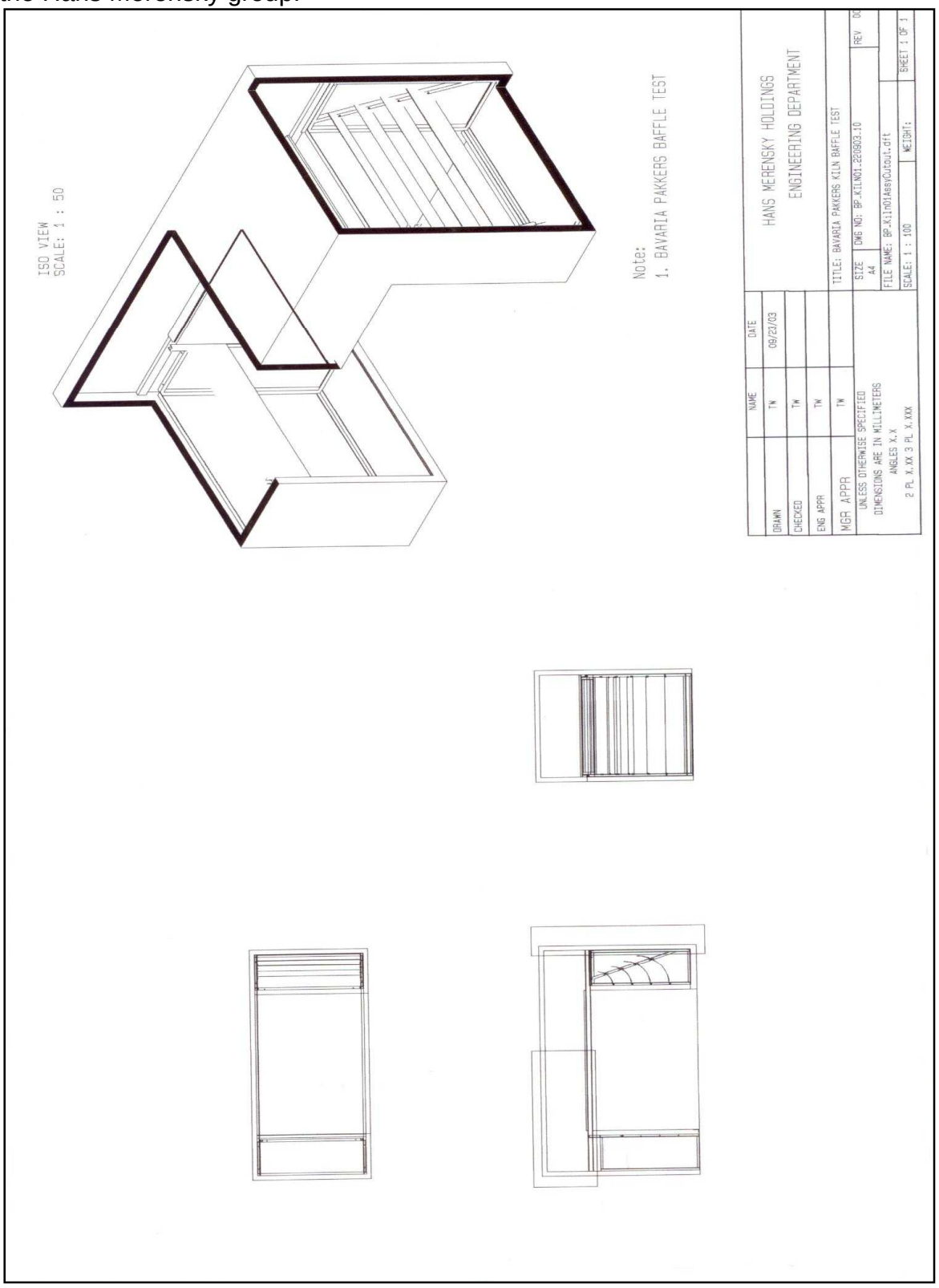

Figure 10-1 Iso-drawing of flow diverters in batch dryer

10.3 Design calculations of M-Pak Musina dryer

Design calculations are based on the methodology used by de Beer and Muller (2003). The analyses are done on the combined heat and mass transfer within the dryer.

The drying capacity of the dryer is:

Table 10-26 Dryer evaporation capacity (M_{evp})

Variable	Value	Unit	Reference
Mass of wet mango slices per tray	5	kg	Par. 4.5.13
Number of trays per trolley	50		Par. 3.2
Number of trolleys per dryer	5		Par. 3.2
Mass of wet mango slices per trolley	250	kg	Par. 3.2
Total mass of wet mango slices in dryer	1250	kg	= 5 × 250
Initial moisture content of product (W.W.B)	86	%	de Beer and Muller (2003)
Initial mass of water in product before drying	1075	kg	= 1250 × 86%
Bone dry mass of product at inlet	175	kg	Equation 3-1
Final moisture content of product (W.W.B)	13	%	de Beer and Muller (2003)
Final mass of product after drying	201.15	kg	Equation 3-1
Final mass of water in product after drying	26.15	kg	= 201.15 - 175
Total mass of water evaporated	1048.85	kg	= 1075 - 26.15
Drying ratio (1kg Wet to 1k dry product)	6.21		= 1250 ÷ 201.15
Drying Cycle	24	h	Par. 3.2
Dryer evaporation capacity (M_{evp})	43.70	kg/h	= 1048.85 ÷ 24

Exhaust fraction:

The mass balance of the water entering and leaving the drying zone as shown in Figure 3-1 is:

$$M_{a_1}\omega_{a_1} + (M_{p_2} - M_{p_3}) = M_{a_1}\omega_{a_4}$$

Equation 10-6

By rearranging the terms:

$$\omega_{a_4} = \omega_{a_1} + (M_{p_2} - M_{p_3})/M_{a_1}$$

Equation 10-7

$$\omega_{a_1} = 0.622\Phi_1 \frac{P_{g_1}}{P_{a_1}}$$

Equation 10-8

$$P_{a_1} = P_m - \Phi P_{g_1}$$

Equation 10-9

$$\omega_{a_1} = 0.622\left[\frac{\Phi_1 P_g}{\left(P_m - \Phi_1 P_{g_1}\right)}\right]$$

Equation 10-10

$$M_{evp} = M_{p_2} - M_{p_3}$$

Equation 10-11

The air entering the drying zone (T_{a_1}) is regulated by the thermal and relative humidity controller to average 55℃ and 20% relativ e humidity (Φ_1) (See Figure 4-3 and Figure 4-4). According to Sonntag et al. (1998) the saturated vapour pressure (P_{g_1}) of water at 55℃ is 15.758 kPa. The pressure of the mixture (P_m) entering the dryer zone was assumed to be the same pressure as the ambient air pressure at 522 m above sea level (See par. 4.3). M_{a_1} was taken as the air displacement of the main fan, which relates to the fan curve in Donkin (2009) at a total gauge pressure of 200 Pa. (See Table 5-3).

Table 10-27 Variables required to determine Exhaust fraction

Variable	Value	Unit
Φ_1 (R.H.)	0.2	
P_{g_1}	15.758	kPa
P_m	95.2	kPa
M_{evp}	43.70	kg/h
Main fan volume flow	10882.44	m^3/h
ρ_a (Table 4-1)	1.1614	kg/m^3
M_{a_1}	12638.86	kg/h
ω_{a_1}	0.021296	
ω_{a_4}	0.024754	

The mass balance on the water entering and exiting the entire system is:

$$M_{a_4}\omega_{a_4} = M_{a_5}\omega_{a_5} + (M_{p_2} - M_{p_3})$$

Equation 10-12

The ambient air conditions were: $T_{a_5} = 34℃$ and $\Phi_5 = 0.4$ (See Third set-up in par. 3.2). According to Sonntag et al. (1998) the saturated vapour pressure (P_{g_5}) of water at 34℃ is 5.628 kPa.

$$\omega_{a_5} = 0.622\left[\frac{\Phi_5 P_{g_5}}{\left(P_m - \Phi_5 P_{g_5}\right)}\right]$$

$$\omega_{a_5} = 0.01506$$

Equation 10-13

A mass balance on the air gives: $M_{a_4} = M_{a_5}$

$$\therefore\ M_{a_4} = (M_{p_2} - M_{p_3})/(\omega_{a_4} - \omega_{a_5})$$

$$M_{a_4} = 4510.3\ \text{kg/h}$$

Equation 10-14

$$Exhaust\ fraction = \frac{M_{a_4}}{M_{a_1}} = 0.3568$$

Equation 10-15

Thus about 35.7 % of the air circulated through the dryer must exit the dryer at the outflow fan to maintain a relative humidity of 0.2 of air entering the drying zone.

Energy requirement for the drying process:

The energy required for the process from an energy balance for the total system using Equation 2-10 without a heat loss (Q_{loss}) of 20%:

$$Q = M_{p_3} C_p\left(T_{p_3} - T_{p_2}\right) + M_{a_5}\left[C_a\left(T_{a_4} - T_{a_5}\right) + \omega_{a_5}(h_{g_1} - h_{g_4})\right] + M_{evp}(h_{g_1} - h_{f_2})$$

Equation 10-16

According to de Beer and Muller (2003) the specific heat (C_p) of the mango product is 1.72 kJ/kg℃. It is unclear where they g ot this value from. The author used the value of 4.5 kJ/kg℃ (C_p value at 50 ℃ for mangoes stored at 8 ℃ for 25 days) given by Suwapanich and Haesungcharoen (2006).

De Beer and Muller (2003) states that the wetted surface temperature will be driven towards the dry bulb temperature of the drying air (After 24 hour drying cycle in the falling rate period). They compute the energy requirement (Q) with T_{p_3} and T_{a_4} equal to 55℃ $\left(T_{a_1}\right)$. The author used Equation 2-21 in order to calculate the variables mentioned above. T_{p_2} equals the ambient temperature of the air (T_{a_5}), after processing the mango (slicing it up in pieces) and placing it onto the trolleys, it can be 4-8 hours before the trolleys is placed into the dryer.

$$T_o - T_i = \pm \frac{h_{fg} m Ln(M_i - M_o)}{C_p \theta \rho V (M_i + 1)}$$

Equation 10-17

Table 10-28 Variables required to determine temperature at exit of drying zone

Variable	Value	Unit	Reference
Mass per tray	5	kg	Par. 4.5.13
Trays per width of drying zone	2		Par. 4.5.12
Trays = width of trolley	0.85	m	Par. 3.2
b	1.565	m	Par. 3.2
m	7.517	kg/m^2	= (5×2)/(0.85×1.565)
L	4.25	m	Par. 3.2
n	14.880	No./m	=(50/2)/1.68
h	1.68	m	Par. 3.2
θ	86400	s	24 hour cycle
M_i (B.D.B)	6.142		Equation 2-19
M_o (B.D.B)	0.149		Equation 2-19
W	0.01213	kg/s	
W (The same as M_{evp})	43.70	kg/h	
Q (Main fan volume flow)	3.0229	m^3/s	Table 5-3
V	1.149	m/s	Equation 2-20
C_{p_a}	1.005	kJ/kg-K	Table 4-1
h_{fg} at 55 ℃	2370.66	kJ/kg	Sonntag et al. (1998)
T_i	55	℃	
T_o	46.84	℃	Equation 2-21

$$\therefore T_{p_3} = T_{a_4} = T_o$$

Table 10-29 Variables to determine energy requirement

Variable	Value	Unit	Reference
M_{p_3}	8.381	kg/h	= 201.15/24
C_p	4.5	kJ/kg-℃	
T_{p_3}	46.84	℃	
T_{p_2}	34	℃	
M_{a_5}	4510.3	kg/h	$M_{a_4} = M_{a_5}$
C_a	1.005	J/kg-K	Table 4-1
T_{a_4}	320	K	= 46.84+273.15
T_{a_5}	307.15	K	= 34+273.15
ω_{a_5}	0.01506		
h_{g_1} at 55℃ (T_{a_1})	2600.86	kJ/kg	Sonntag et al. (1998)

h_{g_4} at 46.84℃ (T_{a_4})	2585	kJ/kg	Sonntag et al. (1998)
M_{evp}	43.70	kg/h	
h_{f_2} at 34℃ ($T_{a_2} = T_{a_5}$)	146.66	kJ/kg	Sonntag et al. (1998)
Q (Q_{loss} of 20% excluded)	55.25	kW	
Q (Q_{loss} of 20% included)	69	kW	

The dryer thermal efficiency is calculated using Equation 2-11:

$$\eta_t = \frac{M_{evap} h_{fg\_vapour}}{Q_{actual}}$$

Equation 10-18

Table 10-30 Variables required to calculate thermal efficiency

Variable	Value	Unit
M_{evp}	43.70	kg/h
h_{fg_vapour} at 55 ℃ (Sonntag et al. ,1998)	2370.66	kJ/kg
Q (Q_{loss} of 20% excluded)	55.25	kW
Q (Q_{loss} of 20% included)	69	kW
η_t (Q_{loss} of 20% excluded)	51.5	%
η_t (Q_{loss} of 20% included)	41.2	%
Q (Q_{loss} of 20% included and 100% recirculation)	30	kW
η_t (Q_{loss} of 20% included and 100% recirculation)	96	%

A 100% recirculation will however not work due to the fact that no drying will take place due to the evaporated water not being removed from the dryer. If ,Φ_1, is raised to 30 % and ,T_{a_1}, to 57.25 ℃, the exhaust air, $M_{a_4,}$ becomes 3400 kg/h. Taking into account the volume flow of Table 5-3 for the outlet fan (This relates to 3660.5 kg/h or air removed from the dryer) the energy required, Q (Q_{loss} of 20% excluded), decreases to 51.5 kW with the thermal efficiency, η_t, increasing to 56 %. The temperature at the exit of the drying zone, T_{a_4}, was calculated to be 49 ℃.

Equation 2-7 is used to calculate the average convective heat transfer coefficient of the dryer in the constant drying period. It should be taken into consideration that this is only an average estimate of the convective heat transfer coefficient for this specific dryer. The area allocated to drying can vary due to the nets that cover the trays and how the slices are placed on the trays.

$$M = \frac{hAT_\infty - T_s}{h_{fg}}$$

Equation 10-19

Table 10-31 Variables used to calculate average convective heat transfer coefficient

Variable	Value	Unit	Reference
M	0.01213	kg/s	$M = M_{evp}/3600$
T_∞	53.17	℃	$(T_{a_1} + T_{a_4})/2$
T_s calculated at $(\omega_{a_1} + \omega_{a_4})/2$	37.5	℃	Psychrometric chart of Sonntag et al. (1998)
h_{fg} at 37.5℃	2412.67	kJ/kg	Sonntag et al. (1998)
Average length of mango slice	0.1	m	Par. 4.5.13
Average height of mango slice	0.025	m	Par. 4.5.13
Average width of mango slice	0.025	m	Par. 4.5.13
Volume of one mango slice	0.0000625	m^3	
Density of mango	1015	kg/m^3	Rajkumar et al. (2007)
Total mass of product inside dryer	1250	kg	
Total volume of product inside dryer	1.2315	m^3	
Number of mango slices inside dryer	19704		
Area of one slice	0.01125	m^2	
Total area of product inside dryer	221.67	m^2	
Percentage not allocated to drying area	20	%	Estimation
Area allocated to drying	177	m^2	
h	0.0105	$kW/m^{2\circ}C$	

Equation 4-16 is used to calculate the Total fan power output, P, and the Equation 4-17 to estimate Fan efficiency,η,. The fan power is calculated using the results of the CFD analysis in Table 5-3 and data from the fan manufacturer (Donkin, 2009). The Fan efficiency is an estimate because the fan manufacturer only gives the maximum mechanical power the fan will require in order to run at the setup stated in paragraph 4.5.9. Table 10-33 gives a more realistic value in terms of the fan efficiency,η, using the values obtained from the CFD analysis on the dryer.

$$P = pQ$$

Equation 10-20

$$\eta = \frac{P}{FP} \times 100\%$$

Equation 10-21

Table 10-32 Variables used from fan manufacturer to obtain Fan power

Variable	Value	Unit	Reference
p	200	Pa	Donkin (2009)
Q (Main fan volume flow)	3.0	m^3/s	Donkin (2009)
P	0.6	kW	
FP	0.85	kW	Donkin (2009)
η	70.6	%	

Table 10-33 Variables used from CFD analysis to obtain Fan power

Variable	Value	Unit	Reference
Diameter of main fan	0.63	m	See Table 5-3
Area of main fan	0.311	m^2	
Q (Main fan volume flow)	3.0229	m^3/s	See Table 5-3
Average fan velocity	9.69	m/s	= 3.0229/0.311
Fan static pressure	72	Pa	See Table 5-3
Fan dynamic pressure ($0.5\rho v^2$)	54.6	Pa	Chadwick and Morfett (1998)
Fan Total pressure	126.6	Pa	= 72 + 54.6
P	0.382	kW	
FP	0.85	kW	Donkin (2009)
η	45	%	

In paragraph 4.5.10 the definition of aspect ratio is given in terms of turning vane and flow diverter.

Table 10-34 Variables used to define the aspect ratio of the dryer configuration described in paragraph 5.4

Variable	Value		Unit	Reference
Angle of vane	13°	0.2268 rad.		Par. 4.5.11
Width of flow diverter	0.865		m	Par. 4.5.11
Height of flow diverter	0.2		m	= TAN(0.2268) × 0.865
Width of duct section	1.565		m	Par. 3.2
Height between roof and the false ceiling	0.87		m	Par. 4.5.11
Height of duct section	0.67		m	= 0.87 - 0.2
Aspect ratio	2.3			= 1.565 ÷ 0.67
Wetted area	0.94			Equation 4-1
Mean radius ratio	0.8			= ((0.87+0.2)/2)/0.67
Ratio of wetted area to cross section	0.89			= 0.94/(1.565 × 0.67)

Table 10-35 Variables used to define the aspect ratio of the duct system above the false ceiling for the dryer configuration in paragraph 6.4

Variable	Value		Unit	Reference	
Angle of vane	13°	0.2268 rad.		Par. 4.5.11	
Width of flow diverter	0.865		m	Par. 4.5.11	
Height of flow diverter	0.2		m	= TAN(0.2268) × 0.865	
Width of duct section	1.565		m	Par. 3.2	
Height between roof and the false ceiling	0.87		m	Par. 4.5.11	
Height of duct section	First section	Second section		First section	Second section
	0.22	0.44	m	= 0.67×1/3	= 0.67×2/3
Aspect ratio	7	3.5		= 1.565/0.22	= 1.565/0.44
Wetted area	0.4	0.7		= 4×(0.22×1.565)/(2×(0.22+1.565))	= 4×(0.44×1.565)/(2×(0.44+1.565))
Mean radius ratio	1.4	1.44		= (0.2+0.22)/2)/0.22	= ((0.87+(0.87-0.44))/2)/0.44
Ratio of wetted area to cross section	1.11	1		= 0.4/(1.565×0.22)	= 0.7/(1.565×0.44)

10.3.1 Cost analysis of improved dryer

Table 10-36 will show the energy requirements of the dryers with and without flow diverters. The CFD results, especially in terms of the main fan flow, are used to determine the energy requirements compared to the theoretical or manufacture values used in paragraph 10.3. Energy values were compared and referenced against the values found in the paragraph mentioned above. The table only shows the input values that have change and the values that are dependent on the input values.

Table 10-36 Energy requirements for various dryer configurations

Variable	Values of Par. 10.3	Excluding Flow Diverter	Including Flow Diverter	Unit	Reference
Main fan volume flow	10882.44	10702.908	10882.692	m^3/h	Table 10-27
M_{a_1}	12638.86	13111.056	13331.304	kg/h	Table 10-27
ω_{a_4}	0.024754	0.024630	0.024630		Table 10-27
M_{a_4}	4510.3	4569.0	4595.5	kg/h	Equation 10-14
$Exhaust\ fraction$	0.3568	0.3484	0.3447		Equation 10-15
Q (Main fan volume flow)	3.0229	2.97303	3.02297	m^3/s	Table 10-28
V	1.14974	1.13077	1.14976	m/s	Table 10-28
T_o	46.84	46.69	46.83	℃	Table 10-28
T_{p_3}	46.84	46.69	46.83	℃	Table 10-29
M_{a_5}	4510.3	4569.0	4595.5	kg/h	Table 10-29
T_{a_4}	319.90	319.84	319.98	K	Table 10-29
Q (Q_{loss} of 20% included)	69	70.10	70.29	kW	Table 10-29
η_t (Q_{loss} of 20% included)	41.2	41.053	40.94	%	Table 10-29

Table 10-37 shows the power required to run the main and outlet fan of the various dryer configurations. The values are obtained through the CFD results of the dryers. Table 10-38 indicates the total power usage of the various dryer configurations. It shows that with the flow diverter added that there is only a 0.33 % increase in power required. Taking into account that the average speed in the drying zone with the flow diverter is 3.4 % higher (See values in Table 10-39 and Table 10-40) the increase in power requirement is negligible.

Table 10-37 Fan Power requirements for various dryer configurations

	Excluding Flow Diverter		Including Flow Diverter		
Variable	**Main Fan**	**Outlet Fan**	**Main Fan**	**Outlet Fan**	**Unit**
Fan velocity (Avg.)	8.53895	7.58175	8.63476	7.54057	m/s
Static pressure (Avg.)	39.2662	57.7609	50.9197	53.7761	Pa
Dynamic pressure	42.3409	33.3803	43.2964	33.018	Pa
Fan Total pressure	81.607	91.1412	94.216	86.7948	Pa
Q	2.97303	0.86317	3.02297	0.87558	m^3/s
P	0.242	0.0786	0.284	0.0759	kW

Table 10-38 Total heating requirements of for various dryer configurations

Variable	Excluding Flow Diverter	Including Flow Diverter	Unit
Heating energy requirement	70.10	70.29	kW
Main Fan Power	0.242	0.284	kW
Outlet Fan Power	0.0786	0.0759	kW
Total energy requirement	70.421	70.652	kW
Energy requirement/hour	253519.0	254349.5	KJ/h
Water evaporation	43.7	43.7	kg/h
Energy requirement/kg	5801.07	5820.07	KJ/kg
% Increase compared to dryer without flow diverter		0.33%	

There are two main criteria in order to determine if the addition of the flow diverter benefits the drying system. The one is by increasing the average speed in the drying zone without increasing the power requirements. The second is if the drying uniformity is increased in the drying zone. The tables above showed that the speed is increased in the drying zone. The figures and tables below will show that at the area covered by the average speed is more uniform in the drying zone with the flow diverter added.

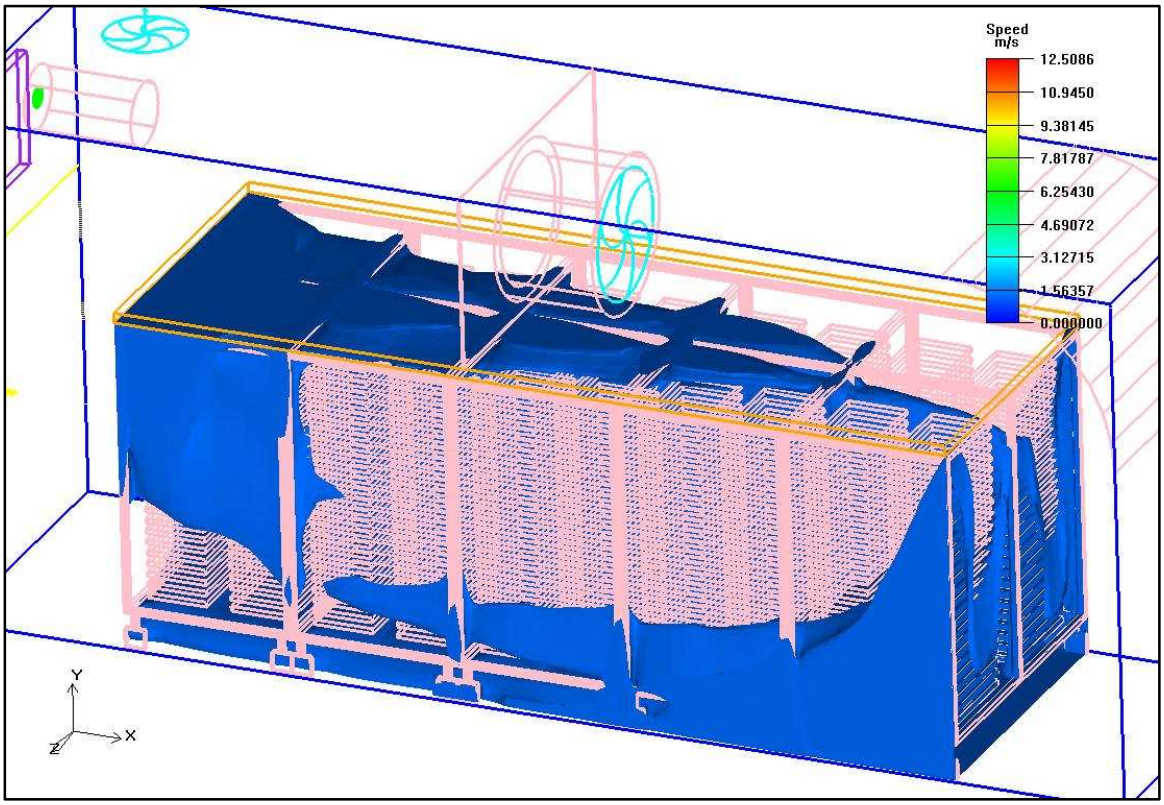

Figure 10-2 Iso-volume of average air speed in dryer without flow diverter

Table 10-39 Iso-volume of average air speed in dryer without flow diverter

Variable	Value	Units	Reference
Average speed	1.48	m/s	Table 5-7
Area covered	74.9	m^2	
Total Iso-volume	111	$m/s\text{-}m^2$	

Figure 10-2 and Figure 10-3 show the iso-volume covered by the average speed within the confined volume of the drying zone. Table 10-39 and Table 10-40 indicates that the area covered by the average speed in the drying zone is 7 % more compared to the dryer without a flow diverter.

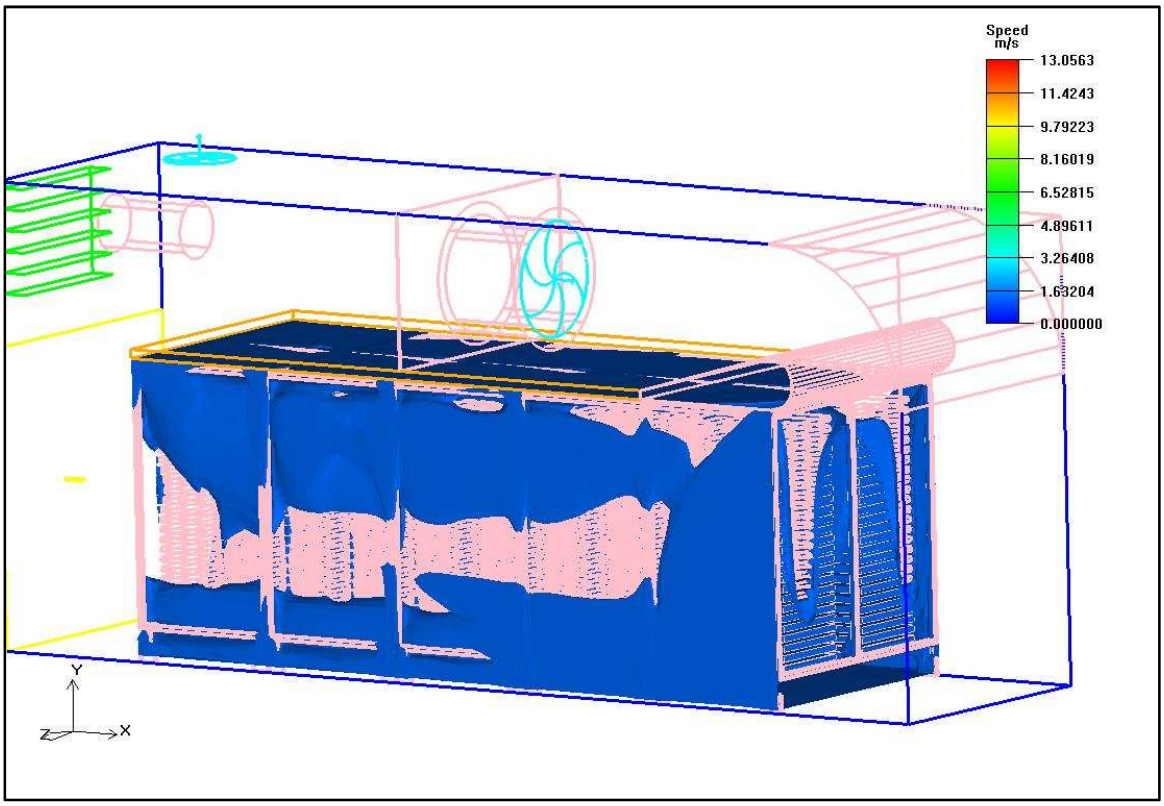

Figure 10-3 Iso-volume of average air speed in dryer with flow diverter

Table 10-40 Iso-volume of average air speed in dryer with flow diverter

Variable	Value	Units	Reference
Average speed	1.53	m/s	Table 5-6
Area covered	80.2	m^2	
Total Iso-volume	123	$m/s\text{-}m^2$	

These tables above show that with the same amount energy input into the various dryer configurations that the dryer with flow diverter has a more uniform velocity distribution in the drying zone, meaning less wet spots. In Table 10-41 the evaporation rate during the constant rate period was determine with the average air speed in the drying zone and the area covered by it. It factors out the chemical treatment and mango structure that influences the drying rate in the falling rate period. It shows that there is a 7 % increase in the evaporation rate with the addition of the flow diverter.

Table 10-41 Water evaporation rate in constant rate period with drying area calculated at average speed in drying zone

Variable	Excluding Flow Diverter	Including Flow Diverter	Unit	Reference
h	0.0105	0.0105	kW/m^2°C	Table 10-31
Area covered	74,9	80.2	m^2	Table 10-39 Table 10-40
T_∞	53.17	53.17	℃	Table 10-31
T_s	37.5	37.5	℃	Table 10-31
h_{fg}	2412.67	2412.67	kJ/kg	Table 10-31
M	18.388	19.689	kg/h	
% Increase compared to dryer without flow diverter		7%		

Table 10-42 and Table 10-43 show the running cost on a yearly basis in terms of the energy requirement to run the various dryer configurations.

Table 10-42 Average cost of L.P.G consumed by gas burner per year

Variable	Values	Units	Reference
L.P.G delivery at 70 kW	2.7	m^3/h (Standard Pressure and Temp.)	F.B.R Gas X3/2CE burner (2009)
Density (gas state)	2.01 1	kg/m^3 (Standard Pressure and Temp.)	Lange Gas (2009)
L.P.G mass delivery per hour	5.43	kg/h	
Average price of L.P.G /kg in S.A, 2009	12	R/kg (Average price for large consumers)	No regulated price available yet in S.A
Cost per hour	R 65.15	R	
Operating hours/year	2400	h	= 24 (hours) × 5 (days) × 4 (weeks) × 5 (months season)
Operating per year of dryer without flow diverter	R 156578.90	R	= (65.15 X 2400) × 1.0014) (70.1 kW relates to 0.14% increase in gas usage - Table 10-38)
Operating per year of dryer with flow diverter	R 157001.07	R	= (65.15 × 2400) × 1.0041) (70.3 kW relates to 0.41% increase in gas usage - Table 10-38)

Table 10-43 Electrical cost of various dryer configurations on a yearly basis

Variable	Excluding Flow Diverter	Including Flow Diverter	Reference
Electrical unit cost	R 0.57/kW·h	R 0.57/kW·h	Average electrical unit cost in S.A (2009)
Main fan	R 329.60	R 386.92	= 2400 h × R 0.57 × kW (Values in Table 10-38)
Outlet fan	R 106.87	R 103.24	= 2400 h × R 0.57 × kW (Values in Table 10-38)
Gas burner	R 149.43	R 149.43	= 2400 h × R 0.57 × 0.11 kW (F.B.R Gas X3/2CE burner ,2009)
Total cost	R 585.90	R 639.59	Electrical usage of sensors and actuators were negligible

A total cost saving of 6 % in terms of energy requirements are shown in Table 10-44 with the flow diverter added.

Table 10-44 Total cost of drying mangoes on a yearly basis

Variable	Excluding Flow Diverter	Including Flow Diverter	Reference
Initial construction cost	R 6666.67	R 6933.33	= R100000/15 year life cycle. Added 4 % to initial building cost of dryer with flow diverter (Par. 7)
Cost of 5 trolleys with trays	R 6666.67	R 6666.67	= R100000/15 year lifespan.
Operating costs (Gas usage)	R 156594.29	R 157016.50	Table 10-42
Maintenance cost	R 666.67	R 693.33	= 10 % of yearly construction cost
Electrical cost (fans and gas burner)	R 585.90	R 639.59	Table 10-43
Total cost per year	R 171180.19	R 172216.09	
Water evaporated per year during constant evaporation period	44132.23	47255.07	= 2400 h × values in Table 10-41
R/kg producing cost in a year	R 3.87	R 3.63	
% Cost saving compared to dryer without flow diverter		6 %	